NOTICE

The quality of this microform is heavily dependent upon the quality of the original thesis submitted for microfilming. Every effort has been made to ensure the highest quality of reproduction possible.

If pages are missing, contact the university which granted the degree.

Some pages may have indistinct print especially if the original pages were typed with a poor typewriter ribbon or if the university sent us an inferior photocopy.

Reproduction in full or in part of this microform is governed by the Canadian Copyright Act, R.S.C. 1970, c. C-30, and subsequent amendments.

AVIS

La qualité de cette microforme dépend grandement de la qualité de la thèse soumise au microfilmage. Nous avons tout fait pour assurer une qualité supérieure de reproduction.

S'il manque des pages, veuillez communiquer avec l'université qui a conféré le grade.

La qualité d'impression de certaines pages peut laisser à désirer, surtout si les pages originales ont été dactylographiées à l'aide d'un ruban usé ou si l'université nous a fait parvenir une photocopie de qualité inférieure.

La reproduction, même partielle, de cette microforme est soumise à la Loi canadienne sur le droit d'auteur, SRC 1970, c. C-30, et ses amendements subséquents.

Behaviour of the Adsorbed Cl· Intermediate in Electrocatalysis of Anodic Cl_2 Evolution at Oxide Film Surfaces at Pt and Ru

By

Ping Gu

A thesis submitted to the School of Graduate Studies in partial fulfillment of the requirements for the degree of

Doctor of Philosophy

in Chemistry

Department of Chemistry
University of Ottawa,
Ottawa, Ontario.

B. E. Conway
Professor of Chemistry
Research Supervisor

Ping Gu
PH.D. Candidate

ISBN 0-315-62315-2

Canada

UNIVERSITÉ D'OTTAWA
UNIVERSITY OF OTTAWA

Abstract

In this thesis, the investigation of the mechanism of chlorine evolution reaction at: i) both freshly reduced and pre-oxidized Pt electrodes; ii) RuO_2-TiO_2 electrodes (DSA); iii) other noble metals such as Pd, Ir, Ru and Rh by means of computer controlled anodic polarization, potential-relaxation transients and a. c. impedance measurements, will be presented.

As described in Chapter V, the influence of co-deposited OH and O species in the surface oxidation process on the extent of chemisorption of the Cl· intermediate in the Cl_2 evolution reaction has been carefully examined. Experimental results reveal that the reaction rate at reduced Pt surfaces is much greater than that at pre-oxidized ones. This is because the oxide species have a significant effect in blocking the Cl_2 evolution kinetics. The detectable surface adsorption pseudocapacitance, which is associated with the "overpotential deposited" Cl· intermediate, at freshly reduced Pt and oxide free Pt surfaces in non-aqueous trifluoroacetic acid (TFA) medium supports this conclusion.

In chapter VI, some exploratory experiments at other noble metal (e.g., Pd, Ir, Ru, and Rh) electrodes in non-aqueous TFA solution have shown very interesting interfacial capacitance information, which must be interpreted probably in terms of more than one adsorbed reaction intermediate being present.

In Chapter VII, a possible mechanism of recombination kinetically control has been proposed for the Cl_2 evolution reaction at RuO_2-TiO_2 electrodes, based on the observations of their steady-state behaviour, and electrochemical data from potential relaxation and a.c. impedance measurements. Local supersaturation of Cl_2 in the microstructure of the oxide film appears to make a contribution to the

pseudocapacitance behaviour.

Some of the results in this work have been published or in press, as listed below:

1. "Surface electrochemistry of the anodic chlorine evolution reaction at Pt: influence of co-deposition of the $Cl^{\cdot}$ intermediate", P.Gu and B.E.Conway, J. Chem. Soc. Farada Trans. 86(6) (1990) 923.

2. "Behaviour of the adsorbed $Cl^{\cdot}$ intermediate in anodic chlorine evolution at thin-film RuO_2 surfaces", P.Gu and B.E.Conway, J. Appl. Electrochem., in press.

3. "Evaluation of $Cl^{\cdot}$ adsorption in anodic chlorine evolution at Pt by means of a.c. impedance and potential relaxation experiments: role of the state of surface oxidation", P.Gu and B.E. Conway, J. Chem. Soc. Faraday Trans., in press.

Acknowledgment

The author wishes to express his deepest and sincere thanks to Professor B.E. Conway for his direction and guidance throughout the course of this work. Professor Conway was not only always willing to give his assistance and suggestions, but also gave encouragement whenever difficulties arose. Without his guidance, the completion of this work would not be possible. The author always remembers what he learned from Professor Conway, regarding both electrochemistry and a good attitude towards science. It was a privilege and honour for the author to work with such a well-known, capable and understanding person.

I would also like to mention how grateful I am to my colleges and my friends; Dr. L.J. Bai, Mr. S.Y. Qian and Dr. R. Brousseau who many times helped me with enlightening discussion. Great thanks extended to Dr. T. Wrzesniewska and Mr. B. Anderson for taking the beautiful SEM micrographs shown in the thesis. The author will not forget Mr. Egon Kristoff, the exceptional master glassblower, and his assistant, Mr. John Hopkins, who provided the glass cells and other work for the author.

Finally, I wish to thank my parents and Miss Pei Li for their supports and encouragement.

List of Contents

List of Tables

List of Figures

CHAPTER I

General Review of the Anodic Chlorine Evolution Reaction

1.1 Introductory Remarks

Electrocatalysis of anodic processes that take place in aqueous solution, is different in an important way from that of cathodic ones, for example, the hydrogen evolution reaction or electrochemical hydrogenation; this is because the anode materials normally develop initially a two-dimensional surface oxide film in the case of noble metals or a three-dimensional bulk phase one in the case of base metals. The anodic reaction, for instance Cl_2 or O_2 evolution, may take place at appreciable current densities on the oxidized anode metal surface. Therefore, the oxide film will directly influence anodic Faradaic reactions. Alternatively, anode materials may be conducting bulk oxides like RuO_2, IrO_2 or SnO_2 supported on corrosion-resistant metal substrates such as Ti or Ta.

The investigations described in this thesis are: i) the influence of pre-build oxide film to the mechanism of chlorine evolution reaction, and ii) the behaviour of the intermediate $Cl^{\cdot}$ species in the Cl_2 evolution mechanism on the noble metal electrode Pt and on pre-formed RuO_2-TiO_2 oxide electrodes in aqueous medium; (iii) studies, as in (ii), applied to the behaviour of chlorine evolution reaction in anhydrous trifluoroacetic acid (TFA) medium in which Pt can be used as an unoxidized metal surface, and (iv) Some preliminary studies at Pd, Ru, Ir and Rh electrodes of the Cl_2 evolution reaction in a non-aqueous TFA solution.

The methods that were employed in this research work are listed below:

a) Digital recording of potential transients on an open-circuit, following the interruption of a polarizing current, the so-called potential-relaxation method. This

technique has been applied to study the adsorption behaviour of the " overpotential deposited " Cl_{ad} generated as an intermediate in the anodic Cl_2 reaction at an appreciable current. A new procedure for the data processing of acquired in the by this method, which we call the potential decay " fitting method ", has been developed by the present author in collaboration with Dr. R. Brousseau in this laboratory and is used to evaluate one of the required the experimental variables.

b) A.c. impedance method was employed to study the adsorption behaviour of the Cl_{ad} and applied both a developed equivalent-circuit treatment and the kinetic mechanistic approach for quantitative interpretation of the obtained a.c. behaviour by means of computer simulation procedures.

c) Cyclic-voltammetry, coupled with computer programmed data-processing. This procedure has been used to study the growth of the oxide film during the chlorine evolution reaction at Pt. This aspect of the work has led to an improved understanding of the properties of the oxide film and the role it plays in determining the electrocatalysis and kinetics of the Cl_2 evolution reaction at the Pt anode surface.

1.2. Introduction Concerning the Anodic Chlorine Reaction

1.2.1. Brief Historical Aspects of Cl_2 Production Technology

Historically, carbon and magnetite anodes were initially used for industrial production of chlorine by the electrolysis of brine at elevated temperatures, 90 ~ 95°C. However, since 1900, graphite has been extensively used, even up to the late 60's. Although the use of carbon anodes has been common for many years, much attention has been given to study of the behaviour of various noble metal and noble metal oxide surfaces as anodes for commercial electrochemical Cl_2 production[1-10] in order to diminish Cl_2 overvoltage and associated power loss and to increase anode lifetimes. These materials are:

(a) titanium electrodes coated with a noble metal.(e.g. Pt, Pd, Ru, Rh, Ir)[1-2]

and (b) titanium electrodes coated with oxides of Ru and Ir[3-7], etc..

Although Pt is considered as one of the best catalysts, it is not commercially used because it is too expensive and also it is known that Pt electrodes undergo strong passivation, furthermore, extensive corrosion occurs when Pt is used as an anode for Cl_2 production. However, Ti-supported Pt-Ir alloy anodes have shown much better performance since Ir contents as low as 0.5% were found sufficient to almost completely eliminate the passivation effects[2].

Special attention has been given to the electrochemical behaviour of metal oxide films, particularly RuO_2 on a passive metal support such as Ti/TiO_2, the so-called dimensionally stable anodes (DSA) which were first developed by Beer[12] in the 1950s. Such oxide films have been found not only to be good electrical conductors but it is likely that they also play an important role in the electrocatalysis and mechanism of the anodic Cl_2 evolution reaction.

Recent technology employs ion-exchange membrane cells in which the anodically generated Cl_2 is completely separated from the cathodically generated H_2. This is accompanied by the production of a pure NaOH solution.

1.2.2. Thermodynamic Aspects of the Cl_2-Cl^- Reaction and its Columbic Efficiency

The thermodynamics of the chlorine - chloride reaction at equilibrium:

$$Cl_2 + 2e^- \rightleftharpoons 2Cl^- \qquad [1.1]$$

are well established[13]. The recommended[14] standard reversible potential is 1.35828 V, R.H.E. corresponding to a Nernst equation:

$$E_{Cl2} = E^\circ_{Cl2} - (RT/F) \ln[a_{Cl^-} / f^{1/2}_{Cl2}] \qquad [1.2]$$

where a_{Cl^-} is the hypothetical activity of the Cl^- ions and f_{Cl2} the fugacity of Cl_2 gas. Reaction [1.1] is very reversible and can be established as a practical reversible electrode at platinized or platinized-iridized Pt surfaces in a way similar to that employed for H_2-H^+ reversible electrodes.

As O_2 has a standard reversible potential of 1.230 V, the thermodynamics indicates that it should evolve before Cl_2 at unit fugacity and unit Cl^- activity. However,

the exchange current densities for Cl_2 evolution on noble metals and carbon are usually substantially greater than those for O_2 evolution. In the other words, Chlorine evolution is kinetically favoured but O_2 evolution is thermodynamically preferred, thus, Cl_2 is normally the preferred anodic process in the electrolysis of an aqueous Cl^- solution, except at high dilutions. Moreover, Cl^- ion adsorption competes with the development of the surface oxide film which is anodically formed at noble metals, and changes the critical state of the film enabling Cl_2 evolution to be even more favoured kinetically.

In commercial Cl_2 evolution from brine, the current efficiency is usually better than 98%. However, in dilute solutions, of course, Cl_2 evolution is less favoured first because its exchange current is diminished in some power of the chloride concentration corresponding to the reaction under determined by the transfer coefficient and mechanism of the reaction; and secondly, because at sufficiently high current-densities, the reaction will eventually become diffusion controlled, allowing O_2 evolution to arise competitively from the discharge of water prior to, or in parallel with, Cl_2 evolution so that the current efficiency for Cl_2 evolution will tend to become diminished. Additionally, these conditions allow the possibility of anodic generation of ClO and ClO_2 gases which further lower the current efficiency.

1.3 The States of Oxide Films on Anode Surfaces

1.3.1 General Behaviour

The states of oxide films on anode surfaces are of major importance in determining the electrocatalysis and pathways of anodic reactions in aqueous solution. Metal surfaces usually undergo, or participate in, several types of oxidation reactions as anodes in suitable electrolyte solutions:

(i) oxidation of the metal to free solvated metal ions; e.g. $M \rightleftharpoons M^{z+} + ze^-$ where M^{z+} is solvated.

(ii) oxidation to form an oxide film by an electrochemical reaction with the

electrolyte; e.g. $M + H_2O \dashrightarrow MOH + H^+ + e^-$.

(iii) dissolution as solvated ions by the passage of metal ions through the oxide film.

(iv) O_2 evolution on the oxidized metal surface is a subsequent reaction but it is often electrochemically coupled with the surface oxidation process.

(v) other anodic gas evolution, e.g. Cl_2, on the oxide covered surface depending on the composition of the solution.

Obviously, whether these reactions occur at a given metal depends on several factors: (a) the properties of the metal itself; (b) the experimental conditions, such as choice of electrolyte, polarization potential and temperature; and (c) pH and electrolyte concentration. This means that some metals such as copper or nickel can undergo anodic dissolution in acidic solution, while, in alkaline solutions, their surfaces become covered with an oxide film of significant thickness (5 to ca. 100nm).

At sufficiently positive anodic potentials, most metals become coated with an oxide film leading eventually to " passivation " of the metal dissolution process. This behaviour occurs in a relatively narrow potential range, and the thickness of the resulting film depends on the metal and on the conditions of the oxide film growth (interfacial field, temperature etc.) and can be in the range of a few layers to a few thousand layers. These films, of course, can be compact or porous depending on the conditions under which they are grown. They also may be distinguished according to their conductivities, for example, oxides formed on Pt are known to be fairly thin and conducting, while those at Ni thicker and conducting and those at the " valve " metals (Ti, Ta, Zr, Al) are thick but behave as insulators[15,16]. Such films are usually highly protective since diffusion of metal cations or O anions through the film is so slow that they almost completely inhibit dissolution of the underlying metal. However, the oxide films on these metals[17] thicken in proportion to the potential applied across them by mechanisms involving either defect cation or anion transport, or in some cases, both. Few leakage currents do arise through the films and this is ascribed to defects in the

film or to the presence of pits[15,16,18].

At extreme positive potentials, O_2 can be made to evolve upon the protective films if sufficient voltage is applied to overcome the high resistivity of the films. At such oxide films, there are two regions where ion or electron-transfer occurs: one at the metal/oxide interface and the other at the oxide/solution interface.

Another type of behaviour can arise at heavily oxide-coated metals where the anodic oxidation process is either partially or completely the anodic dissolution of the metal itself. This process may take place with or without formation of an intermediate reaction film on the electrode surface. In the case of Al or Fe, depending of the type of electrolyte, anodic oxidation is coupled with the anodic dissolution of the metal[17]. Al can develop solid compact oxide films which are virtually insoluble (borate or tartrate buffers, pH = 5 - 7) or finely porous films which result from slow dissolution of the film itself (acidic solution: sulphuric acid). Some metals such as Fe or Ni[15,16,18] exhibit a transition between so-called active and passive states. The first is characterized by either a dissolution of the metal itself or by the formation of a porous salt or hydroxide layer, which becomes transformed into a passive, protective form as the oxidation state of the metal is increased and the oxide film is formed directly or when the lower hydroxide is converted into an higher oxide.

Less noble metals such as Ag, Cu and Ni tend to form thick oxide layers[18,19] depending on the conditions of their formation. In the material which follows, attention will be concentrated upon the behaviour of very thin oxide films formed on the noble metals, especially Pt and on the properties of bulk, conducting oxide films such as RuO_2 or IrO_2 etc.

1.3.2 Thin Oxide Films at the Noble Metal Pt

Since the most detailed mechanistic studies of the Cl_2 evolution reaction have been addressed to Pt and the most extensive knowledge of surface oxidation processes is available for this metal, some account will first be given on the state of

the oxidized Pt electrode surface in the absence of Cl^- ion as this indicates the type of surface oxidation processes that can go on prior to or in parallel with Cl^- ion discharge and will determine the competitive adsorption which Cl^- experiences over the potential range in which an oxide film is formed at Pt.

The interpretation of the properties and formation of the oxygen layer on the Pt surface is rather complex since three factors contribute to the difficulties of studying the system. First, the state of the bare metal surface itself, as it is important that a perfectly clean surface be present initially without any other impurities being adsorbed, except inevitably anions from the electrolyte. Second, the irreversibility of the film formation and reduction processes, leading to a displacement of the potentials of the current peaks for oxide formation and reduction in comparison with those for reversible processes. Third, the possibility of eventual formation of a multi-layer oxide film, beyond the initial monolayer, in contrast to that for H for which only a monolayer film is formed.

The methods that have been applied to the study of oxide films on noble metals are cyclic-voltammetry, ellipsometry, radio-tracer studies of ion adsorption and some modern techniques such as X-ray photo-electron spectroscopy for chemical analysis (ESCA) and Auger spectrometry; some of these will be mentioned below.

1.3.2.1 Information from Cyclic-Voltammetry

A method developed by Breiter, Knorr and co-workers[20,21] and especially by Will and Knorr[22], involves the observation of potential-dependent charging currents which result when a repetitive or a single potential sweep, linearly varying in time ($V_t = V_{ini} \pm st$), is applied to an electrode by means of a potentiostat at a rate $s = dV/dt$, programmed by means of a function generator. The change of potential V with time t is referred to as a " potentiodynamic sweep "; in the repetitive mode, when potential is cycled " anodically " and " cathodically " over some set potential range, this method is called "cyclic-voltammetry".

Many papers have been published on the study of oxide film formation of platinum, especially two groups of investigators: Vetter and Schultze[23,24] and Schultze[25] who reported results of some detailed galvanostatic and potentiostatic experiments. They favour a place-exchange mechanism coupled with high-field ionic transport and they detected a true phase up to three oxide layers in thickness. Another group, Conway, Kozlowska, Sharp[26] with Tilak[27], identified[28-33] three anodic current peaks up to monolayer OH coverage (1.1 V RHE) at Pt corresponding to passage of 1 electron per Pt atom. This resolution can only be achieved with very clean solutions, made up from pyrodistilled water[34]. Conway et al[26] also concluded that the resolution of the i - V profile into three distinguishable peaks below the OH monolayer coverage which corresponded to successive stages of occupation of the surface lattice of Pt in three significantly different overlay structures of OH electrodeposited on Pt from H_2O or OH^- depending on pH. Each 2d sublattice has a different structure identified as " Pt_4OH ", " Pt_2OH ", " PtOH " but these are not stoichiometric compounds. The " Pt_4OH " sublattice corresponds to the first peak in the i - V profile O_{A1} (see Fig.1.1) in which only one OH group is electrosorbed per four Pt atoms on the (100) lattice plane. The maximum adsorption charge in that stage is q_o = 55 $\mu C\ cm^{-2}$. The second peak O_{A2} requires an additional 55 $\mu C\ cm^{-2}$ to fill the " Pt_2OH " sublattice. To attain the monolayer stage, a total charge q_o = 220 $\mu C\ cm^{-2}$ is needed. In the broad region beyond 1.1 V E_H ,"PtO" species arise after further oxidation by processes such as:

$$PtOH \longrightarrow PtO + H^+ + e^- \qquad [1.3]$$

$$PtOH \longrightarrow OHPt \qquad [1.4]$$

$$PtO \longrightarrow OPt \qquad [1.5]$$

The important fact that all species adsorbed in the anodic sweep are reduced apparently in one cathodic peak O_c over a less positive range of potentials, no matter how slow the sweep rate is, can be rationalized in terms of formation of an irreversibly formed, rearranged surface phase of lower free energy than that of species progressively deposited in the anodic sweep.

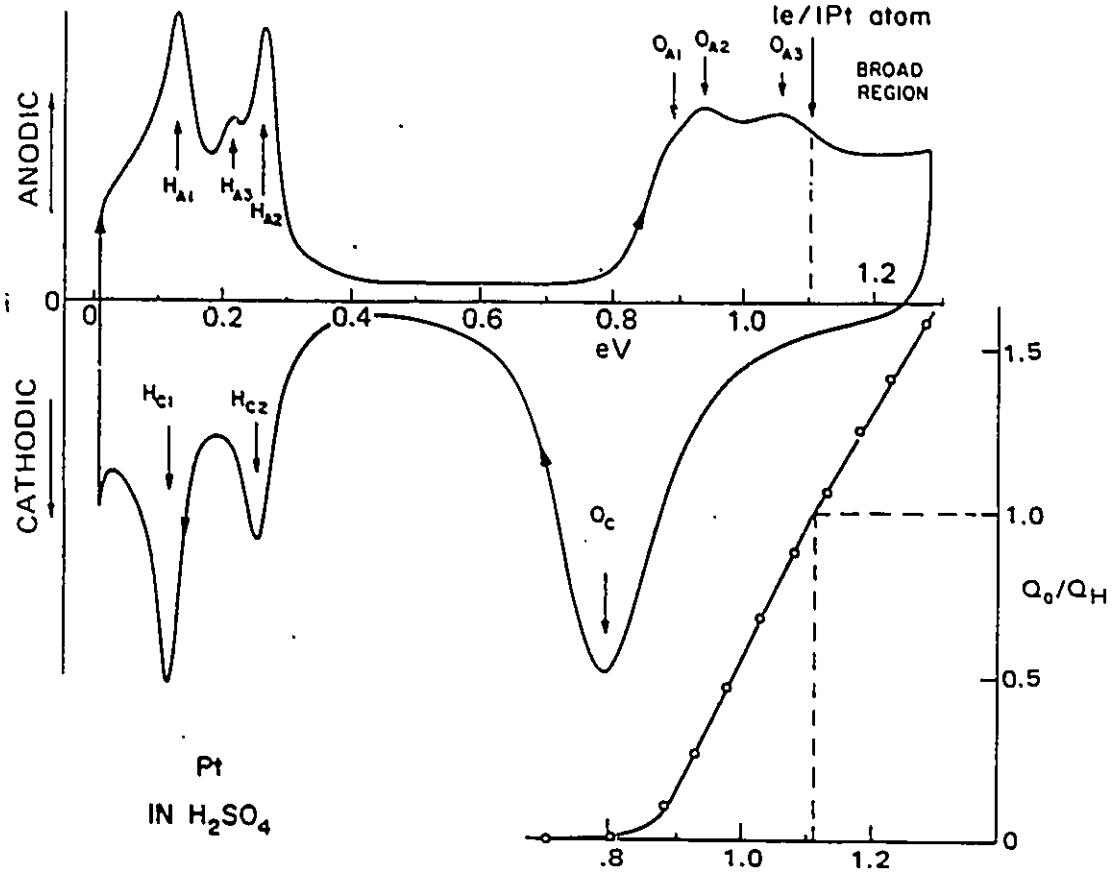

Fig.1.1 Successive stages O_{A1}, O_{A2}, O_{A3}, in Pt surface oxide film formation (ref. 27) corresponding to successively formed OH overlay lattices on Pt. Behaviour depends on geometry and orientation of substrate Pt lattice. Inset : integral relative charge Q_o/Q_H isotherm for surface oxidation as a function of potential.

A rearranged, so-called " phase oxide " film can be more stable than a two - dimensional chemisorbed layer of OH or O species on the Pt surface since lateral repulsions are believed to be smaller or absent. The rearranged states, PtOHPtOH or PtOPtO ... can also be thermodynamically more stable than the 2d Pt-OH surface dipole array . The mechanism can be represented schematically as follows and involves the process of " place-exchange " between chemisorbed OH's and underlying Pt atoms :

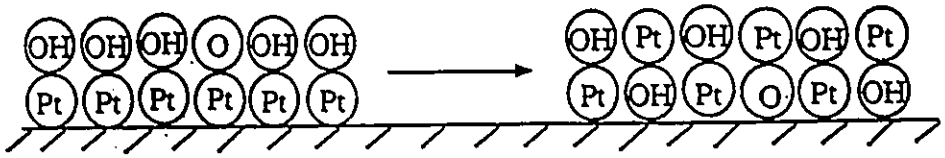

This idea of " place-exchange " originated in the interpretation of the growth of oxide films on Fe by Sato and Cohen[32] and in the treatment of chemisorption of oxygen on metals by Trapnell[35]. The idea was also applied to the problem of anodic surface oxidation of Pt by Reddy, Genshaw, and Bockris[36,37] and by Kozlowska, Conway and Sharp[26] in their interpretation of the irreversibility of Pt surface oxide formation and reduction.

1.3.2.2. Information from Optical and Spectroscopic Methods

In the last decade, electrochemical studies of the formation and reduction of oxide films on noble metals, particularly platinum, have been supported by several complementary non-electrochemical techniques. The earliest optical technique applied to this problem was ellipsometry; other methods such as electrochemical reflectance, Auger, and ESCA spectroscopy have also been used to obtain information on the formation of oxide films, their nature and their properties.

The first report on the application of ellipsometry to the study of oxide formation on platinum were published by Reddy, Genshaw and Bockris[36,37], who calculated from the ellipsometric phase shift Δ and amplitude χ parameters the thickness of the oxide film as a function of potential. However, they failed to detect any change of Δ and χ until a sudden change of optical properties became observable at about 1.0 V RHE. Between 0.8 V and 1.0 V, the Δ and χ did not correlate with the measurable charge q for oxide film formation. Beyond 1.0 V, the optically detectable film grows linearly with increasing potential up to 1.6 V. However, in the later work by Greef[38] and by Conway et al[39,40] using more sensitive instrumentation, it was shown that the very initial stages of oxide film formation also could be detected optically and the Δ , χ and relative reflectivity change does correlate with the oxide formation charge. When a monolayer of OH species is formed at 1.1 V, a discontinuity was observed by Greef[38] between charge,q, and Δ ; hence, the conclusions of Reddy et al[36,37] on the properties of an oxide film above 1.0 V RHE are essentially correct.

1.3.2.3. Growth of the Oxide Film on Platinum

A number of theories of oxide growth on Pt have been presented by Ord and Ho[41], Reddy, Genshaw and Bockris[36,37]; Vetter and Schultze[23,24]; Gilroy and Conway[42]; Gilroy[42,43] and in a series of papers by Damjanovic et al[45-47]. The growth of the oxide film arises because a given coverage of O species at Pt is not a thermodynamically well-defined quantity at any potential as is the coverage by H. Such growth behaviour arises on account of progressive place-exchange which is kinetically controlled and allows more oxygen species to be deposited at a given potential with increasing time, than would correspond to an equilibrium adsorption isotherm for that potential, as for underpotential deposition. Experimentally, the extent of growth of the Pt oxide film at a given potential is logarithmic in time, a relation that has been called the " direct " logarithmic growth law expressed as:

$$Q_t = A \log (t + t_o) \qquad [1.7]$$

where $t >> t_o$ for the main region of logarithmic growth and t_o is an integration constant of the differential kinetic equation for growth. Practically, t_o corresponds to a time of the order of a ms or less, the time required for adjustment of the potential during which some immediate formation of a sub-monolayer of oxide takes place. This type of behaviour was observed by Gilroy and Conway[42] and, in later work, by Gilroy[43,44]. The log growth law applies over 3 to 4 decades of time. However, there appears to be no discontinuity in the film growth kinetics between the growth below monolayer levels and that above, up to thicker films at Pt[47]. Possibly a succession of place-exchange events is involved, as discussed by Sato and Cohen[32] for Fe. For thicker, post-monolayer film growth at base metals such as Ti, Ta, Al and Zn, an " inverse " logarithmic growth law applies having the form $1/Q_t$ vs $\log(V^{-1})$, as described by Mott and Cabrera[48].

1.3.2.4. Ohmic Resistance of the Oxide film on Pt

Consideration has been given to the importance of the conductivity of oxide films in anodic electrode processes. Although only very thin oxide films, several monolayers in thickness[36,37,49-54], can eventually be formed on Pt anodes, their conductivity can somehow change. Thus, it has been found that under conditions of strong anodic polarization, two types of oxide films are, in fact, generated at Pt:

i) a so-called α oxide, PtO, reducible over a broad potential range, is formed only to a limited extent[55,56].

ii) a ß-oxide, PtO_2, is reduced over a narrow potential range which extends into the H deposition region, and is much more negative than that for reduction of the α oxide. This film grows at much slower rate to form a multilayer[57]. The conductivity of these two types oxide has been measured by Shibata[58].

In his experiment, Shibata[58] formed a series of different states of the surface oxide at Pt electrochemically and determined their conductivities in the dry state, ex situ, in a sandwich-like cell between Hg contact electrodes. The oxide films were

formed for various periods of time, 10 sec to 210 min, at 310 K with a current density of 0.2 A cm^{-2}. When t < 4 min, only the PtO α-oxide was formed; this oxide has virtually the same conductivity as Pt until a film, corresponding to a reduction charge over 2100 μC cm^{-2} (approximately five PtO layers) was formed. Beyond the 2100 μC cm^{-2} extent of oxidation, the resistance of the film increased, an effect that was ascribed to the development of the ß-type oxide. The thicker the layer of ß-oxide was, the larger the resistance of the oxide film. The specific conductance of the ß-oxide could not be exactly evaluated as the precise thickness of the ß-oxide was unknown. It might be assumed that the monolayer thickness for the PtO_2 layer is twice as great as that of the PtO layer; the specific conductance of ß-oxide would then be about 1.1-2.1 x 10^{-3} $Ohm^{-1}.cm^{-2}$.

Except at very high anodic current densities for Cl_2 or O_2 evolution or at pre-oxidized electrodes, the less conducting thick ß-oxide film will not normally be formed. Therefore, conduction problems at Pt surface oxide films will not normally be as significant in the kinetics of the above processes under ordinary conditions as they are at metals such as Ti, Zr, Ta, where thick insulating films are normally present when they are used as anodes. However, the oxide film does play a significant role in the kinetic processes involved, e.g. in the anodic Cl_2 evolution reaction, as will be discussed more extensively in later chapters.

1.3.2.5. Conclusions on Oxide Film Growth on Pt

It would be useful to give a summary on surface oxide film formation at Pt. This is conveniently done by means of the scheme shown in Fig.1.2. The oxide film formation involves a transformation associated with place-exchange or reconstruction of the Pt surface as OH or O species are deposited. These processes are of major importance in determining the absorbability of Cl^- and the $Cl^\cdot$ intermediate in the Cl_2 evolution reaction, and the electrocatalytic properties of the external electrode surface for Cl_2 formation or parallel O_2 evolution.

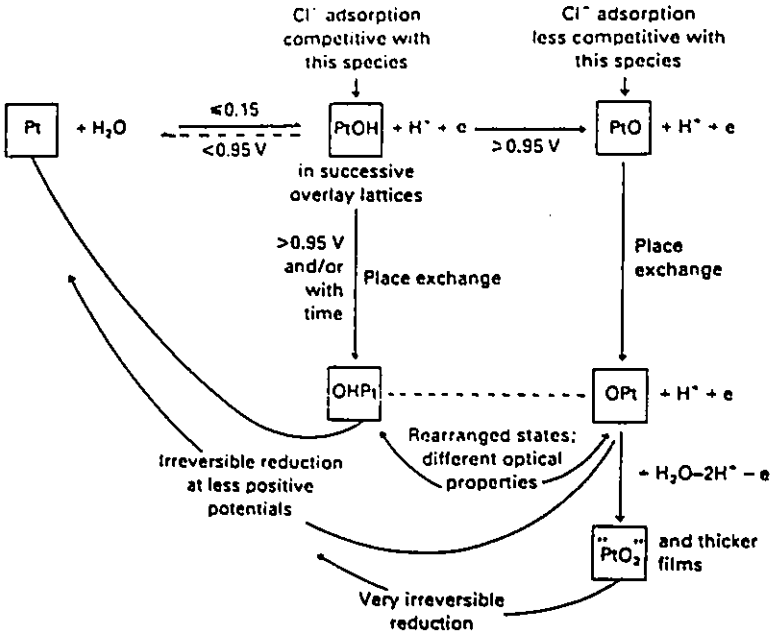

Fig.1.2 Cycle of processes in Pt oxidation and oxide reduction.

1.3.3. Oxide Films on Other Noble Metals(Ru, Ir, Pd, Rh)

1.3.3.1. Ruthenium

There are only relatively few studies on the formation or dissolution of ruthenium oxide. Under anodic polarization in acidic or alkaline solution ruthenium undergoes dissolution, especially at high pH. These processes have been studied by Llopis et al[59,60] and by Gorodetskii et al.[61], Trasatti et al.[4] and Galizzioli et al.[5] have reported on the electrochemical behaviour of chemically prepared RuO_2 which they compared with the behaviour of electrochemically grown RuO_2 on a ruthenium electrode. The cyclic-voltammetric curves for these two kinds of electrodes are presented in Fig.1.3. From the curves they concluded that the formation of RuO_2 on ruthenium occurs at approximately 1.0 V, following the onset of metal surface oxidation at 0.55 V. On ruthenium electrodes, no definite separation between the hydrogen adsorption and the oxide reduction regions is observed, as it is at Pt. Conway et al.[62,63] were able to show more clearly the hydrogen adsorption peaks of electroplated ruthenium and they also detected some absorption of H in Ru. As the potential scan rate increases, the cyclic-voltammetric curve becomes less structured.

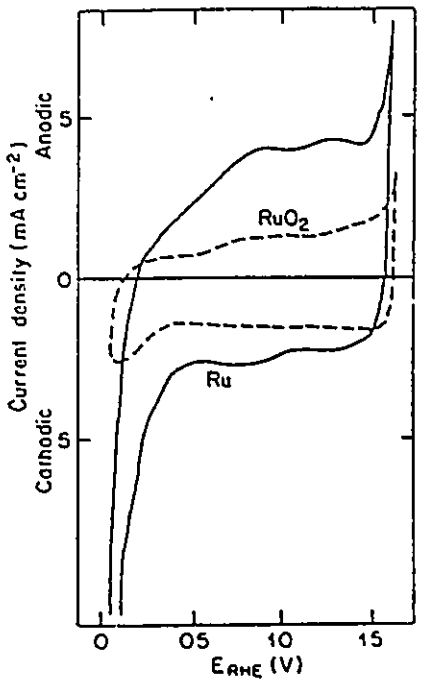

Fig.1.3 Cyclic-voltammograms of a ruthenium electrode and a deposited RuO_2 film

1.3.3.2. Iridium

Ir, with potentiodynamic cycling, shows the characteristics of a reversible oxide film formation reaction. Figure 1.4 depicts the potentiodynamic potential-current relationships in acidic and alkaline media for oxide formation and reduction[64]. These curves are consistent with those reported by other authors[65-69]. The reversible character of oxide formation is illustrated in the instantaneous change of sign of current as the potential scan is changed from the anodic to the cathodic direction. Also, the anodic peak and the corresponding cathodic peaks do not exhibit the pronounced hysteresis characteristic of other noble metals. The reversible character of the oxide formation was also confirmed by optical measurements in work by Conway and Gottesfeld[70].

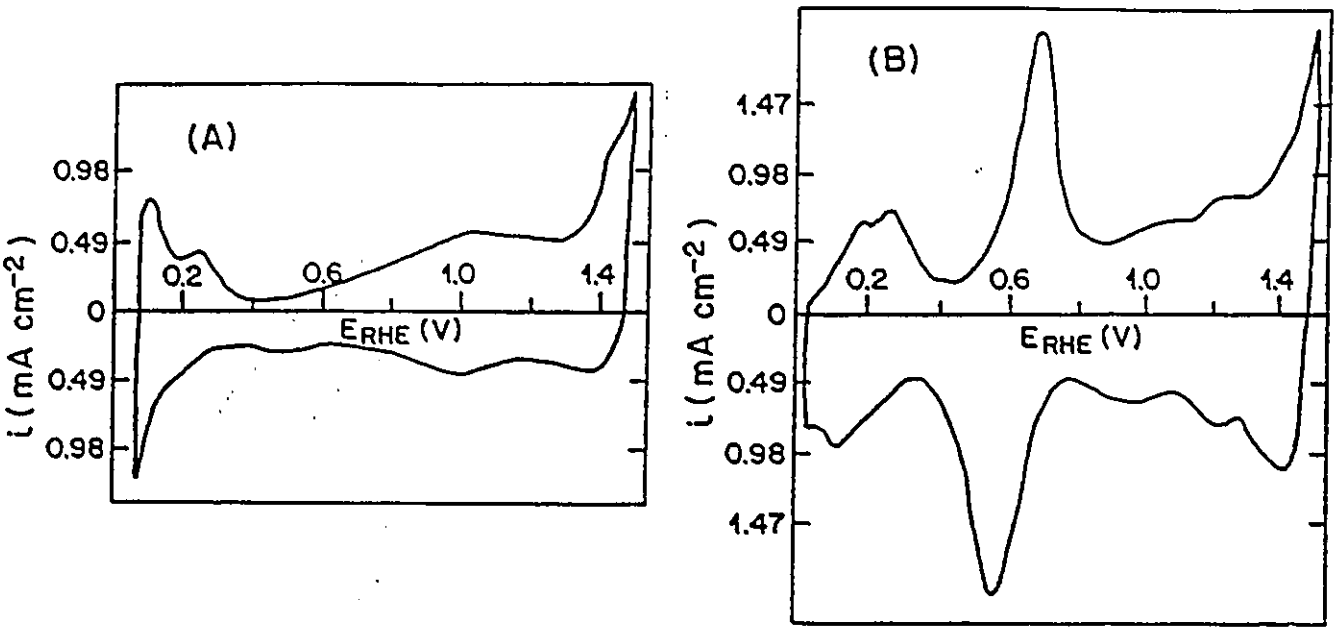

Fig.1.4 Cyclic-voltammograms of an iridium electrode in a) 2.3 M H_2SO_4; b) 0.1 M NaOH at 25°C

The behaviour of iridium on repeated potentiodynamic cycling is unique[71-73]. As the number of cycles increases, the anodic oxide formation current, as well as its reduction current, increase continuously. This effect is not due to a surface roughening since the hydrogen adsorption and oxidation peaks are not modified to such an extent[72,73]. This can be explained by assuming a pit oxidation model where the oxide is formed preferentially in pits or crevices of the iridium electrode. The mechanism for oxide formation on this metal, taking into account the pit model, was proposed[71] as follows: the oxide is formed in pits below 1.2 V but they become full of oxide at 1.2 V. Above this potential, the underlying metal layer is further attacked and penetration becomes important.

1.3.3.3. Palladium

In the case of palladium, the review paper by Hoare[74] shall be mentioned. There is evidence from the charging curves[75,76] that two types of oxides are formed at palladium, namely PdO and PdO_2, as at Pt. The cyclic- voltammetric curve is similar to those for other noble metals such as Pt, Rh and Au in that hysteresis is observed between the oxide formation and reduction processes.

Palladium behaves like gold in this respect; a small limiting oxide coverage is attained in the potential range of 1.5 to 1.7 V, and beyond this potential, the oxide coverage increases, and also a roughening and colouring of the surface occurs. The stoichiometry of the oxide formed at potentials about 1.5 V is concluded to be one oxygen atom per palladium atom, i.e., corresponding nominally to a PdO species.

1.3.3.4. Rhodium

Shibata[77] examined oxide film formation and reduction on rhodium electrodes by means of galvanostatic transients. At constant current, a linear increase of potential with time from 0.6 V (versus SHE) to almost 1.6 V (versus SHE) was observed. In another paper, Khrushcheva et al.[78] studied the time effect in cyclic-voltammetric oxide formation and reduction. They found in acidic media when the potential was held at 1.0 V, the peak for reduction of the oxide film is shifted by a few mV in the cathodic direction. However, if the anodic potential is 1.4 V , the charge in the reduction peak increases as the polarization time is made longer and the cathodic shifts becomes much more significant, as also found at Pt or Au. From these results and similar ones obtained in alkaline solutions, Khrushcheva et al. concluded that there were two types of oxides on the rhodium surface, the more stable one arising from oxidation at 1.4 V. The first state is interpreted as chemisorbed oxygen of the type " RhO ". As the potential increases, the oxide Rh_2O_3 begins to be formed. However, for very thin films, the significance of such bulk stoichiometries becomes indefinite.

1.4. Chloride Ion Adsorption and its Effects on Oxide Film Formation at Noble Metal Anodes (Pt, Ru, Ir)

In anodic Cl_2 evolution, the reacting ion, Cl^-, is not simply the initial reactant in the overall process but it also modifies the state of the anode surface on which it is discharged. On any bare metal sites, for instance at Pt, Cl^- is normally chemisorbed. This leads [79-82] to a strong inhibition of the formation of a monolayer surface oxide, especially at Pt and Rh, that would usually be completed at potentials less positive than those required for Cl_2 evolution. Thus, Cl^- adsorption changes the properties of the electrode surface on which the reaction of Cl_2 evolution occurs. In addition, Cl^- adsorption will tend to increase with increasing positive potentials of the electrode and maintain competitive adsorption with respect to electrodeposition of the monolayer or multilayer surface oxides.

1.4.1. Cl^- Adsorption on Pt and Its Blocking Effect on Oxide Film Formation

The first quantitative studies of Cl^- ion adsorption at noble metal electrodes were made by Breiter[79] and later by Bagotskii et al.[82]. Conway and Novak[80,81] investigated the effects of the Cl^- ion, over a wide range of concentrations, on the blocking of the electrodeposited surface oxide at Pt in relation to the kinetics of anodic Cl_2 evolution. The quantity of surface oxide generated at Pt electrodes up to potentials at which Cl_2 evolution commences significantly, decreases to about 10% of a monolayer as the Cl^- concentration is increased to about 1.0 M.

Two effects are involved: firstly, increasing Cl^- ion concentration progressively diminishes the extent of surface oxidation attained at Pt at a given potential >0.8 V E_H. In fact, a selective effect is involved, the more reversible states, "Pt_4OH" up to "PtOH", of the surface oxide being preferentially blocked by Cl^-. For the initial rise of the extent of surface oxide blocked by adsorbed Cl^- with increasing log[Cl^-], a linear logarithmic relation for Cl^- ion blocking of surface oxidation of Pt is observed over four decades of Cl^- concentration. Secondly, as Cl^- concentration increases, the reversible

potential for Cl_2-Cl^- becomes less positive, so that significant Cl_2 evolution rates tend to arise at potentials for which less surface oxide would have been generated.

The indication of the role of the adsorbed Cl^- ion and its effect on the oxidation isotherm of Pt is obviously important for the understanding of Cl_2 evolution kinetics.

1.4.2. Oxide Film Growth in the Presence of Cl^- Ion

Recent experiments by Conway and Mozata[83], and Conway and Roscoe[84] showed that oxide film growth in the presence of Cl^- on Pt also obeys the so-called direct logarithmic law (q_t = A log $(t+t_o)$). Practically, the A is smaller compared with that for growth in aq. H_2SO_4 solution alone; this is due to the blocking effect of the adsorbed Cl^- ion. One interesting point is that the linear logarithmic relations pass again through the charge value for monolayer coverage by OH species (210 $\mu C\ cm^{-2}$) without any change of slope. This implies that there is no discontinuity in the process of oxide film growth or involvement of Cl^- as the monolayer of OH is completed and further extended in thickness with time or high potential.

The lack of discontinuity in the growth curves through " $\theta = 1$ " arises presumably because there is a continuous and progressive place-exchange reconstruction process taking place with increasing OH- or O- to -Pt ratio as potential and/or time is increasing. Unlike underpotential deposition processes, the process of place-exchange in surface oxidation is not limited by θ_{OH} or θ_O becoming 1.

1.4.3. Cl^- Ion Adsorption at Ir and Ru

Since the surface oxidation for Ir and Ru metals begins at lower potentials than at Pt, viz. 0.2 - 0.3 V R.H.E., the oxide blocking effects by Cl^- ion are much less sensitive with respect to $[Cl^-]$ compared with those at Pt. Usually, appreciable concentrations of Cl^- are required before the region of initial surface oxidation at the above mentioned metals is displaced to more positive potentials; for instance, in the case of Ru, a 5 M NaCl solution required to produces a small but significant shift in the onset of surface

oxidation, revealing then a " double-layer charging " region in the cyclic-voltammetry i-V profile.

1.5. Previous Work on the Study of the Mechanism of the Cl_2 Evolution Reaction

1.5.1. Possible Mechanisms

The anodic Cl_2 evolution reaction is formally one of the simplest gas evolution reactions like that for H_2, cathodically. Also, the reactant ion Cl^- can be much more strongly chemisorbed under certain conditions than H_3O^+, especially at noble metal surfaces, as indicated above. Normally, there are three commonly accepted mechanisms that have been proposed by various workers, which are as follows.

Mechanism I is the so-called " Volmer-Tafel " pathway illustrated by:

$$Cl^- + M \rightleftharpoons MCl^-_{ads} + e \qquad [I]$$

$$2MCl^-_{ads} \longrightarrow 2M + Cl_2 \uparrow \qquad [II]$$

where Cl^- is discharged on the surface of the electrode, followed by a chemical catalyzed recombination reaction. This kind of mechanism appears to apply at Pt electrodes, as reported by Conway and Novak[85,86].

Mechanism II is the so-called " Volmer-Heyrovsky " pathway with the same first step as that in mechanism I but followed by a electrochemical discharge step instead, involving desorption of chemisorbed Cl^-, as represented by:

$$Cl^- + M \rightleftharpoons MCl^-_{ads} + e \qquad [I]$$

$$MCl^-_{ads} + Cl^- \longrightarrow M + Cl_2 \uparrow + e \qquad [III]$$

A different kind of process was suggested by Krishtalik et al[87,88], based on the possibility of formation of the chloronium ion, Cl^+, as represented by:

$$Cl^- + M \longrightarrow MCl^-_{ads} + e \qquad [I]$$

$$MCl^-_{ads} \longrightarrow MCl^+_{ads} + e \qquad [IV]$$

$$MCl^+_{ads} + Cl^- \longrightarrow M + Cl_2 \uparrow \qquad [V]$$

Since the chloronium ion is unlikely exist under normal aqueous electrochemical conditions, the author later suggested OCl^- as the intermediate instead of Cl^+, because

it is a more stable species.

The interpretation of experimental kinetic data for anodic Cl_2 evolution is more complicated because the following factors that must be taken into account :

(a) the presence of oxide films;

(b) their changing catalytic properties with potential, time and extent of coverage;

(c) the adsorption of Cl^- ions and their possible incorporation in the growing oxide film and their competition with the film's formation;

(d) some dissolution of the oxide film or substrate metal.

1.5.2. Consideration of Oxide Film and Cl^- Ion adsorption in the Cl_2 Evolution Reaction

As is well known, the oxide film surface at an anode plays a major role in the kinetics and mechanisms of continuous faradaic anodic electrochemical reactions such as Cl_2 evolution, either by modifying the energy of adsorption of reactants or intermediates on the surface, and/or by changing the catalytic activity of the surface. In some cases, as the oxide film is completed or becomes thicker, a parallel reaction on the oxide-covered areas of the surface can continue but at a different rate and even over a different potential range from that over which it proceeded previously on the "bare" metal. The adsorptive and electrocatalytic properties of an oxide-modified surface of a metal are commonly quite different from those of the free metal itself and the mechanism of the parallel component of the reaction may be different.

Below are listed some of the principal effects of the oxide film on the Cl_2 evolution reaction:

(a) The oxide film blocks initially free metal surface sites on which the Cl_2 reaction may take place, e.g., passivation or inhibition effects[89,90] can arise, and a change of electrocatalytic properties occur (see below).

(b) Once the oxide film has been formed, it usually has different electrocatalytic properties for the parallel reaction from free metal surface. Therefore, the reaction

rates and even the mechanism can vary.[91-93]

(c) Oxide films may, in same cases, be relatively nonconducting and lead to a so-called [94-96] " demetallization " of the surface, e.g. at Ti, Ta, etc.

(d) Also, if a change in the oxidation state of the metal ions in the oxide film occurs with increasing potential or growth of the film, the electrocatalytic properties may vary, especially at transition-metal anode materials, including the noble metals. Also, the conductivity of the oxide film usually changes under such conditions.

(e) The Cl^- ion is initially chemisorbed and blocks irreversibly the initial "PtOH" stage of surface oxidation (at Pt).

1.5.3. Electrocatalytic Properties of the Oxide Film in the Cl_2 Evolution Reaction

1.5.3.1. Electrocatalytic Behaviours

Conway and Novak[85,86] investigated Cl_2 evolution kinetics in anhydrous CF_3COOH containing RbCl as electrolyte and comparatively in CF_3COOH-H_2O mixtures of up to 100% H_2O. In order to evaluate the role of the presence of the oxide film at Pt in aqueous solution vis a vis its absence in the anhydrous CF_3COOH medium. They also compared a bare, oxide-free Pt surface in TFA with that for a pre-formed oxide surface, and found that the current densities on the pre-oxidized Pt surface are about 40 times larger than those on the oxide-free metal surface. In the CF_3COOH-H_2O mixture experiments, the authors were able to control the water percentage so that the oxide film coverage could be varied and determined in separate cyclic-voltammetry experiments. Form their results, a recombination rate constant, k, vs composition of H_2O in TFA plot was derived, from which it was quite clear that k increases with increasing percentage of water, corresponding to increasing extents of oxide film formation of the Pt electrode.

In more recent experiments, Conway and Roscoe[84] were able to illustrate so-called "Volcano" behaviour in the electrocatalysis of anodic Cl_2 evolution. The Pt electrode was polarized anodically first in aqueous H_2SO_4; hence a certain amount of

oxide film could be controllably formed and its reduction charge determined in a cathodic linear sweep. In this way, a series of different extents of oxide film formation could be established on the Pt electrodes, The polarization behaviour of the anodic Cl_2 evolution was then evaluated for each degree of oxide film formation. From these results, the authors concluded that an interesting electrocatalytic effect arises, depending on the state of oxidation of the Pt surface on which the Cl_2 reaction proceeds. A clear " Volcano " plot was demonstrated between the recombination rate constant, k, and the extent of prior surface oxidation of Pt, as measured by the reduction charge Q. An optimum surface oxidation state, corresponding to an oxide film reduction charge of ca. 500 $\mu C\ cm^{-2}$, gave maximum values of k. The oxidation state corresponds to a degree of oxidation of ca. 2.5 e^- per Pt atom which implies that the oxide film is about one layer of O or 2 layers of OH species with a further over layer of half-coverage by OH species.

1.5.3.2. Electronic Effects

Arikado et al[97,98] studied the mechanism of Cl_2 evolution with a series of electrocatalysts aiming to find the relationship between the Cl_2 evolution mechanism and the catalytic activities of the oxide electrodes by taking into account the electronic structures of the oxides. They reached the conclusion that if the oxide surface of the electrode contains a transition metal cation with partially filled t_{2g} levels and empty e_g levels, such as RuO_2 or IrO_2, the Volmer-Heyrovsky mechanism (I-III) could apply. However, if the electrode surface contains a transition metal cation with half or just filled t_{2g} and partially filled e_g levels, such as TiO_2-PtO_2, it was suggested that the Volmer-Tafel mechanism (I-II) applied[99].

Fig.1.5 shows how the state of adsorbed Cl atoms at a Ru cation site in two types of electrode surface preparation may determine whether the " Volmer-Tafel " or the " Volmer-Heyrovsky " type of mechanism determine the kinetics, as well as the Tafel slope. As a summary, Table 1.1 shows various anode electrocatalysts in relation

to the d-electron configuration.

Table 1.1 Summary of the Reaction Mechanism and i_o Values for Cl_2 Evolution as Function of d-Electron Configuration at Various Electrocatalysts.

Electrode	Tafel slope	R. D. S. Mechanism	*d*-Electron configuration	$i_0(A/100\ \mu F)$
RuO_2	$2RT/3F$	II	$(t_{2g})^4$	0.118
IrO_2	$2RT/3F$	II	$(t_{2g})^5$	0.390
$Eu_{0.1}WO_3$	$2RT/3F$	II	d^0 or $(t_{2g})^1$	0.019
Graphite	$2RT/3F$	II	—	—
$Pt-MnO_2$	$RT/2F$	I	$(e_g)^1$	0.410
$Ti-PtO_2$	$RT/2F$	I	$(e_g)^x$	0.550
$La_{0.6}Sr_{0.4}CoO_3$	$RT/2F$	I	$(e_g)^{0.4}$	0.433
$LaNiO_3$	$RT/2F$	I	$(e_g)^1$	0.144

i_0 expressed as mA/100 μF of double-layer capacitance, hence real area. Mechanisms I and II were defined earlier in this chapter. From Arikado, *et al.*

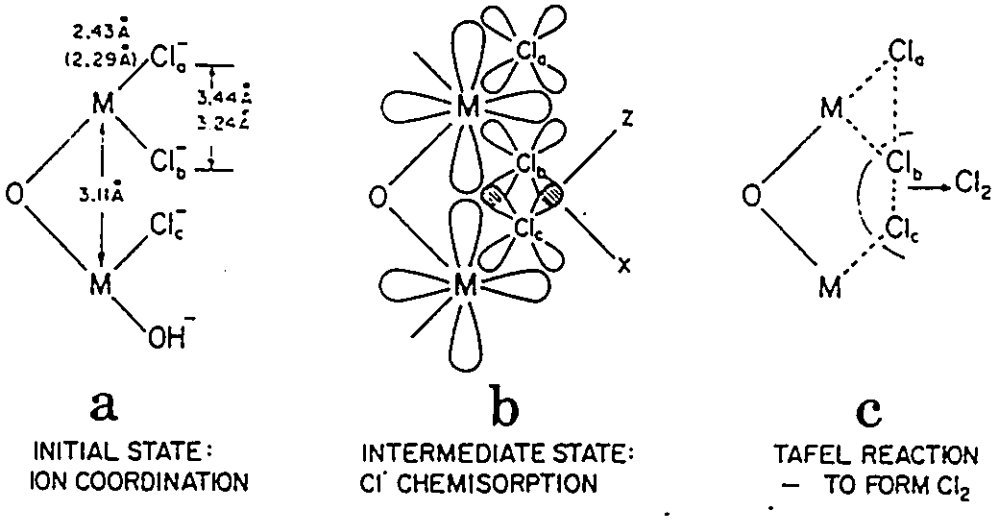

Fig.1.5 Cl$^-$ coordination at Ru(III) providing active site in Cl_2 evolution electrocatalysis, according to Arikado et al.

Fig.1.6 illustrates a plot of the d-band vacancy against quantity of electricity consumed in the reduction of the oxide layer formed under Cl_2 evolution conditions; this result shows that the coverage of the oxide on the electrode surface can be linearly related to d-band vacancy. However, the coverage by the oxide is considered to be a function of electrode potential, pH, and concentration of Cl^-; thus, when all these conditions are constant, a linear function of the d-band vacancy can be observed. This relation suggests that unpaired d-electrons participate in the bonding, even when specifically adsorbed Cl^- is replaced by oxygen atoms at high anodic potentials.

The relationship between current-density, electrode potential and d-band vacancy can be considered with respect to coverage by the oxide film. Other plots by Arikado et al. [97,98] show the rates of Cl_2 evolution at various potentials against the d-band vacancy of some alloys (see Fig.1.7) and an attempt to relate the exchange current-density for Cl_2 evolution to the metal-to-Cl bond energy (see Fig.1.8).

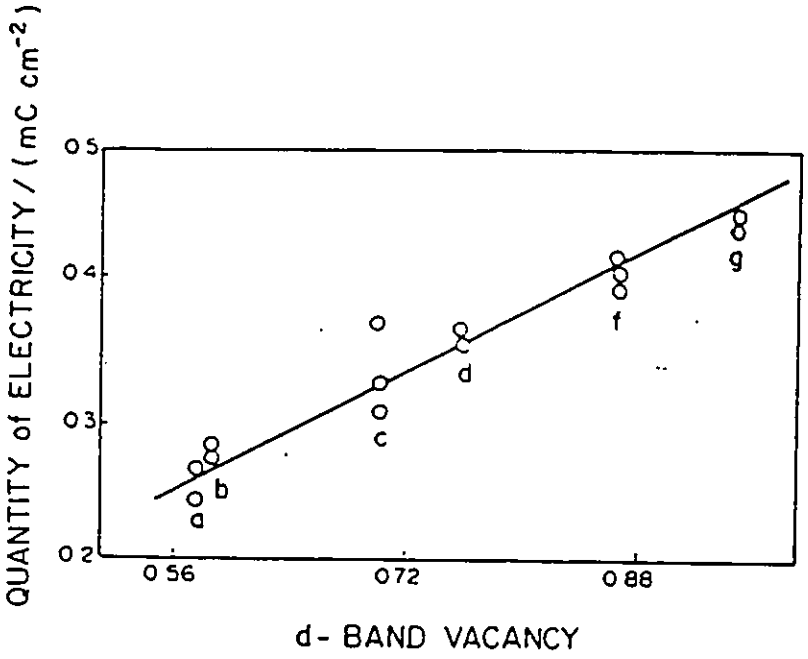

Fig.1.6 Relation of extent of oxide film formation at several metals, under Cl_2 evolution conditions, (measured as oxide reduction charge) to the d-band vacancy. a) Pt; b) Pt-Ir 10.1%; c) Pt-Ir 15.2%; d) Pt-Ru 17.6%; e) Pt-Pd 17%; f) Pt-Pd 24%; g) Pt-Rh 32.4%.(Times of formation of these oxide film are not recorded in the original papaers;98,99).

The latter quantity is based on allotments of the chlorine bond energy for pure metals in proportion with the atomic percentages of their respective alloys. Since, however, the Cl_2 evolution reaction always occurs in aqueous solution on an electrode surface completely or partially covered by an oxide film, the attempts to correlate i_o values simply with the metal-Cl^- bond strength, $\Delta H_{M\text{-}Cl}$ are highly questionable. However, a better approach used by Arikado et al. was to utilize MO-Cl bond strengths instead M-Cl's.

Both $\Delta H_{MO\text{-}Cl}$ and ΔH_{MCl} can be calculated by means of the Pauling formula:

$$\Delta H_{M\text{-}Cl} = 1/2(D_{M\text{-}M} + D_{Cl\text{-}Cl}) + 23.06(X_M - X_{Cl})^2 \qquad [1.8]$$

where $D_{M\text{-}M}$ and $D_{Cl\text{-}Cl}$ refer to the dissociation energies of the metal lattice and of Cl_2, respectively, and the X's to the corresponding electronegativities; and:

$$X_{M_yO_z} = (yX_M + zX_O)/(y+z) \qquad [1.9]$$

It is unfortunate that substrate-Cl^- interactions are very complicated when an oxide film is present and thus there remain a number of matters that have not yet been clarified.

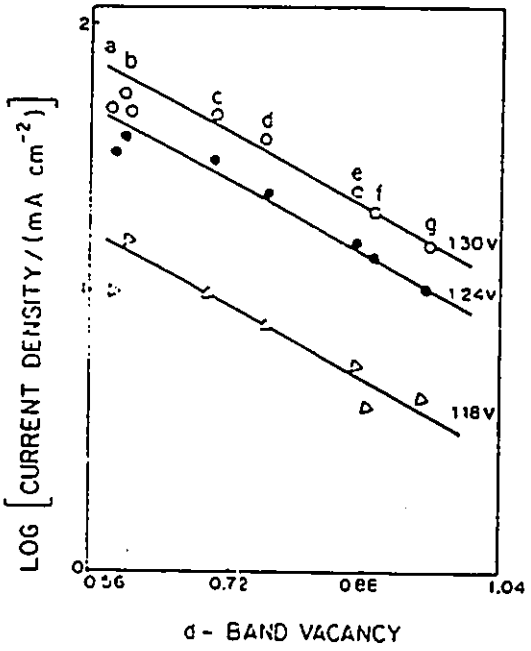

Fig.1.7 Rate of Cl_2 evolution at various alloy metal surfaces at three potentials in relation to d-band vacancy. a) Pt-Pd 24%; b) Pt; c) Pt-Ir 10.1%; d) Pt-Ir 15.2%; e) Pt-Ir 25.3%; f) Pt-Ru 17.6%; g) Pt-Rh 32.4% (ref.98,99).

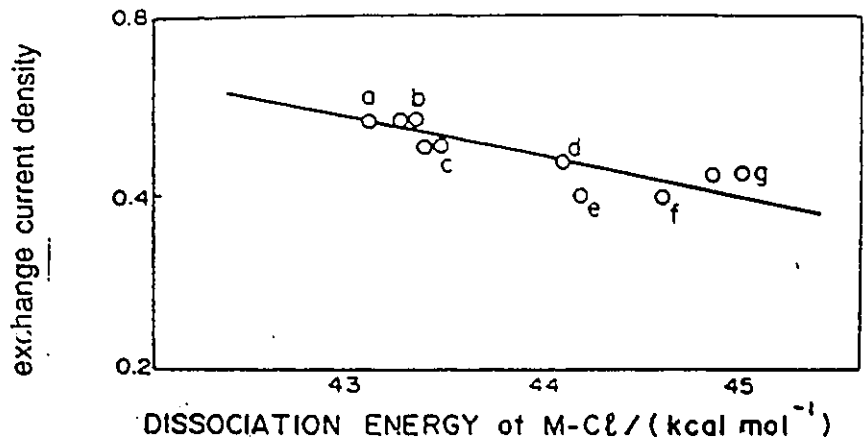

Fig.1.8 Relation between exchange current density for Cl_2 evolution from aq. Cl^- at various metal anodes and the metal-to-Cl bond energy as evaluated from data for corresponding metal chlorides. a) Pt; b) Pt-Ir 10.1%; c) Pt-Ir 15.2%; d) Pt-Ru 17.6%; e) Pt-Pd 17%; f) Pt-Pd 24%; g) Pt-Rh 32.4% (ref.98,99).

1.6. Dimensionally Stable Anode Electrodes

In the early days of chlorine production, graphite was used as the anode. However, these anodes have inherent problems which include high Cl_2 overpotential, a consequently large electrical energy consumption and dimensional instability by gradual oxidation of C to CO_2. However, the advent of noble metal oxide coatings on a titanium substrate, i.e. so-called " dimensionally stable anodes " (DSA), has revolutionized the whole chlorine production industry. The most widely used anodes are RuO_2/TiO_2 coated on Ti which diminished power consumption and operational costs and accelerated the Chlor-Alkali industry in the mid-1970s.

The $RuO_2 + TiO_2$ solid solution coating is formed by thermal decomposition of Ru and Ti salts applied to the Ti substrate and baked at about 450° C in air to obtain the mixed oxides of Ru and Ti. The original Beer-type anode is believed to contain a Ru/Ti mole ratio of 1/2, whereas a three component coating developed by O'Learg[11] consists of a metal mole ratio of 3Ru : 2Sn : 11Ti.

DSA electrodes exhibit low chlorine overvoltage and long life time, usually greater than 5 years. Their performance characteristics depend on the composition of the coating and the method of preparation. The latter is important since one of the failure

mechanisms of these coatings is via the formation of a nonconducting TiO_2 layer at the interface of the Ti with the applied catalytic RuO_2 coating.

Various attempts to understand the excellent electrocatalytic characteristics of RuO_2-based coated electrodes have been made in recent years[101-102]. In this thesis, an investigation of Cl_2 evolution on RuO_2-TiO_2 electrodes forms part of the research reported and discussed in later chapters. The study includes: the kinetic process of Cl_2 evolution on RuO_2, the behaviour of the Cl· intermediate and the reaction mechanisms in relation especially to new data on the adsorption of the Cl· species.

CHAPTER II

The Principles of Electrochemical Kinetics of Processes Involving Adsorbed Intermediates

2.1. General Kinetic Aspects of Electrode Processes

The major differences between electrode reactions and regular redox reactions in solution are that electrode reactions are heterogeneous processes and the overall reaction can be treated in terms of two half-cell reactions, one a cathodic process and the other anodic. As they are heterogeneous, their rates are affected by some or all of the following factors :

(i) the surface concentration of reactant ions adsorbed at the interface;

(ii) the activation energy for the heterogeneous reaction at the surface, which depends on the electrochemical nature of the reactants, and the catalytic and adsorptive properties of the surface;

(iii) the extents of surface coverage by adsorbed intermediates and/or reaction products;

(iv) the metal or metal-oxide/solution potential difference at the interface, which controls the rate of the charge-transfer reaction.

The last factor is the principal one that distinguishes electrochemical reactions from other heterogeneously catalyzed reactions at solid-solution interfaces. Also, the potential normally influences the surface coverage by the intermediates.

The rates of electrochemical reactions are usually expressed in terms of product moles cm^{-2} sec^{-1} but it is more convenient to express the latter units in terms of the equivalent current passing, provided the current-efficiency is known or is simply 100 %. If the overall reaction involves the passage of zF coulombs $mole^{-1}$ of products cm^{-2}, the electrochemical rate, v, in terms of current can be simply described by zFv Amp

cm^{-2}. With respect to the usual way of representing a reaction velocity, that of an electrochemical process will be given as:

$$i = zFv$$
$$= nF\{(\tau kT/h)\exp[-\Delta\overline{G}^{o\ddagger}/RT]\}(C_R)_s(1-\theta) \quad [2.1]$$

where the rate constant is equal to:

$$\overline{k}_r = (\tau kT/h)\exp(-\Delta\overline{G}^{o\ddagger}/RT) \quad [2.2]$$

according to absolute rate theory[103] where τ is the transmission coefficient, taken as approximately equal to unity[103], k, T and h are well known constants and $\Delta\overline{G}^{o\ddagger}$ is an electrochemical standard Gibbs energy of activation analogous to a chemical Gibbs energy of activation, $\Delta G^{o\ddagger}$, for an ordinary chemical reaction but dependent on potential according to :

$$\Delta\overline{G}^{o\ddagger} = \Delta G^{o\ddagger} - \beta F(\Delta\phi_r + V) \quad [2.3]$$

In the second term on the right hand side of the eqn.[2.3], is an electrical energy factor consisting of the metal-solution potential difference, $\Delta\phi$, at the electrode interface given by the sum of $\Delta\phi_r$, the absolute metal-solution potential difference when the system is at equilibrium, plus an overpotential, V, corresponding to the electrical energy required to drive the reaction at a net current density i. β is a barrier symmetry factor analogous to Brønsted's factor α in his linear free energy relationship since it represents the fraction of the electrical free energy provided to the system which changes its Gibbs energy of activation. It is widely accepted that the symmetry factor β is close to one half for a more or less symmetrical energy barrier, and this value will be assumed in the subsequent discussion.

For a single electron transfer reaction, eqn.[2.1] can be expressed by:

$$i = (\tau kT/h)\exp(-\Delta G^{o\ddagger}/RT)F(C_R)_s(1-\theta)\exp[\beta F(\Delta\phi_r+V)/RT]$$
$$= Fk^\circ_s\,(C_R)_s(1-\theta)\exp[\beta F(\Delta\phi_r + V)/RT] \quad [2.3]$$

where:

$$k^\circ_s = (\tau kT/h)\exp(-\Delta G^{o\ddagger}) \quad [2.4]$$

and θ is the fractional coverage of the electrode surface by the discharged adsorbed

intermediate processed in eqn.[2.1], the quality k°_a is the specific rate constant for the anodic reaction under zero potential difference conditions. The net anodic current density measured is the difference between the partial currents in the anodic (i_a) and cathodic (i_c) directions, which leads to a form of the Butler-Volmer equation. i_a and i_c are comparable in magnitude only at, or near $\Delta\phi_r$. Since, generally,

$$i = i_a - i_c$$

$$= i_o\{\exp(\beta FV/RT)-\exp[-(1-\beta)FV/RT]\} \qquad [2.5]$$

where i_o is the so-called exchange-current density at overpotential, V, equal to zero, and can be written as :

$$i_o = Fk^\circ_a C_i(1-\theta)\exp(\beta F\Delta\phi_r/RT)$$

$$= Fk^\circ_c C_i\theta\exp[-(1-\beta)F\Delta\phi_r/RT] \qquad [2.6]$$

Two limiting cases of eqn.[2.5] are of special interest. At high values of overpotential, where $(\beta FV/RT) >> 1$, the second term on the right hand side of eqn.[2.5] becomes negligible with respect to the first term so that :

$$i = i_o\exp(\beta FV/RT) \qquad [2.7]$$

or $$V = (RT/\beta F)\ln i - (RT/\beta F)\ln i_o \qquad [2.8]$$

This is the well known Tafel equation ($V = a - b \log i$) proposed by Tafel in 1905, where b, the Tafel slope,is equal to $2.303RT/\beta F$.

The other limiting case corresponds to the system being very close to equilibrium. Then, at low values of overpotential for which $|\beta FV/RT| \leq 0.1$ eqn.[2.5] takes a linear form upon expansion of the exponents, taking the first two terms ; thus

$$i = (i_o F/RT)V \qquad [2.9]$$

This enables a Faradaic resistance R_f to be defined as $R_f = dV/di = RT/i_oF$. This may be regarded as an "Ohmic region" of the kinetic behaviour where a linear relationship between the applied potential and current density is maintained to a good approximation. Equation [2.9] is important in the analysis of the frequency response of electrode processes under low amplitude potential modulation (see chapter IV and V) in impedance spectroscopy studies of electrode reactions.

2.2. Adsorbed Intermediates in Consecutive and Alternative processes[104]

As is well known, most electrochemical reactions except one-electron ionic redox processes, proceed by at least two consecutive steps, and in some cases alternative pathways may be involved. In consecutive reactions, it is always the step with the smaller(est) rate constant, sometimes referred to incorrectly as the " slow " step, that is rate-determining. In alternative pathways, it is the pathway that proceeds with the greater(est) velocity that characterises its kinetics. Since the electrochemical rate constants of various steps depend on potential, a step which is rate-controlling at one potential may not be the kinetically limiting step at another potential. For two consecutive steps, I and II, with Tafel slopes b_1 and b_2 ($b_2 > b_1$), the current-potential plot will be as illustrated in Fig.2.1a where, at high potentials, process II with the smaller electrochemical rate constant and larger Tafel slope, is rate-controlling, while, at lower potentials, step I is rate-controlling. This change of rate-controlling mechanism arises because the electrochemical rate constant of process I, in this example, changes more rapidly with potential, by the factor $\exp(V/b_1)$, than does process II, which can change only by the factor $\exp(V/b_2)$. Therefore, for a given change of overpotential, V, a smaller change in the electrochemical rate constant will arise for process II than for I for the same change in V, b_2 being supposedly greater than b_1. Conversely, for alternative processes I and II , the faster characterises the kinetics and the current-potential relation will be as shown in Fig.2.1b. At a critical potential, the two processes will have comparable rates, and a smooth inflection will arise in the ln(i) vs. V curve.

2.3. A Multistep Process Model of the Cl_2 Evolution Reaction

The chlorine evolution reaction is apparently one of the simplest gas evolution reactions, formally like the hydrogen evolution process except that it is an anodic reaction. Its mechanisms have been considered in a number of earlier papers[85,86,105-107]; the most simple and commonly accepted ones are the so-called

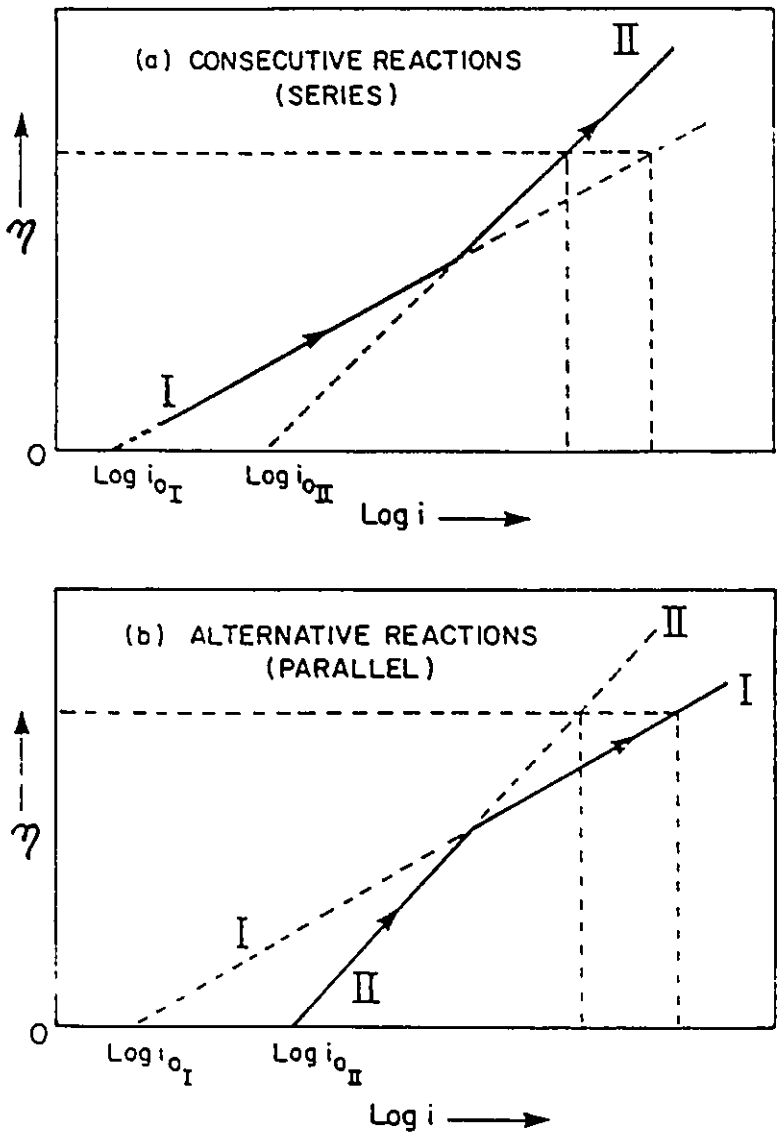

Fig.2.1 Examples of Tafel relations for overpotential, V, as a function of log[current-density, i] for a) consecutive or b) parallel reaction pathways, designated I and II for a reaction.

"Volmer-Tafel" and "Volmer-Heyrovsky" pathways, as indicated in Chapter I. However, a mechanism combining the both has been considered in later treatments, as given below :

$$M + Cl^- \rightleftharpoons MCl^- + e \qquad [I]$$

$$MCl^- + Cl^- \dashrightarrow M + Cl_2 \uparrow + e \qquad [II]$$

or $$2MCl^- \dashrightarrow 2M + Cl_2 \uparrow \qquad [III]$$

Since steps [I] with [II] or with [III] are alternative pathways, the faster step will characterize the kinetics, contributing the major current. When the step [II] is much slower than step [III], the pathway is a "Volmer-Tafel" one while, on the other hand, if step [II] is much faster than step [III], that is the "Volmer-Heyrovsky" pathway. Step [III] is also called the chemical recombination step, and leads to a limiting current density at a higher V, since this step is independent of potential except indirectly on account of the dependence of θ_{Cl} on V.

2.4 Methods of Kinetic Treatment

The adsorption behaviour of kinetically-involved species in an electrode reaction may be examined in terms of the either of two approaches.: (1) the quasi-equilibrium hypothesis, in which it is supposed that all steps prior to the rate-determining one in the reaction sequence are almost at equilibrium, i.e. the rate constant of the rate-determining step is at the least ten times smaller than those of all the antecedent steps in both directions; or (2) the steady-state method in which the rate of change of concentration of the intermediates with time is equal to zero. The steady-state method is, in general, to be preferred but usually leads, for some mechanisms such as I with III, to cumbersome expressions thus numerical computing is required in order to derive the theoretically predicted behaviour.

2.4.1. Quasi-Equilibrium Approach with the Assumption of the Langmuir Isotherm

The Langmuir isotherm is the simplest expression for representing adsorption as

described in 1916 by Irving Langmuir[108]. The basic assumptions involved are: (a) a fixed-side adsorption, which implies immobility of the adsorbate; (b) the absence of lateral interactions or heterogeneity of the surface, i.e. a Gibbs energy of adsorption that is independent of coverage, θ; and (c) the equilibrium between the interphase or surface and the bulk phase for adsorption up to a monolayer (θ = 1).

For now we will only consider the case for which step [II] is less significant than step [III], i.e. the "Volmer-Tafel" case, since the recombination pathway seems to apply (see chapter V and refs. 85,86) to the real mechanism for Cl_2 evolution on Pt and some other noble metals. A further discussion will be introduced in the next section using the steady-state approach.

The rate equations for the discharge step (I) and its reverse for Cl_2 evolution are given by:

$$i_1 = nFk_1C_{Cl^-}(1-\theta)\exp(\beta FV/RT) \qquad [2.10]$$

$$i_{-1} = nFk_{-1}\theta\exp(-(1-\beta)FV/RT) \qquad [2.11]$$

The fractional coverage θ is proportional to the surface concentration of adsorbed intermediates and the fraction (1-θ) is proportional to the concentration of free sites on the surface, which are to be regarded as reactants in the adsorption, step I. Since quasi-equilibrium is assumed, the forward and backward currents of eqns. [2.10] and [2.11] can be equated. This gives rise to an electrochemical adsorption isotherm relating the fractional surface coverage θ to the potential difference across the interphase or to the overpotential, V :

$$\theta_{Cl^-}/(1-\theta_{Cl^-}) = KC_{Cl^-}\exp(FV/RT) \qquad [2.12]$$

where $K=k_1/k_{-1}$. Equation (2.12) is a Langmuir adsorption isotherm modified to apply to the case of electrochemical adsorption involving charge transfer, sometimes referred to as an electrosorption isotherm.

For the Cl_2 evolution reaction in the case of the " Volmer-Tafel " pathway, we

assumed step [III], the recombination of two adsorbed Cl· atoms on the surface, to be the rate-controlling step, so that the rate of the overall reaction is :

$$i = 2Fk_3\theta^2_{Cl\cdot} \qquad [2.13]$$

Then, from eqn. [2.12], $\theta_{Cl\cdot}$ can be expressed by :

$$\theta_{Cl\cdot} = [K_1C_{Cl^-}\exp(VF/RT)]/[1+ K_1C_{Cl^-}\exp(VF/RT)] \qquad [2.14]$$

Inserting the value of $\theta_{Cl\cdot}$ from equations [2.14] into [2.13] gives :

$$i_3 = 2Fk_3\{[K_1C_{Cl^-}\exp(VF/RT)]/[1+ K_1C_{Cl^-}\exp(VF/RT)]\}^2 \qquad [2.15]$$

For the limit of relatively low coverage for which $(1-\theta) \approx 1$ and $K_1C_{Cl^-}\exp(VF/RT) << 1$, the coverage becomes a simple exponential function of V and the rate equation takes the more convenient form :

$$i_3 = 2Fk_3K_1^2C_{Cl^-}^2\exp(2VF/RT) \qquad [2.16]$$

giving a corresponding Tafel slope of $b' = 2.303RT/2F$, about 29 mV; the other limiting case is when $\theta \rightarrow 1$, i.e. full coverage. Equation [2.13] then gives rise to an activation-controlled limiting current density of $2Fk_3$, which is independent of overpotential and of any mass-transfer in the solution.

In the usual case, the current density can be obtained by eqn.[2.15]. However, it is convenient to rearrange it to the form [85,86]:

$$\exp(VF/RT)/i^{1/2} = 1/[(2Fk_3)^{1/2}K_1C_{Cl^-} + \exp(VF/RT)/(2Fk_3)^{1/2} \qquad [2.17]$$

Hence, a plot of $\exp(VF/RT)/i^{1/2}$ vs. $\exp(VF/RT)$ will give a straight line of slope $(2Fk_3)^{1/2}$ and an intercept of $[(2Fk_3)^{1/2}K_1C_{Cl^-}]$ if recombination control through III determines the kinetics.

Another alternative procedure, which provides a more sensitive basis for examining the kinetic behaviour at high θ_{Cl^-}, follows the rearrangement of eqn.[2.15] in another way thus:

$$i^{-1/2} = (2Fk_3)^{-1/2} + (2Fk_3)^{-1/2}(K_1C_{Cl^-})^{-1}\exp(-VF/RT) \qquad [2.18]$$

which again enables both k_3 and K_1 to be evaluated, in this case, from the slope and intercept of the plot of $i^{-1/2}$ vs. $\exp(-VF/RT)$.

This procedure, developed by Conway and Novak[85,86], provided a new way of testing the applicability of the "recombination-controlled" mechanism and evaluating quantitatively both parameters K_1 and k_3 for steps [I] and [III].

2.4.2. Quasi-Equilibrium Approach with Assumption of Temkin Isotherm

In this section, the " Volmer-Tafel " type mechanism will be examined further. In a number of systems of practical interest, interactions and heterogeneity effects usually arise at a real surface. The former can be taken into account by introducing a coverage-dependent interaction energy in the configurational partition function. This factor can be taken into account in several ways, the best is the one described by Temkin[109]. For immobile adsorption, heterogeneity will not be detectable by observation of coverage-dependent heat of adsorption, since sites of varying energy will be filled at random and the measured heat of adsorption will be an average value. However, lateral interaction effects, if significant, lead to a coverage-dependent adsorption energy since the probability of near neighbour configurations increases with θ. The basic assumption in the Temkin isotherm is that varying energies of adsorption can arise on account of heterogeneity so that the surface is regarded as made up of a distribution of patches, at each of which the Langmuir isotherm holds independently with a characteristic local standard Gibbs energy or heat of adsorption, depending on the patch distribution, and decreasing linearly with coverage, which can be expressed by :

$$\Delta G^\circ_\theta = \Delta G^\circ_{\theta=0} + r\theta \qquad [2.19]$$

It is important to note that the ΔG°_θ does not, of course, always vary in an exactly linear manner with θ, so that it is better to modify eqn.[2.19] by raising the θ term in the exponent to the power n, so that eqn.[2.19] becomes :

$$\Delta G^\circ_\theta = \Delta G^\circ_{\theta=0} + r\theta^n \qquad [2.20]$$

However, in most cases encountered, eqn.[2.19] give satisfactory results. Also, it is a specific case of eqn.[2.20] for n=1. Therefore, in later discussion, eqn.[2.19] will be

used.

If an interaction term is taken into account, eqns.[2.10], [2.11] and [2.13] can be rewritten as:

$$i_1 = Fk_1^{\circ}C_{Cl^-}(1-\theta)\exp(-\beta g\theta)\exp(\beta FV/RT) \qquad [2.21]$$

$$i_{-1} = Fk^{\circ}_{-1}\theta\exp((1-\beta)g\theta)\exp(-(1-\beta)FV/RT) \qquad [2.22]$$

and, $$i_3 = 2Fk^{\circ}_3\theta^2\exp(2g\theta) \qquad [2.23]$$

where $g = r/RT$ and $K^{\circ}_1 = k^{\circ}_1/k^{\circ}_{-1}$. According to the quasi-equilibrium assumption, eqn.[2.21] with [2.22] gives rise to a Frumkin-type isotherm viz:

$$(\theta/(1-\theta))\exp(g\theta) = K^{\circ}_1C_{Cl^-}\exp(VF/RT) \qquad [2.24]$$

from which the Langmuir isotherm is recovered as a special case for $g = 0$ or $r = 0$. At intermediate values of coverage $0.2<\theta<0.8$ and with an appreciable value of g, the exponential term in equation [2.24] predominates and, upon taking logarithms of both sides and noting the $\ln(\theta/(1-\theta))$ term is ca. 1, there results :

$$\theta = \ln K^{\circ}_1C_{Cl^-}/g + VF/gRT \qquad [2.25]$$

This equation is formally equivalent to the Temkin isotherm. It is characterized by a linear dependence of θ on the overpotential V and a logarithmic dependence on the concentration C_{Cl^-}. However, if eqns. [2.21], [2.22] and [2.23] are combined, the total current can be obtained as :

$$i_3 = 2Fk_3[K^{\circ}_1C_{Cl^-}\exp(VF/RT)/(1+K^{\circ}_1C_{Cl^-}\exp(-g\theta)\exp(VF.RT))]^2 \qquad [2.26]$$

and the equation can be rearranged to another form :

$$i^{-1/2} = (2Fk_3)^{-1/2}\exp(-g\theta) + (2Fk_3)^{-1/2}(K_1C_{Cl^-})^{-1}\exp(-VF/RT) \qquad [2.27]$$

The initial Tafel slope at low overpotential still remains RT/2F but the limiting current density depends on the lateral interaction parameter, g; when g has a greater positive value, it gives rise to a larger value of the limiting current for $\theta_{Cl^-} \rightarrow 1$ than that for $g = 0$.

2.4.3. Steady-State Approach

It is convenient to apply the steady-state treatment when more than one pathway

arises in the overall reaction, for instance, in oxygen or hydrogen evolution reactions. Here, this approach will be used to treat the Cl_2 evolution mechanism referred to an earlier section, which includes the electrochemical step [II], in parallel with the recombination pathway, through step [III].

In the state of steady current, the surface concentration, related to $\theta_{Cl\cdot}$, of adsorbed $Cl\cdot$ will be time-independent and this condition may be written in terms of the rates of the indicated steps :

$$d\theta/dt = i_1 - i_{-1} - i_2 - i_3 = 0 \qquad [2.28]$$

using the abbreviated representation for the i_1, i_{-1}, i_2 and i_3 of the steps involved. In the case where the Langmuir isotherm applies, we have :

$$i_1 = Fk_1C_{Cl^-}(1-\theta)\exp(\beta FV/RT) = k'_1(1-\theta) \qquad [2.29]$$

$$i_{-1} = Fk_{-1}\theta\exp(-(1-\beta)FV/RT) = k'_{-1}\theta \qquad [2.30]$$

$$i_2 = Fk_2\theta\exp(\beta' FV/RT) = k'_2\theta \qquad [2.31]$$

and :

$$i_3 = 2Fk_3\theta^2 = k'_3\theta^2 \qquad [2.32]$$

where β and β' are symmetry factors for charge transfer, and k'_1, k'_{-1}, k'_2, k'_3 are defined according to eqns. [2.28] to [2.32]. Thus, the $Cl\cdot$ coverage is given from

$$k'_1(1-\theta) - k'_{-1}\theta - k'_2\theta - k'_3\theta^2 = 0 \qquad [2.33]$$

Neglecting a negative solution which has no physical significance, it is found that :

$$\theta = -(k'_1 + k'_{-1} + k'_2)/(4k'_3) + [(k'_1 + k'_{-1} + k'_2)^2 + 8k'_1k'_3]^{1/2}/(4k'_3) \qquad [2.34]$$

and the steady-state current is contributed by both pathways, through step [II] and [III], so that :

$$i_t = i_2 + i_3 = 2F(k'_3\theta^2 + k'_2\theta) \qquad [2.35]$$

2.5 The Adsorption Pseudocapacitance

2.5.1. Definition of Pseudocapacitance

When a chemisorbed species arises in an electrode reaction, e.g. as in underpotential deposition of H on Pt or Pb on Au, an equilibrium pseudocapacitance

C_ϕ arises, determined by the potential dependence of coverage, θ, by the ad-species and characterized by an equilibrium electrochemical adsorption isotherm for all potentials corresponding to an observable range of θ, > 0 and < 1.

In a process for which a net Faradaic current is passing, a non-equilibrium situation is obtained. If the reaction is a multistep one involving an adsorbed intermediate, the steady-state coverage, θ_{ss}, of this intermediate can depend on potential so that a variation of θ_{ss} with overpotential, V, can arise. This gives rise to a "non-equilibrium", steady-state pseudocapacitance $C_{\phi,ss}$. In the present work, methods are developed and used for evaluating this kind of C_ϕ for the adsorbed Cl· intermediate in the anodic Cl_2 evolution reaction.

Normally, because significant $C_{\phi,ss}$ arises in processes taking place at appreciable net current, the cyclic-voltammetry method used for evaluation of u.p.d. C_ϕ, is not applicable. Other "modulation" methods are therefore required, e.g. potential relaxation on an open-circuit and/or a.c. impedance spectroscopy, as used in the present work.

Since the formation of adsorbed intermediates is associated with charge transfer across the interphase (as in step I), if a potential is applied, a transient Faradaic current will flow to establish the equilibrium value of the coverage θ of the intermediates together with a smaller non-faradaic current component for the change of charge in the double layer. The total charge q_F will be proportional to θ or the change of θ caused by the change of the potential plus C_{dl} dV/dt. Neglecting the latter quantity,

$$q_F = q_o\theta \qquad [2.36]$$

where q_o is the charge needed to form a complete monolayer of the adsorbed intermediates. Its value is about 210 $\mu C/cm^2$ for a monovalent species, e.g. H or Cl, each occupying a single site on the surface. Because θ is a function of potential, θ=f(V), a differential capacity may be defined as:

$$C_\phi = (dq_F/dV) = q_o(d\theta/dV) \qquad [2.37]$$

where C_ϕ is the so-called adsorption pseudocapacity. It is noted that an adsorption pseudocapacity cannot exist at a ideal polarized electrode. The prefix " pseudo " is used because C_ϕ refers to a leaky capacitor. Usually, the pseudocapacity is proportional to the value of change of coverage with potential.

Under Langmuir conditions, from equations [2.14] and [2.36], C_ϕ is :

$$C_\phi = (q_o F/RT)[K_1 C_{Cl^-}\exp(FV/RT)/(1+K_1 C_{Cl^-}\exp(FV/RT))^2] \qquad [2.38]$$

Alternatively, C_ϕ can be expressed as a function of coverage :

$$C_\phi = (q_o F/RT)[\theta/(1-\theta)] \qquad [2.39]$$

If the Frumkin isotherm applies, (see eqn. [2.24]), θ cannot be written as an explicit function of potential,V, so C_ϕ can only be expressed as a function of θ.

$$C_\phi = (q_o F/RT)[\theta(1-\theta)/(1+g\theta(1-\theta))] \qquad [2.40]$$

The dependence of C_ϕ on V can, however, be easily obtained by numerically calculating V as a function of θ from eqn.[2.38][110,111].

2.5.2. Cl^- Coverage, θ_{Cl^-}

From eqn. [2.37], the coverage by the intermediate, in this case, Cl^-, can be evaluated by the integration of the C_ϕ vs. V profile.

Since : $$q_1 \int d\theta = \int C_\phi(V)dV \qquad [2.41]$$

then : $$\theta_{Cl^-} = (1/q_1)\int C_\phi dV + \theta_o \qquad [2.42]$$

where θ_o is an initial coverage at V=0, i.e. the condition of equilibrium. The C_ϕ vs. V relation can be experimentally obtained by means of the potential-decay method (see chapters V and VI) so that the integration of the $C_\phi(V)$ and θ vs. V plot can also be made numerically.

The relationships of $C_\phi(V)$ to V and θ to V are very important for understanding the Cl_2 evolution mechanism. Even though there are a number of papers on the subject of anodic Cl_2 evolution, no previous papers have examined the pseudocapacitance behaviour of the Cl^- intermediate and the corresponding dependence of coverage by Cl^- on potential which is an essential requirement for

understanding electrocatalysis and adsorption, and their mechanism.

Therefore, it is one of the main purposes of the work described in this thesis to characterize quantitatively the role of adsorption behaviour of the intermediate, $Cl^{\cdot}$, in the Cl_2 evolution reaction and to describe the basis of the experimental procedures required for providing this kind of information.

2.6. The Adsorption Factor in Electrocatalysis

One of the particular requirements is the experimental evaluation of the potential dependence of coverage, θ, by the electroactive intermediates in the reaction in relation to reaction mechanisms and the Tafel slope, b, of the process representing the dependence of ln[current-density,i] on the overpotential, V. Thus, characterization of b values in relation to potential dependence of coverage by the intermediates is as important for evaluation of electrocatalysis as derivation of i_o values, especially for comparing electrocatalysis in a given reaction at various electrode materials with appreciable current densities. For example, for the electrochemical desorption step of the electroactive adsorbed intermediate(step II, above), the reciprocal of the Tafel slope can be expressed as:

$$1/b = d \ln i/ dV = d \ln \theta/dV + \beta F/RT \qquad [2.43]$$

where the first term on the right hand side can be recognized as an "adsorption factor" and the second term as the "charge-transfer factor". When $d \ln \theta/dV$ is significant, i.e. for an appreciable and potential-dependent θ, b is << 2RT/F, which is a feature desirable for good electrocatalysis.

The determination of b, through b^{-1} in eqn.[2.43] in relation to chemisorption effects has, surprisingly, not been treated theoretically to any great extent in the literature except in recent work by Conway et al[111] and Srinivasan[112], where the term $d \ln \theta/dV$, which is as important as i_o and surface structure and composition evaluation

in electrocatalysis, has been considered. It is to be considered as a major factor in electrocatalysis especially with regard to comparison of performance of electrocatalysts for faradaic reactions proceeding at practical high current-densities on the order of 100 mA cm^{-2} or more.

CHAPTER III

Experimental

3.1. Selection of Systems

The aim of this research project was : (a) to investigate the behaviour of the adsorbed intermediate $Cl^{\cdot}$ in the Cl_2 evolution reaction; (b) to try to understand the mechanism of Cl_2 evolution at various materials such as Pt, Ru and RuO_2-TiO_2 etc.; (c) to evaluate the role of the oxide film that is unavoidably electrogenerated concomitantly on the surface of Cl_2-evolving anodes and its electrocatalytic or inhibition properties for the Cl_2 evolution reaction. A fuller understanding of the mechanism of Cl_2 evolution is essential for finding improved electrocatalysts for industrial Cl_2 production and rationalizing choice of materials.

The research work has been principally conducted at : (i) a Pt rotated disc electrode in 1 N aq. HCl; (ii) in 0.5 M RbCl + trifluoro-acetic acid solutions; (iii) Ru, Pd, Ir and Rh electrodes in some complementary experiments and (iv) at RuO_2-TiO_2 DSA-type electrodes in aqueous $Cl^{\cdot}$ solution.

The use of a non-oxidizable non-aqueous solvent allows anodic Cl_2 evolution experiments to be carried out under conditions such that no oxide film is formed (ref.85,86), thus this behaviour can be compared with that in aqueous solution in order to extract information concerning the role that the oxide film plays. In the aqueous solution work, experiments on Cl_2 evolution kinetics and $Cl^{\cdot}$ involvement were conducted both on " reduced " and " oxidized " (see below) surfaces.

3.2. Electrodes

3.2.1 Working Electrode

3.2.1.1. Pt Electrode

Pt electrodes were made from 0.5 mm diameter high-purity grade Pt wire from Johnson Matthey and Mallory Co.. The Pt wire samples were first degreased by refluxing in acetone in a Soxhlet-type extractor for 24 hours, then heated and sealed in soft-glass tubes which were used as electrode holders, and finally soaked in 98% H_2SO_4 solution. Before use, the electrodes were washed in many changes of distilled water in an ultrasonic cleaner, and never left to become dry in the air.

3.2.1.2. Ru, Pd, Rh and Ir Electrodes

The preparation of Ru, Pd, Rh and Ir electrodes was similar to that for the Pt electrode. The respective, degreased Johnson Matthey and Mallory high-purity grade wires, of diameter ca. 0.5 mm, were sealed in soft-glass tubes and also soaked in 98% H_2SO_4 before use.

3.2.1.3. The Rotating Pt Disc Electrode

A Pt rotating disc electrode, obtained from Pine Instrument Co. (Grove City Pa.), mounted in Teflon, had a geometric area of 0.47 cm^2. The main purpose of using a rotating electrode was to eliminate or minimize the possibility of mass- transfer effects since, in the experimental observations, a limiting current-density was consistently obtained in the current vs. potential relation that could have arisen from diffusion limitation. Also, electrode rotation seems to remove adhering chlorine bubbles formed anodically on the electrode surface, which can cause significant fluctuations in the current at an active electrode. Additionally, rotation spins away any local boundary layer of solution supersaturated with Cl_2 [113-115].

In the measurements, especially those of a.c. impedance, the rotating disc electrode has to used in order to avoid " noise " problems arising in the experiment caused by the presence of anodically generated Cl_2 bubbles. However, it was found that with a reasonable rotation speed ca. 3600 r.p.m. under the experimental

conditions used, very reproducible i vs V relations could be established which were independent of any further increase of rotation frequency beyond the above rate.

3.2.1.4. RuO_2-TiO_2/Ti Electrodes

RuO_2-TiO_2/Ti DAS-type electrodes were prepared according to the recommendations given by Beer[12] and elsewhere[11,100]. The procedure includes two steps, the first step is the substrate pretreatment: the Ti wire, 0.9 mm diameter, sealed in a soft-glass holder, ca. 0.4 cm^2 in surface area, was first roughened with fine-grade emery paper, cleaned in an ultrasonic bath for 30 minutes and then degreased in acetone; it was then pickled in boiling dilute HCl; washed; briefly immersed in hot 10-15% HNO_3; rinsed in double-distilled water and finally dried in hot air. The second principal step consists of the active film preparation: a suspension of ruthenium(III) chloride, $RuCl_3$, and titanium(IV) butoxide, $Ti(OC_4H_9)_4$, in acidified butyl alcohol was adjusted in composition to give an electroactive layer containing about 30 mole percent RuO_2 and the remainder TiO_2. This suspension was applied to the pre-treated Ti-substrate by a repetitive brushing, drying and baking procedure. After application of each layer, the electrodes were dried at 343-363K and then baked at 673-773K in a hot air oven for two hours.

3.2.1.5. Determination of Real Surface Area

Unfortunately, no general electrochemical method for surface area determination, similar to the B.E.T. method, is available, but, depending on the specific character of the electrode material, various electrochemical data can be used for surface area calculations based on one or more of the following quantities: (a) the double-layer capacity value; (b) the charge for electrochemical deposition of a monolayer of adsorbed H or O species; (c) the values of the diffusion-controlled limiting currents for the oxidation or reduction of a known species, e.g. $Fe(CN)_6^{-4}$, $Fe(CN)_6^{-3}$.

The estimation of real surface area of electrodes from the value of the double-

layer capacity was first introduced by Frumkin[116] and involves the assumption that the capacity of the double-layer is the same for different metals, that is, having a value of about 25 μF cm^{-2} for the cation and 40 μF cm^{-2} for anion adsorption regions, depending on the sign of surface charge at the electrode. This procedure has been used in determinations of the surface area of RuO_2-TiO_2 electrodes in the present work.

In the case of the Pt and Rh electrodes, the estimation of the true surface area is based on the assumption that one atom of hydrogen is electrodeposited, or adsorbed from the gas phase, on each metal atom of the surface, and that a monolayer of hydrogen is completed at the reversible potential of the hydrogen electrode[117]. The real area can be obtained from the charges under the hydrogen u.p.d. peaks[118] determined by cyclic-voltammetry in 0.5 M H_2SO_4 at 298K, taking 210 μC cm^{-2} as the charge required for the formation of a monolayer of H in the usual way.

3.2.2. Reference Electrode

3.2.2.1. Platinized Reference Electrode

Platinized Pt reference electrodes were prepared according to the procedure given by Ives and Jantz[13]. Lead acetate, sometimes recommended as an additive, was not used in the platinizing solution (2% H_2PtCl_6 in 2N HCl) because of the possibility of introducing undesirable impurities into the working electrode electrolyte. In the experiments, the platinized Pt reference electrode was bubbled with pure Cl_2 gas in a way similar to that used in the case of a H_2 reference electrode. The equilibrium $Cl_2 + 2e^- \equiv\equiv\equiv 2Cl^-$ can easily be established and gives a very stable potential of 1.358 V vs the R.H.E. Since the working electrode was also bubbled with pure Cl_2 gas, the open-circuit potential is about 0 ± 1.5 mV.

3.2.2.2. Silver-Silver Chloride Reference Electrode

The silver-silver chloride reference electrode was formed by successive

anodization/cathodization of a Ag wire mounted within a thin-walled capillary tube which acted as a Luggin probe. The potentials of the test electrode were referred to that of the silver-silver chloride electrode in the same solution (1 mole dm^{-3} of Cl^-). The open-circuit potential vs Ag/AgCl was 1.135 V when the solution was saturated with Cl_2 and its hydrolysis products.

3.2.3. Counter Electrode

A platinized-platinum gauze having a large surface area was used as the counter electrode. The large surface area minimizes the reaction resistance and the polarization of the electrode and dissolution of Pt.

3.2.4. Electrolyte

All aqueous solutions were made up in pyrodistilled water[120] using BDH 98% Aristar grade H_2SO_4 or HCl, and from NaCl that had been recrystallized and dried at 423 K. The trifluoroacetic acid was purified by drying followed by multiple distillation by a method described previously[121]. The anhydride used for " gettering " any remaining traces of water was purified similarly. RbCl required for the work in TFA was also recrystallized and dried at 423 K (NaCl or KCl are insufficiently soluble in this solvent for purposes of the electrochemical experiments involved).

3.3. Cell

A conventional three-compartment all-glass cell was used as described in previous work[65,86]. In most measurements, since the current densities were relatively high, the stopcock between the working and counter electrode compartments could be opened as necessary. Pure Cl_2 gas was bubbled continuously through the working electrode compartment.

3.4. IR-Drop Measurement

Because relatively high current densities up to the -1 to 0 decade in log [current-density] were involved in the measurements, and because of the approach to apparent limiting currents, IR drop corrections were important in most of the present work. The uncompensated resistance between the Luggin capillary of the reference electrode and working electrode was determined at various current-densities by means of a Nicolet digital oscilloscope using the current interruption procedure[122]. The solution resistance was also measured by means of a newly developed open-circuit potential decay "fitting method" (see section 3.6.3) and by a.c. impedance. The resistances involved usually were 1.0 to 4.0 Ohm. Values obtained by the above three methods were in a good agreement and could be determined with an accuracy of ca. 5% prior to each experiment. IR-drop corrections, based on these resistances, were applied in all the polarization measurements by means of a computer program.

3.5. Instrumentation

A PAR model 173 potentiostat/galvanostat and a PAR model 376 logarithmic current converter, coupled with an Hewlett Packard model 216 computer, were used in most of the electrochemical measurements, including the recording of Tafel relations and potential relaxation transients (see section 3.6.2) following the interruption of the anodic polarization currents.

In order to record the fast potential relaxation transients (potential decay curves), a Nicolet 2090 digital oscilloscope was used to acquire the data and store them on a floppy disk. The recorded information was then transferred to an HP216 computer for further data processing.

The a.c. impedance measurements were made using a Solartron 1250 Frequency Response Analyzer (FRA), equipped with a Solartron potentiostat, 1286 Electrochemical Interface (ECI) which controlled the electrode system. The data was first stored on a 31/4 inch disk then transferred to an IBM clone small PC computer which could also communicate with the University of Ottawa main-frame computer

network for further analysis with data fitting treatments. The fitting procedure (see section 3.6.3) was carried out using a software package called " Statistical Analysis System " (SAS), which allowed a nonlinear regression subroutine (NLIN) to be applied to fit the data.

3.6. Methods

3.6.1. Computer-Programmed Data Acquisition of Steady-State Polarization Data (Tafel plots)

The steady-state current-density, i vs overpotential V plots, or so-called Tafel plots, not only provide information on the kinetics of electrode processes, for example, from the Tafel slope b or the limiting current density (in the case of a recombination-controlled process as involved the present Cl_2 evolution reaction), but also enable the reaction mechanism to be determined. Additionally, information on the electrocatalytic properties of electrode materials are provided, since electrodes exhibiting low Tafel slopes, b, and large exchange current-densities, i_o, can be considered good electrocatalysts. Recently, Conway et al[123-125] have combined steady-state polarization and open-circuit potential decay results in order to derive information about the pseudocapacitance and surface coverage of adsorbed intermediates in an electrode reaction as an important direction for characterization of electrocatalysis in electrode processes.

In practice, in an anodic reaction such as Cl_2 evolution, the steady-state current can be appreciably affected by the simultaneously grown anodic oxide film, since the oxide film developed during the reaction may change the electrocatalytic properties of the electrode surface. Thus, if the state of oxidation of the electrode surface changes, the steady-state current may not be easily reproduced. Therefore, control and characterization of the state of oxidation of the anode surface is an important but difficult aspect of anodic process studies. However, during this project, three different programmes for the computer control of the pre-conditioning of the electrode surface

were developed to deal with this problem.

In order to obtain stable steady-state currents in Tafel measurements, two limiting states for the oxidation of the surface of Pt electrodes were studied in order to compare how the oxidation of the Pt surface affects the behaviour and coverage by the adsorbed intermediate, Cl, in the Cl_2 evolution reaction. One was attained by anodically holding the overpotential at a given value, say +500 mV, for 30 minutes to form a well defined surface oxide film and to attain a stable anodic current; then the Tafel measurement could be made. The resulting log(i) vs V results were found to be reproducible so that it could be assumed that the surface oxide film had reached a relatively stable state of formation, and no significant further change would arise during the short time when the experimental data was being acquired (note that oxide film formation at noble metals depends on potential and the log of time of growth[83,84]).

The second extreme state is achieved by cathodically reducing the surface for 30 seconds immediately before each anodic polarization point is taken. Since for each point, the surface has been "reduced", it could be considered that each measurement is being made on a "clean", reduced surface without any significant oxide film being present initially.

Fig.3.1 illustrates the three computer programmes for control of the potential; 3.1a shows the normal one, a stair-type control and 3.1c is for long-term potential-holding experiments for eleven successive measurements; 3.1b is for obtaining the so-called initial "reduced" surface, before each anodic polarization potential is applied; in this, the electrode potential was cathodically scanned to a negative potential, say 0.35~0.4 V R.H.E. where any previously formed oxide film should be reduced but H_2 would not evolve. In this way, the Tafel plots are reproducible. The data for ascending potential change actually overlay those for descending change, which incidentally also confirms minimum surface oxide film formation under these conditions. However, the points are not overlaid in the case where the stair-type program was applied. The overlay arises because, at the cathodically reduced Pt electrodes, an active state of the electrode

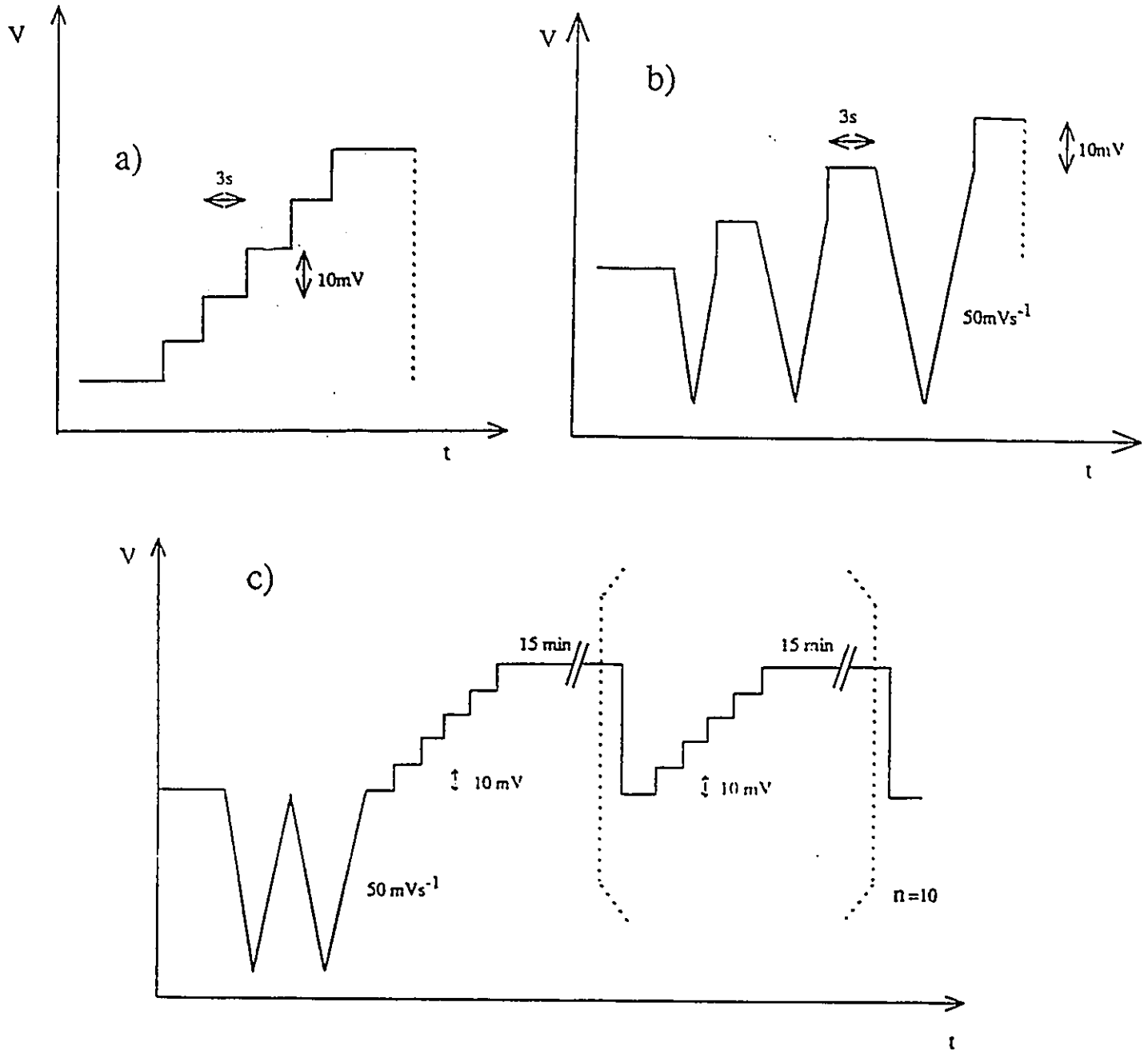

Fig.3.1 Three computer control programs for the steady-state polarization measurements on the Cl_2 evolution reaction at Pt electrodes. (a) "stair" type; (b) "reduced" type; and (c) the long-term holding.

surface is well controlled but in the stair-type program, progressive and cumulative surface oxidation has time to take place.

3.6.2. Open-Circuit Potential Decay Method

The open-circuit potential decay method for the derivation of information about chemisorbed intermediates, recently developed by Conway and Bai[123-125] in a relatively new way, involves numerical data treatment for obtaining accurate dV/dt values, with complementary determination of Tafel plots. This enables information concerning the pseudocapacitance and coverage of the adsorbed intermediates (here Cl·) to be determined. For this method, since both experimental potential relaxation transients and Tafel polarization measurements are required in the experiments, it becomes very important to control, in the same way, the experimental conditions for these separate experiments in order to obtain accurate and reliable information. Terefore, open-circuit potential relaxation transients, for the case of the Cl_2 evolution reaction, as described in Chapters V, VI and VII, were recorded as quickly as possible after determining the Tafel measurements.

The Nicolet digital oscilloscope provides a satisfactory means of recording fast potential vs time relaxation transients which can be stored digitally on floppy disks for later analysis. The required current interruption is made by means of a Clare vacuum mercury relay which gives quick enough response. The electric circuit for the potential decay measurements is shown in Fig.3.2.

In order to record the transients over significantly long time scales, three separate transients were made over three different time ranges :

(i) 0.5 - 50 μs per point.

(ii) 100 - 500 μs per point.

and (iii) 1 - 5 ms per point.

The V(t) data was acquired in channel A of the oscilloscope and the current i(t) was also recorded in channel B, so that both V(t) and i(t) could be recorded at the same

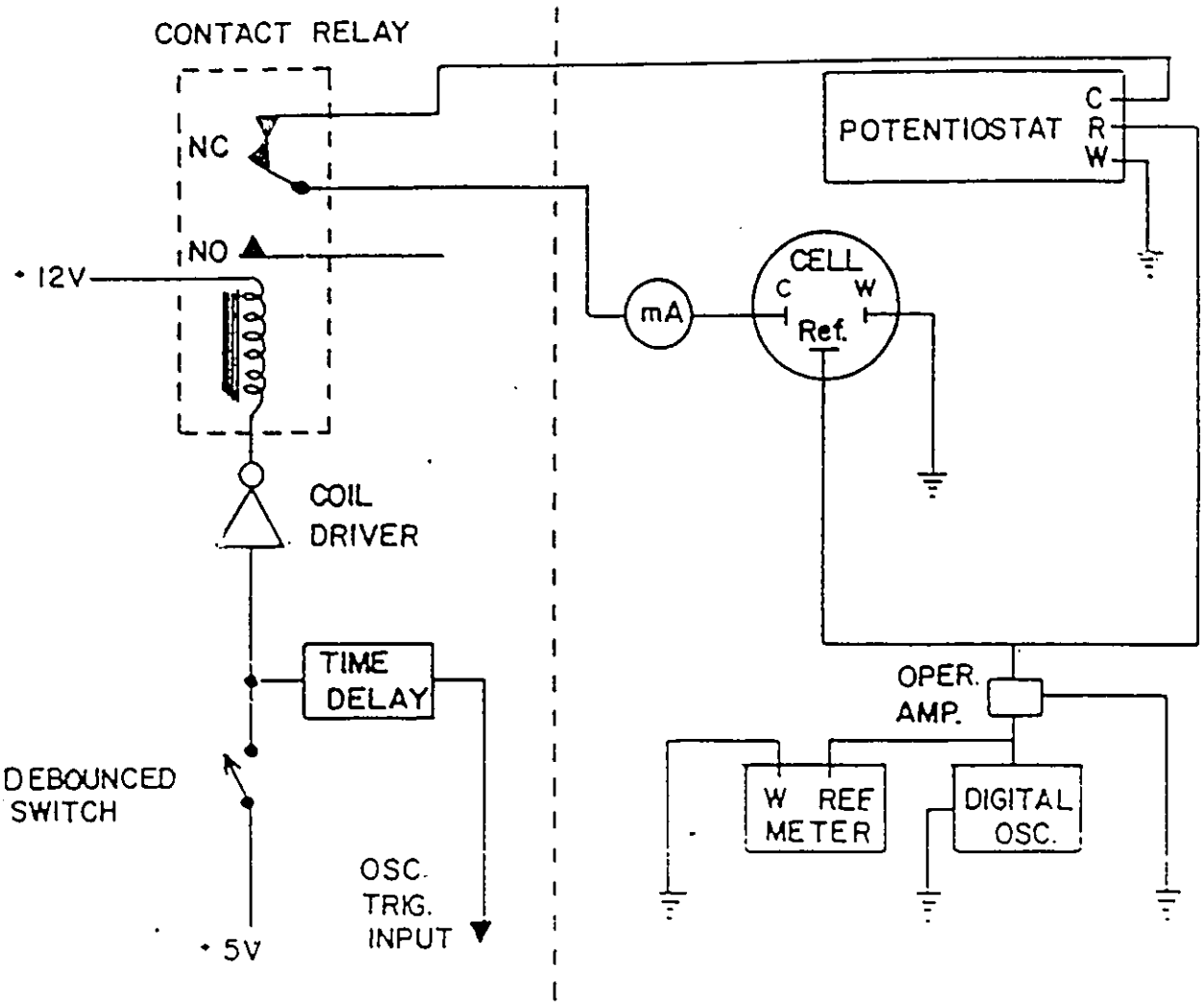

Fig.3.2 Electrical circuit for steady-state polarization and potential decay measurements.

time when the potential decay transient was initiated. This procedure gave very accurate potential V(t) and current i(t) values which were required for later pseudocapacitance calculations.

During the process of recording each decay transient the circuit needed to be "open" for less than a few seconds. Determination of the next decay transient could not be made until the reaction of Cl_2 evolution had returned to a new controlled steady-state rate (usually requiring only a few seconds).

As in the study of the anodic Cl_2 evolution Tafel measurements, two extreme states of surface oxidation were investigated in the potential relaxation experiments. Fig.3.3 illustrates the procedure for taking the decay transients, where (a) is for holding at a given determined time, t_h, for the measurements at the pre-oxidized electrode while (b) shows the programme for a cathodic potential scan applied first to completely reduce the oxide on the electrode surface and then followed by a jump of potential to the next desired value to record the new potential transient at a different initial potential.

The recorded V(t) data was then processed in the HP 216/217 computer to join three sets of data according to the time scales for which the kinetic parameters of the Cl_2 evolution reaction and the adsorbed $Cl^{\cdot}$ behaviour and coverage, were to be obtained. The $Cl^{\cdot}$ pseudocapacitance was then evaluated according to eqn.[4.1], by dividing the steady-state current densities i(V) by respective dV/dt values derived from the potential relaxation transients calculated by application of a differentiating program to the V(t) data.

3.6.3. Initial Potential Decay Rate $(dV/dt)_{t=0}$: Extrapolation by Means of a Fitting Function for the V(t) Transient

For the first time, a new treatment based on the fitting of the potential-relaxation curves, V(t), recorded on open-circuit following interruption of the polarizing current of an electrode reaction, has been developed in collaboration with Dr. R. Brousseau in

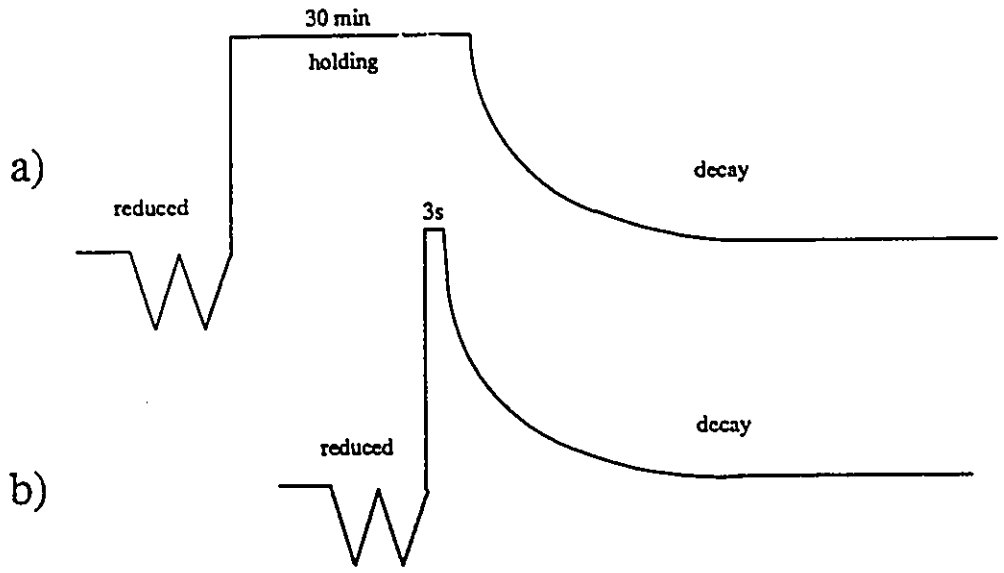

Fig.3.3 Potential relaxation programs for: (a) the pre-oxidized electrode; (b) the reduced electrode for study of the Cl_2 evolution reaction at Pt electrodes.

our laboratory. This new procedure can be used to obtain conveniently both the interfacial capacitance behaviour of the electrode and the noncompensated solution resistance giving rise to the IR drop (see section 3.5) in an electrochemical cell for appreciable current-densities of the faradaic process.

This proposed technique has clear advantages over other previously published methods for evaluation of the interfacial capacitance at the electrode in a state just prior to current interruption. The procedure for collection of the potential relaxation curves for this fitting method was similar to that described in an earlier section 3.6.2. However, only the short-time transients (0.5 - 5 μs per point range) were used. Again both channels A and B were utilized to record V(t) and i(t) curves from which, i(t=0) and V(t=0), viz, the current and potential just before each open-circuit current interruption was initiated could be very accurately recorded. These two values for each potential and corresponding current-density were the basic data for calculation of interfacial capacitance at each potential and evaluation of the uncompensated resistance.

Another application arises on account of the fact that the pseudocapacitance discharges much slower than does the double-layer capacitance, so that this method can be used to estimate the real electrode surface area by evaluation of the C_{dl} especially for porous electrode surfaces such as arise at baked RuO_2-TiO_2 films. The principle is rather simple: since the transients treated by the fitting method were recorded over a short time scale, only the double-layer capacitance becomes discharged in such a short times (from the V vs log(t) curve, it can be seen that the double-layer capacitance, in most cases, becomes discharged first; thus, because of the time constant defined as τ=RC, the process having the smallest τ will discharge first). The surface area can therefore be evaluated, based on the assumption that the double-layer capacitance is equal to 40 μF cm^{-2} on the anodic side of the p.z.c. in the normal way.

The curve fitting procedure, mentioned in section (3.5), was carried out using the University of Ottawa mainframe computer and employed a non-linear regression programme (SAS) corresponding to a nonlinear representation of the time course of V(t). An example of a fitted V(t) curve is shown in Fig.3.4 and further examples will be given in section (4.1.3).

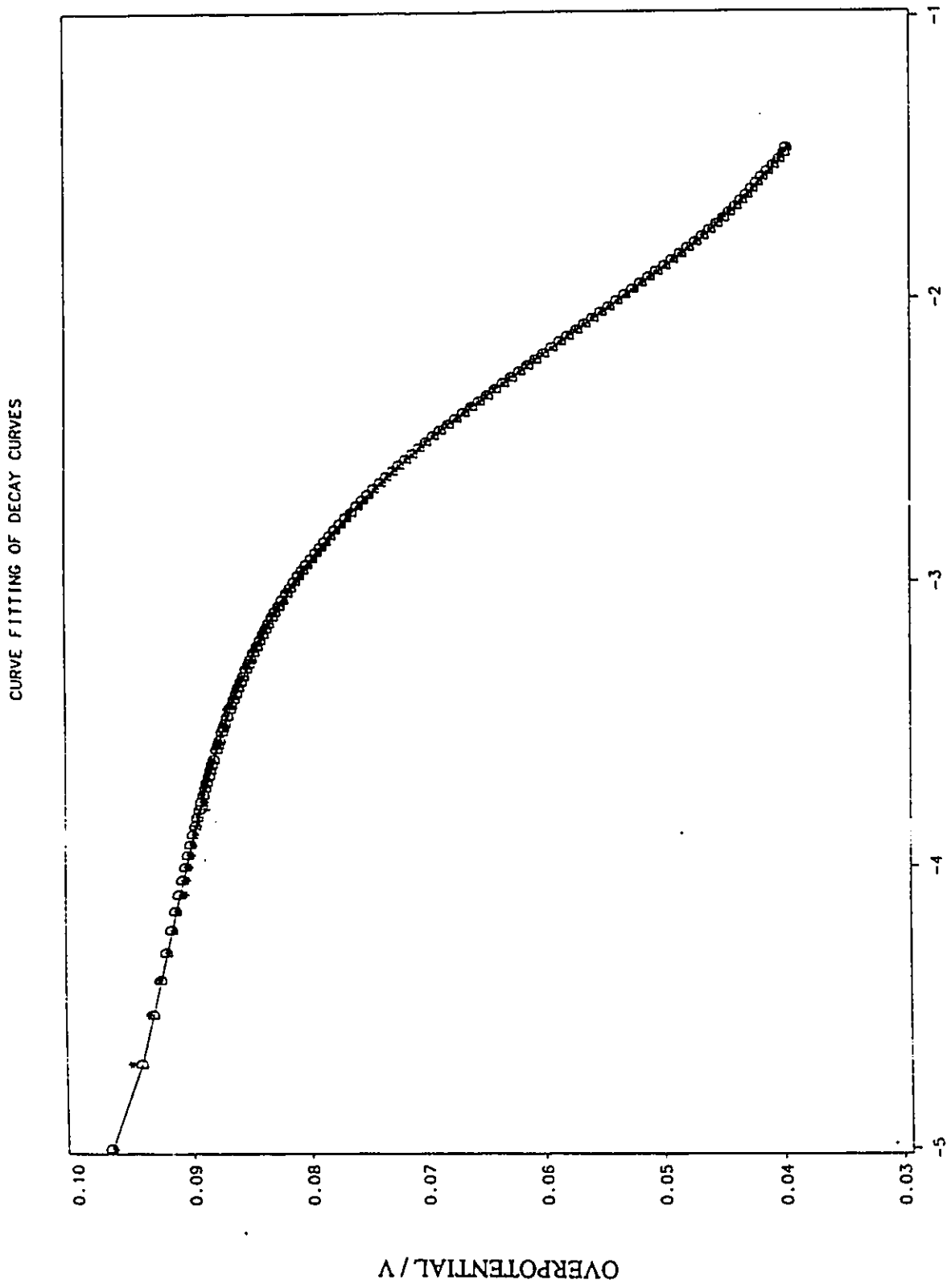

Fig.3.4 A sample of initial data Fitting of potential relaxation transient data.

3.6.4. A.C.Impedance Method

A.c. impedance measurements not only provide a useful approach to the study of the kinetics and mechanism of complex electrode reactions but are also complementary to the potential-decay method just described for extracting information concerning pseudocapacitance and coverage behaviour of the Cl· intermediate in the Cl_2 evolution reaction.

The system consisted of a Solartron 1250 Frequency Response Analyzer (FRA) and potentiostat (ECI 1286). The ECI provides given potentials to control the electrochemical process in the anodic polarization experiments (here for Cl_2 evolution) while the FRA, consisting basically of a programmable sinusoidal signal generator and analyzer, provides an output signal of amplitude 5 mV and variable frequency which is in the form A $\sin(\omega t)$. The sinusoidal signal is superimposed on the given " d.c. " anodic polarization potential and is applied to the electrochemical interface. The response of the electrochemical reaction to the a.c. modulation signal in the form $A'\sin(\omega t+\psi)$ is returned back to the analyser in which the phase shift and amplitude are analyzed and evaluated. Finally, the real (Z') and the imaginary (Z") components of the impedance vector are obtained as the output experimental data from the analyser. The data (Z') and (Z") being a function of frequency, ω, can be displayed on a graphics screen or plotter, using the HP 217 computer and can be also transferred to an IBM-PC and mainframe computer for functional fitting or simulation treatments. For the reaction studied (Cl_2 evolution), the impedance components were measured at various controlled anodic overpotentials over the frequency range 65,000 to 0.005 Hz(or lower if necessary).

In order to study the "reduced" Pt surface, the electrode had to be pre-reduced to remove any oxide film existing on the electrode surface before each measurement was taken. A switch box was used to control the electric circuit which could select either the a.c. measurement mode or cathodic scanning reduction (see Fig.3.5). Before the a.c. measurement, the switch was put in position C , allowing cathodic scanning to

be applied to reduce any oxide on the surface of the electrode (arising e.g. from the previous polarization measurements); then the switch was set to position I, corresponding to running the a.c. impedance measurement scan. Since each measurement takes only a few minutes with much of the frequency scan covered in a few seconds, the measurements can be considered as approximately corresponding to a "clean" or a less oxidized electrode surface, especially over low overpotential range where the oxide film grows very slowly in a Cl^- containing solution.

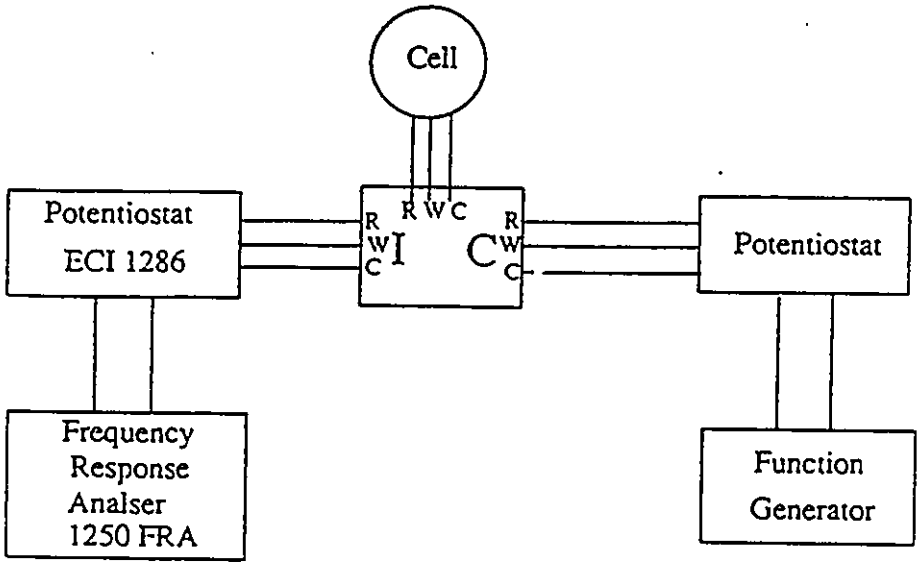

Fig.3.5 Diagram of the system for controlling oxide formation on Pt electrode surfaces in a.c. measurements.

3.6.5. Cyclic-Voltammetry

Although this technique has been mentioned in an earlier chapter, here it is still necessary to emphasise that this method was not only used in the study of oxide film growth but was also applied in almost all the experiments to the course of preparation of the "reduced" electrode surfaces. In the quantitative measurements, a linearly swept potential signal, V(t), was applied to the electrochemical system and the response signal, viz, the current i(t), was recorded. Both the current and potential curves were recorded by means of the Nicolet oscilloscope and transferred to the HP 216/217 computer for further processing; for example, the oxide reduction peak in the voltammogram can be integrated by computer to evaluate the oxide reduction charge, corresponding to the coverage of the anode at a given potential by OH and/or O species. Also, the cyclic-voltammograms can be plotted on the screen or by means of a plotter, as desired.

CHAPTER IV

Theories of Methods

In order to reach a fuller understanding of the kinetic and mechanistic behaviour of an electrode reaction, information about the capacitance at the electrode surface has to be obtained since the pseudocapacitance, which is the capacitative component due to the adsorbed or chemisorbed species, is necessary in order to calculate the coverage by the adsorbed intermediates. Thus, this capacitance component, C_ϕ, is related to the derivative of the coverage, θ, with the electro-active species by the relationship $C_\phi = q_1 d\theta/dV$ as defined in section 2.5.1. The basis of the various methods used for determining the capacitance behaviour in this work are presented in this chapter, including the recording of open-circuit potential decay transients and the determination of initial potential decay rates by the new curve-fitting method, as well as determination of a.c. impedance.

The study of electrocatalysis in electrochemical reactions requires not only characterization of the steady-state kinetics of the process as a function of electrode material, state and composition of the electrode surface, etc. but also, additionally, information concerning the coverage behaviour of the chemisorbed intermediates generated, in relation to the reaction mechanism.

In order to provide, experimentally, information on the behaviour of adsorbed intermediates, methods must be used that generate a recordable response of the reaction to a modulation of some kind, of either the current, or conjugately of the electrode potential. Such a response arises from the dependence of the activation energy or of the equilibrium Gibbs energy of the process upon potential, a fundamental aspect of electrode processes distinguishing them from the regular heterogeneous reactions. Modulation procedures are normally used in a

complementary way with steady-state kinetic methods, e.g. evaluation of log[current-density] vs potential (Tafel) curves.

The types of modulation commonly applied are: a) a step-function in potential or current; b) self-relaxation of the potential on an open-circuit from an interrupted previous steady-state polarization; c) linear potential sweep variation of the activation energy or of the (quasi-) equilibrium Gibbs energy and d) small amplitude sinusoidal alternating variation of potential or current. The modulation procedures normally involve a non-steady-state of the reaction, analysis of which gives rise to additional information, e.g. the interfacial capacitance, complementary to the kinetic information derived from steady-state experiments as a function of potential.

In the present work, methods (b) and (d) have principally been used (together with steady-state measurements) and supplemented by method (c) for characterization of the state of surface oxidation of Pt anodes.

4.1. Open-Circuit Potential Relaxation Transient Technique for Study of the Pseudocapacitance

4.1.1. Mechanism of Self-discharge

Following interruption of a polarization current, no net passage of electron charge can continue to occur. The observed potential decay must therefore take place by one of the following three mechanisms, depending on the rate-determining mechanism of the reaction and the electrode at which it takes place:

(a) In the absence of significant coverage by adsorbed intermediates, as with the h.e.r. at Hg, decay of potential from a state of prior polarization can only occur by discharge of the double-layer capacitance, C_{dl}, through the parallel, potential-dependent reaction resistance.

(b) When there is appreciable coverage, θ, by a chemisorbed intermediate, a pseudocapacitance, C_ϕ, arises ($>>C_{dl}$), as described in section 2.5.1 and this must be discharged during an open-circuit potential decay. A charge much larger than that on

C_{dl} is involved so the process must differ from that in (a) above. For mechanism I,II, discharge of C_ϕ and associated decrease of θ can only take place by a mixed cathodic anodic process, e.g. for the case of adsorbed Cl^-:

$$M_{ox.Cl\cdot} + Cl^- \longrightarrow M_{ox} + Cl_2 + e \text{ (continuing rate-determining step)} \quad (II)$$

coupled with

$$M_{ox.Cl\cdot} + e(\text{from II}) \longrightarrow M_{ox} + Cl^- \text{ (reverse of step I)}$$

This is equivalent to the formation of Cl_2 from two adsorbed $Cl\cdot$, and no net electron transfer is required from or to the electrode surface in this mechanism.

(c) If is the rate-controlling step, I and its reverse determine the potential as $f(\theta_{Cl\cdot})$ through the electrochemical adsorption isotherm (eqn.[2.14]), as $\theta_{Cl\cdot}$ decreases by continuation of the chemical recombination step III:

$$2M_{ox.}Cl\cdot \longrightarrow M_{ox} + Cl_2 \quad (III)$$

or an equivalent process on the "reduced" Pt surface. A small flew of charge, $C_{dl}\Delta V$, also takes place through the process

$$M_{ox}Cl\cdot + e \rightleftharpoons M_{ox} + Cl^-$$

enabling the C_{dl} to be discharged through the decaying potential range ΔV. The charge involved in discharging C_ϕ is equivalent to $C_\phi\Delta V$ or $\int_{V_1}^{V_2} C_\phi dV$ if $\Delta V = V_2 - V_1$, and a corresponding change θ occurs determined by the difference of θ at V_2 compared with V_1, according to eqn.[2.14].

4.1.2. Theory of the Potential Relaxation Transient Method

A simple electrode charge-transfer reaction under kinetic control may be described by an electrical equivalent circuit in which the double-layer capacitance and Faradaic resistance associated with the electrochemical reaction are in parallel. The capacitance will be discharged after the current is interrupted, the discharge current-density i being expressed as :

$$i = - C (dV/dt) \quad [4.1]$$

The kinetics of the electrode process, characterized by a rate equation, which

determines the current density i, is given by

$$i(V) = i_o \exp(\alpha FV/RT) \qquad [4.2]$$

where 2.303 (RT/αF) = b, the Tafel slope [dV/d(log(i))]; the polarization conditions are for the potential region where the back reaction can be neglected. Then combining eqns. [4.2] and [4.2] gives :

$$-C\,(dV/dt) = i(V) \qquad [4.3a]$$

$$= i_o \exp(\alpha FV/RT) \qquad [4.3b]$$

where C is the total capacitance of the electrode interface, which may be potential-dependent, and i(V) is the internal, also potential-dependent, self-discharge current assumed to have the same potential-dependence as the steady-state, experimentally measured current-density[123-125]. It is considered that, under certain conditions, the double-layer capacitance and the C_ϕ for the electroactive adsorbed intermediates at appreciable coverage can be represented as though in parallel in an equivalent circuit.

The simplest case is when C is constant, i.e. for the pseudocapacitance, C_ϕ =0 and the double-layer capacitance, C_{dl}, being to a good approximation, a potential-independent constant, then eqn. [4.3b] can be integrated easily as :

$$\int -\exp(-\alpha FV(t)/RT)\, dV = \int (i_o/C)\, dt \qquad [4.4]$$

so that :

$$(RT/\alpha F) \exp(-\alpha FV(t)/RT) = (i_o/C)(t+\tau) \qquad [4.5a]$$

and $$\tau = (b'RT/\alpha F)(C/i) \qquad [4.5b]$$

or eqn.[4.5] can be written in the simple form :

$$V(t) = a - b \log(t + \tau) \qquad [4.6]$$

in which $a = -b \log(i_o/b'C)$ and $b = \alpha F/RT$.

From eqn.[4.5], it is seen that the decay of potential, V(t), follows a linear relationship with log(t+τ) having a slope of -b, the negative of the Tafel slope. The integration procedure involves a constant, τ, that usually can be obtained empirically[123-125]. However, in the present work, the appropriate τ value was evaluated by a computer program by fitting the experimental V(t) data with a nonlinear

approximation method. Furthermore, it can be seen that dV/d(log(t)) = -b', as $\tau << t$. Also evaluation of the capacitance (usually the double-layer capacitance C_{dl}) can be made from τ knowing $i_{t=0}$, the current-density before interruption, and the Tafel slope,b.

Alternatively, if integration between finite limits is applied, eqn.[4.3] could be expressed in the form :

$$\exp(-\alpha nFV/RT)\, dV = i_o/C\, dt \qquad [4.6]$$

Then, after some re-arrangement eqn.[4.6] can lead to [126-127]:

$$V = V_{t=0} + (RT/\alpha nF) \ln[(\alpha nFi_{t=0}/CRT)t + 1] \qquad [4.7]$$

where $i_{t=0}$ is the current-density before the interruption and $V_{t=0}$ is the potential immediately after the interruption. The difference between the potential just before the interruption V_{int} and $V_{t=0}$ also gives the uncompensated ohmic iR drop in the solution. Differentiating eqn.[4.7] with respect to t and rearranging the resulting equation yields :

$$dt/dV = C/i(t=0) + (\alpha nF/RT)t \qquad [4.8]$$

This eqn. indicates the plots of dt/dV against t will give a straight line, of which the slope and the intercept are $\alpha nF/RT$ and $C/i(t=0)$, respectively. Once these values are obtained, it is possible to plot the values of $\exp(\alpha nFV/RT)$ against t. The plot will also be linear and the V(t=0) value can be evaluated.

If the back reaction is significant, as at low overpotentials, a similar procedure can be applied to the analysis of the potential decay behaviour by writing the following equation, related to eqn.[4.3a]:

$$-C(dV/Dt) = i$$

$$= i_o [\exp(\alpha FV/RT) - \exp(-(1-\alpha)FV/RT)] \qquad [4.9]$$

in a Butler-Volmer type representation of i at low overpotential,V.

Often, the capacitance is by no means found to be constant, which means that C(V) itself is a function of potential in some way, e.g. $C_\phi \neq 0$. For such a condition, $C_\phi >> C_{dl}$ in most cases. The integration of eqn.[4.3] then has to be reconsidered if C(V) is also dependent on potential, a case of special interest in this work. In the usual way

of treating of potential decay results, the C vs V relation can be assumed [124] to take the two limiting forms, corresponding to low(-) or high(+) coverage:

$$C(V) = C_o \exp(\pm V/d) \qquad [4.10]$$

Then, with this equation applied to eqn.[4.3],

$$-\exp[(-V(t)/b')]\, dV = (i_o/C_o) \exp(\pm V/d)\, dt$$

is obtained; i.e.

$$-\exp[-V(t)\ (1/b' \pm 1/d')\ ]\, dV = i_o/C_o \qquad [4.11]$$

which leads to

$$dV/d(\ln (t+\tau)) = 1/(\ 1/b' \pm 1/d') \qquad [4.12]$$

Therefore, when C_ϕ is significant and dependent on V, the V vs log(t+τ) relation might not be a straight line any more, but could be represented by two or more linear regions depending on the behaviours of the intermediates adsorbed on the electrode surface. The numerical values for the slopes of the linear region will not any longer be necessarily equal to the Tafel slope dV/d(ln(i)). Generally, the plot may be a curve with limitingly linear regions.

Another plot that can be obtained from the potential relaxation data is V vs log(-dV/dt). This arises from eqn.[4.3] after rearrangement; viz.

$$C = i_o \exp(V/b)/(-dV/dt) \qquad [4.13]$$

which, in logarithmic form, is :

$$\ln C = -\ln (-dV/dt) + \ln i_o + V(t)/b' \qquad [4.14]$$

In the limiting case, with C constant and $C = C_{dl}$ with $C_\phi = 0$, the plot log(-dV/dt) vs. V(t) will be linear having a slope equal to -b (Tafel slope). Knowing i_o, the interfacial capacitance can be evaluated from the slope and the intercept. However, the pseudocapacitance, C_ϕ, for the adsorbed intermediates, is usually a function of potential so that the total capacitance, $C = C_\phi + C_{dl}$, will not generally be constant. Then the plot of log(-dV/dt) against V(t) will not necessarily be linear and will not have a slope equal to -b. Analogous to the plot of log(t) vs V for this case, more than one slope would then be observed for the log(-dV/dt) vs. V(t) plots as is experimentally

observed for some cases.

4.1.3. Evaluation of the Interfacial Capacitance

In order to obtain adsorption information relevant to the kinetic and mechanistic behaviour of the electrode process at the interface, it is necessary to evaluate the pseudocapacitance, the component due to the adsorbed species, which can lead to information about the coverage by the adsorbed intermediates in the reaction as a function of potential. The following are a list of several ways of evaluating the interfacial capacitance from potential transient or modulation methods :

(a) By knowing the exchange current-density, Tafel slope and the constant τ (eqn.[4.5b]), the capacitance can be estimated from the intercept of the log(t) vs V(t) plot. Thus, according to eqn.[4.6]:

when $V(t) = 0$,

$$-\log(i_o/b'C) = \text{intercept (on t axis)} \qquad [4.15]$$

or from eqn.[4.5].

(b) From eqn.[4.14] , the capacitance can also be estimated from the intercept of log(-dV/dt) on the V(t) plot when the exchange current density is known. Thus,

when $V(t) = 0$,

$$(2.303RT/\alpha F)\log(i_o/C) = \text{intercept (on t axis)} \qquad [4.16]$$

(c) According to eqn.[4.8], the intercept of the plot of dt/dV vs t can be expressed, when t = 0, by :

$$C/i(t=0) = \text{intercept (on Y axis)} \qquad [4.17]$$

so that , if the current before interruption is known, the capacitance can be evaluated for that initial potential corresponding to i(t = 0).

(d) A more general treatment of the potential decay data involves the use of the actual i(V) data from the steady-state polarization measurement in the derivation of C(V). From eqn.[4.1], the i(V) and (dV/dt) from separate experimental measurements are combined to derive a C(V) vs V relation according to :

$$C(V) = C_\phi + C_{dl}$$
$$= i(V)/(-dV/dt) \qquad [4.18a]$$

so that

$$\log C(V) = \log (i(V)) - \log (-dV/dt) \qquad [4.18b]$$

Therefore, C_ϕ as a function of V can be directly evaluated from the experimental i(V) and related dV/dt data without any empirical parameters being involved or any assumption being made about the form of the adsorption isotherm for the electroactive species.

(e) A different kind of basis for evaluation of capacitance arises in the a.c. impedance method as will described in section 4.2.

The different ways in which the capacitance can be evaluated have themselves limitations and approximations. Normally, approach (d) is more precise for evaluating the pseudocapacitance,C_ϕ, over a range of V's. However, the quantity obtained is the total interfacial capacitance C which is taken as approximately equal to $C_\phi + C_{dl}$. The C_ϕ is of general interest in electrode kinetics and in particular here for evaluation of the adsorption behaviour of Cl^- in the Cl_2 evolution reaction. Here, two limiting cases can arise ; (i) when $C_\phi >> C_{dl}$ and is potential-dependent; (ii) when $C_\phi \rightarrow 0$, i.e. $C = C_{dl}$, so that C is approximately independent of potential.

In the case of $C = C_{dl}$, potential relaxation takes place[124] simply by self-discharge of the double-layer capacitance through the continuing passage of electronic charge across it at a rate determined by the potential-dependent Faradaic resistance as characterized by the charge transfer kinetics. When $C_\phi >> C_{dl}$ and the electrode surface is appreciably covered by the reaction intermediates, the relationship between the Tafel slope b and the potential decay slope d, [$d = d\log(-dV/dt)/dV$], can be derived from eqn.[4.14]; viz.

$$d \log(C(V))/dV = 1/b - 1/d \qquad [4.19]$$

From eqn.[4.19], it can be seen that, when $d = b$, $d \log(C(V))/dV = 0$, which means the interfacial capacitance is independent of potential; when $d > b$, d

$\log(C(V))/dV > 0$, which indicates that the capacitance increases as the potential is numerically increased while for $d < b$, $d \log(C(V))/dV < 0$, the capacitance decreases as the potential is increased. From the derived C_ϕ vs V data, the coverage, or the change of the coverage, can be calculated as a function of V ($f(\theta)$ vs V) by integration of the experimentally determined C_ϕ vs V profile (see eqn. [2.39])

4.1.4. Interfacial Capacitance Evaluation from Initial Decay Curves by the "Fitting Method"

Fitting the potential decay curves, digitally recorded on an open-circuit following the interruption of a polarizing current of the electrode reaction, is used to obtain the interfacial capacitance behaviour of the electrode together with the uncompensated solution resistance in the electrochemical cell during a continuous Faradaic process. This method has been developed recently in this laboratory. The basic idea of this "fitting method" is that the digitized potential relaxation transients are empirically represented* by a polynomial function :

$$V(t) = a_0 + a_1 t + a_2 t^2 + a_3 t^3 + a_4 \log(t + a_5) \qquad [4.20]$$

by computer fitting of the data of each transient to the above function. Such a third-order polynomial, plus the log term, provides an excellent empirical fit for the transients with different values of the constants a_0 to a_5 for each transient recorded. Extension to a fifth or sixth order polynomial gives no further improvement.

This procedure enables both V(t=0) and $(dV/dt)_{t=0}$ to be accurately evaluated, for t = 0, i.e. just after the current interruption has taken place. Since eqn.[4.20] corresponds to the following expression when t = 0 :

$$V(t=0,i=0) = a_0 + a_4 \log(a_5) \qquad [4.21]$$

the " iR " drop, $\Delta V = V(i) - V(t=0,i=0)$, can be accurately determined and gives the

---

* The fitting function [4.20] has no fundamental meaning and is applied only to represent accurately the observed V(t) transient over relatively short time in order to estimate by extrapolation, the dV/dt at t = 0 and V(t=o).

uncompensated resistance as this ΔV divided by i. The differential of eqn.[4.20] is:

$$(dV/dt)_t = a_1 + 2a_2t + 3a_3t^2 + a_4/(t + a_5) \quad [4.22]$$

Then, when t = 0 :

$$(dV/dt)_{t=0} = a_1 + a_4/a_5 \quad [4.23]$$

From the curve fitting constants a_0 to a_5, the capacitance, C, can hence be directly evaluated from $(dV/dt)_{t=0}$ and the current-density i(V), before the current interruption, from the equation :

$$C = i(V)/(-dV/dt)_{t=0} \quad [4.24]$$

The uncompensated solution resistance, " R ", is also obtained as :

$$R = (V(i) - V(t=0,i=0))/i(V) \quad [4.25]$$

The resulting values are in good agreement with those obtained by the conventional current interruption method or by means of a. c. impedance as well.

This curve fitting technique has a number of advantages over other methods for the evaluation of the apparent capacitance of the electrode interface :

(a) No assumptions are made about the change of capacitance with overpotential in the derivation of the equation.

(b) Only the steady-state current-density before the opening of the circuit, together with the potential decay curve in digitized form, are required as the basic experimental data.

(c) The capacitance is obtained directly from eqn.[4.24] using the current density before the opening of the circuit, together with the derivative of the potential decay curve (eqn.[4.22]) at t = 0, obtained from the curve fitting function. Further discussion of the application and possible limitations of this curve fitting method will be given in later chapters.

4.1.5. "Kinetic Constants" Simulation of the Potential Decay Transient

The kinetic theory of open-circuit potential decay behaviour was recently given by Harrington and Conway [128], extending the treatment of Tilak and Conway[129,130] for the

case of the hydrogen evolution reaction. In the essential ways, the Cl_2 evolution reaction is formally very similar to that of hydrogen evolution, both in its kinetics and mechanism. However, since Cl_2 evolution is an anodic reaction and usually involves, in water, oxide film formation on the electrode, the reaction is rather more complicated than H_2 evolution. In this section, the Cl_2 evolution reaction will be treated in terms of the mechanistic model given in section (2.3), viz the electrosorption step (I) followed by either the " atom-ion " electrodesorption step (II) or the chemical recombination step (III) as parallel alternative steps, the faster of which will characterize the kinetics..

Since the oxidation of the electrode surface is also an anodic reaction, the following processes should be considered at the same time for Cl_2 evolution at Pt electrodes :

$$M + OH^- \longrightarrow MOH + e \qquad [IV]$$

$$MOH + OH^- \longrightarrow MO + H_2O + e \qquad [V]$$

where the adsorbed OH can easily be replaced competitively by Cl^- [80], but the adsorbed O species is more irreversibly generated and cannot be displaced by Cl^- ion. Therefore, the O species ,in fact, will occupy some of the surface area and reduce the "active area" fraction available for Cl^- and $Cl^\cdot$ adsorption and desorption in the Cl_2 evolution reaction.

In this treatment, there no assumption is made about which step is rate-determining, only mass transfer effects are considered to be negligible, so that the surface concentration of Cl^- (and Cl_2) are assumed to be constant. For the case where Langmuir adsorption behaviour applies (eqns. [2.29] to [2.32]) the net rate of Cl_2 evolution (steps I, II and III), can be written in the form :

$$v_1 = k_1(1-\theta)\exp(\beta FV/RT) - k_{-1}\theta\exp(-(1-\beta)FV/RT) \qquad [4.26]$$

$$v_2 = k_2\theta\exp(\beta FV/RT) - k_{-2}(1-\theta)\exp(-\beta FV/RT) \qquad [4.27]$$

$$v_3 = k_3\theta^2 - k_{-3}(1-\theta)^2 \qquad [4.28]$$

where θ is the coverage by the Cl· intermediate. The Faradaic current is proportional to the rate of electron production, r_o (mole cm^{-2} s^{-1}) which, in the case of Cl_2 evolution, is equal to the sum of v_1 and v_2 (eqns.[4.26] and [4.27]). The contribution by oxygen evolution is assumed to be too small to consider. Hence :

$$i_f/F = r_o(\theta, V) = v_1 + v_2 \qquad [4.29]$$

Likewise, dθ/dt is proportional to r_1, the rate of production of MCl·, which is equal to v_1 minus v_2 and twice v_3, i.e.

$$(q_o/F)(d\theta/dt) = r_1(\theta, V) = v_1 - v_2 - 2v_3 \qquad [4.30]$$

where q_o is the charge required per cm^2 for complete monolayer coverage by the Cl· intermediate. Since the MO adsorption is irreversible, it will not make a significant contribution to dθ/dt, so that eqns.[4.29] and [4.30] can therefore still be applied to anodic Cl_2 evolution in an approximate but fairly reliable way.

If double-layer capacitance is taken into account, assuming the simple Helmholtz parallel plate model, on opening the circuit, the potential difference, V, across the double-layer must be reduced by diminution of the "charge on each plate". In the case of the anodic Cl_2 reaction, each electron being transferred from adsorbed Cl· to the metal across the interface effects an elementary act of reaction and reduces the charge, q_o. As a result, the rate of reduction of this charge is equal to the faradaic current, leading to eqn.[4.31]:

$$i_f = -dq/dt = (-dq/dV)(dV/dt) = -C_{dl}(dV/dt) \qquad [4.31]$$

Combining eqns. [4.29] and [4.31] gives a relation for dV/dt in terms of the kinetics of the reaction :

$$-(C_{dl}/F)(dV/dt) = r_o(\theta, V) = v_1 + v_2 \qquad [4.32]$$

Solution of eqns. [4.30] and [4.32] leads to determination of the time evolution of V and θ during the decay of potential. However, these equations can only be solved numerically by Harrington's program (available in this laboratory) which enables V(t) and θ(t) to be found, given the (θ,V) dependence of v_1, v_2 and v_3. The potential decay transients, V(t), thus obtained, may be compared directly with the appropriate

experimental transient, and the rate constants which represent the behavicur can then be derived by seeking the best agreement between the calculated and experimental transients for various rate constant values required to simulate the experimentally observed V(t) behaviour.

4.2. Theory of A.C. Impedance Behaviour of Electrode Reactions*

4.2.1. General Introduction

A.c. impedance spectroscopy has been widely applied to the study of electrochemical systems, especially in recent years, but originating in about 1947. Randles[131] introduced the so-called "Randles circuit" for first order, single step reactions, and later Gerischer[132,133] considered the case of an homogeneous chemical reaction step coupled to a charge transfer step. Lorenz[134,135], following an approximate treatment by Gerischer, dealt with the impedance due to adatoms in metal deposition but without taking into account diffusion effects that were considered later by Rangarajan, Fleischmann and Thirsk[136]. The impedance associated with adsorbed intermediates in the hydrogen evolution reaction was first treated by Gerischer and Mehl[137] and extensively by Epelboin[138]. The a.c. impedance behaviour of multistep reactions involving adsorbed intermediates was treated by Armstrong and coworkers[139-145].

The basic principle of the a.c. impedance technique is the application of a small amplitude (± 5mV) sinusoidal voltage or current signal, so that, a response current or potential signal, respectively, is generated. By analysis of the ratio of the amplitudes and phase shift, Φ, between the voltage and current, the impedance can easily be evaluated. A wide range of frequencies is scanned; in modern work from mHz to

---

* This is a major topic about which many papers have been written. Therefore, only a brief description of relevant aspects, required for the work, will be given here. For a more detailed review see e,g. ref. 146-151.

hundreds of kHz.

The electrodynamic theory of sinusoidally alternating currents and voltages is based on relatively simple laws. In order to introduce the principles involved, it is necessary first to consider the relation between electrical current and applied voltage in the cases of an ohmic resistor, a capacitor and an inductor, following from their phenomenological definitions.

If the alternating voltage is given by :

$$V = V_m \sin(\omega t) \qquad [4.33]$$

then : (i) the resulting current for a resistance R would be :

$$i = (V_m/R) \sin(\omega t) \qquad [4.34]$$

(ii) the resulting current for a capacitance C would be :

$$i = dq/dt = C\,(dV/dt)$$

$$= \omega C V_m \sin(\omega t + \pi/2) \qquad [4.35]$$

so that a phase shift of $+\pi/2$ is introduced for the response of a purely capacitative component.

And (iii) for an inductance L :

$$V = L\,(di/dt)$$

$$i = 1/L \int V dt = (V_m/\omega L) \sin(\omega t - \pi/2) \qquad [4.36]$$

so that a phase shift of $-(\pi/2)$ is introduced for an inductive component. In all these cases, it follows that the time dependence of current and voltage have the same mathematical form, i.e. both i and V are sinusoidal functions of time.

The impedance Z is defined as a vector with modulus $| Z | = V_m/i_m$ and phase angle Φ. According to the graphical representative in Fig.4.1 :

$$Z' = | Z | \cos \Phi \qquad [4.37]$$

$$Z'' = | Z | \sin \Phi \qquad [4.38]$$

The corresponding admittance Y, is equal to $1/| Z |$, so that similarly :

$$| Y | = Y' \cos \Phi \qquad [4.39]$$

and

$$| Y | = Y'' \sin \Phi \qquad [4.40]$$

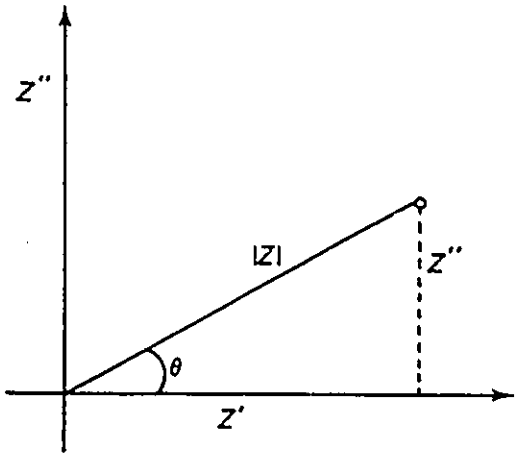

Fig.4.1 Impedance plotted in the complex plane.

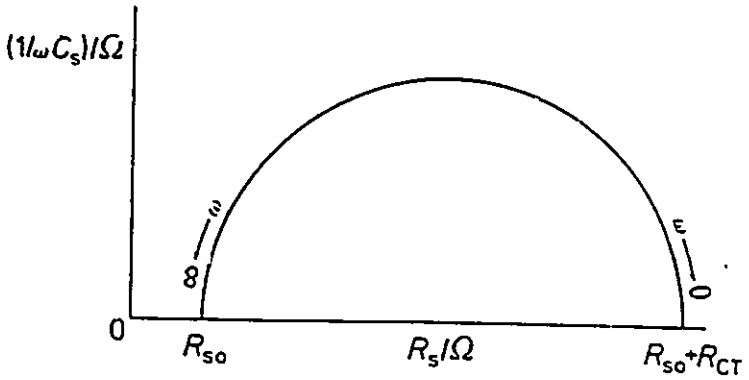

Fig.4.2 Complex-plane spectrum impedance for a R-C in parallel circuit

The Fig.4.1 represents the impedance behaviour, analogous to that of a complex number a + jb, represented in the so-called " complex plane " plot, in which the real component is plotted as the abscissa and the imaginary component as the ordinate. This leads to definitions of impedance and admittance in terms of the complex quantities:

$$Z = Z' - jZ'' \qquad [4.41]$$

$$Y = Y' + jY'' \qquad [4.42]$$

where Z' and Y' are the real components and Z" and Y" are the imaginary components of the impedance or admittance, respectively.

The complex plane type of plot was first applied by Cole and Cole[152] in their study of relaxation effects in dielectric polarization of a polar medium. They plotted the real vs the imaginary components of the dielectric constant giving a so-called Argand diagram. It was recognized by Rehbach and Sluyters[153] in 1961 that a similar expression could be applied to the kinetic behaviour of electrode processes. Later, the complex-plane method of analysis became very widely used in many treatments of the kinetics of surface and other processes at electrodes by various authors, e.g. Armstrong et al [140-145] and Epelboin and Keddam et al [138,154].

For the simplest case, the interfacial process can be described by an equivalent circuit comprised of only a resistance (R_π) and a capacitance (C_π) in parallel, with (R_{so}) a solution resistance in series. Upon plotting the real part, R_π against the imaginary part, $1/\omega C_\pi$, a semi-circle is obtained in the complex-plane plot, (see Fig.4.2). If a diffusion process is involved, a so-called Warburg impedance component (W) arises and can be derived from Fick's laws. In this case, the impedance relationship between Z' and Z" in the complex plane is a straight line of slope 45°. Another representation that has been used is the so-called "Randles plot", first proposed by Randles[131] and also by Ershler[155] in 1947. The Randles method involves plotting R_π and $1/\omega C_\pi$ against $\omega^{-1/2}$ in order to extrapolate the effects of diffusion which depend on the square-root of the frequency. From Fig.4.3, the R_π and $1/\omega C_\pi$ vs. $\omega^{-1/2}$ plots are two parallel straight lines, one of them, $1/\omega C_\pi$ vs $\omega^{-1/2}$ extrapolates through zero, but the other R_π vs $\omega^{-1/2}$ has an intercept on the Z axis, giving the value of R_{ct}.

Besides the Randles and the complex plane plots, there is an alternative method, the so-called "Bode plot"[156], that can be used to represent a.c.
impedance behaviour, since ln (Z) can be represented as :

$$\ln (Z) = \ln (X + jY) = \ln (|Z| e^{j\Phi})$$
$$= \ln |Z| + j\Phi \qquad [4.43]$$

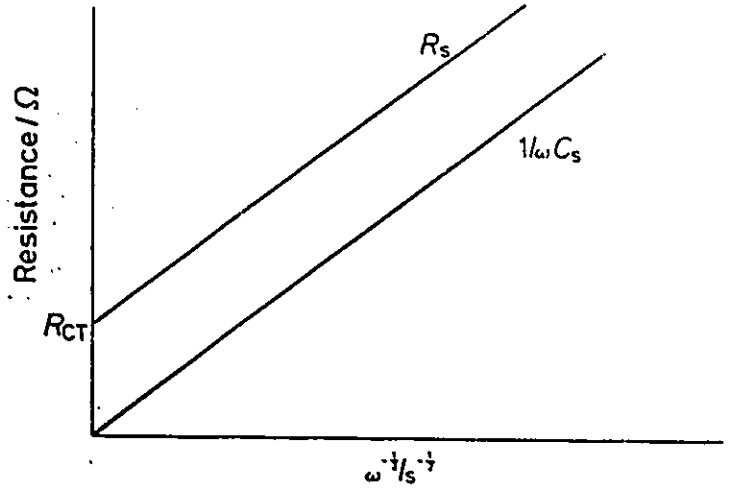

Fig.4.3 The Randles method: plots of $1/\omega C_s$ against $\omega^{-1/2}$.

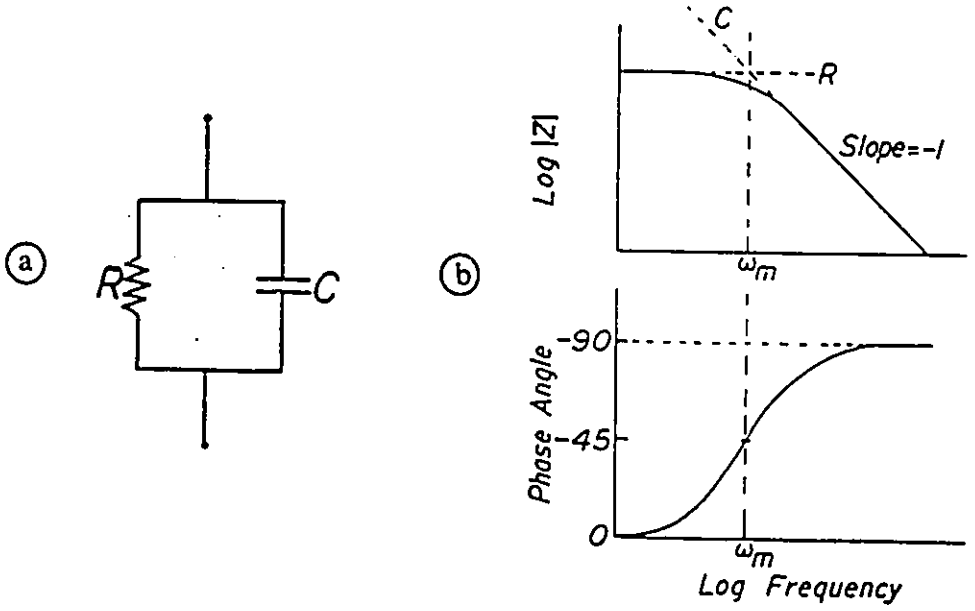

Fig.4.4 (a) A parallel R-C circuit; (b) Bode and phase angle plots for the circuit shown in (a).

where Φ is the phase angle. It can be seen that a plot of both the logarithm of | Z | and Φ vs. log [frequency] can be employed to provide a description of impedance behaviour; such graphs are referred to as "Bode plots".

In such a plot, the impedance of a " perfect capacitance " can be represented as a straight line with a slope of -1 and a phase angle of -90°. For a pure resistance, the plot will be a horizontal line for log | Z | with a phase angle of 0°. A Warburg impedance is represented by a straight line with a slope of -1/2 and a phase angle of -45°. Fig.4.4a shows the impedance of a series and a parallel RC configuration and Fig.4.4b represents the corresponding, Bode plots, i.e. log | Z | vs log frequency and the phase angle vs log frequency. More complex networks can also be resolved by visual inspection of the Bode plots. In a later discussion, the complex-plane and Bode plot methods will be used to present a.c. impedance results.

4.2.2. Equivalent circuits

Even in early works, electrochemists considered the kinetics of electrode processes as equivalent to certain kinds of electrical circuits consisting of resistance and capacitance components in order to represent the observed electrode kinetic behaviour. For example, Helmholtz considered the compact double-layer as a model "capacitor" which, after some modification by other workers, became well accepted as a basis for the representation of the electrode (and colloid interfaces). In treatments of a.c.impedance, it is also useful to apply the equivalent circuit concept in the analysis of the experimental data. Equivalent circuits of the electrode interface are comprised of a double-layer capacitance, a charge-transfer resistance, a pseudocapacitance and possibly also a Warburg impedance if diffusion is involved. Fig.4.5 exemplifies six different equivalent circuits for various electrode processes. Circuit (a) is for a simple kinetic charge-transfer process occurring across an interface exhibiting a double-layer capacitance and which gives a semi-circle in the complex-plane plot, lying on the ohmic resistance (Z') axis. The circuit (b) is for a process

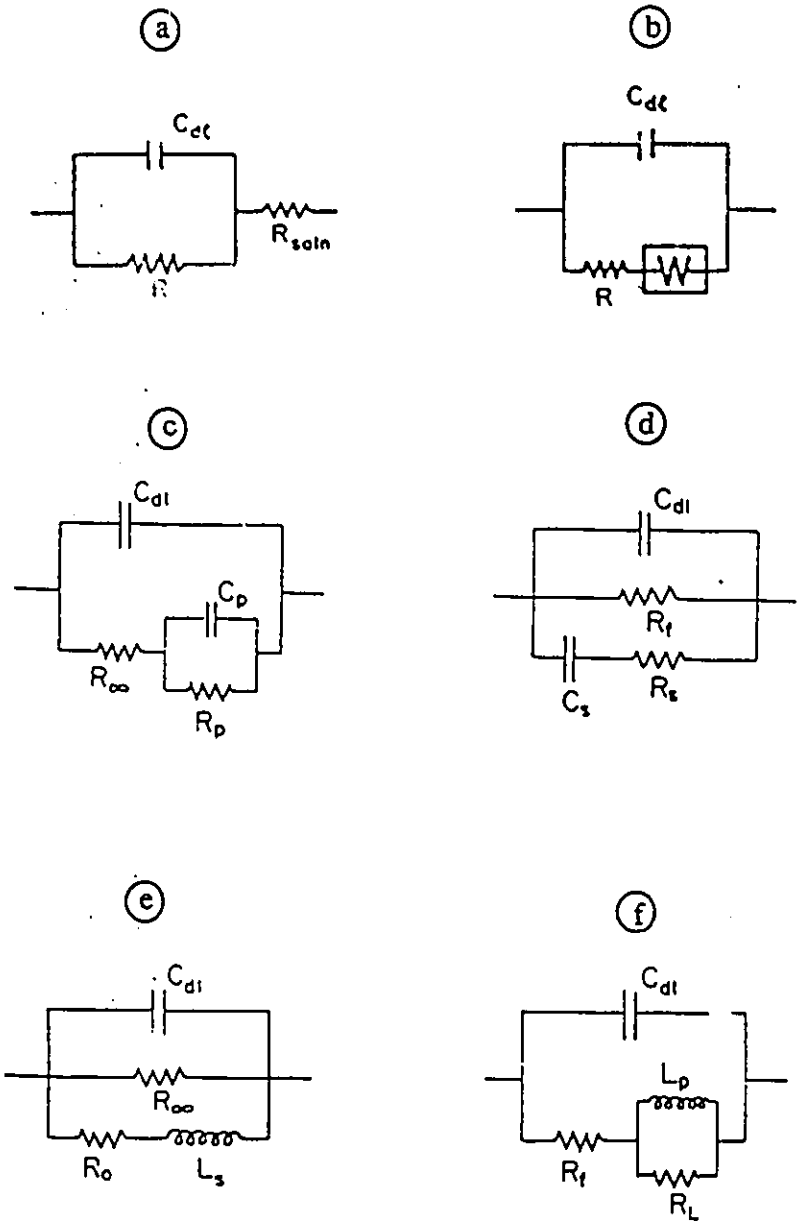

Fig.4.5 Six different equivalent circuits for various electrode processes.

coupled with diffusion which gives rise to a Warburg impedance generating a straight line of 45° slope in the complex-plane plot. The circuits (c) to (f) are for more complicated cases of electrode interfacial kinetic behaviours involving one or more adsorbed intermediates. In particular, they involve an additional component, the pseudocapacitance, C_ϕ, associated with the potential dependence of coverage by adsorbed intermediates. Circuit (c) has been given by Armstrong[139-145], and both (d) and (e) have been used by Epelboin and his co-workers[138,154]. The capacitative components are usually used, for example, to represent the behaviour of the hydrogen evolution reaction while circuits involving an inductive element are required to represent the phenomenon of passivity, leading to S-shaped i vs V profiles. This kind of behaviour results from negative resistance and capacitance which correspond to a pseudoinductance element.

4.2.3. Fitting Observed Impedance Behaviour to that of Model Equivalent Circuits

The basic idea for representing electrode reaction behaviour in terms of an equivalent circuit involves the choice of circuit elements of various values in an arrangement that mimics the observed frequency response of the experimentally studied electrode process. Circuit (c) in Fig.4.5 would be used, for example, to deal with the Cl_2 evolution reaction, where the experimentally acquired impedance spectrum would be fitted by various values of the equivalent circuit components. For circuit (c), the overall impedance can be expressed by :

$$Z = \{[R_\infty + (1/(j\omega C_p + 1/R_p))]^{-1} + j\omega C_{dl}\}^{-1} \qquad [4.44]$$

Then, according to eqn.[4.41], after the necessary mathematical operations have been performed, the real, Z' and the imaginary, Z", components can be extracted as the following quantities by rationalization of the complex terms involved :

$$Z' = \frac{R_\infty + R_p + R_\infty(\omega C_p R_p)^2}{(1 - \omega^2 C_{dl} C_p R_\infty R_p)^2 + \omega^2(C_{dl}R_\infty + C_{dl}R_p + C_p R_p)^2} \qquad [4.45]$$

and

$$Z'' = \frac{\omega[C_{dl}(\omega C_p R_- R_p)^2 + 2C_{dl}R_- R_p + C_{dl}R_-^2 + C_{dl}R_p^2 + C_p R_p^2]}{(1-\omega^2 C_{dl}C_p R_- R_p)^2 + \omega^2(C_{dl}R_- + C_{dl}R_p + C_p R_p)^2} \qquad [4.46]$$

where R_-, R_p, C_{dl} and C_p, (see Fig.4.5c), as well as all constant parameters would be determined by means of the fitting procedure. These quantities may be varied in a computer-based fitting procedure until the calculated behaviour, according e.g. to eqns.[4.45] and [4.46], becomes a best fit to the experimental variation of Z' and Z" with ω. From the analysis of the best fit parameters, the best representation of the impedance response of e.g. the Cl_2 evolution reaction, is obtained since:

(i) $\underline{R_-}$ is the electron transfer faradaic resistance associated with the Cl^- electrosorption (step I), which indirectly provides explicit information about the activation energy barrier for the Cl^- discharge and adsorption step, and the oxidation state of the electrode surface. Oxidation of the electrode surface (Pt) would lead to larger values of R_-, which means the step of Cl^- adsorption would be more difficult (see the example treated in Chapter V).

(ii) $\underline{R_p}$ is the resistance related to desorption of the Cl^- intermediate in steps II or III. Small R_p values would indicate a fast Cl^- desorption rate in either step (II) or (III); of course, the faster one (smaller R_p) would contribute most to R_p (for Cl_2 evolution at Pt, step (III), the recombination pathway, is found to be dominant).

(iii) $\underline{C_{dl}}$ is the well known double-layer capacitance having values between ca. 20 to 40 μF cm^{-2}. It can provide information on interfacial structure and an estimate of the real surface area of the electrode.

(iv) $\underline{C_p}$ is the capacitative component due to the adsorption behaviour of the intermediate on the surface of the electrode. It gives information concerning the pseudocapacitance and coverage by the adsorbed species but it is not exactly numerically equal to the value of pseudocapacitance, C_ϕ. C_p is, however, as important

as C_ϕ in understanding the kinetic and mechanistic behaviour of an electrode reaction (here the Cl_2 evolution reaction) as it is related to the potential dependence of the steady-state coverage of the electrode surface by intermediates and is hence related in an important way to the electrocatalysis in the process involved.

4.2.4. Simulation Approach to the Kinetic Behaviour by Fitting through Assignment of Kinetic Rate Constants

An alternative and important approach, proposed by Harrington and Conway[157] and later with Bai[158], to analysis of the a.c. impedance spectrum is by simulation through fitting behaviour kinetically in terms of the appropriate rate constants. With respect to the mechanism model for Cl_2 evolution given in section (2.3), with steps (I), (II) and (III), the rate of electron transfer and production of adsorbed "MCl" species can be represented by eqns.[4.29] and [4.30]. It is convenient to rewrite these equations as :

$$i/F = r_o = v_1 + v_2 \qquad [4.47]$$

$$(q_1/F)(d\theta/dt) = r_1 = v_1 + v_2 + 2v_3 \qquad [4.48]$$

where r_o again is the net rate of electron transfer; it is a function of potential, coverage and concentration of adsorbed species, i.e. $r_o = f((\theta,V,C_{Cl^-})$. r_1 is the net rate of production of the adsorbed intermediate; similarly, $r_1 = f(\theta,V,C_{Cl^-})$. For simplicity, the actual observed behaviour of the Cl_2 evolution reaction studied in the present work, kinetics without influence from diffusion will be considered :

Then $$r_o = f(\theta, V) \qquad [4.49]$$

and $$r_1 = f(\theta, V) \qquad [4.50]$$

In the a.c. measurements, a small amplitude sinusoidal a.c. component is applied which means :

$$V = V_{ss} + \Delta V\, e^{(jwt)} \qquad [4.51]$$

where V_{ss} is the steady-state potential. The response of i and θ, of course, will follow the same variation sinusoidally, viz.

$$\theta = \theta_{ss} + \Delta\theta\, e^{(jwt)} \qquad [4.52]$$

and $$i = i_{ss} + \Delta i\, e^{(jwt)} \qquad [4.53]$$

For small amplitude modulation, the rate of electron transfer and the corresponding rate of change of coverage can be expressed by using a Taylor expansion, neglecting second and higher order terms; then

$$i/F = r_o = r_{o,ss} + (\partial r_o/\partial V)\Delta V + (\partial r_o/\partial\theta)\Delta\theta \qquad [4.54]$$

and $$(q_o/F)(d\theta/dt) = r_1 = (\partial r_1/\partial V)\Delta V + (\partial r_1/\partial\theta)\Delta\theta \qquad [4.55]$$

since :

$$d\theta/dt = jw\Delta\theta; \qquad [4.56]$$

$$r_o - r_{o,ss} = \Delta r_o = \Delta i/F \qquad [4.57]$$

and $$r_1 - r_{1,ss} = (q_o/F)\, j\omega\Delta\theta \qquad [4.58]$$

combining eqns [4.54] to [4.58] leads to :

$$\Delta i/F = (\partial r_o/\partial V)_\theta\, \Delta V + (\partial r_o/\partial\theta)_V\, \Delta\theta \qquad [4.59]$$

and $$(q_o/F)j\omega\Delta\theta = (\partial r_1/\partial V)_\theta\, \Delta V + (\partial r_1/\partial\theta)_V\, \Delta\theta \qquad [4.60]$$

dividing eqns [4.59] and [4.60] by ΔV and rearranging then gives :

$$(1/F)\,(\Delta i/\Delta V) + (\partial r_o/\partial\theta)_V(\Delta\theta/\Delta V) = -(\partial r_o/\partial V)_\theta \qquad [4.61]$$

$$[(\partial r_1/\partial\theta)_V - (q_o/F)j\omega](\Delta\theta/\Delta V) = -(\partial r_1/\partial V)_\theta \qquad [4.62]$$

therefore;

$$\Delta\theta/\Delta V = \frac{\begin{vmatrix} (1/F) & -(\partial r_o/\partial V)_\theta \\ 0 & -(\partial r_1/\partial V)_\theta \end{vmatrix}}{\begin{vmatrix} (1/F) & (\partial r_o/\partial\theta)_V \\ 0 & [(\partial r_1/\partial\theta)_V - (q_o/F)j\omega] \end{vmatrix}} \qquad [4.63]$$

then;

$$\Delta\theta/\Delta V = (\partial r_1/\partial V)_\theta/[(q_o/F)j\omega - (\partial r_1/\partial\theta)_V] \qquad [4.64]$$

and

$$\Delta i/\Delta V = \frac{\begin{vmatrix} -(\partial r_o/\partial V)_\theta & (\partial r_o/\partial \theta)_V \\ -(\partial r_1/\partial V)_\theta & [(\partial r_1/\partial \theta)_V - (q_o/F)j\omega] \end{vmatrix}}{\begin{vmatrix} (1/F) & (\partial r_o/\partial \theta)_V \\ 0 & [(\partial r_1/\partial \theta)_V - (q_1/F)j\omega] \end{vmatrix}} \qquad [4.65]$$

and the admittance is given by :

$$Y_f \equiv \Delta i/\Delta V = F(\partial r_o/\partial V)_\theta + F^2[(\partial r_1/\partial V)_\theta(\partial r_o/\partial \theta)_V] / [j\omega - (F/q_o)(\partial r_1/\partial \theta)_V] \qquad [4.66a]$$

$$= A + B/(j\omega + C) \qquad [4.66b]$$

so that :

$$A = F\,(\partial r_o/\partial V)_\theta \qquad [4.67]$$

and

$$B = (F^2/q_o)(\partial r_1/\partial V)_\theta(\partial r_o/\partial \theta)_V \qquad [4.68]$$

$$C = -(F/q_o)(\partial r_1/\partial \theta)_V \qquad [4.69]$$

Consider the admittance for circuit (c) in Fig.4.5 :

$$Y_f = [\, R_\infty + 1/(1/R_p + j\omega C_p)\,]^{-1} \qquad [4.70]$$

Comparing eqns. [4.66] and [4.70] leads to :

$$R_\infty = 1/A \qquad [4.71a]$$

$$R_p = -B/[A(CA + B)] \qquad [4.71b]$$

$$C_p = -A^2/B \qquad [4.71c]$$

$$R_o = C/B \qquad [4.71d]$$

and

$$\tau_{ac} = [-(F/q_o)(\partial r_1/\partial \theta)_V]^{-1} = 1/C \qquad [4.71e]$$

where τ_{ac} is the relaxation time parameter defined by Armstrong[139-145]. It is usually accepted that the double-layer capacitance, C_{dl}, is in parallel with Y_f so that the total interfacial impedance will then be given by :

$$Z = 1/(Y_f + j\omega C_{dl}) \qquad [4.72]$$

Since r_1 is zero in the steady-state situation, its derivative with respect to V_{ss} is also equal to zero so that :

$$dr_1/dV_{ss} = (\partial r_1/\partial\theta)_V(d\theta_{ss}/dV_{ss}) + (\partial r_1/\partial V)_\theta = 0 \qquad [4.73]$$

This leads to :

$$C_\phi = -q_o(d\theta/dV_{ss})$$

$$= q_o(\partial r_1/\partial V)_\theta/(\partial r_1/\partial\theta)_V \qquad [4.74]$$

Because the derivative $(\partial r_1/\partial V)_\theta$ cannot be obtained from knowledge or assignment of values of the parameters A, B and C (see eqns. [4.71a-e]), it has to be calculated from the rate constants. Its value, however, is not quite the same as C_p which is the capacitance in the equivalent circuit (c), but the C_p is found to be similar to C_ϕ over a limited potential range and can be written as :

$$C_p = -A^2/B$$

$$= -q_o[(\partial r_o/\partial V)_\theta]^2 / [(\partial r_o/\partial\theta)_V(\partial r_1/\partial V)_\theta] \qquad [4.75]$$

Comparison of eqns.[4.74] and [4.75] shows that they will be equivalent if $-r_o$ and r_1 are identical functions of θ and V to within an additive constant. Another complex quantity, $q_o(\Delta\theta/\Delta V)$, demonstrates how the sinusoidal variation of charge for the adsorbed intermediate depends on the sinusoidal change of the potential; this quantity, also having the dimensions of capacitance, may be termed the a.c. pseudocapacitance, C_{ac}, viz :

$$C_{ac} = q_o/(\Delta\theta/\Delta V)$$

$$= q_o(\partial r_1/\partial V)_\theta/[j\omega q_o/F + (\partial r_1/\partial\theta)_V] \qquad [4.76]$$

The amplitude of its variation is :

$$| C_{ac} | = q_o|(\partial r_1/\partial V)_\theta|/[\omega^2 q_o^2/F^2 + (\partial r_1/\partial\theta)_V^2]^{1/2} \qquad [4.77]$$

From eqn.[4.77], it can be seen that C_{ac} is frequency dependent with maximum equal to C_ϕ when the frequency is limitingly equal to zero !

The evaluation of kinetic constants required to simulate the a.c. impedance spectrum is a rather cumbersome procedure. However, powerful computer software makes this possible. In the work presented in this thesis, this method is used to investigate the behaviour of the Cl· intermediate in the Cl_2 evolution reaction. Here again we should briefly rewrite relevant rate equations for the Cl_2 evolution steps (see

section (2.4.3) and eqns [2.29] to [2.32]) in a short form :

$$v_1 = k'_1(1-\theta) - k'_{-1}\theta \qquad [4.78a]$$

$$v_2 = k'_2\theta \qquad [4.78b]$$

$$v_3 = k'_3\theta^2 \qquad [4.78c]$$

where the back reaction terms in the rate equations for steps II and III are neglected because the analysis refers practically to appreciable overpotentials. By employing the steady-state assumption, the coverage for the intermediate species (here Cl·) can be derived by setting $d\theta/dt = 0$ and the coverage, θ, is then (see section 2.4.3 and equation [2.34]) :

$$\theta = -Lp/4k'_3 + [Lp^2 + 8k'_1k'_3]^{1/2} / 4k'_3 \qquad [4.79]$$

and

$$C_\phi = q_o d\theta/dV$$

$$= (q_o \beta F Lq/4RTk'_3) \{[(Lp/4k'_3 + k'_1/Lq)/$$

$$[(Lp/4k'_3)^2 + k'_1/2k'_3]^{1/2}] - 1\} \qquad [4.80]$$

where $Lp = k'_1 + k'_{-1} + k'_2$, $Lq = k'_1 - k'_{-1} + k'_2$.

Also, the steady state current is given by :

$$i = 2F(v_2 + v_3)$$

$$= 2F(k'_2\theta + k'_3\theta^2) \qquad [4.81]$$

Inserting eqns.[4.67] to [4.69] into eqns.[4.71a] to [4.71e], the expressions for R_∞, R_o, R_p, C_p and τ_{ac} are obtained, as follows :

$$1/R_\infty = F[(\partial v_1/\partial V)_\theta + (\partial v_2/\partial V)_\theta] \qquad [4.82a]$$

$$1/R_o = (F^2\tau/q_o)[(\partial v_1/\partial \theta)_V + (\partial v_2/\partial \theta)_V]$$

$$.[(\partial v_1/\partial V)_\theta - (\partial v_2/\partial V)_\theta] \qquad [4.82b]$$

$$R_p = - R_\infty^2/(R_o + R_\infty) \qquad [4.82c]$$

$$\tau_{ac} = (F/q_o)[2(\partial v_3/\partial \theta)_V + (\partial v_2/\partial \theta)_V - (\partial v_1/\partial \theta)_V] \qquad [4.82d]$$

$$C_p = -R_o\tau/R_\infty^2 \qquad [4.82e]$$

From eqns.[4.78a-c] :

$$(\partial v_1/\partial V)_\theta = (\beta F/RT)[k'_1(1-\theta) + k'_{-1}\theta] \qquad [4.83a]$$

$$(\partial v_2/\partial V)_\theta = (\beta F/RT)k'_2\theta \qquad [4.83b]$$

$$(\partial v_1/\partial\theta)_V = -k'_1 - k'_{-1} \qquad [4.83c]$$

$$(\partial v_2/\partial\theta)_V = k'_2 \qquad [4.83d]$$

$$(\partial v_3/\partial\theta)_V = 2k'_3\theta \qquad [4.83e]$$

The real and imaginary components, Z' and Z" can be calculated from :

$$Z' = Y'/(Y'^2 + Y''^2) \qquad [4.84a]$$

$$Z'' = Y''/(Y'^2 + Y''^2) \qquad [4.84b]$$

where

$$Y' = 1/R_\infty + i/[R_o(1+\omega^2\tau^2)] \qquad [4.85a]$$

and $$Y'' = \omega\{C_{dl} - \tau/[R_o(1+\omega^2\tau^2)]\} \qquad [4.85b]$$

The simulation procedure consists of selecting a set of k_i constants to evaluate the parameters C_p, R_∞, R_o, R_p and τ_{ac} through eqns.[4.82] and [4.83] so that both the real part, Z', and the imaginary part, Z", of the complex impedance can be obtained by numerical simulation, giving the best fit to the experimentally evaluated frequency dependence of Z' and Z".

If the simulated behaviour is not in good agreement with the experimental data, this means that the set of constants is not that for a best fit. Therefore, a further set of rate constants must be used until those corresponding to the best-fit constants are found. From the best fit rate constants thus evaluated, the C_p, R_∞, R_o, R_p, τ_{ac}, C_ϕ and θ can all be evaluated from the corresponding equations shown above. The set of best-fit rate constants is not only potential independent but also should fit the steady-state current as well. One thing that has to be emphasised is that the set of best-fit rate constants is not necessarily the only possible set; however, it is usually difficult to find another equivalent set of rate constants as good as the set of best-fit values, ?? in ?? that the optimized set fit the impedance behaviour not only over a wide range of frequencies but also for different d.c.-level potentials.

CHAPTER V

Results and Discussion: Study of the Cl_2 Evolution Reaction at Platinum Electrodes

Results of the investigations of the Cl_2 evolution reaction at Pt electrodes will be presented in this chapter. The reactions conducted in aqueous 1 N HCl and 0.9 N NaCl + 0.1 N HCl solutions and in a non-aqueous 0.5 RbCl + trifluoroacetic acid solution were studied by means of programmed anodic Tafel polarization study, open-circuit potential relaxation, the initial decay curve fitting method (see section 5.1.5) and a.c. impedance spectroscopy. As will be discussed below, the effect of co-deposited OH and O species in the surface oxidation process on the kinetics of the Cl_2 reaction and on the associated extent of chemisorption of the Cl· intermediate in anodic Cl_2 evolution was determined both in aqueous and non-aqueous solutions. It will be shown that the presence of coverage by surface oxide film species has a major effect on the electrode kinetics of Cl_2 evolution that is associated with large changes in the adsorption pseudocapacitance and Cl· coverage arising from adsorption of the Cl· intermediate. The results also indicate that recombination-controlled kinetics apply, which are related to the Cl· coverage and to the competitive presence of co-deposited OH and O species at Pt surface.

5.1. Results for Aqueous Solution

5.1.1. Log[current density,i] vs. Overpotential, V, Relations

Since the Cl_2 evolution reaction is an anodic reaction, as explained previously, an important feature that has to be taken into account is that an oxide film is usually present on the surface of the test electrode. This determines in an important way the

catalytic properties of the electrode surface since the catalytic surface is an oxide rather than the metal. Therefore, three specially designed computer-controlled procedures were applied in the log(i) - V polarization study in order to regulate oxide film formation and establish reproducibly oxidized or freshly reduced Pt surfaces, as described in Chapter III.

First, we show the Tafel relations for Cl_2 evolution at a freshly reduced Pt surface (Fig.5.1a) and at Pt that had been potentiostatically held in 1.0 mol dm^{-3} aq. HCl at V = 0.5 V for 30 min. (Fig.5.1b). In each of these experiments, the electrode was rotated at rates between 400 and 4900, or 3600, r.p.m. At the pre-oxidized electrode there is almost no effect of mass transfer on the log[current] vs V relation while at the more active " reduced " electrode there is a small but hardly significant effect beyond about 10^{-1} A cm^{-2}.

As was mentioned in the experimental section, these rotation experiments were conducted not so much as to facilitate Cl^- mass transfer (though some small effect will arise for this reason) but rather to check the extent of any supersaturation effect[159] involving dissolved Cl_2 that could give rise to a Tafel plot with the form of the curves of Fig.5.1 a,b. Evidently, as shown by the only small effect of electrode rotation, supersaturation by Cl_2 is not a major effect in determining the shape of the kinetic relations of Figs. 5.1a,b. Hence the form of the relationships in these figures is , as deduced previously by Conway and Novak (cf. refs.85,86), probably associated with the approach to a recombination-controlled (step [III]) limiting current rather than a diffusion effect involving the product Cl_2[159].

Upon comparison of the limiting current-densities for the "oxidized" and "reduced" surfaces, it is seen that the "reduced" Pt electrode sustains a much higher limiting current-density than that for the oxidized Pt surface. The shapes of both sets of curves are, however, quite similar, and the curves are almost superimposable at low overpotentials but are appreciably different in the high overpotential range. This may be a hint in the comprehension of the effects of the oxide film, since it seems that , in

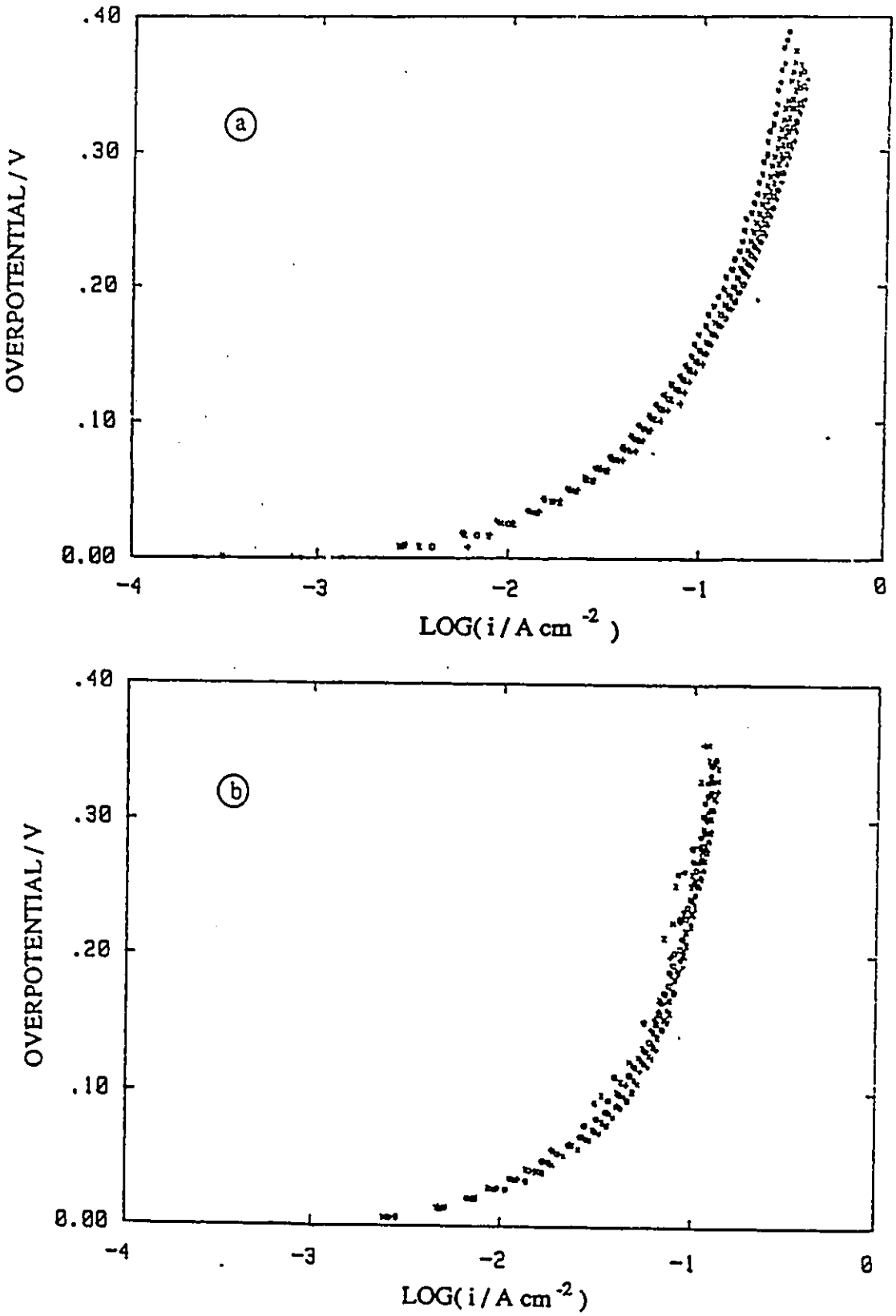

Fig.5.1 a) Log[current-density] vs overpotential relations for anodic Cl_2 evolution at a previously "reduced" rotated Pt electrode (298 K) in 1 mol dm^{-3} aq. HCl. Rotation rates: "*" 400; "x" 900; "z" 1600; "+" 3600 and "o" 4900 r.p.m.

b) As in a) but for the Pt electrode pre-oxidized for 30 min. at V = 500 mV.

the case of the oxidized electrode, some of the "active-area" for adsorbed Cl· has been blocked by OH or O species and thus would not be available for Cl_2 evolution, (the blocking effect is not serious in the low overpotential region since the coverage is probably too small to affect the current but it is serious at high overpotentials); that is why the limiting currents become smaller with increasing extent of surface oxide film formation (see Fig.5.2).

The effect of co-adsorbed OH and/or O species on the kinetics and Cl· adsorption behaviour in the Cl_2 evolution reaction was further examined by extending the duration of the pre-oxidation treatment by holding the potential at V = 0.5 V for a cumulative time up to 135 min. and then examining the Tafel plots (Fig.5.2). The potential-time programme for this series of results is shown in the inset of Fig.5.2.(also see Fig.3.1c). Progressive inhibition of Cl_2 evolution kinetics evidently arises and employment of the Conway-Novak test equation (cf.85,86) for recombination control (viz. plots of $\exp[VF/RT]/i^{1/2}$ vs $\exp[VF/RT]$) shows (Fig.5.3) excellent linearity between these quantities, confirming the recombination process (step [III]) as the probable rate-controlling step in the Cl_2 evolution reaction under the present conditions at Pt. From the intercepts and slopes of these straight lines of Fig.5.3, the values of the recombination rate constant, k_3, for step III can be evaluated as a function of surface oxidation time, t_h, as shown in Fig.5.4. There is evidently a progressive decrease of k_3 with t_h during the pre-oxidation treatment, indicating deactivation of the electrode surface by an electrodeposited oxygen species in the surface oxide film at Pt. The causes of the diminishing k_3 are probably decrease of active site density and/or higher activation energy for Cl· recombination due to the presence of OH or O on the surface. Also surface diffusion of Cl· to recombination sites will be inhibited.

Under conditions of recombination control in the kinetics, leading from a linear Tafel region to a kinetically-controlled limiting current, it is expected, according to the Conway-Novak test plots illustrated in Fig.5.3, that the fractional coverage by the Cl· intermediate should increase from a low value to near unity as the Tafel curve ap-

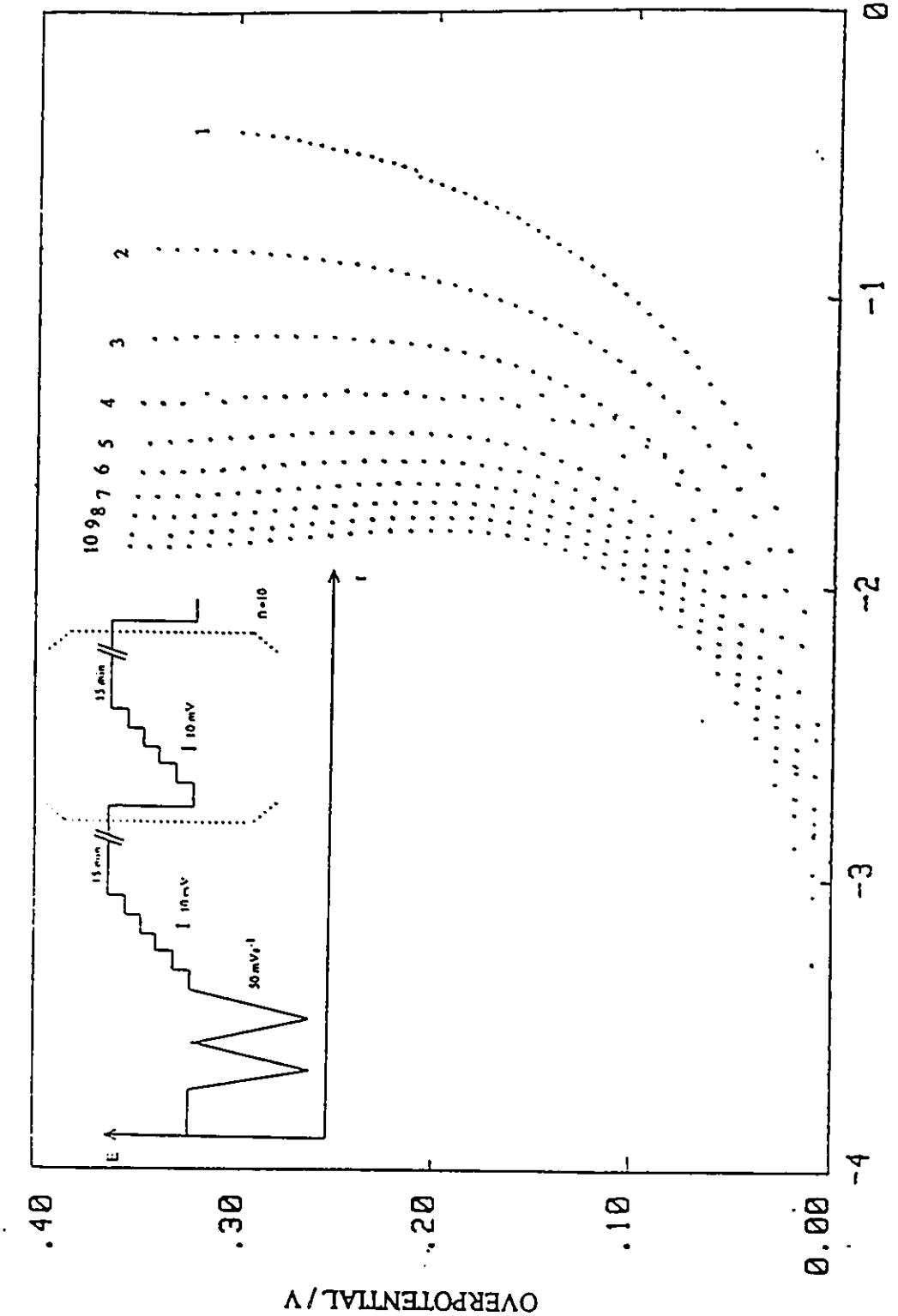

Fig.5.2 Series of log[current-density] vs potential relations, 1 to 10, for anodic Cl_2 evolution at Pt after pre-oxidation treatments at V= 500 mV for up to 135 min. cumulative time of anodic treatment (program as per inset): 1) first I vs V relation, on the freshly reduced Pt surface; 2)...10) with anodic holding time t_h/min. = 15, 30, 45, 60, 75, 90, 105, 120 and 135, respectively, i.e. with Cl_2 being evolved.

proaches the limiting current. This expectation is not entirely realized, although the observed approaches to limiting currents do arise from kinetic rather than diffusional limitations in the cases examined here. The reasons for this divergence of the observed behaviour from expectation of the simple model are connected with effects due to the co-adsorption of the oxide species, as will be argued below.

5.1.2. Nature of the Oxidized Pt Surface on which Cl_2 Evolution Takes Place

The state of the Pt anode surfaces involved in the experiments described above is determined by competition between the process (1) of surface oxidation which can be written more descriptively, for its early stages, by

$$Pt + H_2O \longrightarrow Pt_xOH + H^+ + e \qquad [5.1a]$$

where Pt_xOH represents a 2d lattice of OH on Pt (ref. 26), and the process of Cl^- chemisorption, with partial charge transfer (ref.86,179):

$$Pt + Cl^- \longrightarrow PtCl^{(1-\delta)-} + \delta e \qquad [5.1b]$$

The cyclic-voltammetry results in Fig.5.5 that show adsorbed chloride species remain on the Pt surface, co-adsorbed with OH or O species, up to and including potentials where Cl_2 molecule formation is proceeding at appreciable rates. Cl_2 evolution therefore takes place on an electrode surface jointly oxidized by $Cl^{(1-\delta)-}$ and OH or O species. Unlike chemisorption of HSO_4^- on Au, where the adsorbed ion is desorbed as soon as appreciable coverage by electrosorbed OH or O species appears on the surface (ref.80), adsorbed chloride species are not displaced from the Pt surface when its oxidation by OH or O species takes place; therefore a two-component Cl + OH or O film determines the nature of the electrocatalytic surface on which the steps of the Cl_2 evolution process take place. Only on a Pt surface, separately pre-oxidized in Cl^--free aq. H_2SO_4, as studied in ref.84, can the kinetics of Cl_2 evolution be studied on oxide films initially free from co-adsorbed chloride species (Cl^- is then probably electrostatically adsorbed at the outside of the oxide films, in the oxide film's Helmholtz layer).

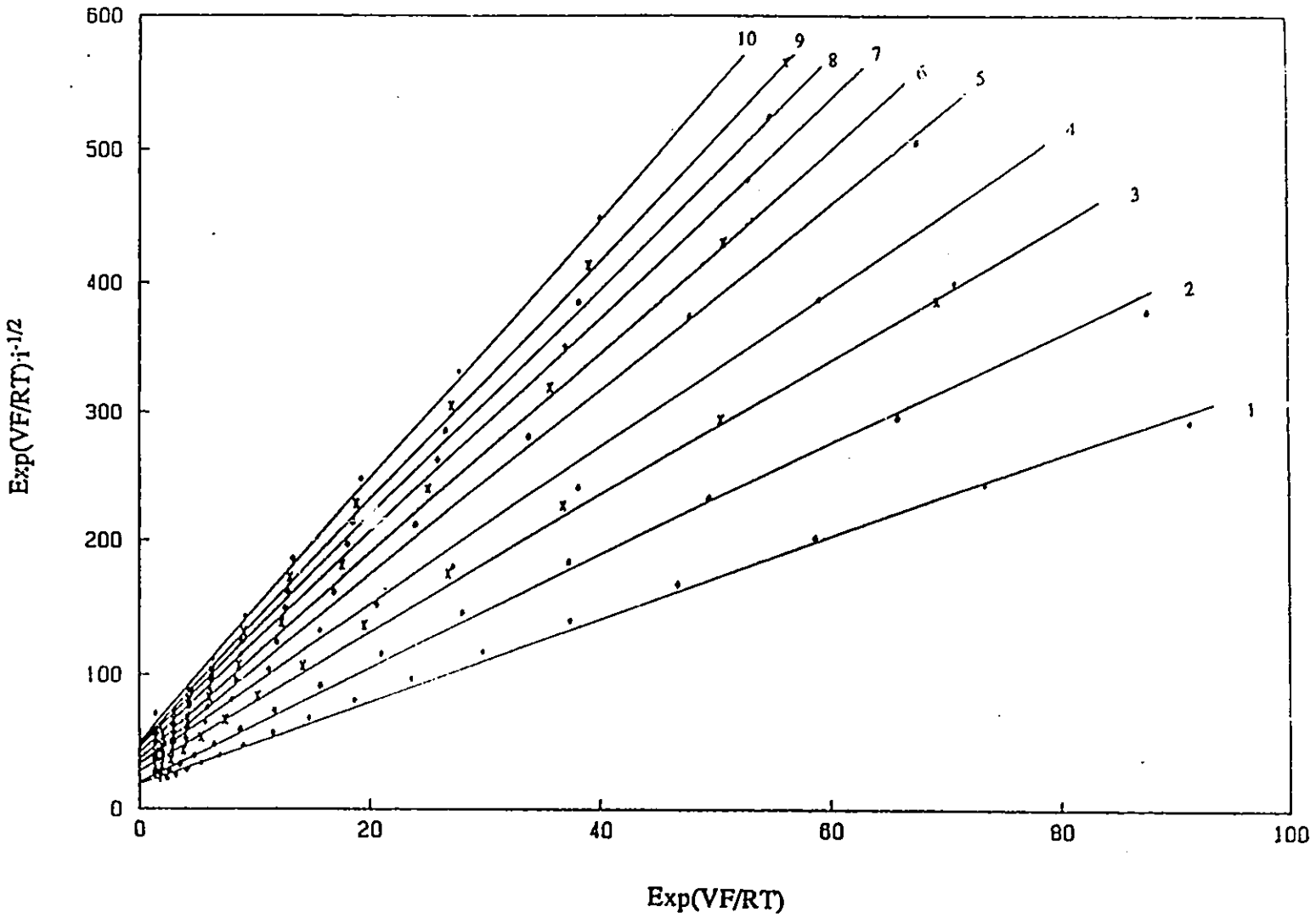

Fig.5.3 Series of Conway-Novak plots for testing applicability of recombination controlled kinetics to the Cl_2 evolution kinetic behaviour recorded in the series of curves of Fig.5.2. Numbered lines correspond, respectively, to those of Fig.5.2.

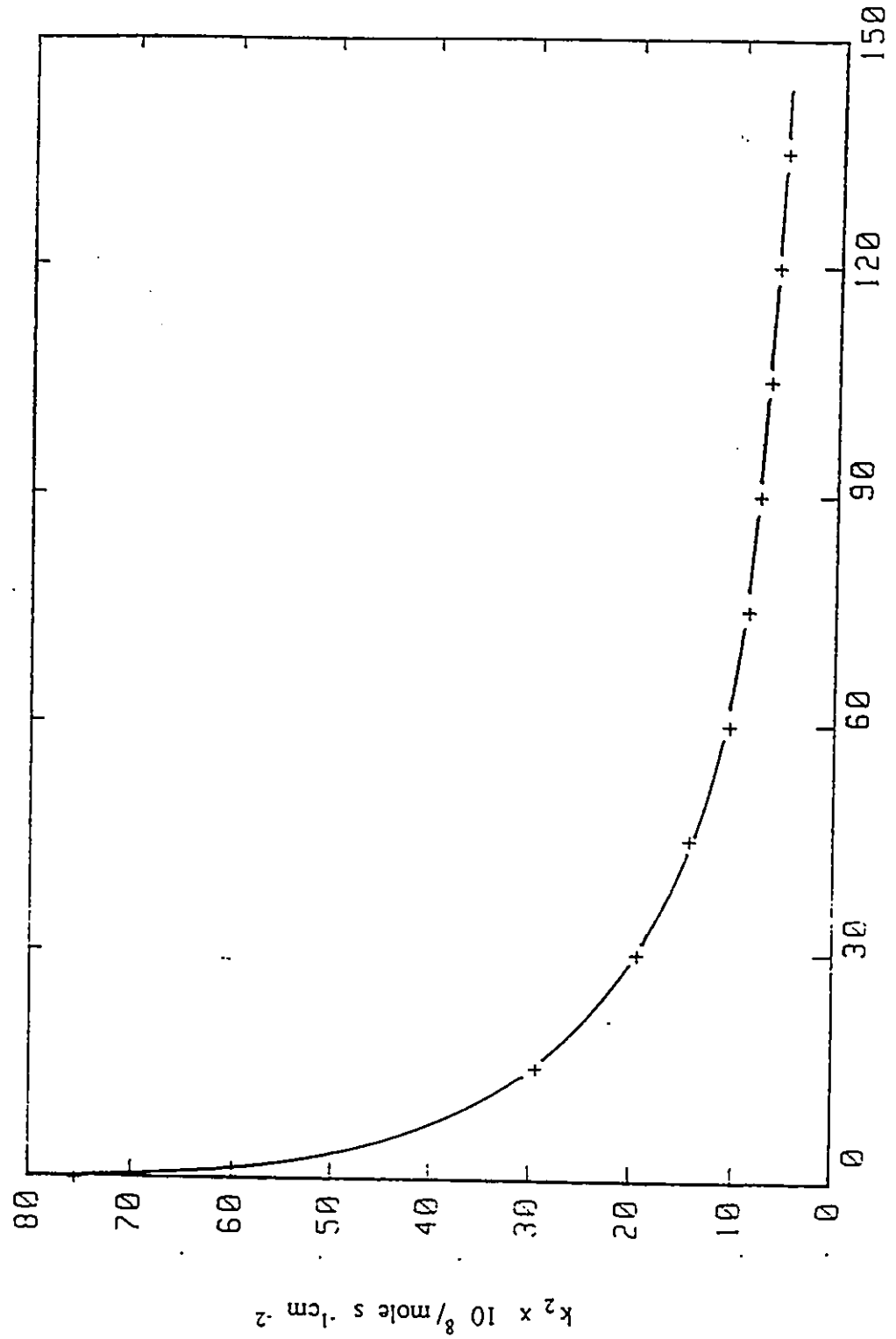

Fig.5.4 Dependence of recombination rate constants, k_2, for the Cl_2 evolution reaction at Pt on time of pre-oxidation, derived from the plots of Fig.5.3.

The effect of co-adsorption of Cl^- ion on the surface oxidation of Pt can be quantitatively evaluated, as in ref.80, by following the effects of progressive increase of Cl^- concentration from 10^{-7} mol dm^{-3} by micrometric titration of a dilute Cl^- solution into a supporting electrolyte of 0.1 mol dm^{-3} of H_2SO_4 or $HClO_4$, on successive cyclic-voltammograms at Pt taken over e.g. the potential range +0.05 V to +1.70 V RHE (i.e. into the range where Cl_2 is evolved) as illustrated in Fig.5.5.

The addition of Cl^- first progressively and selectively blocks the initial stages of Pt surface oxidation with little effect beyond 1.1 V where the second stage of surface oxidation ($PtOH \longrightarrow PtO + H^+ + e$) commences (ref.26). After addition of a substantial quantity of Cl^-, a series of curves is built up (see Fig.5.5) which shows an isosbestic type of point or isopotential point at ca. 1.05 V, which corresponds to the potential at which the $Pt_{x-1}OH$ lattice monolayer is completed. The whole i vs V profile is similar to that reported by Conway and Novak (ref.80) except that the potential range covered is much larger here, being taken up to +1.7 V E_H. The results reveal some further important information about Cl^- adsorption. From Fig.5.5, besides the Cl^- blocking effect in the i vs V profile, there is a "shoulder" which becomes detectable as the Cl^- concentration is increased. The potential of the " shoulder " starts at 1.5 V and ends at 1.7 V, corresponding to a concentration of Cl^- of 4.1×10^{-4} mol dm^{-3}. The mid-point of this range is consistent with the reversible potential for Cl_2 evolution at a concentration of 4.1×10^{-4} of Cl^- since, according to the Nernst equation, the Cl_2 reversible potential is given by:

$$E = E^\circ - 0.059/n \log(1/[Cl^-]) \qquad [5.2]$$

$$= 1.358 - (- 0.203)$$

$$\approx 1.56 \text{ V } E_H$$

This suggests that the " shoulder " may be caused by the onset of Cl^- adsorption on the surface of the Pt electrode. It is not quite clear if a Cl^- desorption peak can be distinguished but there is an isopotential point at about 1.5 V, which might correspond to the Cl^- desorption starting at that point where significant rates of desorptive recom-

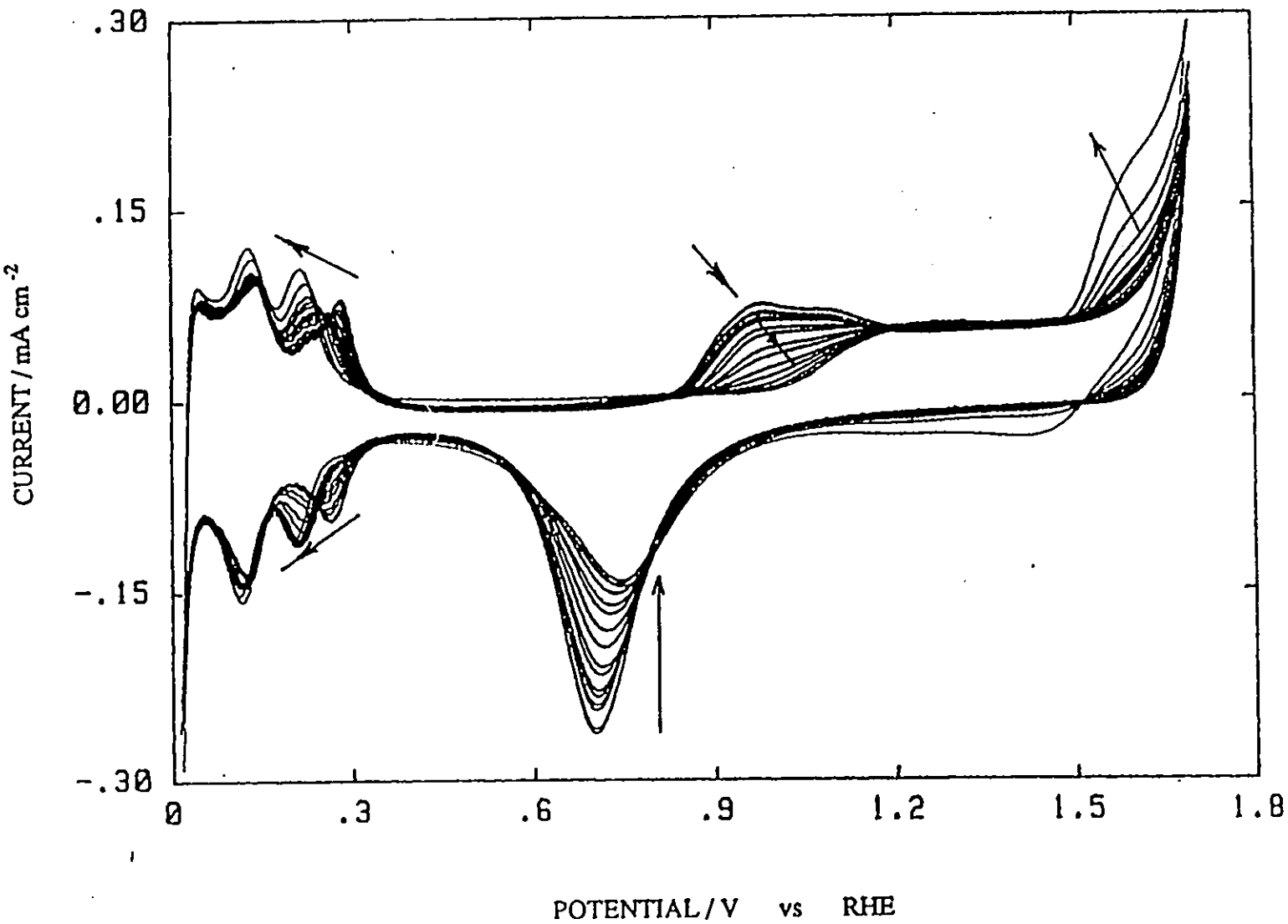

Fig.5.5 Successive series of cyclic-voltammograms for Pt in 0.1 mol dm^{-3} aq. H_2SO_4, with additions of Cl ion giving concentrations from $5x10^{-7}$ to $4x10^{-4}$ mol dm^{-3}, covering the potential range from onset of Pt surface oxidation(+0.8 V,RHE) to +1.7 V, RHE, where Cl_2 begins to be evolved at appreciable rates. Arrows show directions of change of current with increasing Cl^- ion concentration.

bination to Cl_2 arise.

Fig.5.5 show the effects of Cl^- on the H underpotential deposition and ionization behaviour at Pt in the potential range -0.37 to -0.05 V E_H. It is observed that isopotential points also arise in the anion - induced redistribution of electrodeposited H among the four distinguishable states of H adsorption, as reported elsewhere (ref.80).

5.1.3. Oxide Growth During Anodic Cl_2 Evolution

As represented in eqn.[1.7], oxide film growth at Pt obeys the direct logarithmic law in time; the charge required for building up a certain amount of oxide is a function of both the holding potential and time, i.e. high potentials or long holding times at a lower potential would give comparable behaviour in the development of the oxide film. During the time that Cl_2 evolution is proceeding in the steady-state, the oxide film also continues to be generated on the electrode surface. The OH or O species, as soon as they are adsorbed on the Pt surface, are not easy to displace, with the result that further Cl^- adsorption on the electrode surface is inhibited. Significant blocking by O or OH species causes a decrease of current and gives rise to a somewhat S-shaped in its i vs V curve, especially when the potential becomes high.

An experiment was carried out to determine the rate of oxide film growth during the actual process of Cl_2 evolution by means of holding the Pt electrode at various times and potentials, then measuring the reduction charge in an i vs V profile using cyclic-voltammetry. The resulting reduction charge, Q vs log(t), for five potentials are plotted in Fig.5.6. The linear relationship is not unexpected since most thin oxide film growth is logarithmic in time. As can be seen, the higher holding potential leads to a larger slope of this plot, corresponding to a greater logarithmic rate of oxidation. Table 5.1 lists the slopes dQ/d(log(t)) for five holding potentials, for comparison, with Q in units of $\mu C\ cm^{-2}$.

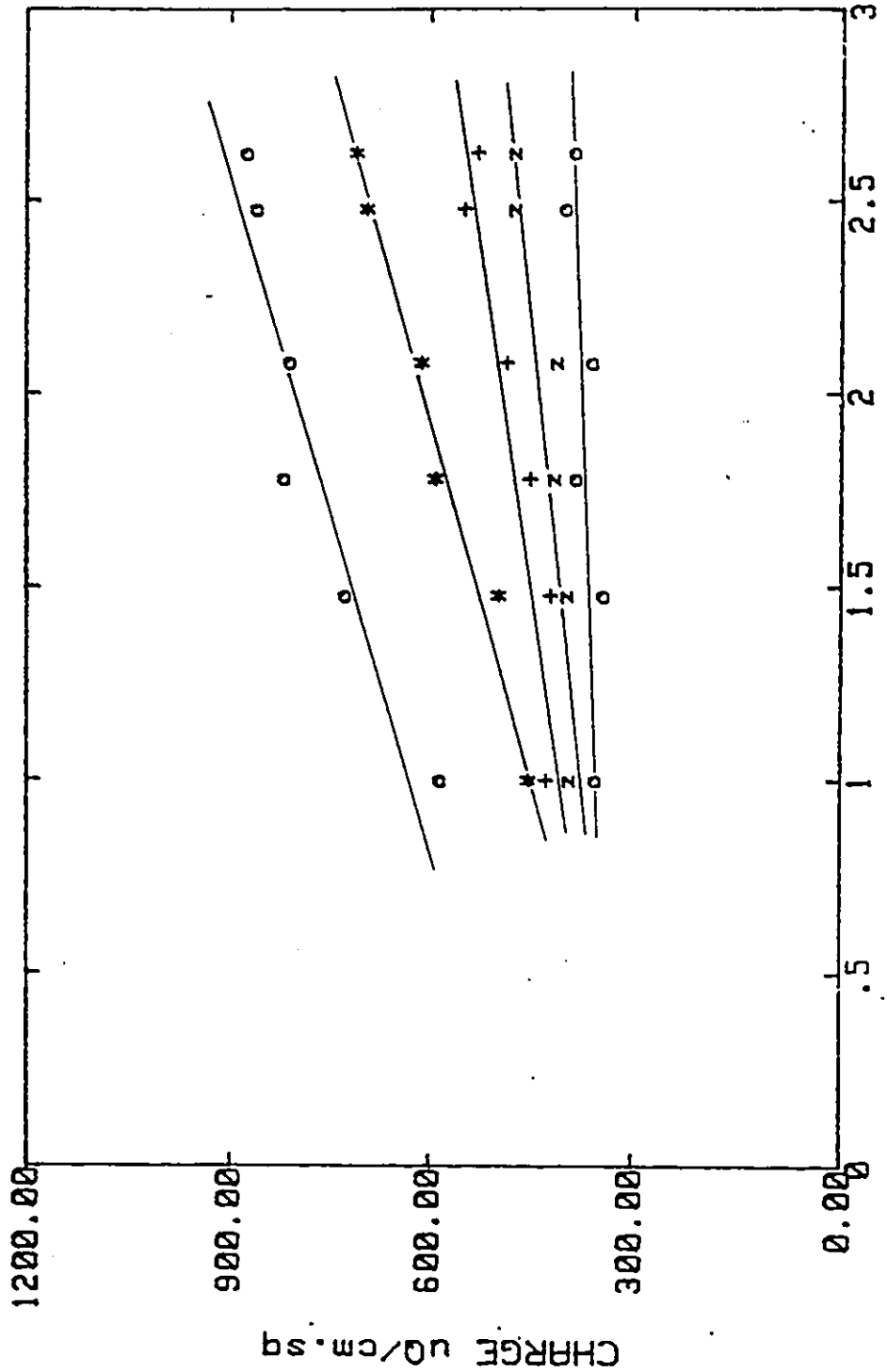

Fig.5.6 Plots of charge for reduction of oxide formed under the conditions of anodic evolution of Cl_2 vs log(t) for various holding overpotentials. "o" 550; "*" 400; "+" 300; "z" 200 and "o" 100 mV, respectively.

Table 5.1 Comparison of slopes of dQ/d(log(t)) for various anodic holding potentials of the oxide formation under conditions of Cl_2 evolution.

Holding overpotential (mV)	dQ/d(log(t) ($\mu C\ cm^{-2}$)
500	171
400	159
300	84
200	64
100	19

The holding potentials were 100, 200 and 300 mV (expressed as overpotentials for Cl_2 evolution). Even for the longer times of holding, the oxide film reduction charges do not change appreciably, which means, for overpotentials lower than 300 mV, the rate of extension of the oxide film is small (see Fig.5.6 and Table 5.1, from which it is seen that there is not much charge difference for holding times of 1 and 15 minutes in the oxide reduction peaks). Tafel polarization measurements usually only take a few minutes (less than 5), so that the growth of oxide does not significantly effect the i vs V polarization in the low potential range. However, for holding at higher potentials, say at 400 or 500 mV, there is a larger difference. The reduction charge then changes substantially, which means that co-deposition of O species then becomes significant and has a stronger competitive effect vis a vis Cl^- and Cl^- adsorption.

5.1.4. Open-Circuit Potential Relaxation Results

The method for processing open-circuit potential relaxation measurements, as described in a previous section (3.3), was employed to derive the adsorption pseudo-

capacitance of Cl^- as a function of overpotential for Cl_2 evolution at the Pt electrode surface. From the decay curves, based on several thousand points recorded by digital oscilloscopes, can be derived the following information : (a) V(t) vs log(t) plots ; (b) V(t) vs log(-dV/dt) plots; (c) the capacitance C(V) vs V(t) plots and from the latter, information about change of coverage by adsorbed intermediates with potential. In the following discussion the potential decay behaviour at the so-called "pre-oxidized" Pt electrode will be compared with that at the "reduced" one.

The relaxation transient data was acquired according to the programme shown in Fig.3.3, the Pt electrode being anodically pre-polarized for 30 minutes or being reduced before each decay transient was initiated and recorded. The resulting data were then processed using a software called " PDDT-2000 ". written by the present author.

5.1.4. Potential Relaxation Behaviour at "Pre-oxidized" Platinum Electrodes

Digitally acquired potential relaxation data, expressed as V(t) vs. log(t) plots for the oxidized Pt electrode in acidic solution, is shown in Fig.5.7 where two regions can be distinguished. Fig.5.8 shows the corresponding V(t) vs. log(-dV/dt) plots. The V(t) to log(t) curves taken from various initial potentials exhibit a flat region at the beginning of the decay, lasting for ca. 10^{-3} s., depending little on the initial polarization potential and time. As discussed by Elam and Conway[160,161], this indicates a high value of R_{∞}, the nonlinear Faradaic resistance most probably associated with the primary discharge step I (eqn.[I]) in the Cl_2 evolution reaction. The large R_{∞}, corresponding to low exchange current density i_o (as well as to current density at any given potential), indicates that the activation energy for step [I], the Cl^- adsorption step, is high. This is because the oxide film on the surface of Pt electrode blocks the Cl^- adsorption step or increases the activation energy for adsorption of Cl^- on the oxidized Pt electrode surface (However, the recombination pathway is still the rate-determining step having the highest activation energy. The co-deposited O or OH species also limit the "active-

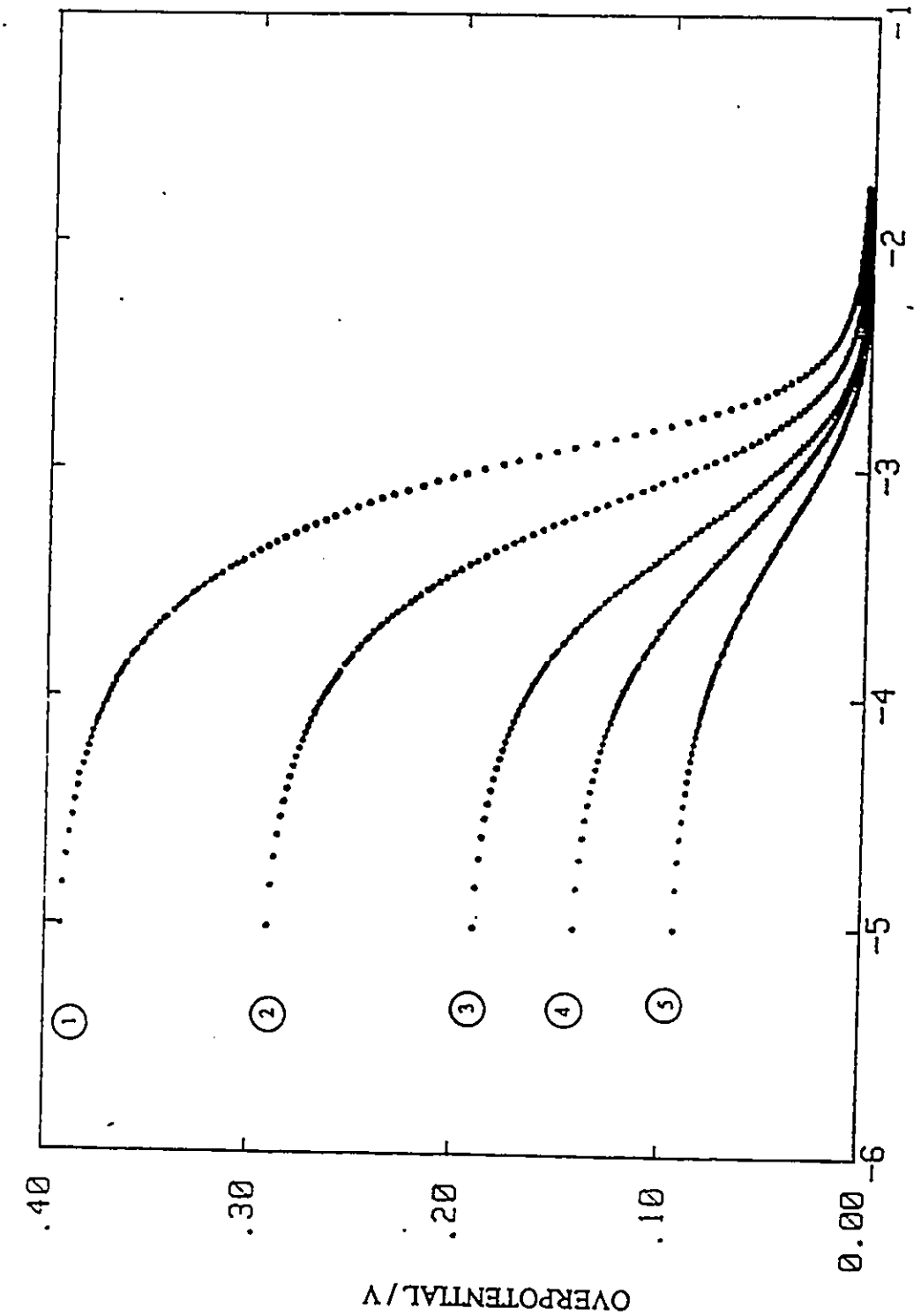

Fig.5.7 Digitally recorded potential-relaxation transients taken from a series of 5 initial anodic overpotentials for the Cl_2 evolution at Pt electrode pre-oxidized at V = 550 mV for 30 min. 1) V = 500; 2) 400; 3) 300; 4) 200 and 5) 150 mV.

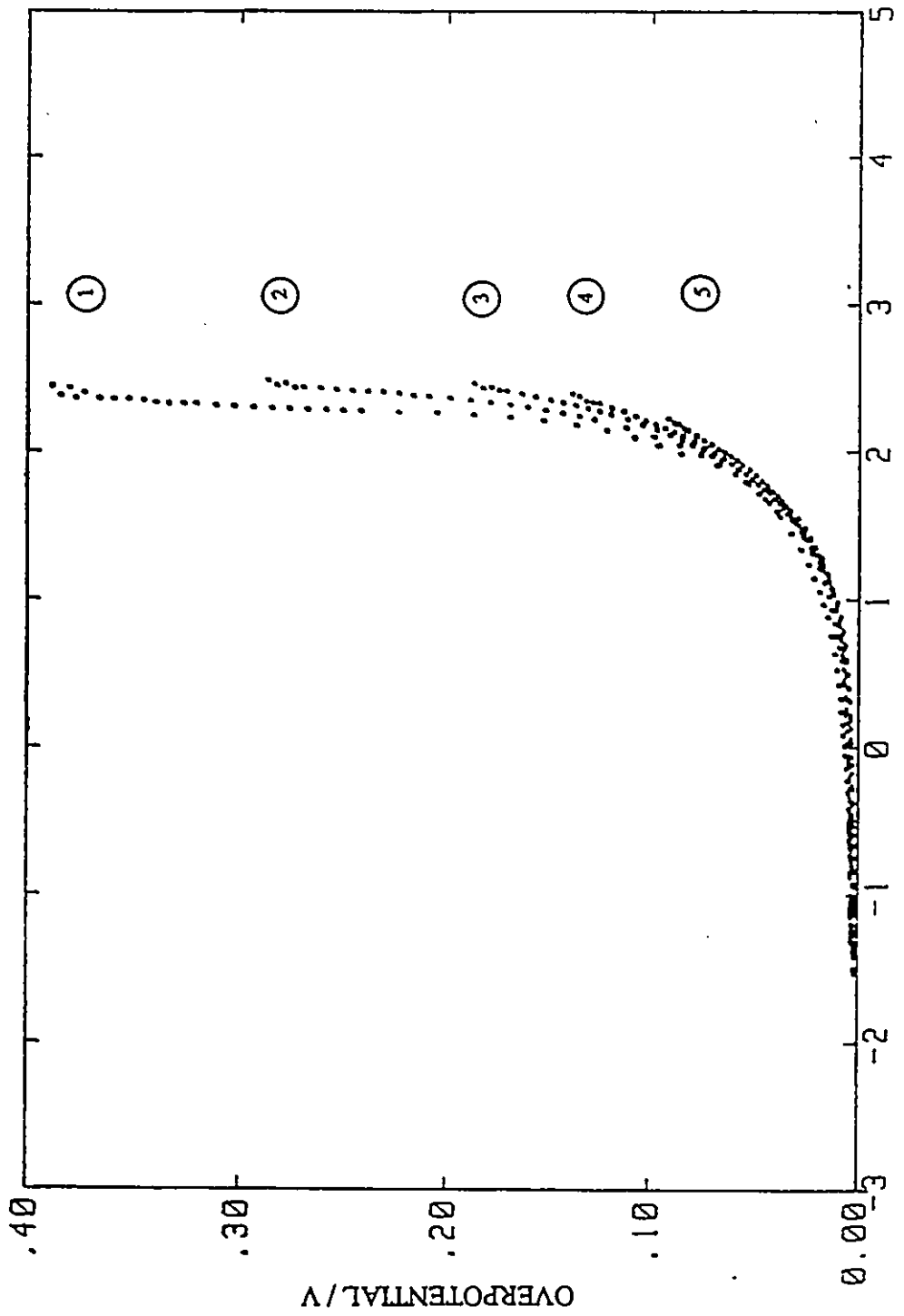

Fig.5.8 Computer-plotted values of log[-dV/dt] vs V derived from the data of Fig.5.7 for 5 initial anodic polarization overpotentials; curves numbered, respectively, as in Fig.5.7.

area" for Cl· desorption and recombination).

The second region is where the potential decays quite quickly and is completed in 10^{-4} to 10^{-2} seconds; this corresponds presumably to the discharge of the double-layer capacitance, C_{dl}, but could involve some contribution from the pseudocapacitance C_ϕ, associated with the adsorbed Cl· intermediate. Because, at the oxidized Pt electrode , only a relatively small fraction of the surface is available as "active-area" for Cl· and Cl· adsorption (step I), the value of C_ϕ can actually be quite small, in fact, comparable with the value of the double-layer capacitance, i.e. $C_\phi \approx C_{dl}$ or even less, so that the second region could be due to the discharge of the total capacitance (C_ϕ + C_{dl}). In other words, C_ϕ and C_{dl} would discharge over the same order of time. How long the practical discharge time is depends on the resistance R_- which is largely affected by the oxidation state of the Pt electrode surface. More extensive surface oxidation gives rise to a larger R_- due to the oxide inhibition effect, so that the "buffering" period of almost constant potential in the decay transient (Fig.5.7) would tend to be longer; however, the C_ϕ under these conditions is much smaller (see Fig.5.11).

In contrast to the V(t) vs log(t) plots shown in Fig.5.7, the plots of V(t) against log(-dV/dt) are all coincident (especially at low overpotentials V < 0.15 V), which indicates that all the decay plots have about the same rate of decrease of V with time after the initial period τ (ref.124). Another significant aspect of the shapes of the V(t) vs log(-dVdt) plots are very similar to those of the V vs log(i) (Tafel) plots, a limiting (dV/dt) value being attained at high overpotentials.

5.1.4.2. Potential Relaxation Behaviour at " Reduced " Pt Electrodes

The potential relaxation curves for the "reduced" Pt electrodes in acidic solution are shown in Fig.5.9 these exhibit three distinguishable regions. The corresponding V(t) vs. log(-dV/dt) plots are given in Fig.5.10 and also have three different regions corresponding to those of the V(t) vs log(t) curves. The initial rapid decay is completed

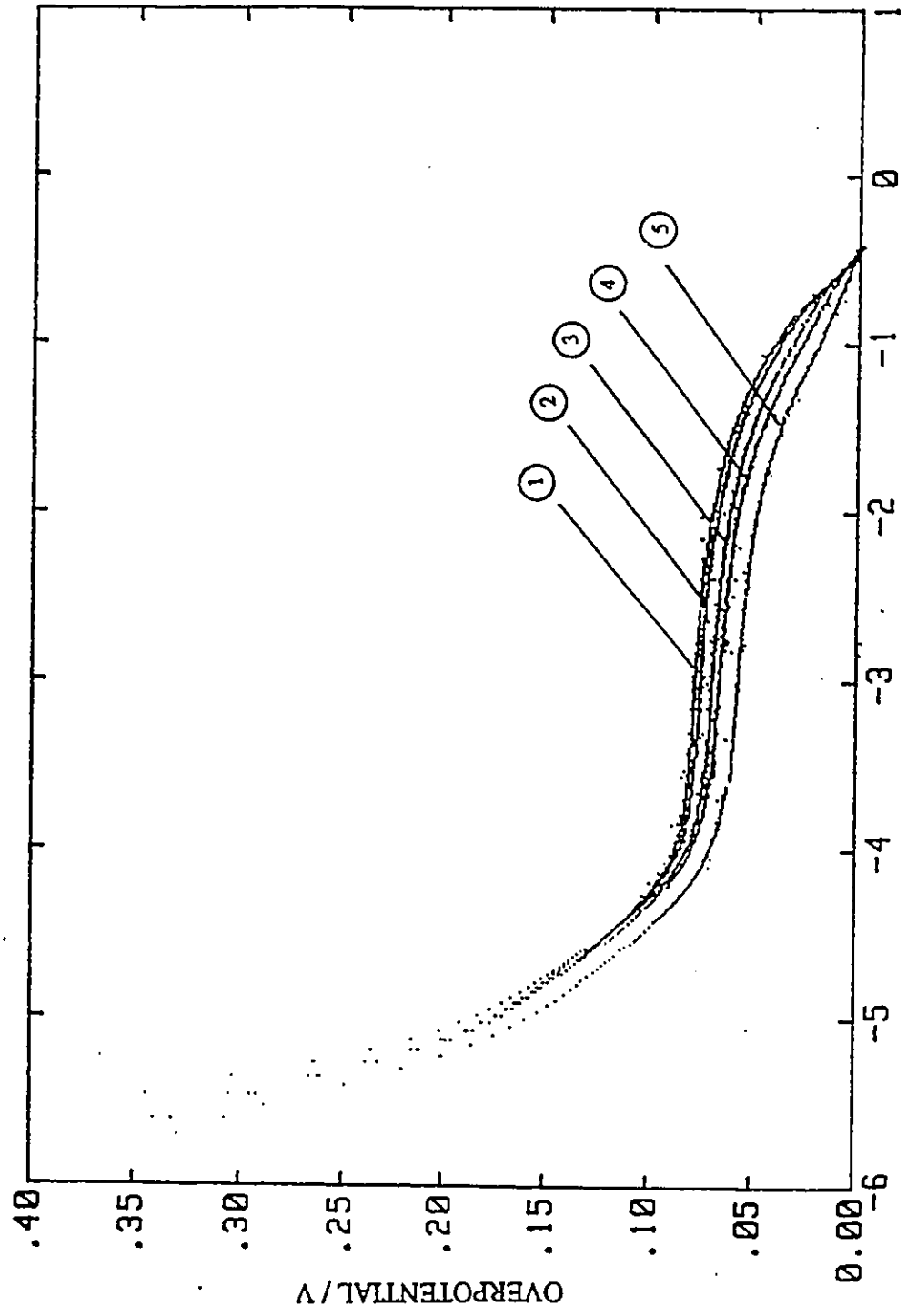

Fig.5.9 Digitally recorded potential-relaxation transients from a series of 5 anodic overpotentials for the Cl_2 evolution at a freshly "reduced" Pt electrode. 1) 300; 2) 350; 3) 400; 4) 450 and 5) 500 mV (compare with Fig.5.7).

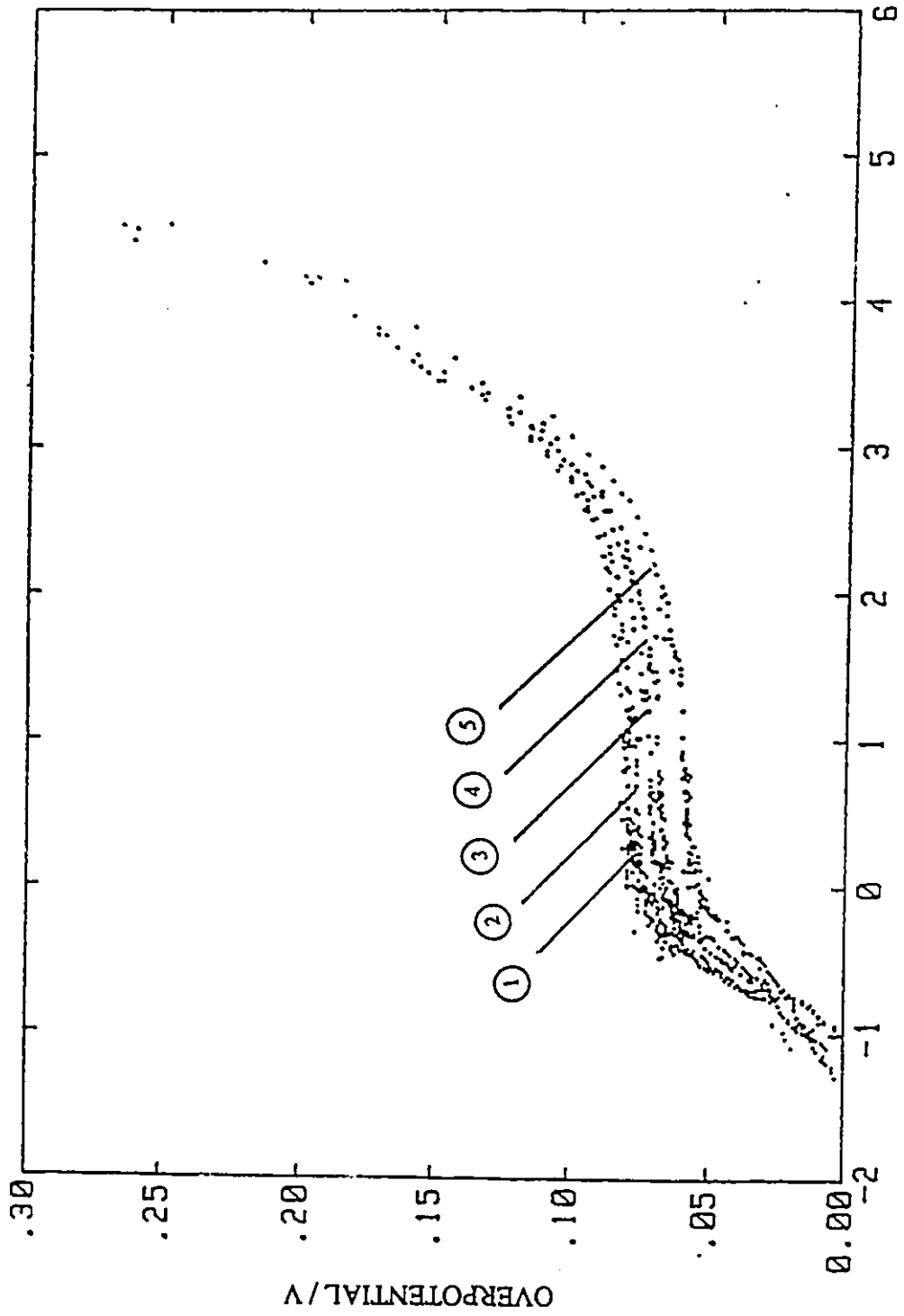

Fig.5.10 Computer-plotted values of log[-dV/dt] vs V derived from the data of Fig.5.9 for 5 initial anodic polarization overpotentials; curves numbered, respectively, as in Fig.5.9 (compare with Fig.5.8).

in $\leq 10^{-4}$ second and is attributed to the discharge of the double-layer capacitance (refs.160, 161) C_{dl} through nonlinear faradaic resistance, R_{∞}. In this case, R_{∞} is much smaller which means the Cl^- adsorption (step I) is much more facile or, correspondingly, the activation energy for the Cl^- adsorption step is smaller and there is a higher surface density of "active-area" available for Cl^- adsorption in the Cl_2 evolution reaction. This is, of course, because the surface has been reduced so that a less oxide-covered surface is available which favours Cl^- adsorption. Also, since the R_{∞} is small, the discharge of C_{dl} is virtually completed within a short period of time.

The second region in the curves of Fig.5.9 is rather flat and lasts from 10^{-4} to 10^{-5} seconds. This region corresponds to the beginning of "discharge" of the Cl^- pseudocapacitance, which is potential dependent and large in comparison with C_{dl} in the low potential region. The plateau corresponds to the situation in which mixed anodic and cathodic Cl^- desorption processes take place, involving the back reaction of step I and the forward direction of step III (here step III is shown by the plots of Fig.5.3, to be the predominant desorption pathway but step II could contribute, in parallel, a pathway of smaller rate). This buffers the potential at relatively constant values for some time until θ_{Cl^-} or the surface quantity of adsorbed Cl^- per cm^2 becomes insignificant.

The third region is due to the continuing discharge of the Cl^- pseudocapacitance, C_{ϕ}, as the coverage of Cl^- declines to its value at the reversible potential and causes the overpotential to decrease towards zero.

The two dV/d(log(-dV/dt)) slopes correspond to the initial discharge of the component involving C_{dl} and later the Cl^- pseudocapacitance, C_{ϕ}.

5.1.4.3. Cl^- Pseudocapacitance Behaviour of " Pre-oxidized " Pt Electrodes

This discussion will focus on the topic of principal interest that arises in this work, that is, the pseudocapacitance, C_{ϕ}, associated with the potential-dependence of the fractional coverage, θ_{Cl^-} of adsorbed Cl^- present as the kinetically-significant reaction

intermediate in the Cl_2 evolution reaction, and the values of $\theta_{Cl\cdot}$ themselves as a function of potential. C_ϕ was defined in eqn.[2.37] for ad-species ($C_\phi = q_o\, d\theta/dt$) where q_o is the charge required for monolayer formation or reduction of the ad-species. Here, it is to be defined as the charge needed to change the fractional coverage, $\theta_{Cl\cdot}$ of the adsorbed $Cl\cdot$ intermediate in the Cl_2 evolution reaction on the exterior surface of the Pt electrode from zero to unity. The charge q_o is taken as 210 $\mu C\ cm^{-2}$, based on the geometry of the Pt surface*.

The C_ϕ vs V curves were derived by treating the combination of V vs log(i) and V to log(-dV/dt) data in terms of eqn.[4.1]. Fig.5.11 shows the resulting C vs V plots for $Cl\cdot$ in the Cl_2 evolution reaction at the pre-oxidized Pt electrodes.

In the case of the oxidized Pt, the C vs V curves evidently do not have a significant peak and the apparent capacitance seems independent of potential, except that only a small increase arises, but without any maximum, just below V ≈ 0.02 V. The main C vs V profile corresponds to an almost constant value of ca. 60 $\mu F\ cm^{-2}$, presumably corresponding to the double-layer capacitance of the oxidized Pt surface. This behaviour is confirmed by the values of C determined by a.c. impedance shown in Fig.5.12 which are evidently in good agreement with those derived from analysis of the potential relaxation transients.

This low constant capacitance is unexpected because, from the previous work[85,86], the recombination mechanism has been strongly suggested for Cl_2 evolution at Pt from the limiting current density behaviour observed in the V vs log(i) plots, and hence would imply an appreciable $\theta_{Cl\cdot}$ over a 200 mV range. However, the blocking effect caused by the oxide film formed on the surface of the Pt electrode presumably largely reduces the availability of "active-area" for $Cl\cdot$ adsorption and recombination,

---

* This depends on the crystal face orientation but here work was conducted only on polycrystalline Pt since single-crystal surfaces do not survive anodic Cl_2 evolution for any extended period of time.

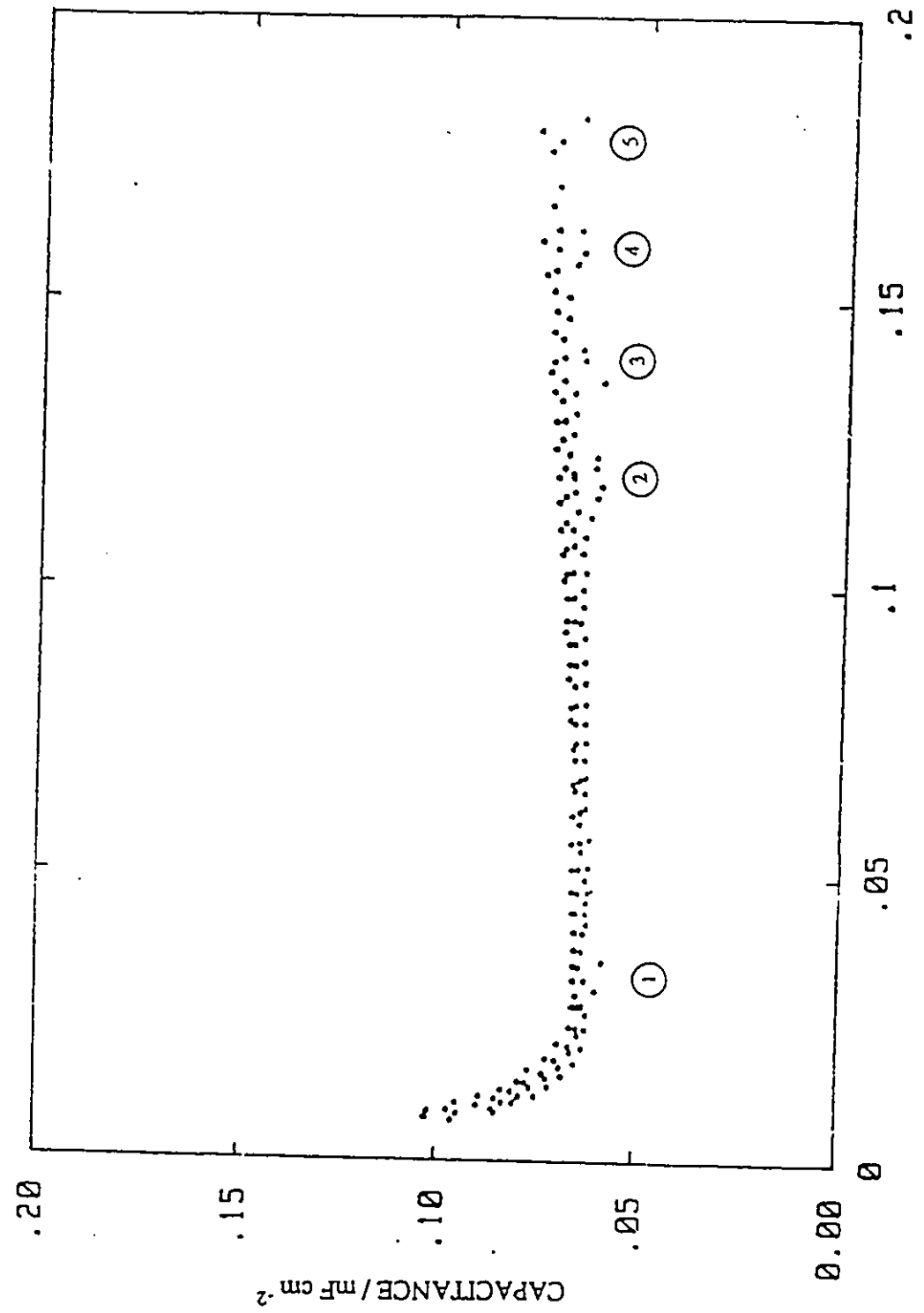

Fig.5.11 Capacitance derived from the potential-relaxation transients and Tafel plots for the pre-oxidized Pt electrode, at overpotentials numbered as on the curves of Fig.5.8.

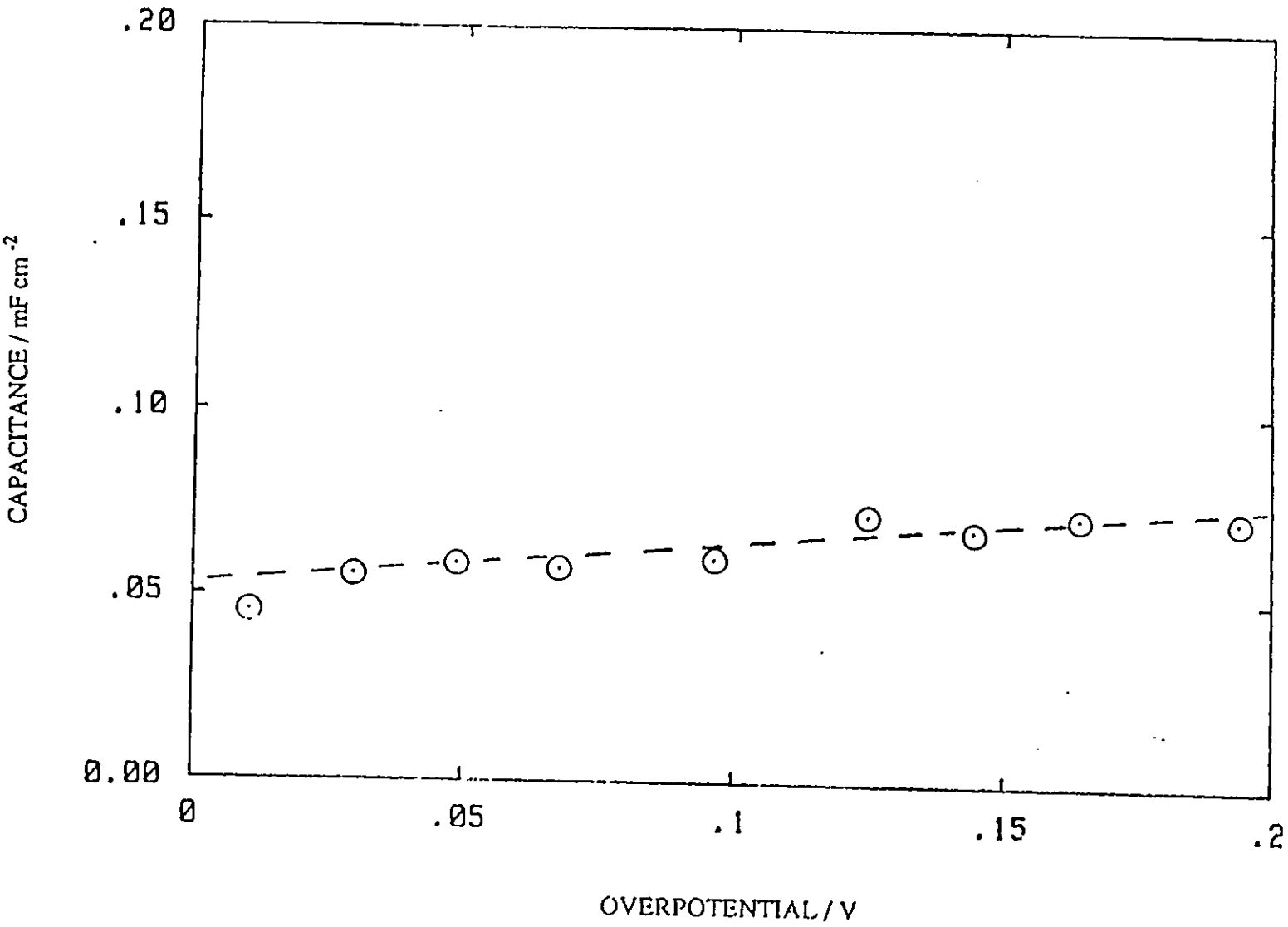

Fig.5.12 Interfacial capacitance vs overpotential for the pre-oxidized Pt electrode evolving Cl_2 as determined by a.c. impedance measurements. (Compare with the results of Fig.5.11).

and leads to an effectively small q_o for the so-called "monolayer charge" required for the adsorption of the Cl_{ad} intermediate covering the available "active-area" fraction, giving rise to a small value of change of coverage, $d\theta/dV$, related to C_ϕ. Therefore, it can be understood how the values of $d\theta/dV$ and q_o can be small in the case of the pre-oxidized Pt electrode. In other words, the charge for full monolayer coverage on the available surface would be much smaller than the 210 $\mu C.cm^{-2}$, normally taken for q_o (for H) on the free metal surface. The apparent capacitance is probably mainly associated with the double-layer capacitance of the oxidized surface with the pseudocapacitance of the Cl_{ad} adsorbed intermediate contributing only a small fraction to the measured C corresponding to the V vs log(t) curves. Both C_{dl} and C_ϕ discharge in about the same time scale, i.e. $C_\phi \approx C_{dl}$.

5.1.4.4. Capacitance Information for the Cathodically Reduced Pt Electrode Surfaces

It must be mentioned again that in the experiments at "reduced" electrodes, in contrast to those conducted earlier on Pt surfaces separately pre-oxidized in Cl^--free electrolytes, some co-deposition of OH and/or O species arises unavoidably during the course of the Cl_2 evolution reaction, depending on the anode potential, though on the "reduced" Pt electrode surfaces, no surface oxide film is initially present. As expected from the observed effects of reduction on the Tafel plots and potential-relaxation transients, a large "active-area" fraction should be available for Cl_{ad} adsorption at the reduced Pt surface, and a major difference arises at the Cl_2-evolving electrode in its capacitance behaviour involving now a substantial pseudocapacitance, C_ϕ, associated with the potential dependence of coverage by the Cl_{ad} intermediate. As shown in Fig.5.13 for the C vs V behaviour, substantial pseudocapacitance values arise over the V range 0.01 to 0.09 V, depending on the initial potentials of the transients. Of course, this is not surprising since, according to the recombination mechanism with step III rate-controlling, a maximum in the capacitance vs potential curve is theoretically

expected. Fig.5.13, shows 5 sets of potential dependent capacitance curves corresponding to the 5 initial anodic polarization potentials i.e. (1) 300 mV; (2) 350 mV; (3) 400 mV; (4) 450 mV; and (5) 500 mV, and the log(-dV/dt) plots in Fig.5.10. The C vs V curves exhibit maximum values of C in the potential range V = 50 to 70 mV and the half-widths of the peaks are ca. 50 mV. The capacitance curves rise rapidly around V = 60 to 80 mV with corresponds to the plateaux in the log(t) and log(-dV/dt) curves.

The appreciable pseudocapacitance exhibited by the reaction at the "reduced" electrodes is not, in any way, connected with evolved molecular Cl_2 as (a) the solution is already pre-saturated with Cl_2 and (b) the behaviour is almost independent of electrode rotation rate.

It is interesting that initiation of the potential-relaxation transients from different initial potentials leads to very different values for the maximum capacitances; the initial potential of 300 mV gives the biggest peak in the whole set of curves while for an initial potential of 500 mV, the smallest peak in C arises at this point. This must be due to the effect of development of the oxide film, since, after cathodic reduction of the Pt electrode surface, the potential is jumped back anodically to the potentials required for taking the decay measurements as explained earlier. During the short time of anodic polarization required to achieve this condition, some adsorption of O and OH species (see eqns.[IV] and [V]) unavoidably arises and competes with the Cl^- adsorption reaction (step I). At a high anodic potential more rapid oxide film formation will take place leading to more O or OH species being adsorbed on the surface of the Pt electrode. The results in Fig.5.13 suggest that for the higher initial potentials, more surface space (active sites) is being initially occupied by oxide species than at low initial potentials.

The change of charges associated with potential dependence of coverage by the Cl^- species, giving rise to the C_ϕ vs V profiles, can be estimated by integration of the profiles. The resulting plots are shown in Fig.5.14 for the 5 initial polarization

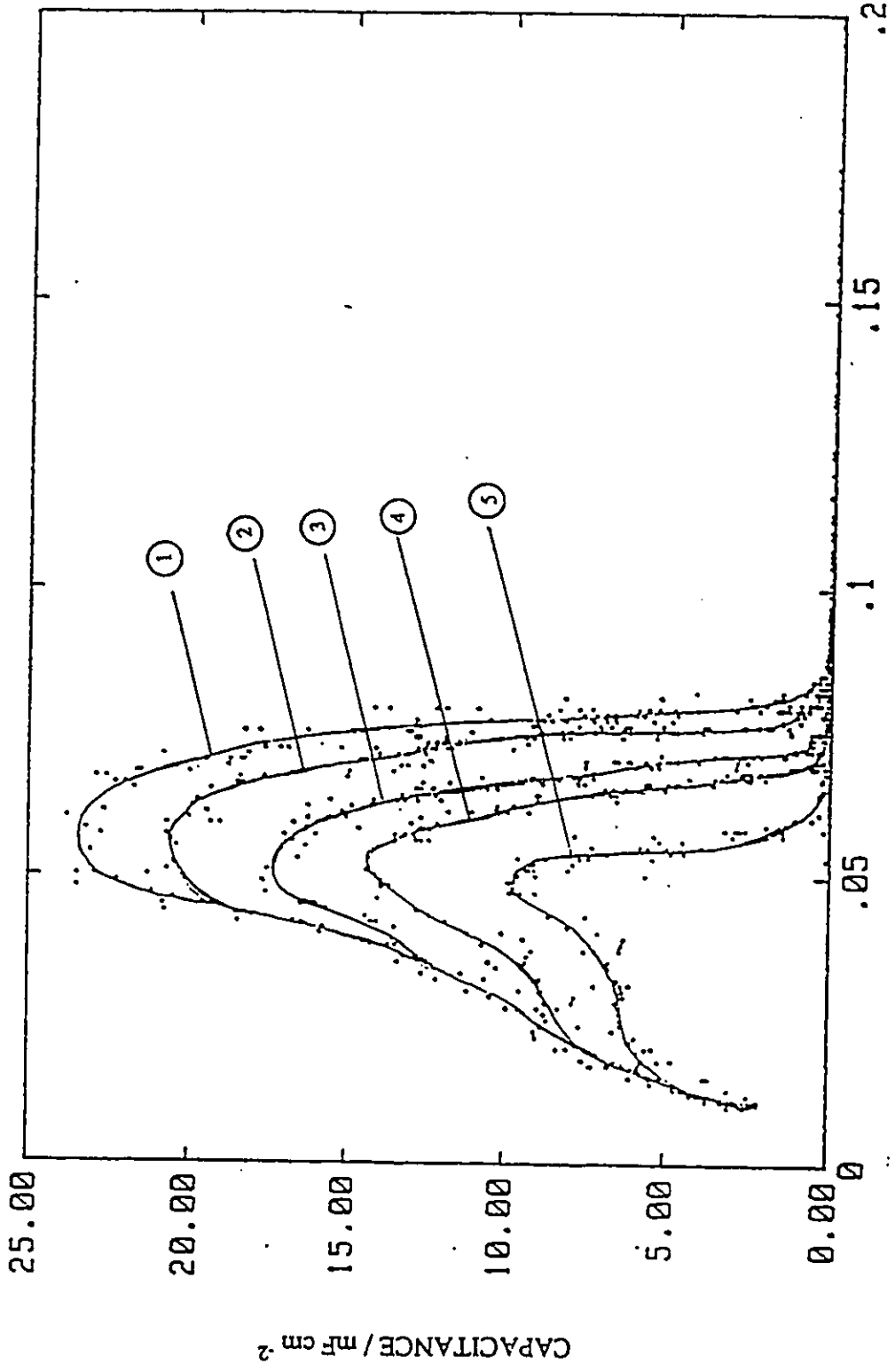

Fig.5.13 Capacitance derived from the potential-relaxation transients and Tafel plots for the freshly "reduced" Pt electrode, at overpotentials numbered as on the curves of Fig.5.10.

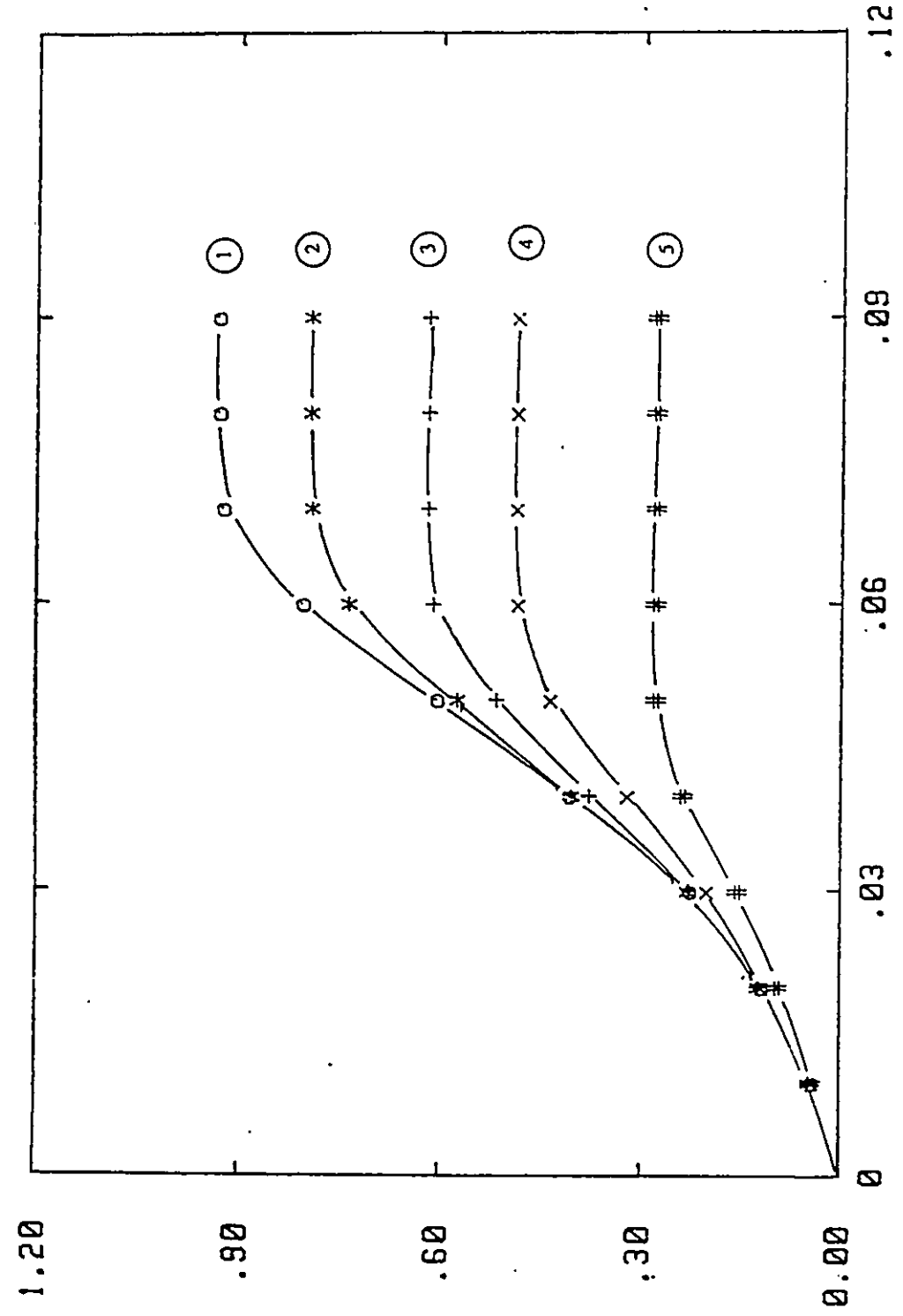

Fig.5.14 Integrated changes of charge associated with potential dependence of coverage by the Cl intermediate at the reduced Pt electrodes, derived for various initial potentials from the curves of Fig. 5.13. (The numbers on the curve correspond, respectively, to those of Fig.5.13).

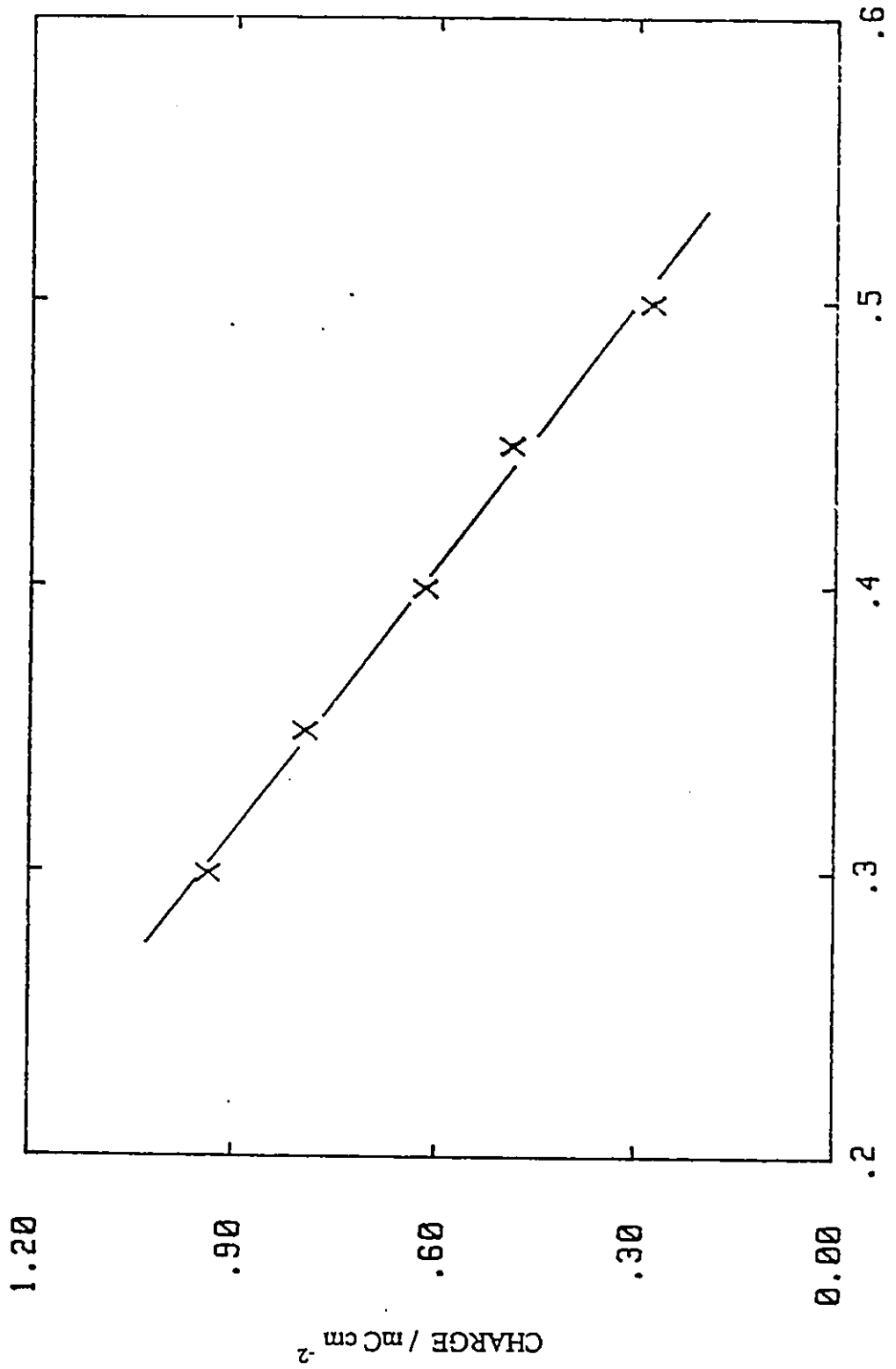

Fig.5.15 Change of the limiting charge attained for the adsorption of the Cl intermediate with increasing initial potential of the relaxation transient, derived from the plots of Fig.5.14 for the respective indicated potentials.

potentials corresponding to those for the C_ϕ vs V plots; the attainment of limiting charge values as V is increased is clearly seen in these plots and the values are shown as f(V). It will be seen from Fig.5.14 that Cl· charge values are larger than that (ref.26) for an O monolayer, especially on the less oxide-covered Pt surface. The reasons for this behaviour are discussed in section 5.1.6.2.

It is evident, from Fig.5.15, that the charges (and corresponding C_ϕ values in Fig.5.13) diminish with initial polarization potential in a substantially linear way. Under the conditions of the experiments conducted, this behaviour originates from the presence of increasing co-coverage by electrodeposited oxygen species on the surface since, at initially reduced Pt surfaces, some co-deposition of OH or O species, as surface oxide, arises in the course of the Cl_2 evolution reaction, to greater extents with increasing anode overpotential, as has been mentioned in earlier paragraphs.

The above series of results demonstrate, in a clear way, the sensitivity of the electrocatalytic properties of Pt anode surfaces for electrolytic Cl_2 evolution to the state of surface oxidation of the Pt and the related coverage by the adsorbed Cl· intermediate in the reaction steps.

5.1.5. Capacitance Information from the Initial Potential Decay Fitting Method

The capacitance values obtained from the initial potential decay rates of transients treated by the fitting method (Chapter IV) are shown in Fig.5.16 for the pre-oxidized Pt electrodes. "x" points represent the capacitance values from the initial decay fitting method and "*" and "+" represent the results obtained from a.c. impedance and whole potential decay transient treatments, respectively. It seems that, in most cases, the fitting of fast transients to a polynomial function with evaluation of the initial slope, (dV/dt) t=0, gives only the double-layer capacitance unless the pseudocapacitance is very small with about the same magnitude as the double-layer capacitance (in that case, both capacitances are involved in the self-discharge in fast decay transients). This can be understood, if one considers the electrode reaction

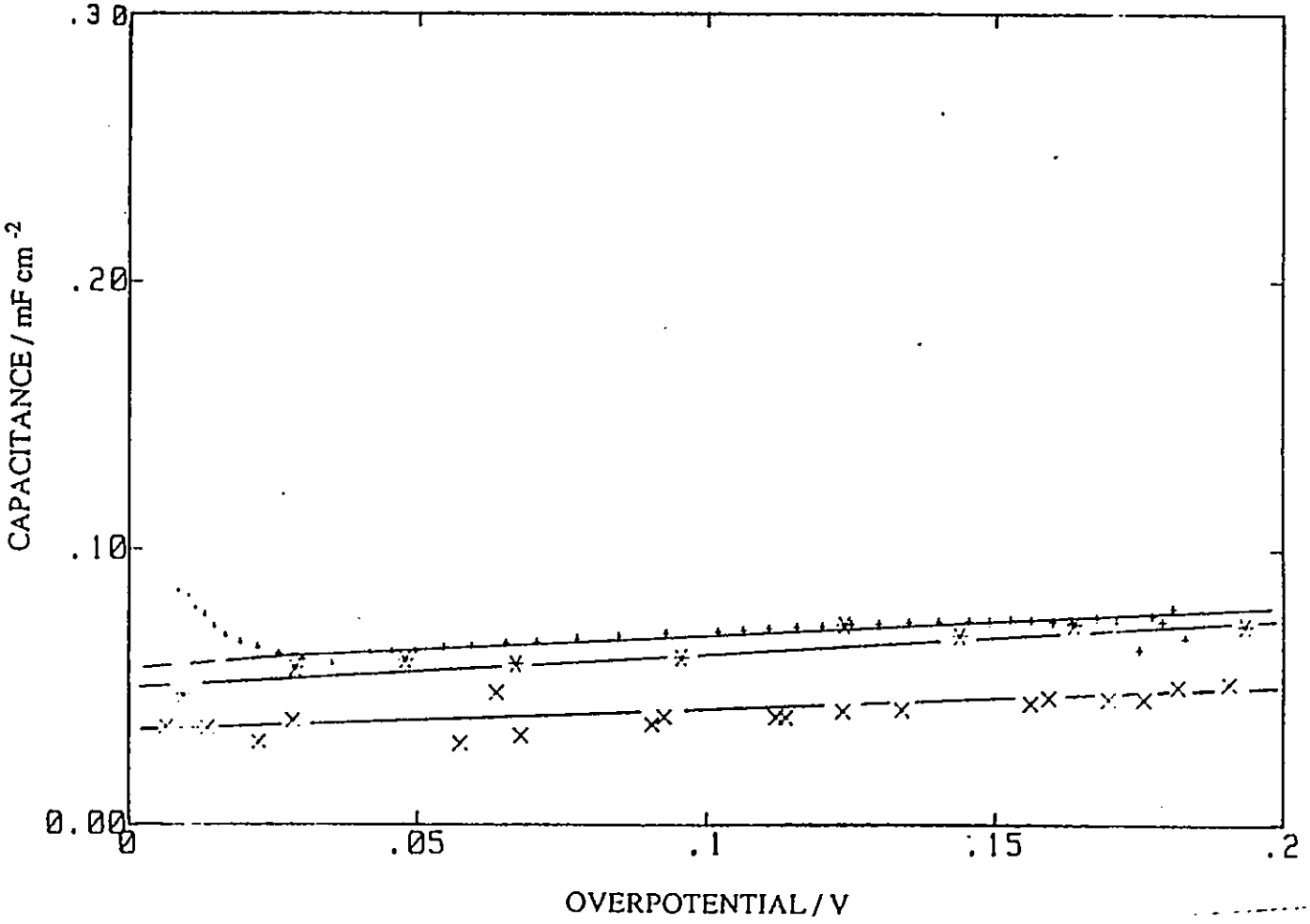

Fig.5.16 Comparison of capacitance values derived from the three different methods for examining Cl adsorption at pre-oxidized Pt electrodes. "+" conventional potential relaxation method; "x" fitting method for potential-relaxation transients and "*" results from a.c. impedance measurements.

with one adsorbed intermediate, for which case the equivalent circuit (in Fig.4.5c) can be used to represent the electrical response of the reaction. The discharge time-constant for an RC circuit (i.e. the "RC" constant) involving the double-layer capacitance is equal to $\tau_{RCdl} = C_{dl}(R_\infty + R_p)$ and the time constant for the pseudocapacitance of adsorbed Cl· is equal to $\tau_{RC\phi} = C_\phi(R_\infty + R_p)$. However, usually $C_\phi >> C_{dl}$ for most cases (in fact, this is the case for Cl_2 evolution at the reduced Pt electrode) over an appropriate potential range, so that $\tau_{RC\phi} >> \tau_{RCdl}$. The small RC time constant will lead to discharge first in the fast decay transient. In the other words, the initial decay rate fitting method always measures the smaller capacitative component first since $-[dV/dt]_{t\to 0} > -[dV/dt]_{t>0}$.

5.1.6. Results from A. C. Impedance Measurements

In order further to clarify the Cl· adsorption behaviour at Pt electrodes, the a.c. impedance method was applied in a complementary way in investigations on both the pre-oxidized and the reduced Pt electrodes according to the procedure described in section (3.6.4). As will be seen later, the a.c. impedance results for the pre-oxidized and the reduced electrodes show one semi-circle and two semi-circles, respectively, in the complex-plane plots of Z" vs Z'. It is evident that , for the reduced Pt electrode, the behaviour of the Cl· intermediate can be distinguishably detected while for the pre-oxidized one, only 2 ~ 5 % of the total surface seems available as "active-area" for Cl· chemisorption. All the a.c. results are in good agreement with those from the potential-relaxation transients. In the following discussion, the "equivalent circuit" and "kinetic constants" approaches will be applied to both states of the Pt electrode surfaces.

5.1.6.1. A.C. Results for " Pre-oxidized " Pt Electrodes

Here, the results from a.c. impedance measurements on the Cl_2 evolution reaction at the "pre-oxidized" Pt electrode are first presented in Figs.5.17a-d for four given "d.c. level" overpotentials : a) 10 mV; b) 100 mV; c) 150 mV; d) 300 mV, from

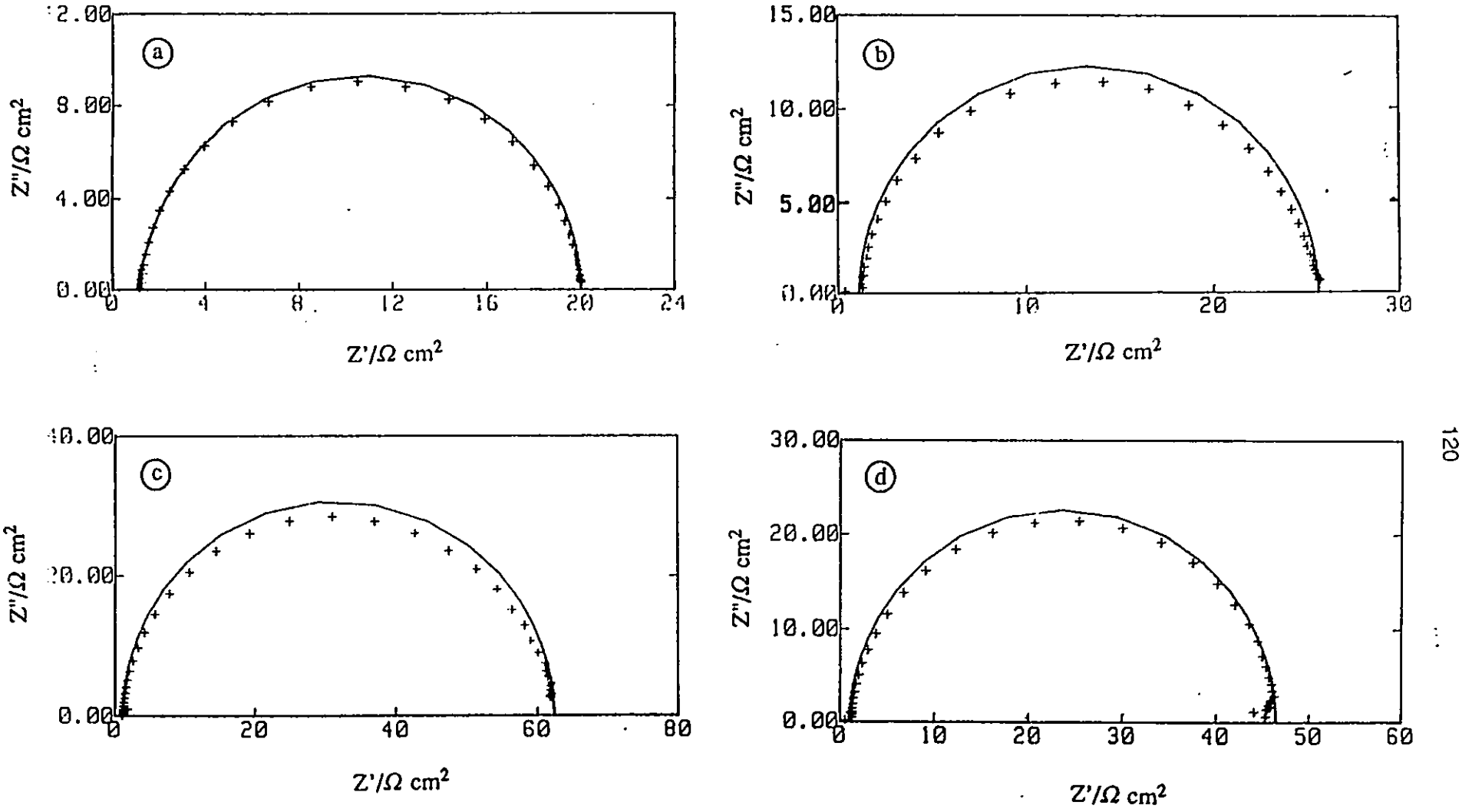

Fig.5.17 The a.c. impedance plots in the complex-plane for Cl_2 evolution at pre-oxidized Pt electrodes for various overpotentials : a) 10 mV; b) 100 mV; c) 150 mV and d) 300 mV as indicated in the diagrams. "+" represent the experimental points and the lines represent the theoretical simulations.

which it can be seen that , for all the potentials, a set of single semi-circles is obtained from the experimental observations. The estimated values of capacitance derived from the top frequency point are about 60 μF cm^{-2}, presumably corresponding to the double-layer capacitance of the oxidized Pt surface. These values of capacitance are in quite good agreement with those from the potential-relaxation measurements (see Figs.5.11 and 5.12). The single semi-circle plots of the impedance response in the complex-plane suggest that only C_{dl} and R_∞ in parallel are the significant components in the equivalent circuit (see Fig.4.5c.) and not much adsorption pseudocapacitance, C_ϕ, is involved; this indicates that the pseudocapacitance associated with the adsorbed Cl_{ad} intermediate is small at the "pre-oxidized" Pt electrode due to low $\theta_{Cl_{ad}}$. This, as we have suggested, must be due to the situation at the "pre-oxidized" Pt electrode surface where the OH or O species have already occupied those low activation energy sites so that the Cl_{ad} adsorption (step I), as well as the recombination (step III), are blocked.

The equivalent circuit fitting was made using the Armstrong equivalent circuit (cf.ref.139). Results (Figs.5.17a-d) are given in the complex-plane impedance diagrams for various potentials, as mentioned above. The experimental data is represented by "crosses" points while the points, connected by solid lines, represent the behaviour simulated by eqns.[4.45] and [4.46] with the parameters listed in Table 5.2. Comparing the experimental and simulated impedance spectra, it can be seen that there is an excellent fit between the solid lines and the points. From the fitting parameters (R_∞, R_p, C_{dl} and C_p), it is evident that the single semi-circles correspond to relaxation involving the double-layer capacitance since the C_{dl} value, derived from the fitting over the whole potential region, is constant at about 50 μF cm^{-2}, in good agreement with the values estimated from the top frequency points and those from the independent potential-relaxation measurements. The values of C_p (C_p is related to the C_ϕ, but is not exactly identical with it; see ref.157) are extremely small, so that this qualitatively indicates a small value also for the C_ϕ pseudocapacitance associated with the adsorbed Cl_{ad} intermediate.

Table 5.2 List of A.C. Fitting Parameters for the Pre-oxidized Pt Electrodes

parameters / over-potential	$R_\infty (\Omega.cm^2)$	$R_p (\Omega.cm^2)$	C_p (F/cm2)	C_{dl} (F/cm2)
10 mV	5.26	13.65	2.2×10^{-5}	4×10^{-5}
100 mV	3.72	20.8	5.8×10^{-6}	5×10^{-5}
150 mV	3.59	57.7	1.9×10^{-6}	5×10^{-5}
300 mV	5.55	39.8	3.5×10^{-8}	5×10^{-5}

Figs.5.18 and 5.19 show the kinetic constant simulation of the same data as those in Fig 5.17 in Bode plots of log| Z | vs log(ω) with | Z | = | $(Z')^2 + (Z'')^2|^{1/2}$, $\omega = 2\pi f$, where f is the frequency in Hz and the phase angle, $\alpha = \tan^{-1}(-Z''/Z')$ vs log(ω). The experimental conditions and simulation parameters for curves (1), (2), (3) and (4) in Figs.5.18 and 5.19 are the same as those for (a), (b), (c) and (d) in Fig.5.17, respectively. It is seen that the numerically simulated behaviour (solid lines in Fig.5.18 and solid and dashed lines in Fig.5.19) provides a very good fit to the experimental data in both log| Z | vs log(ω) and phase angle vs log(ω) plots except for the very high frequency region where some points are "noisy". The single peaks observed in the phase angle vs log(ω) plots indicate that only one capacitative component is involved. All the simulated curves are based on approximately the same set of rate constants, viz : $k_1 = 1 \times 10^{-7}$; $k_{-1} = 8 \times 10^{-8}$; $k_2 = 1 \times 10^{-12}$; $k_3 = 4.35 \times 10^{-8}$ mole cm^{-2} s^{-1}. However, in order to get a "perfect" fit, a slight variation in k_3 is necessary (see Table 5.3); this may be due to some small change in the oxidation state of the Pt electrode surface during the experiment.

Table 5.3 List of kinetic rate constants simulation of the a.c. impedance data for the pre-oxidized Pt electrode interfaces.

Rate constant / Over-potential	k_1 ($cm\ s^{-1}$)	k_{-1} ($cm\ s^{-1}$)	k_2 ($cm\ s^{-1}$)	k_3 ($mol\ cm^{-2}s^{-1}$)	q_o (C/cm^2)	C_{dl} (F/cm^2)
10 mV	1×10^{-7}	8×10^{-8}	1×10^{-12}	3.5×10^{-8}	1×10^{-5}	4×10^{-5}
100 mV	1×10^{-7}	8×10^{-8}	1×10^{-12}	5.2×10^{-8}	5×10^{-6}	5×10^{-5}
150 mV	1×10^{-7}	8×10^{-8}	1×10^{-12}	5.4×10^{-8}	5×10^{-6}	5×10^{-5}
300 mV	1×10^{-7}	8×10^{-8}	1×10^{-12}	3.3×10^{-8}	5×10^{-6}	5×10^{-5}

Form above, it is seen that $k_3/k_2 = 4 \times 10^4$ and, in accordance with experimental behaviour, it is evident that the recombination pathway makes the major contribution to the steady-state current as expressed by the log(i) vs V profiles. Since pathway III is in parallel with pathway II, the recombination pathway is the principal rate-determining step, which explains the observation of attainment of limiting currents in the Tafel relations for the pre-oxidized Pt electrodes.

Further support for the argument that a small "active-area" fraction is involved in Cl^- adsorption at the pre-oxidized electrodes also follows from the results of the kinetic constants simulation of the a.c. impedance spectra since the q_o, supposedly the charge for adsorption or desorption of a full monolayer of the intermediate (here, the Cl^-), was not equal to ca. 210 $\mu C\ cm^{-2}$ (1 Cl^- per surface Pt atom) as was expected but had a value of only ca. 10 $\mu C\ cm^{-2}$ or less, 20 times smaller then it would have been for a free metal surface. This means that only about 5% of the total surface area is available for Cl. and Cl^- adsorption, the remaining fraction being occupied by the oxide that was pre-formed on the Pt electrode surface. Fig.5.20 shows the simulation curves

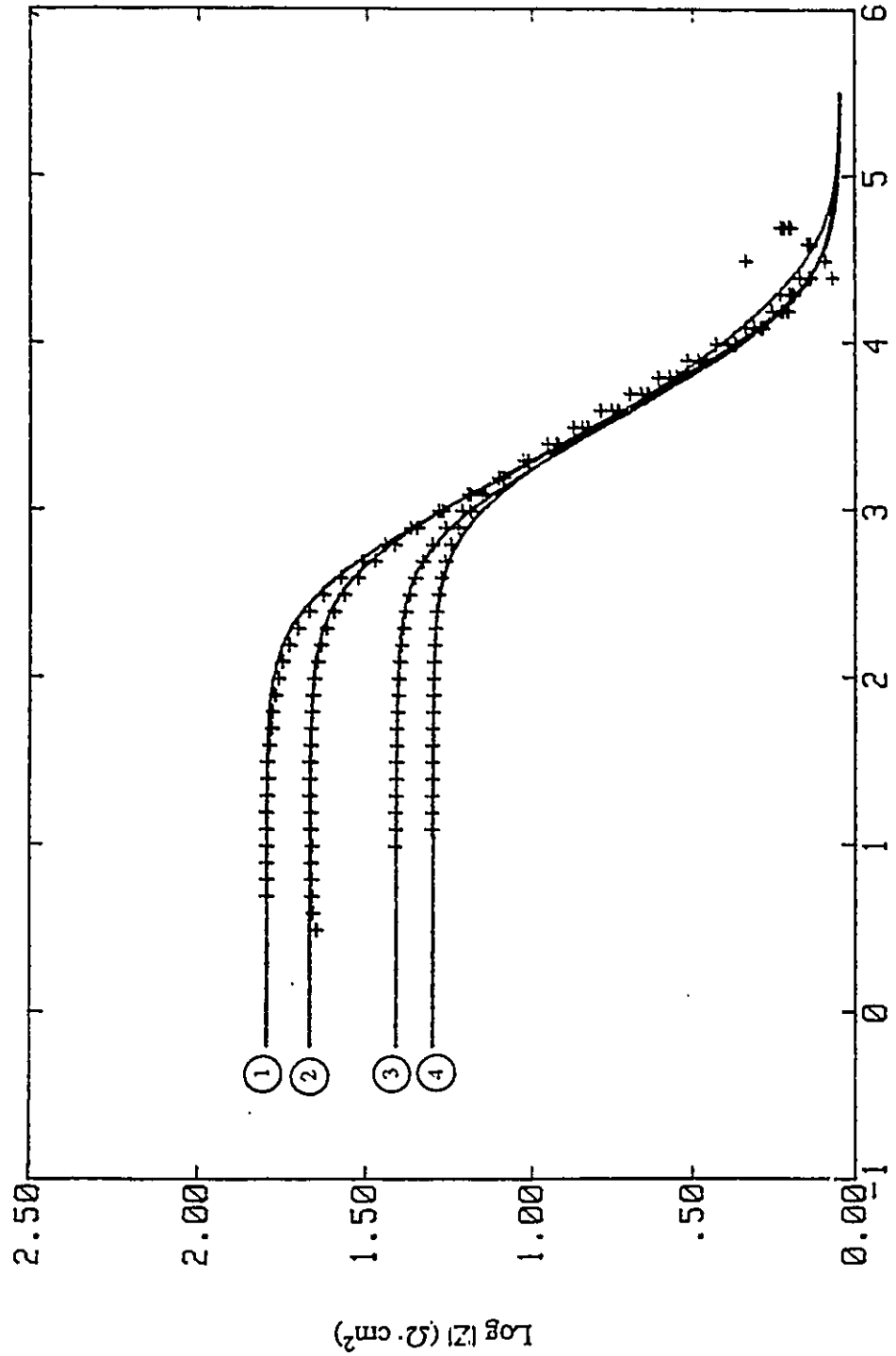

Fig.5.18 Experimental (crosses) and simulated (solid lines) Bode plots for Cl_2 evolution at pre-oxidized Pt electrodes. The experimental conditions and simulation parameters for curves 1), 2), 3) and 4) are the same as those for Figs.5.17 a), b) c) and d), respectively.

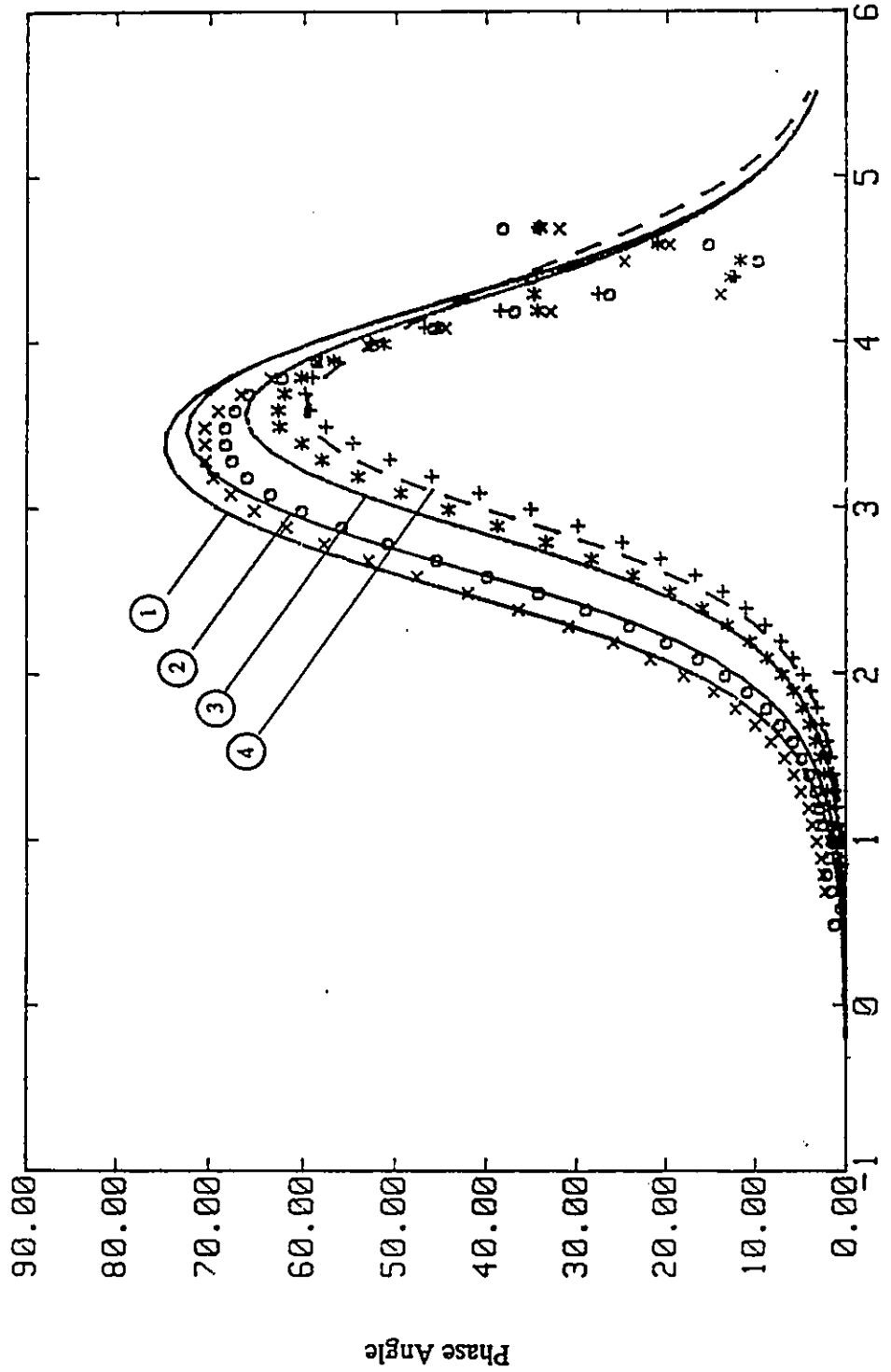

Fig.5.19 The same experimental and simulated data as for Fig.5.18 except being plotted as phase angle vs log| Z |. Lines and points represent the theoretical simulation and experimental data, respectively. "x", "o", "*" and "+" correspond to a), b), c) and d) in Fig.5.18.

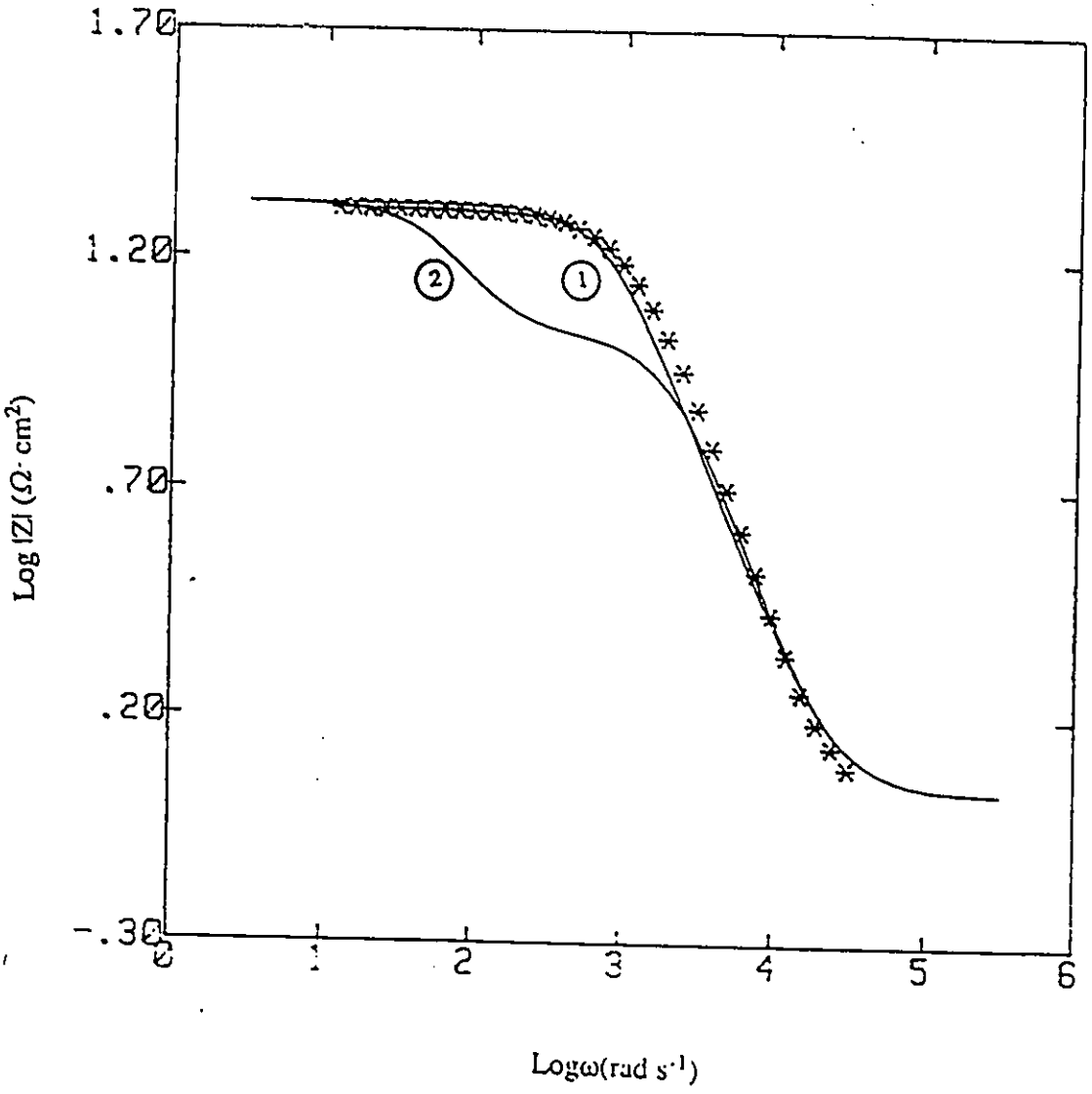

Fig.5.20 Experimental (crosses) and simulated (solid lines) Bode plots, log| Z | vs log(ω), for Cl_2 evolution at pre-oxidized Pt electrodes. Curve 1) taking the value of q_a = 10 μC cm^{-2} and 2) q_a = 210 μC cm^{-2}.

(1) with q_o = 210 μC cm^{-2} and (2) with q_o = 10 μC cm^{-2}. It is clear that only curve (2) has a good fit with the experimental points.

The simulated log[current-density] and log($1/R_-$) behaviours using the eqns. [4.81] and [4.82a], are shown in Fig.5.21. In contrast to the result for the HER reported by Bai and Conway [158], the variation of log($1/R_-$) with V was similar to log(i) behaviour. This is consistent with the electrochemical adsorption step [I] playing a very significant role in the kinetics of the overall Cl_2 evolution process since R_- is associated with step [I].

The simulated behaviour of the pseudocapacitance, C_ϕ, and the Cl_{ad} intermediate coverage, $\theta_{Cl_{ad}}$, calculated by means of eqns.[4.80] and [4.79], as well as C_p by eqn.[4.82e] and τ_{ac}, the relaxation time by eqn. [4.82d] are shown in Fig. 5.22. Interestingly, the curves of C_p and C_ϕ vs V have similar shapes (but the value of C_p is larger) with no capacitance peak being observed in the 0 to 0.5 V overpotential range. This situation is close to that experimentally observed: only a rise in C_ϕ at low overpotentials near the equilibrium potential is found. The coverage by Cl_{ad}, $\theta_{Cl_{ad}}$, starts with a non-zero value and reaches a limiting small value of about θ = 0.02, which relates to the small fraction of surface area available for Cl_{ad} adsorption on the oxidized surface. The change of θ with potential, i.e. $d\theta/dV$, is small. Thus the C_ϕ, = $q_o d\theta/dV$ will not be significant since both q_o and $d\theta/dV$ are small. The τ_{ac} vs V plot (cf.eqn.4.82d) also has a similar shape to that of the C_ϕ vs V plot; this is because τ_{ac} has a similar physical significance in some cases to that of C_ϕ(refs.157,158,124).

5.1.6.2. A.C. Impedance Results for the "Reduced" Pt Electrodes

In contrast to the case of the "pre-oxidized" electrodes, the a.c. impedance spectra for Cl_2 evolution at the reduced Pt electrodes, in 1 N aq. HCl solution, are substantially different. Instead of a single semi-circle, two semi-circles arise in the complex-plane plots for various potentials, as shown in Fig.5.23 under conditions of which N_2 was bubbled in the working electrode compartment, i.e. with virtually no

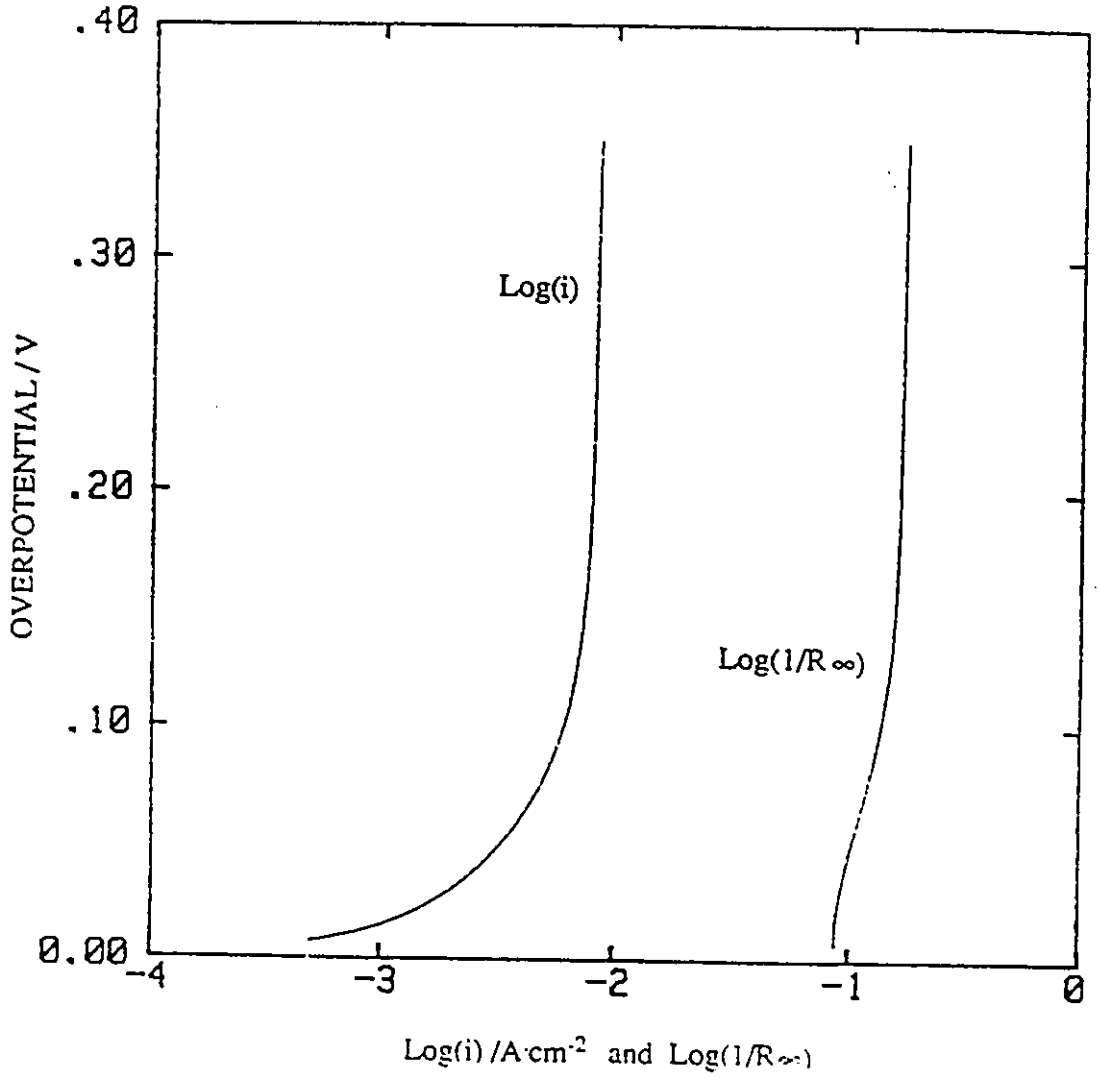

Fig.5.21 Simulated log(*i*) vs V and log(1/R_∞) vs V behaviour for Cl_2 evolution in aqueous solution at a pre-oxidized Pt electrode according to eqns.[4.81] and [4.82a], using rate constant values k_1 = 1.0x10^{-7}; k_{-1} = 8.0x10^{-6}; k_2 = 1.0x10^{-12}; k_3 = 4.35x10^{-6} mol cm^{-2} s^{-1}.

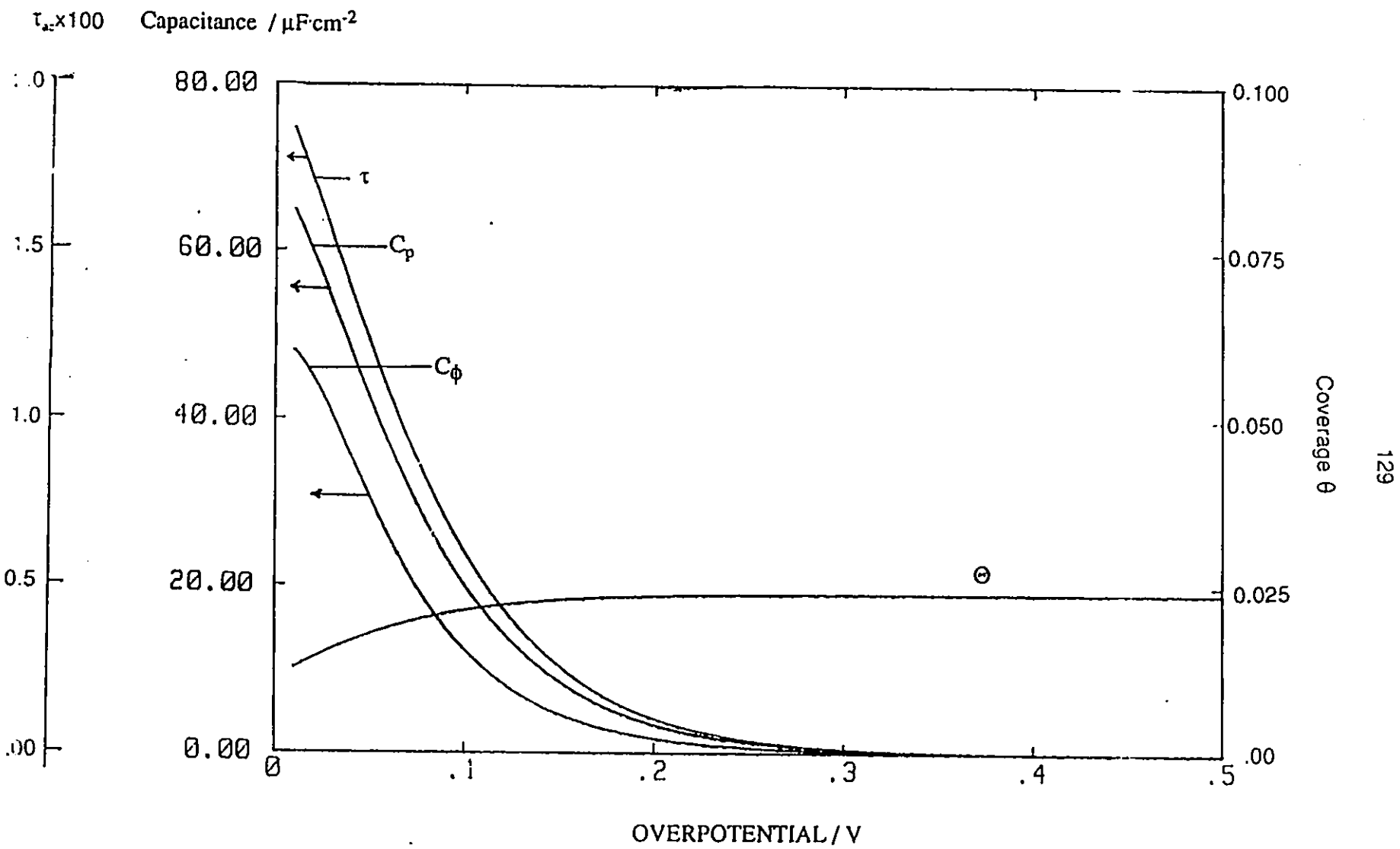

Fig.5.22 Simulated C_p vs V, C_ϕ vs V, θ vs V and τ vs V behaviour for Cl_2 evolution in aqueous solution at pre-oxidized Pt electrodes according to eqns.[4.82e], [4.80], [4.79] and [4.82d] using rate constant values $k_1 = 1.0\times10^{-7}$; $k_{-1} = 8.0\times10^{-6}$; $k_2 = 1.0\times10^{-12}$; $k_3 = 4.35\times10^{-6}$ mol cm^{-2} s^{-1}.

molecular Cl_2 being present. The observation of two semi-circles qualitatively indicates, in the case of the reduced Pt electrode surface, that adsorption of the $Cl^{\cdot}$ intermediate is now significant and appreciable.

As will be discussed further below, that the first semi-circle in the impedance complex-plane plot corresponds to the relaxation of the double-layer capacitance while the second corresponds to the pseudocapacitance, C_ϕ, associated with the adsorbed intermediate, $Cl^{\cdot}$ in the Cl_2 evolution reaction. (The second semi-circle cannot be due to the adsorption of O or OH species because the deposition and reduction of such species is irreversible except at low coverage at Pt. Thus, small amplitude potential modulation [±5 mV] would not affect the O or OH species which will remain in the state in which they were initially deposited. Also, under otherwise the same experimental conditions as for the Cl_2 evolution experiments, a.c. impedance measurements at Pt, taken in a 0.5 M H_2SO_4 aqueous solution in the absence of Cl^- gave no second semi-circle over a wide potential range, even up to +1.90 V vs RHE.). The adsorbed $Cl^{\cdot}$ intermediate therefore plays a very important and observable role in Cl_2 evolution kinetics at the freshly reduced surfaces of Pt and its behaviour can be detected not only by a.c. impedance but also by the potential relaxation method, and indirectly by cyclic-voltammetry as well.

The second semi-circle becomes smaller as the potential increases and eventually almost disappears at ca. 60 mV overpotential (Fig.5.23d). This potential region corresponds to that where the pseudocapacitance peaks arise for the reduced Pt electrode in potential relaxation measurements (Fig.5.13).

The goodness of fit of the simulated impedance spectra for the Cl_2 evolution reaction at the reduced Pt electrodes was tested, using the equivalent circuit (Fig.4.5c) and the results are shown in Figs.5.23a-d, for various potentials : a) 1.33 V; b) 1.35; c) 1.37 V and d) 1.42 V vs RHE. The solid lines again represent the simulation fitting and the small "crosses" the experimental data. It is seen in all the diagrams that very good agreement between the theoretical and the experimental

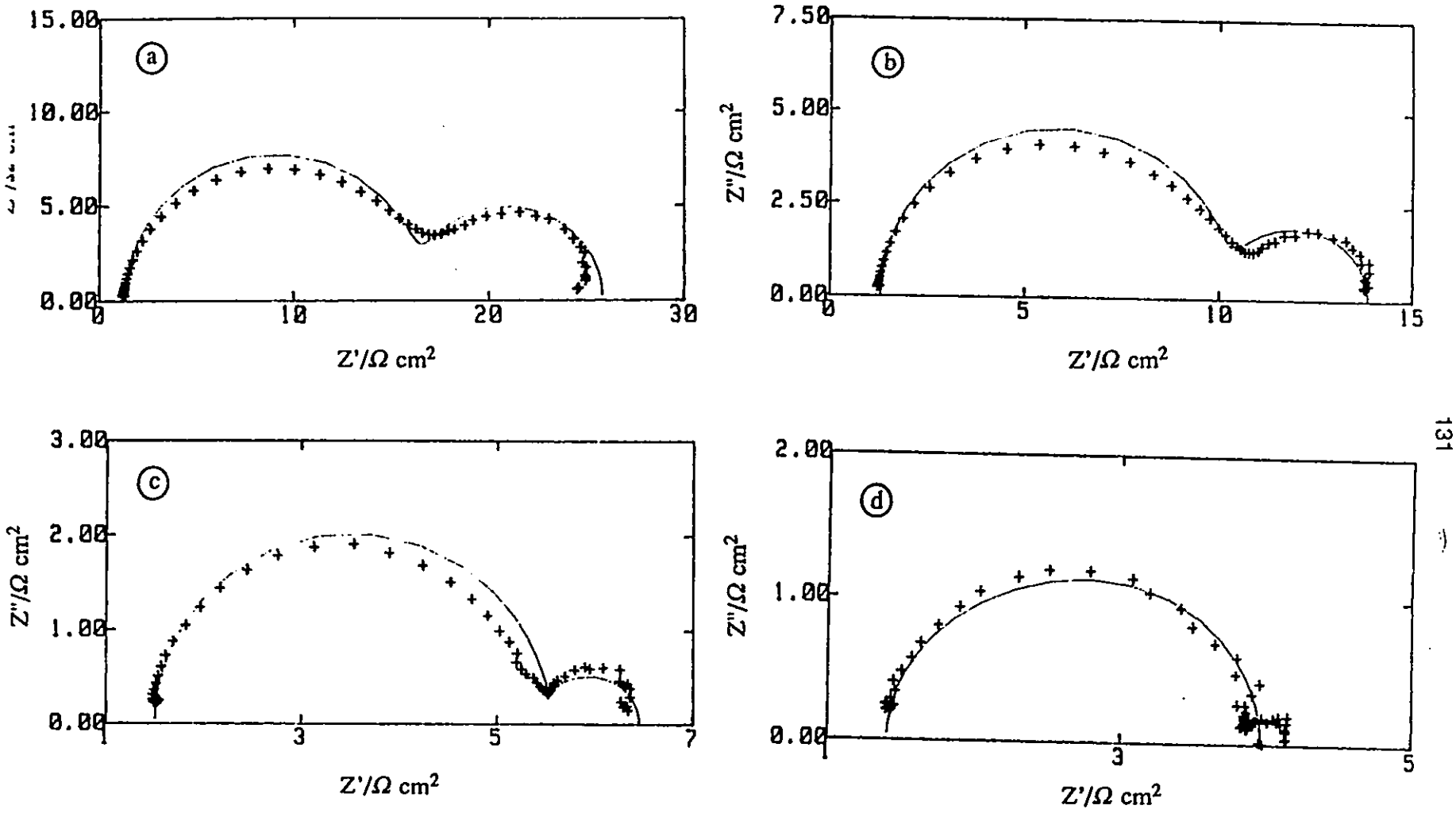

Fig.5.23s.a-d A.c. impedance plots in the complex-plane for the Cl_2 evolution reaction at reduced Pt electrodes at various potentials (vs RHE) : a) 1.33 V; b) 1.35 V; c) 1.37 V and d) 1.42 V, as indicated in the diagrams. "+" represent the experimental points and the line represents the theoretical simulation.

points is achieved. The required values for the parameters C_p, R_∞, R_p and C_{dl}, corresponding to these fitted curves*, are given in Table 5.4 below:

The value of the double-layer capacitance required for the equivalent circuit fitting is ca. 50 μF cm^{-2} (the same as for the kinetic constants simulation below). Both R_∞ and R_p, in this case, decrease with increasing potential because increase of potential reduces the activation energy of the discharge reaction step so that R_∞ and R_p, the reaction resistances, become experimentally smaller.

Table 5.4 List of A.C. Fitting Parameters for Reduced Pt Electrodes

Parameters / Potential vs RHE	R_∞ (Ωcm^2)	R_p (Ωcm^2)	C_P ($F cm^{-2}$)	C_{dl} ($F cm^{-2}$)
1.33 V	15.1	8.38	5.5×10^{-3}	5×10^{-5}
1.35 V	9.1	3.45	8.8×10^{-3}	5×10^{-5}
1.37 V	3.8	0.89	1.5×10^{-2}	5×10^{-5}
1.38 V	3.6	0.73	1.6×10^{-2}	5×10^{-5}
1.42 V	2.0	0.61	6.2×10^{-4}	5×10^{-5}

* The fitting, it is to be stressed, is not entirely arbitrary since (a) a series of double curves is simulated and (b) a series of values of the parameters, self-consistent for four d.c.-level potentials, over a wide frequency range must be sought.

Even though C_p does not exactly correspond to the capacitance of the adsorbed intermediate, Cl, it is quite closely related to the pseudocapacitance, C_ϕ. The large values of C_p, about ~16 mF cm^{-2} at the maximum, indicate qualitatively that appreciable values of the pseudocapacitance must arise being comparable in magnitude to C_p.

The most interesting simulation results are those in the form of Bode plots, log|Z| vs log(ω) and phase angle vs log(ω), obtained by applying the kinetic constants approach to the same data as those shown in Fig.5.23 and are given in Figs.5.24 and 5.25, respectively. The numbers 1, 2, 3 and 4 in both Figs.5.24 and 5.25 correspond to the a, b, c and d in Fig.5.23. From these two figures, it can be seen that an excellent numerical fit is achieved between the experimental points (shown as crosses, circles and stars etc.) and the theoretical data (shown as lines). In the phase-angle vs log(ω) plots, two peaks are observed which correspond to the two capacitative components involved in the electrochemical process. The second peak in the low frequency region becomes smaller with increase of potential, so that, at sufficiently high potentials, no significant pseudocapacitance is measurable, i.e. θ has reached a certain limiting value (usually ≈ 1, see Fig.5.14) or the change of θ, dθ/dV, approaches zero (for the full coverage situation). The values of the best-fit simulation parameters: k_1, k_{-1}, k_2, k_3, q and C_{dl} are listed in Table 5.5 for various potentials. The set of k_3 constants for different potentials are about the same while, as expected, k_1 and k_{-1} in the low potential region, where the kinetics of the first step may play a significant role, vary. However, the set of average rate constants from Table 5.5 is as follows: k_1 = 1.63×10^{-7}, k_{-1} = 2.3×10^{-8} , k_2 = 3.5×10^{-10} and k_3 = 9.2×10^{-7} mole cm^{-2} s^{-1}.

Since it is found that the rate constant of the recombination step, $k_3 >> k_2$ the electrochemical desorption pathway, this explains how the same reaction mechanism arises apparently for the Cl_2 evolution at the reduced Pt surface as at pre-oxidized one, which the results also indicate as being recombination-controlled.

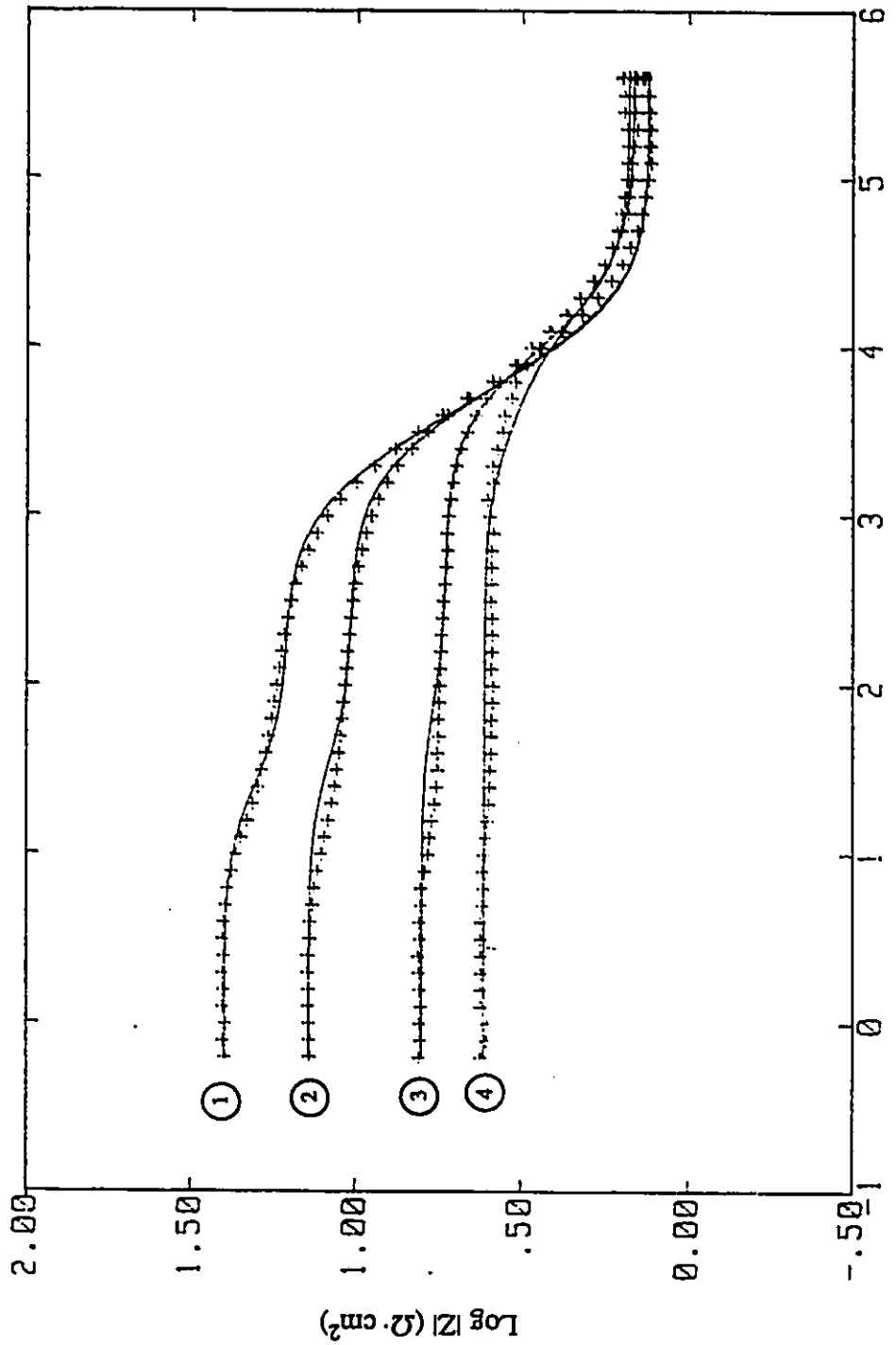

Fig.5.24 Experimental (crosses) and simulated (solid lines) Bode plots for Cl_2 evolution at reduced Pt electrodes. The experimental conditions and theoretical simulation parameters for curves 1), 2), 3) and 4) are the same as those for Figs.5.23 a), b) c) and d), respectively.

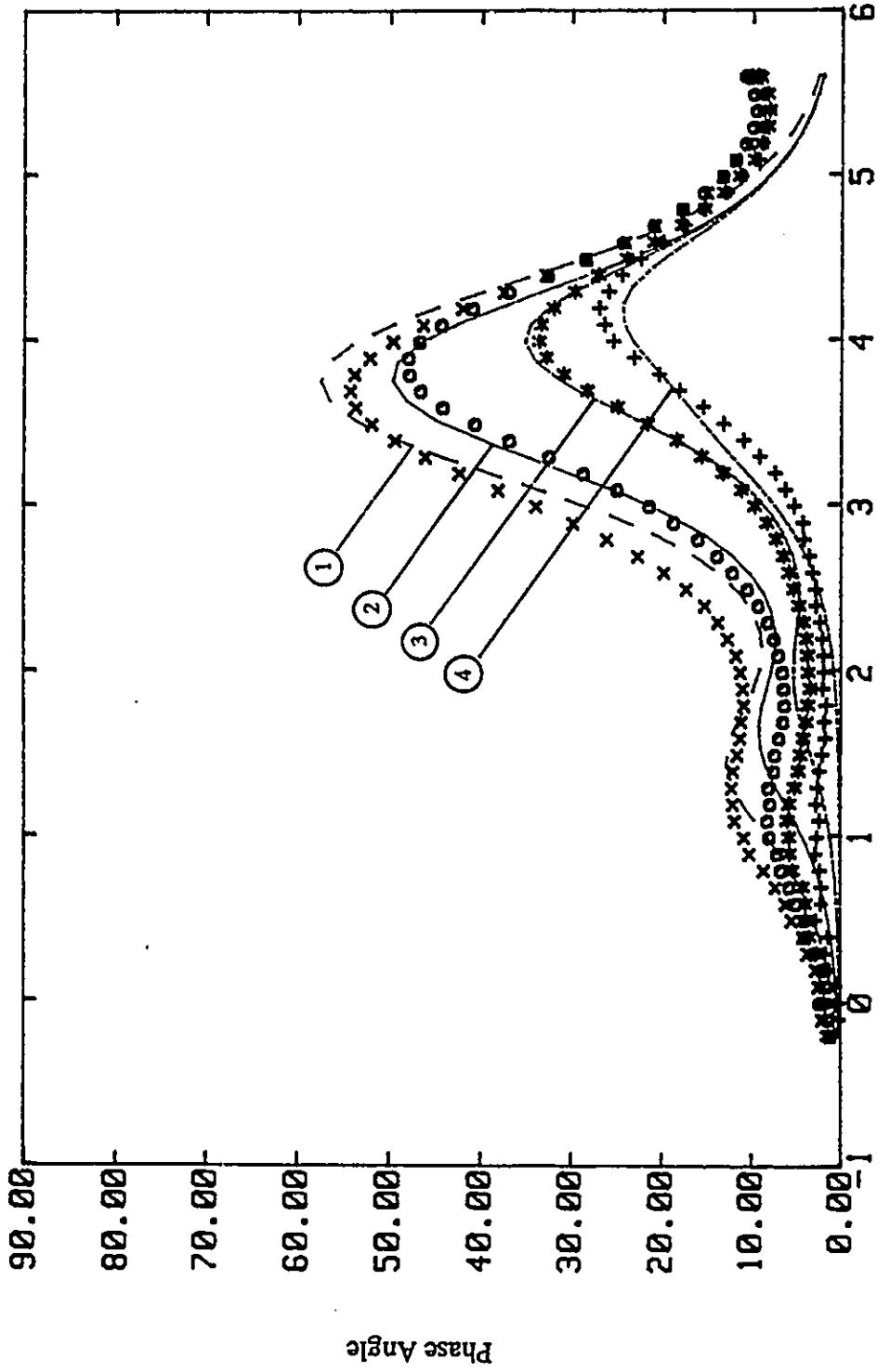

Fig.5.25 The same experimental and theoretically simulated data as in Fig.5.24 except plotted as phase-angle vs log(ω). Lines and points represent the theoretical simulation and experimental data, respectively. "x", "o", "*" and "+" points correspond to a), b), c) and d), respectively, in Fig.5.24.

Table 5.5 List of kinetic rate constants simulation of the a.c. impedance data for the freshly reduced Pt electrodes.

Rate constant / Potential vs RHE	k_1 ($cm\ s^{-1}$)	k_{-1} ($cm\ s^{-1}$)	k_2 ($cm\ s^{-1}$)	k_3 ($mol\ cm^{-2}\ s^{-1}$)	q_o ($C\ cm^{-2}$)	C_{dl} ($F\ cm^{-2}$)
1.33 V	4.6×10^{-8}	7×10^{-8}	3.5×10^{-10}	7.2×10^{-7}	1.2×10^{-3}	4×10^{-5}
1.35 V	6×10^{-8}	9×10^{-8}	3.5×10^{-10}	7.2×10^{-7}	1.2×10^{-3}	5×10^{-5}
1.37 V	1.6×10^{-7}	5×10^{-8}	3.5×10^{-10}	9.2×10^{-7}	1.2×10^{-3}	5×10^{-5}
1.38 V	1.6×10^{-7}	1×10^{-8}	3.5×10^{-10}	9.2×10^{-7}	1.2×10^{-3}	5×10^{-5}
1.42 V	1.8×10^{-7}	1×10^{-8}	3.5×10^{-10}	9.2×10^{-7}	5.1×10^{-4}	5×10^{-5}

Comparing the k_1 and k_3 values in the Cl_2 evolution mechanism for both the reduced and the pre-oxidized cases, k_1 (reduced) $\approx 1.63\times10^{-7} > k_1$ (oxidized) $\approx 1\times10^{-7}$ and k_3 (reduced) $= 9.2\times10^{-7} > k_3$ (oxidized) $\approx 4\times10^{-8}$. These data indicate that, for the reduced Pt, both k_1 and k_3 are larger than the corresponding values for the oxidized Pt electrode. This clearly reflects the role of the oxide film in affecting the kinetics of the Cl_2 evolution reaction and the adsorption of its intermediate, $Cl^{\cdot}$. The presence of co-deposited O or OH species on the surface of the Pt electrode would not necessarily change the mechanism of the reaction but it evidently does block the "active-area" thus diminishing adsorption of $Cl^{\cdot}$ or $Cl^{\cdot}$ and changing the electrocatalytic properties of the Pt surface. In a state of extended surface oxidation, the oxide film makes the Cl_2 evolution reaction kinetically more difficult by reducing the rate constants k_1 and k_3 for the $Cl^{\cdot}$ adsorption and recombination desorption steps, respectively.

According to eqns.[4.82a] and [4.81], the behaviour of log(1/$R_{\_}$) and log(i) as $f(V)$, can be simulated, taking the average rate constants from Table 5.5 for the reduced Pt electrode; the resulting behaviour is shown in Fig.5.26. The shape of the

log(1/R_-) curve is also similar to that of log(i) vs V which means that, for the reduced surface, the adsorption of Cl^-, and $Cl^\cdot$ as well is still an essential step. As mentioned earlier, at the reduced Pt electrode, a greater active-site density is available for $Cl^\cdot$ adsorption, which enables the currents to remain large. Comparing this with Fig.5.21, the C_ϕ, C_p, θ and τ_{ac} behaviours are quite different, especially that of the pseudocapacitance, which has a maximum in Fig.5.27, in qualitative agreement with the experimental behaviour observed. However, the rather narrow peak observed experimentally may be due to attractive interactions between the adsorbed species as represented by a negative g factor in the adsorption isotherm (eqn.[2.40]). Another difference is that the relaxation time, τ_{ac}, is much larger for the reduced electrode than that for the pre-oxidized one. The reason, again, is that the greater surface density of the adsorbed species corresponds to a longer relaxation time because of the larger C_ϕ.

Another significant difference between the behaviour of the reduced and oxidized electrodes is the charge value q. For the reduced electrode, a much larger value of q (1.2 mC cm^{-2}) is required in the simulation than it is needed for the pre-oxidized one (10 μC cm^{-2}). This large difference must be a principal basis for the big difference in their pseudocapacitance profiles as derived from both the potential relaxation and a.c. impedance methods. These results are thus in good agreement with those from the potential relaxation measurements, and also support the argument in terms of "active-area" density since the reduced Pt surface has a much greater free site density available for $Cl^\cdot$ adsorption and recombination. The large value of q may arise for the following reasons : first, the roughness factor should be considered, since even for a fresh and smooth Pt electrode, the intrinsic roughness factor can be 1.2 to 1.3, allowance for which would diminish the q value by 20 to 30 %. Secondly, as for the O_2 evolution reaction at Pt studied by Conway and Liu (refs.119), a place-exchange effect may arise in the co-deposited oxide film in the case of the Cl_2 evolution reaction at Pt, which means the adsorbed $Cl^\cdot$ may to some extent exchange places with Pt atoms so

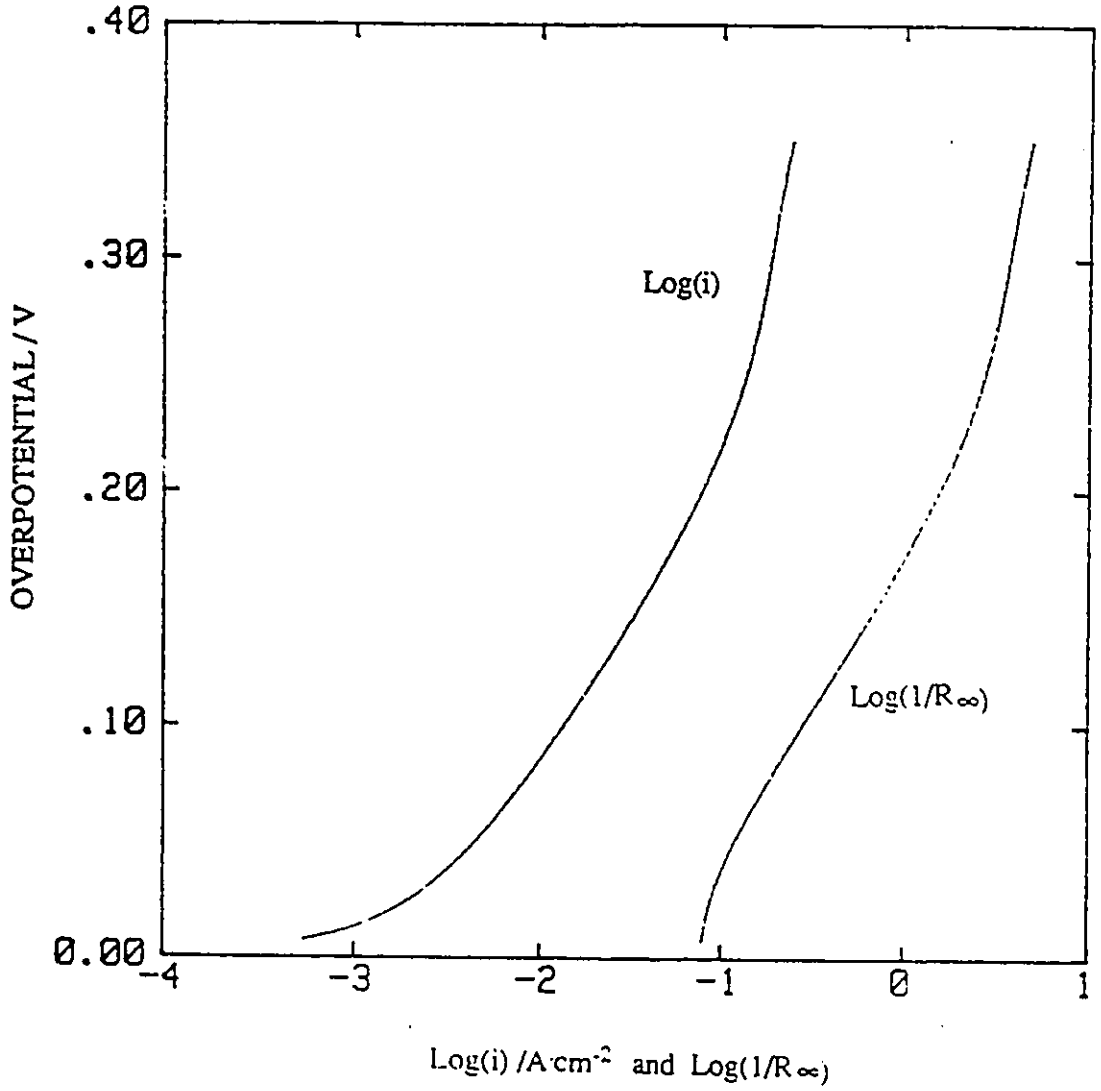

Fig.5.26 Simulated log(i) vs V and log(1/R_∞) vs V behaviour for the Cl_2 evolution reaction in aqueous solution at reduced Pt electrodes according to eqns.[4.81], [4.82a] and [4.82c] using rate constant values k_1 = 1.63x10^{-7}; k_{-1} = 2.3x10^{-6}; k_2 = 3.5x10^{-6}; k_3 = 9.2x10^{-7} mol cm^{-2} s^{-1}.

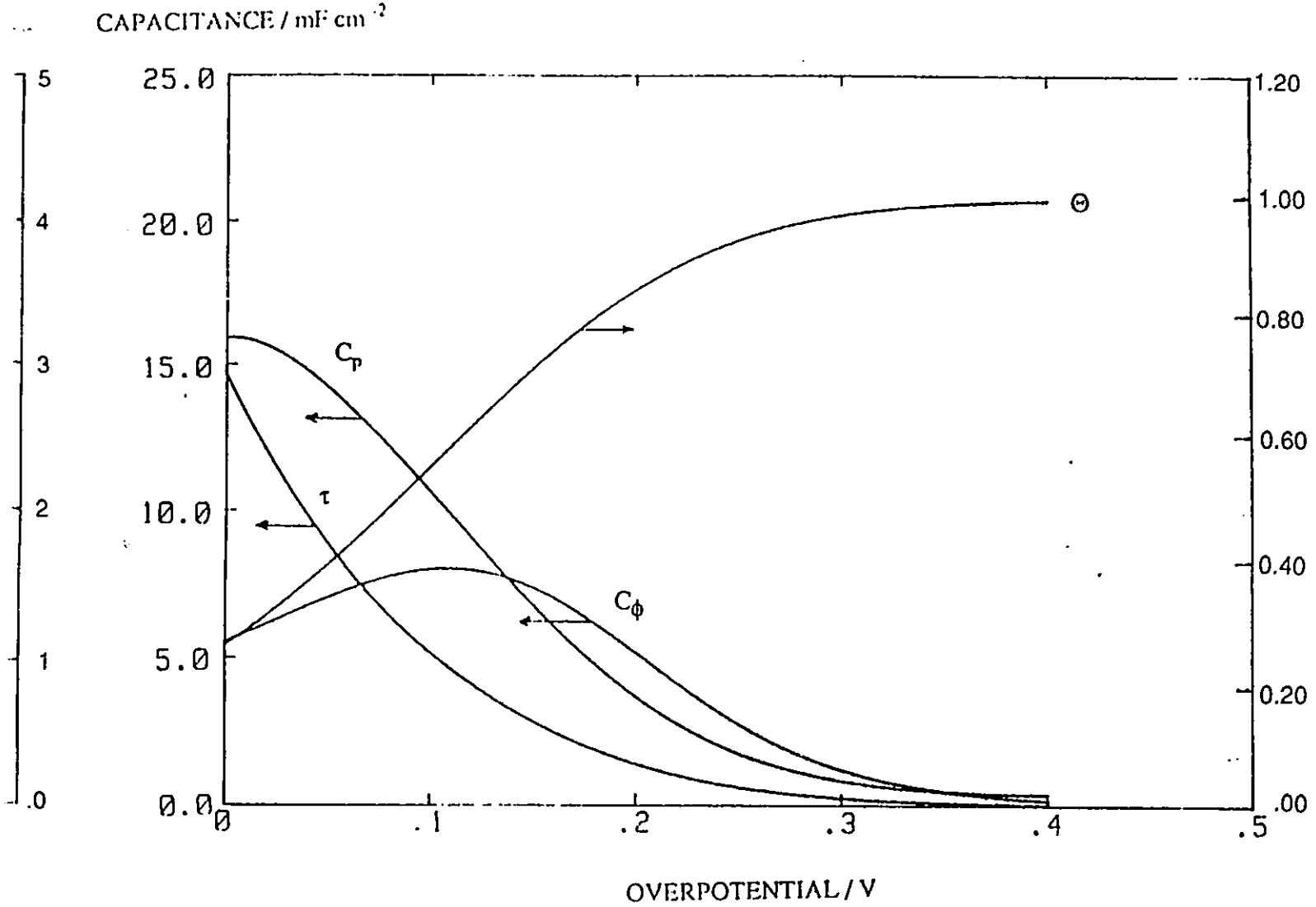

Fig.5.27 Simulated C_p vs V, C_ϕ vs V, θ vs V and τ vs V behaviour for the Cl_2 evolution reaction in aqueous solution at reduced Pt electrodes according to eqns.[4.82e], [4.80], [4.79] and [4.82d] using the average rate constant values $k_1 = 1.63\times10^{-7}$; $k_{-1} = 2.3\times10^{-6}$; $k_2 = 3.5\times10^{-10}$; $k_3 = 9.2\times10^{-7}$ mol cm^{-2} s^{-1}.

that one Pt atom could actually interact with more than one Cl· Thirdly, the Pt becomes more rough after multiple oxidation-reduction cycles. As suggested by Burke[162], the surface Pt atoms, like Ir, cannot come back to the same places they were originally in, following successive oxidation-reduction cycles. An overall schematic outline of processes of oxide growth under potential-cycling conditions is illustrated in the diagram below. As can be seen, each surface Pt atom could possibly be effectively involved in adsorption of more than one Cl· atom after a reconstructed state of the oxide film has been generated, as in (4) below, but this is only a tentative suggestion.

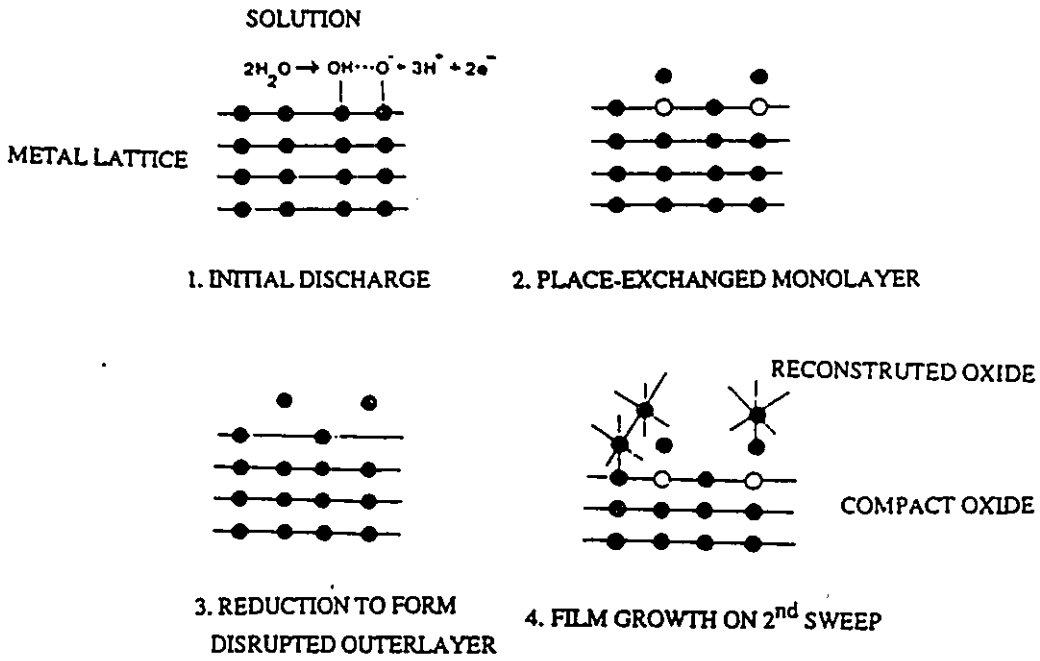

5.2. Results at Pt in Non-aqueous Trifluoroacetic Acid Solution

The possibility of examining the kinetics of anode Cl_2 evolution in the complete absence of an oxide film, e.g. at Pt, was demonstrated by Conway and Novak (ref.86). As was mentioned earlier, in aqueous Cl^-, at any metal including the noble ones, Cl^- discharge and Cl_2 evolution takes place always on an oxide-film covered surface of the metal. However, by conducting studies of the reaction (at Pt) in anhydrous triflouroacetic acid (TFA), "gettered" from traces of water by reaction with this acid's own anhydride, it was shown that the Cl_2 evolution reaction from RbCl (chosen for reason of favourable solubility) in TFA could be studied in the complete absence of surface oxide at Pt; the kinetics were shown still to be recombination controlled.

The Cl_2 evolution reaction on Pt electrodes in a non-aqueous 0.5 M RbCl in TFA solution was investigated in the present work by means of potential relaxation and a.c. impedance methods, as well as by steady-state polarization measurements. It will be shown, in this section, that the Cl_2 evolution kinetics remain recombination controlled under these conditions and non-diffusion controlled limiting current densities are again observed. However, the limiting currents are much smaller than in the case of aqueous solutions. This is presumably due to the strong bonding of the Cl^- on the "bare" oxide-free Pt electrode surface and/or to strong adsorption of the TFA anion.

Information concerning the behaviour of the adsorbed $\dot{Cl}$ intermediate in Cl_2 evolution is also derived from the C vs V profile obtained, as before, by processing the potential-relaxation measurements. From corresponding a.c. impedance results, complex-plane plots comprised of two semi-circles were obtained and it is evident that the second semi-circle is due to the adsorbed Cl^- intermediate in Cl_2 evolution kinetics under these H_2O-free conditions.

5.2.1. Steady-State Polarization Behaviour

First, the steady-state polarization (Tafel plots) for Cl_2 evolution at " bare " Pt in a

0.5 M RbCl solution in TFA taken at various electrode rotation rates from 400 to 4900 rpm. are shown in Fig.5.28. The current, i, for anodic Cl_2 formation, becomes significant at ca. 1.1 V vs Ag/AgCl and reaches limiting values (cf.ref.86) of current-density at about the 1 mA cm^{-2} level. Since the significance of i_{lim} is important with regard to $Cl^{\cdot}$ recombination-controlled kinetics, two types of experiments were performed to identify it as a kinetically limited-current : i) ohmic polarization "IR" was checked over a wide current range by the current interruption technique; "IR" drops were, however, negligible in the anhydrous TFA experiments. ii) Current vs potential plots were established at a rotating Pt disc electrode, as shown in Fig.5.28, and were found to be independent of r, the rotation rate. Thus, the log(i) vs V curves and the limiting currents observed are kinetically controlled, confirming previous conclusions.

5.2.2. Potential Relaxation Transients and C(V) vs V Profiles

We have discussed the influence of the oxide film on Cl_2 evolution reaction kinetics in an aqueous solution at the Pt electrode. In order to study the effect of the oxide film in the Cl_2 evolution in a non-aqueous solution, three differently prepared Pt electrodes were used. They were : (a) without any pre-oxidation of the Pt electrode surface; (b) with the Pt electrode being pre-oxidized in a 0.1 M aq. H_2SO_4 solution to form approximately a monolayer of the oxide by holding the electrode at a polarization potential of ca. 1.0 V RHE and (c) the same procedure as in (b) except that the oxide was formed to an extent greater than a monolayer. The corresponding charges for their reduction are listed in Table 5.6 below :

The potential relaxation results, expressed as V vs log(t) and the corresponding V vs log(-dV/dt) plots for cases (a), (b) and (c) are shown in Figs.5.29a-c and 5.30a-c, respectively. In all the V vs log(t) curves taken from various initial polarization potentials, three regions are barely distinguished.

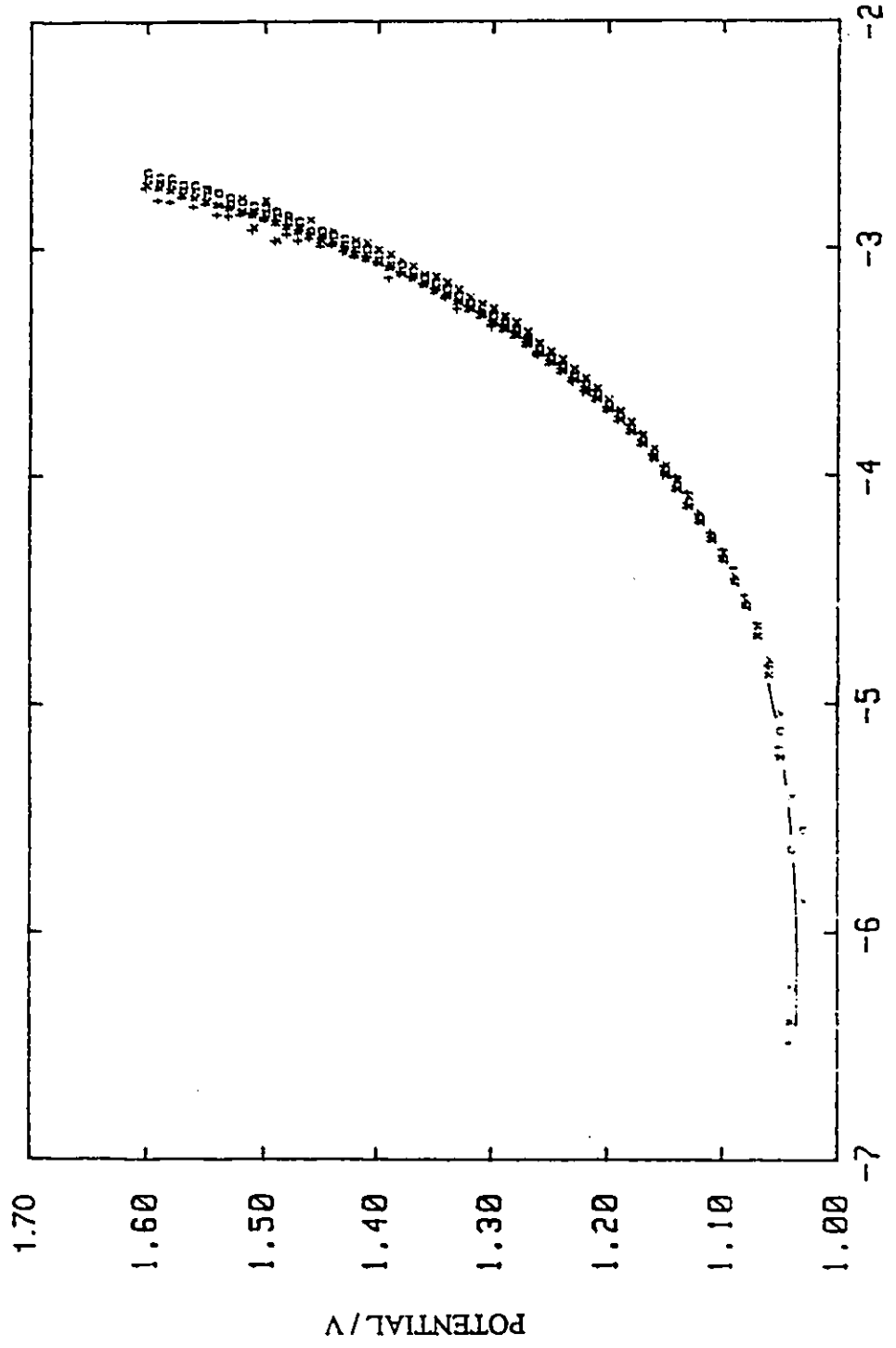

Fig.5.28 Log[current-density] vs overpotential relations for Cl_2 evolution at a rotated Pt disc electrode (298 K) in 0.5 mol dm^{-3} RbCl + TFA non-aqueous solution. Rotation rates: "+" 400; "*" 900; "z" 1600; "o" 2500 and "x" 3600 r.p.m.

Table 5.6 Charges for Pre-oxidation of Pt electrodes used in TFA Solutions

Cases	Pre-oxidation charge ($\mu C\ cm^{-2}$)
a	~ 0
b	127
c	625

A flat area is approached after times of ca. 10^{-3} s in both cases (a) and (b) while the time is 10^{-2} s for case (c). Over the time range 10^{-2} s (for (c) it is ~ $10^{-1.5}$) to ~ 1 s, the decay slopes change continuously. This may be due to the discharge of the double-layer capacitance coupled with that of the Cl^- adsorption pseudocapacitance. The corresponding set of V vs log(-dV/dt) plots have hyperbolic shapes, no linear relationship being observed. This could arise because of the existence of the pseudo-capacitance which may be small and hence relatively close to the value of the double-layer capacitance. The discharge time constant for the Cl^- intermediate adsorption capacitance is then not much larger than that for the double-layer capacitance, so a broad relaxation region in time arises.

The C vs V profiles for the three cases are shown in Fig.5.32 and exhibit quite appreciable differences. the "star" points represent results for case (a), the "circles" for case (b) and "crosses" for case (c). It is not surprising that a capacitance maximum arises in cases (a) and (b), but it is unexpected that, in case (c), the C vs V profile is without a significant C(V) maximum, and also much larger capacitance values arise in the higher potential region where only the double-layer capacitance

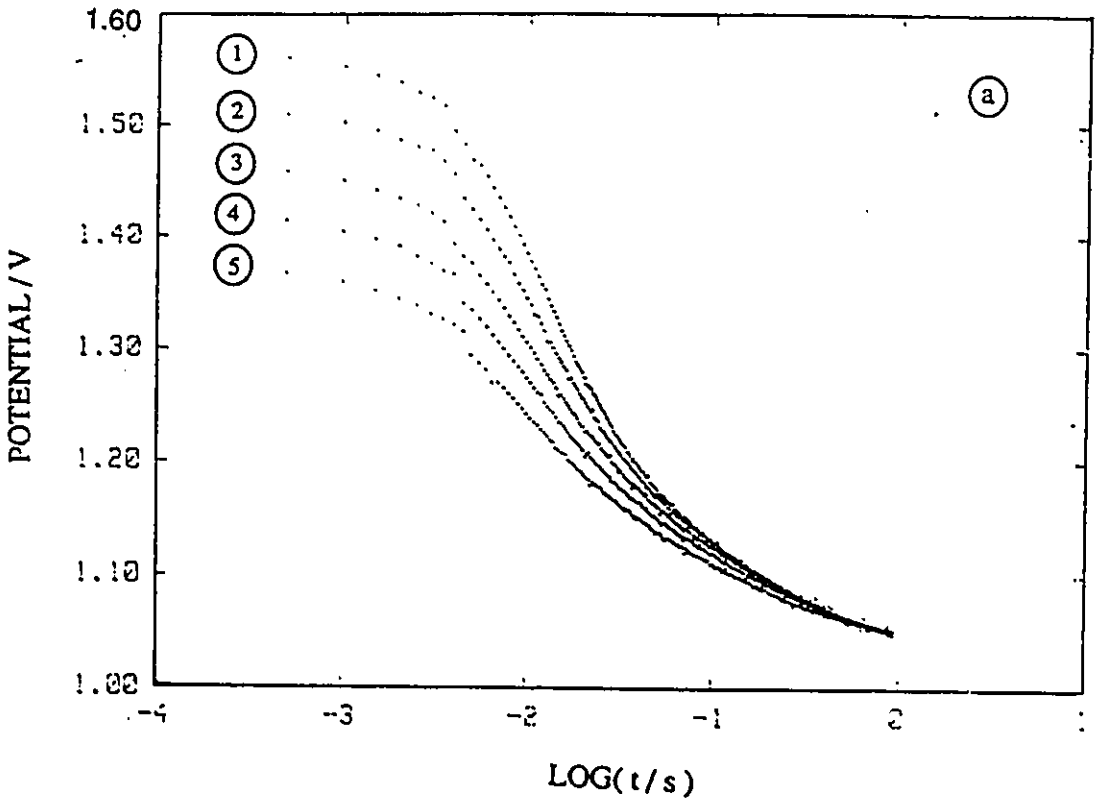
1.60
1.50
1.40
1.30
1.20
1.10
1.00
POTENTIAL / V
-4
-3
-2
-1
0
LOG(t / s)
1
2
3
4
5
a

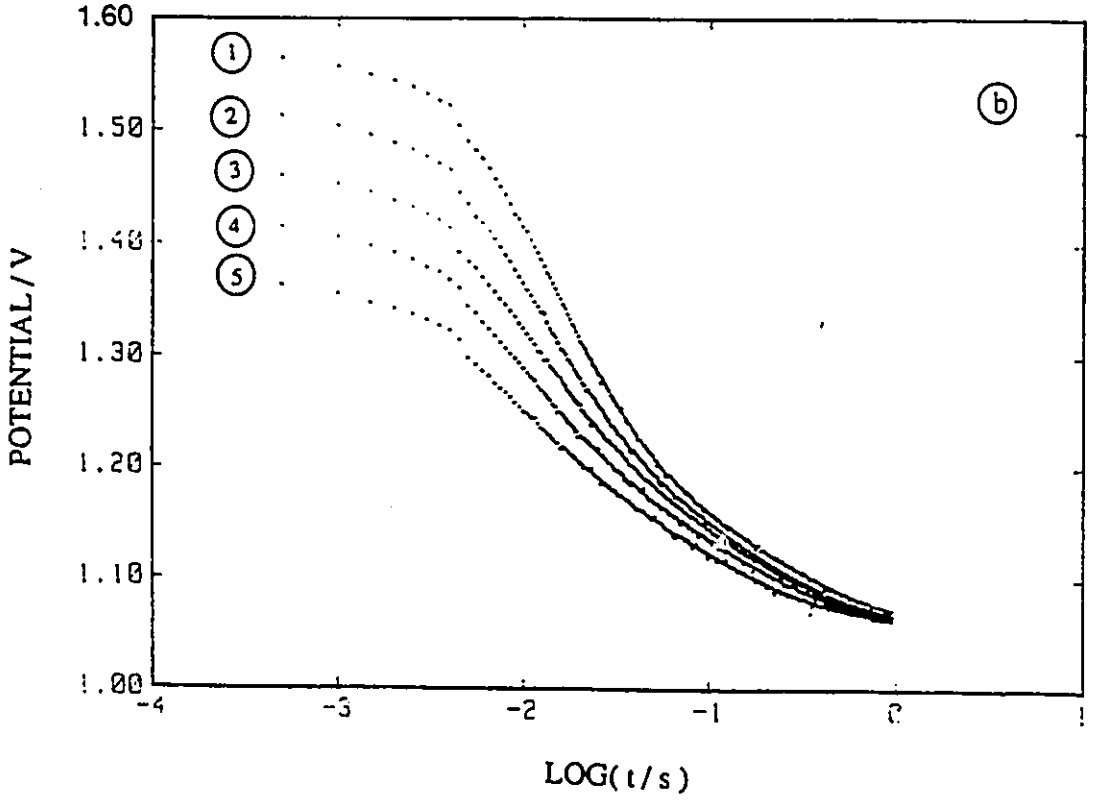
1.60
1.50
1.40
1.30
1.20
1.10
1.00
POTENTIAL / V
-4
-3
-2
-1
0
LOG(t / s)
1
2
3
4
5
b

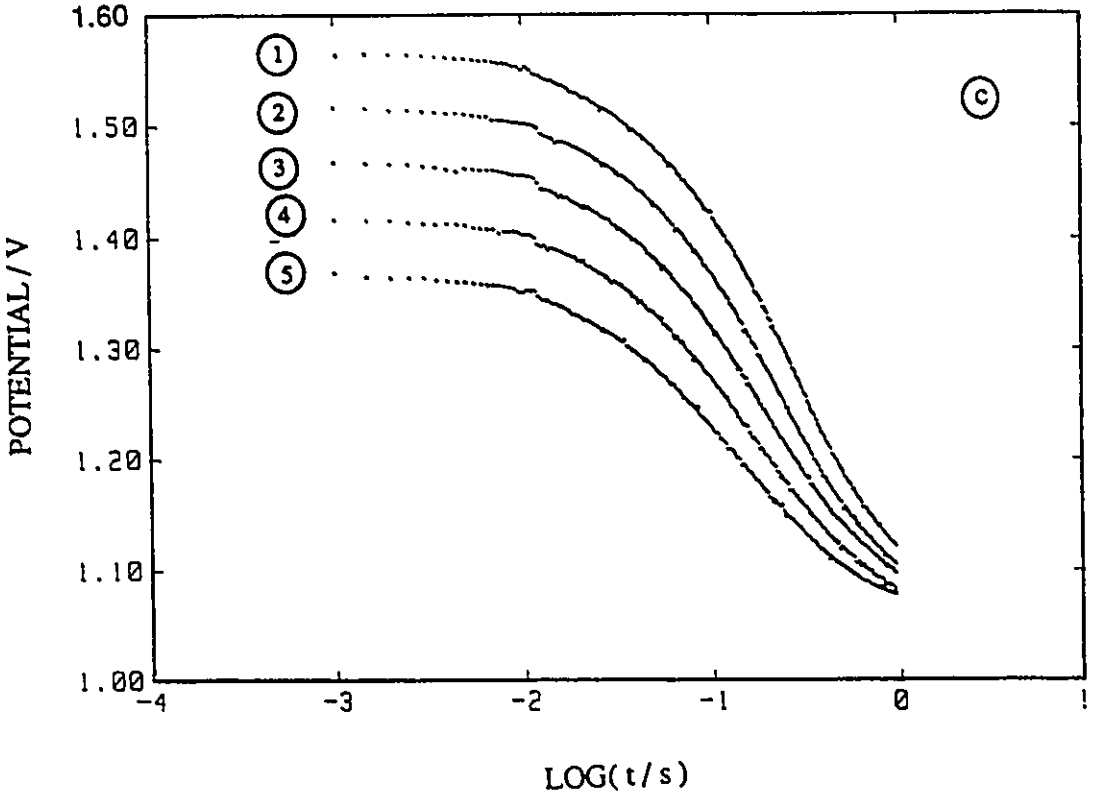

Fig.5.29 a) Digitally recorded potential-relaxation transients, V(t) vs log(t), from a series of 5 anodic overpotentials for the Cl_2 evolution at a Pt electrode in non-aqueous TFA solution. 1) 1.6 V ; 2) 1.55 V; 3) 1.50 V; 4) 1.45 V and 5) 1.40 V vs Ag/AgCl. b) the same as a) except for the case of a pre-formed oxide film at the Pt, q = 127 $\mu C\ cm^{-2}$ and c) for q = 625 $\mu C\ cm^{-2}$.

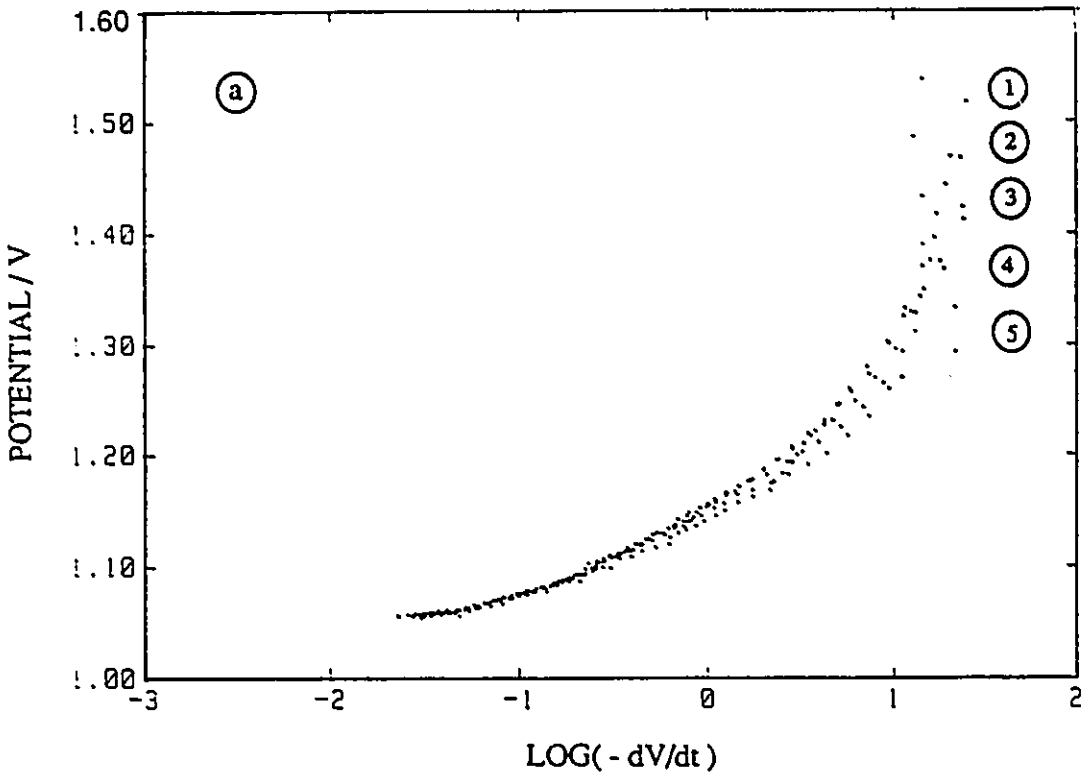
a
1
2
3
4
5
1.60
1.50
1.40
1.30
1.20
1.10
1.00
POTENTIAL / V
-3
-2
-1
0
1
2
LOG(- dV/dt)

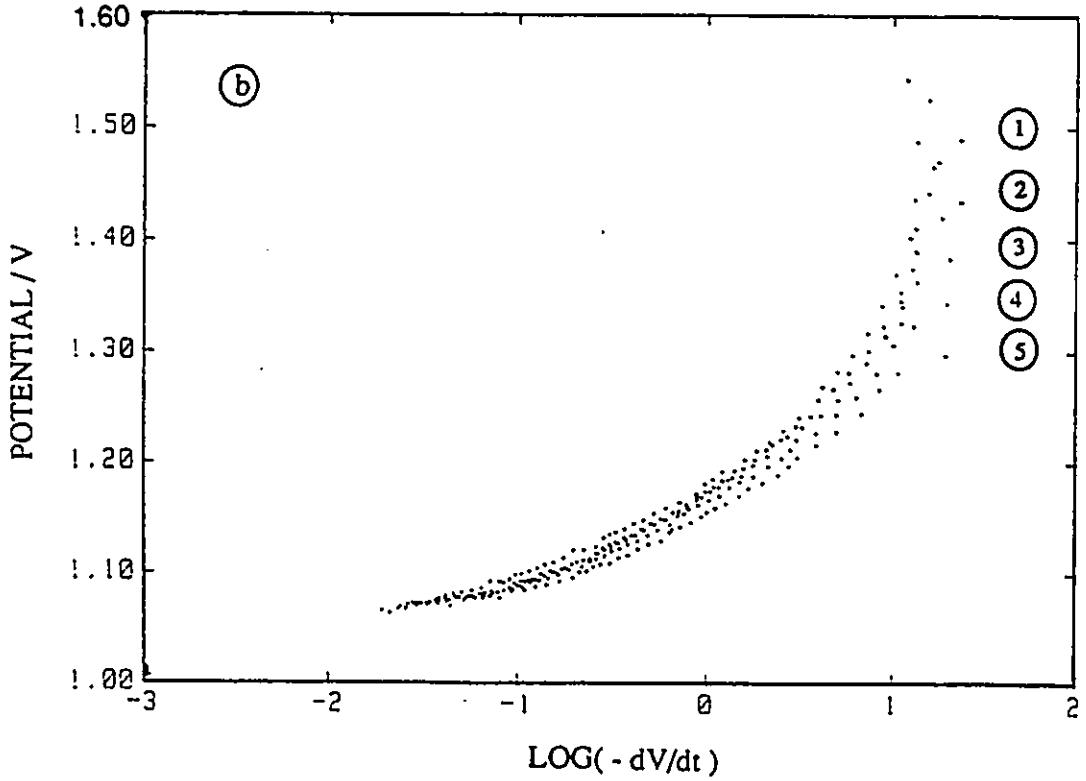
b
1
2
3
4
5
1.60
1.50
1.40
1.30
1.20
1.10
1.00
POTENTIAL / V
-3
-2
-1
0
1
2
LOG(- dV/dt)

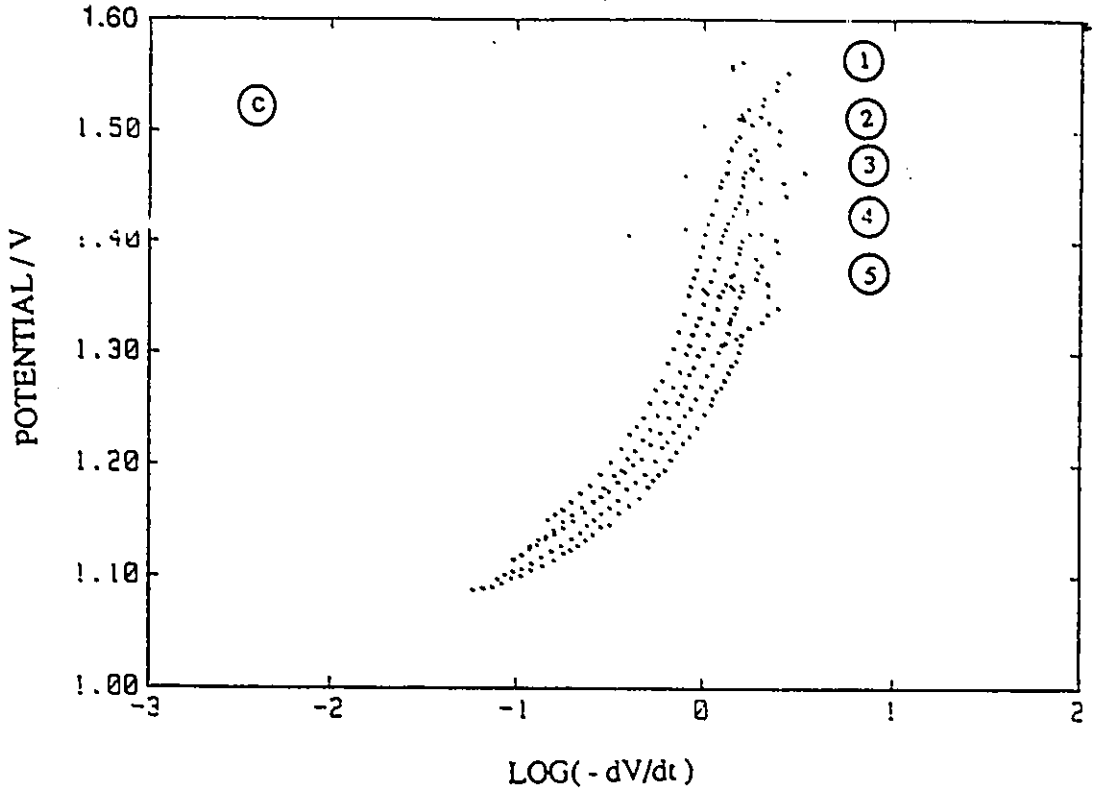

Fig.5.30 a) Computer-plotted values of log[-dV/dt] vs V derived from the data of Fig.5.29 for the same 5 initial anodic polarization potentials: curves numbered, respectively, as in Fig.5.29. b) the same as a) except for the case of a pre-formed oxide film at the Pt, for q = 127 μC cm^{-2} and c) for q = 625 μC cm^{-2}.

normally arises, as in cases (a) and (b).

Fig. 5.31 clearly demonstrates the influence of the oxide film. The greater the extent of oxide film formation on the Pt surface, the smaller the maximum in the corresponding C(V) vs V profile. It seems that this effect arises from the different rates of change of coverage with potential, associated with competitive adsorption between Cl^- and O or OH species. The total charge for Cl^- adsorption is found (Fig.5.33) to be about the same in all three cases.

Compared with the behaviour in an aqueous solution, the pseudocapacitance associated with Cl^- adsorption is much smaller in the non-aqueous medium. There is evidently little adsorption of Cl^- (the limiting charge for Cl^- adsorption being only ca. 30 $\mu C\ cm^{-2}$). The reason is not simply the absence of the oxide film since case (a) exhibits the same phenomenon. The TFA could poison the surface or cause an inhibition effect. The TFA molecules can be chemisorbed on the Pt surface since the electronegativites of -F and -COOH are large. These large size neutral molecules can occupy the Pt surface and give rise to two major effects: i) poisoning or inhibition of the "active-sites" for Cl^- adsorption, and also a spatial effect ; and ii) a low value of double-layer capacitance, since the neutral TFA molecules are large and un-ionized. The adsorption of TFA can be detected even in a 0.1 M H_2SO_4 aqueous solution at low concentrations ca. $2x10^{-4}$ mole dm^{-3} as shown in Fig.5.32.

A similar blocking effect of the adsorbed TFA (probably TFA^-) is observed in the reduction peak of the oxide film at Pt in an aqueous medium and a significant displacement of the oxide formation region also arises, as shown in Fig.5.32. The TFA blocking effect is probably the principal factor that explains the observation of smaller currents for Cl_2 evolution in the non-aqueous TFA solution. Even though the bonding effect between " bare " Pt and Cl^- would be a important factor in Cl_2 evolution in a non-aqueous solution, a significant poisoning effect by TFA adsorption must be taken into account.

A low double-layer capacitance (only 5 $\mu F\ cm^{-2}$) is observed in the C(V) vs V

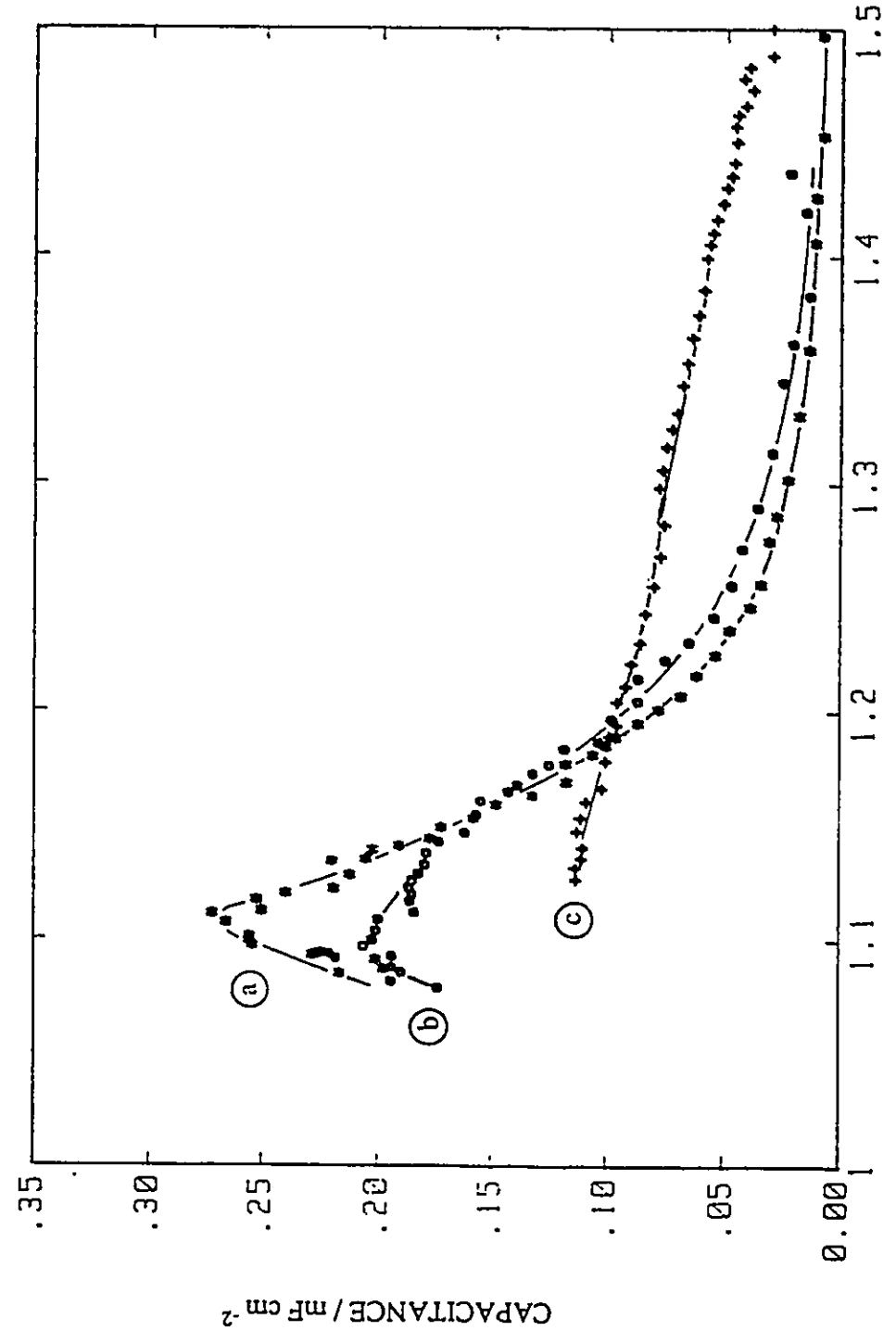

Fig.5.31 Capacitance derived from the potential-relaxation transients and Tafel plots for Cl_2 evolution at an oxide-free Pt electrode in non-aqueous TFA solution, The letters a), b) and c) correspond to those of Fig.5.28 and 5.30.

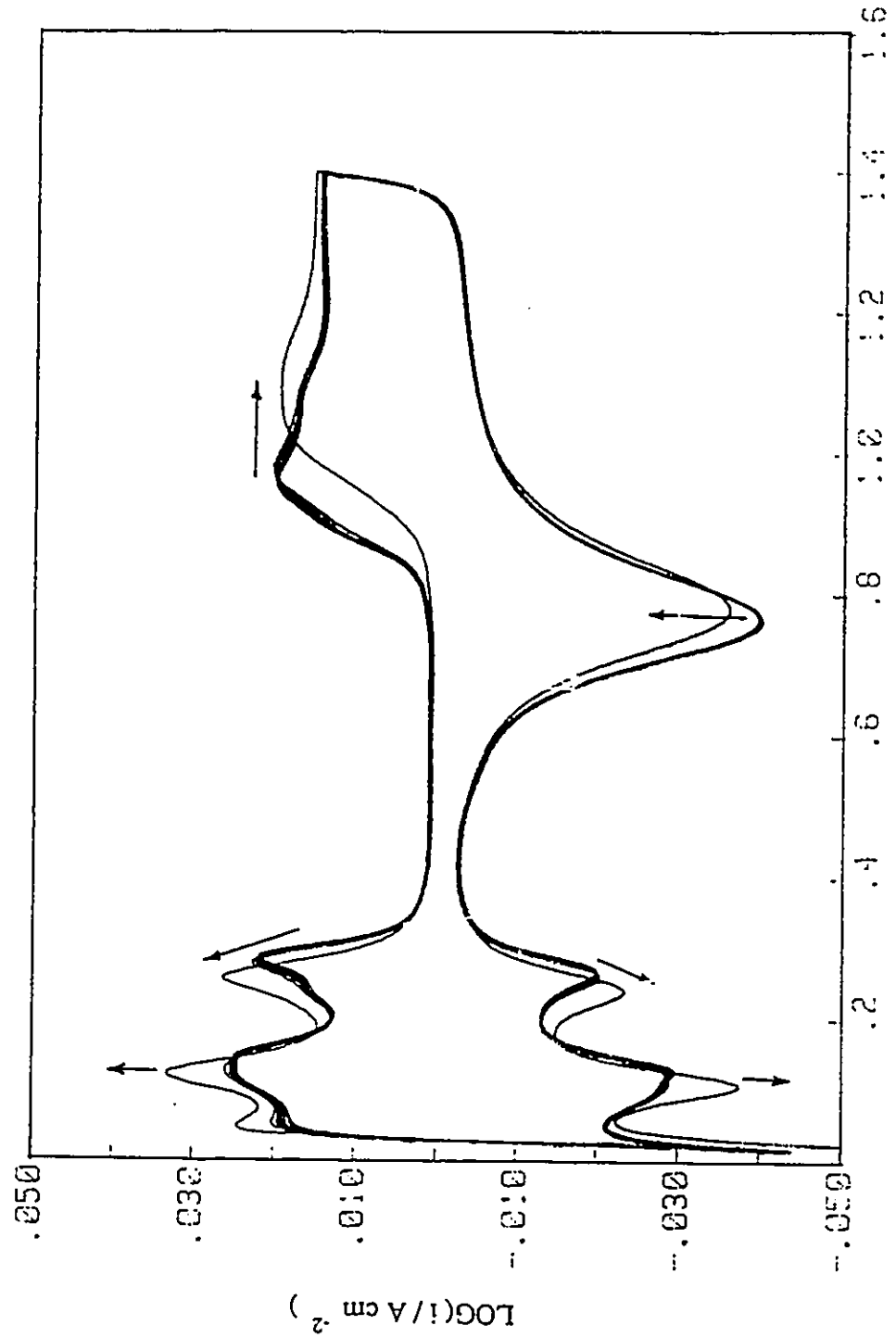

Fig.5.32 Successive series of cyclic-voltammograms for Pt in 0.1 mol dm^{-3} aq. H_2SO_4, with additions of TFA giving concentrations from $2x10^{-6}$ to $2x10^{-4}$ mol dm^{-3}, covering the potential range from onset of Pt surface oxidation(+0.8 V,RHE) to +1.4 V, RHE. Arrows show directions of change of current with increasing TFA concentration.

curve (case a) in the high potential region. A similarly low value is also obtained from the a.c. impedance spectra for which the first semi-circle in the high frequency region corresponds to a small double-layer capacitance. This is as expected for a non-aqueous solvent such as TFA.

5.2.3. The Coverage by Cl· at Pt in the TFA Medium

Besides the information on pseudocapacitance of adsorbed Cl·, the coverage by the Cl· intermediate can also be derived from the potential relaxation transients simply by integration of the C(V) vs V curves using eqn:[2.42] and division by 210 μC cm^{-2} as the required charge for formation of a full monolayer of the adsorbed Cl· intermediate, in the usual way. The results are given in Fig.5.33, curves a, b, and c for cases (a), (b) and (c), respectively. As remarked earlier, only a small limiting coverage, θ = 0.12 - 0.15 is attained, corresponding to possible poisoning or inhibition of Cl· adsorption by the organic solvent, TFA and/or the anion of TFA.

Theoretical simulation of the pseudocapacitance behaviour of Cl· adsorption in the Cl_2 evolution reaction at Pt in a non-aqueous solution are given in Fig.5.34; curves a, b and c correspond to the cases (a), (b) and (c). All of the curves are obtained by using the same set of constants or parameters except for the values of the g-factor representing the lateral interaction effect. In order to relate these curves to experimental behaviour, the required g factor should become larger as more oxide is deposited on the Pt surface The constants used for the simulation are $K_1 = k_1/k_{-1}$ = 0.8, k_2 = 0, $k_3 = 4.87 \times 10^{-8}$ and q = 30 μC cm^{-2}, and the g values are 0.8, 2 and 10, respectively. The more oxide that is formed, the larger is the required g value because an increase in coverage by the polar oxide species would lead to greater lateral interaction between the adsorbed Cl· intermediate and a weakened the bond between the Pt atom and this species so that a lower capacitance maximum results, as illustrated in the simulation curves (Fig.5.34). Evidently, beyond monolayer oxide coverage, the Cl· must become deposited on the completed oxide film so that the

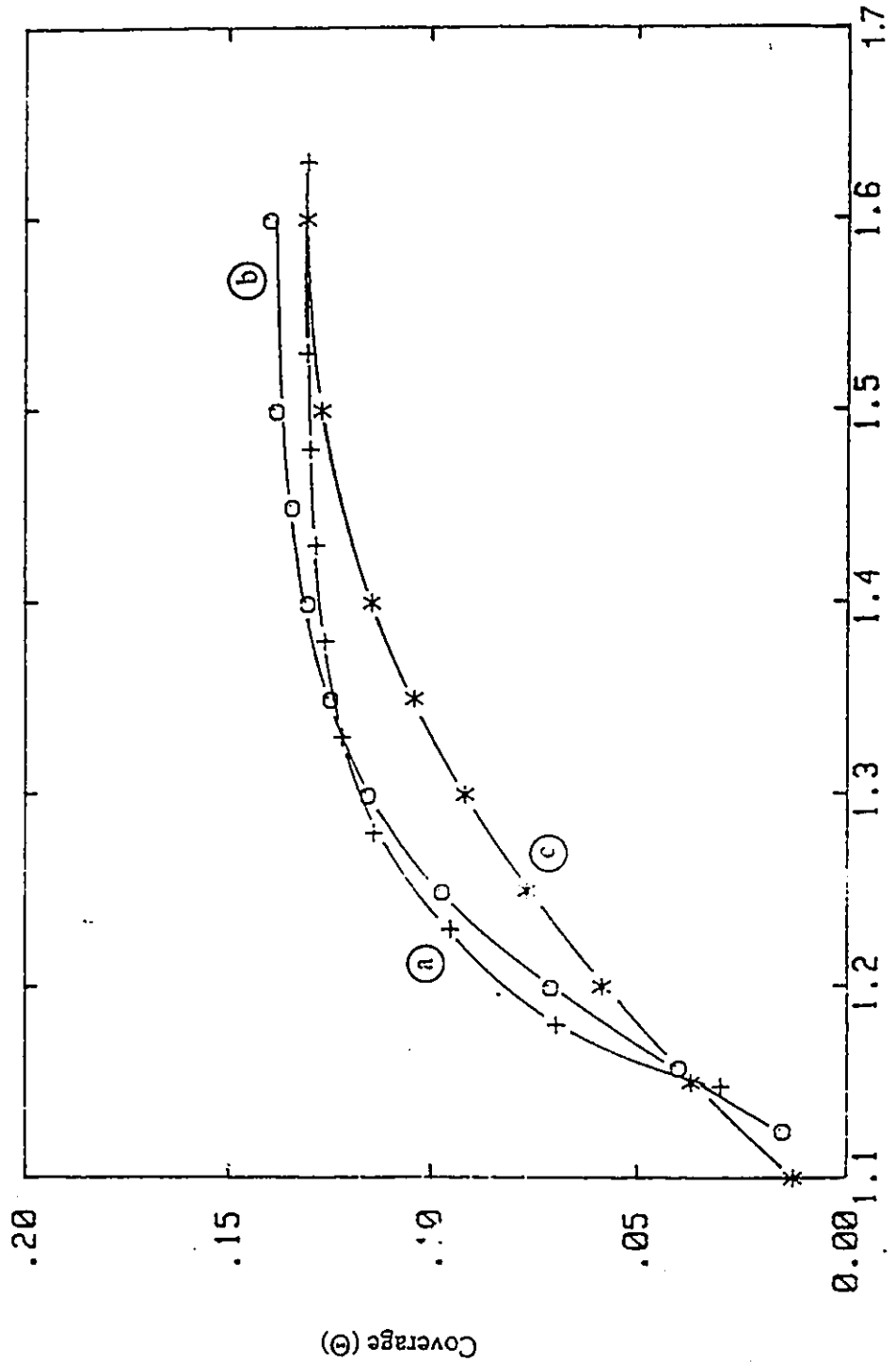

Fig.5.33 Coverage, θ, of Cl vs potential for the Cl_2 evolution reaction at a Pt electrode in non-aqueous TFA solution assuming a real/apparent area ratio corresponding to ca. 210 μC cm^{-2} hypothetical for monolayer coverage. The letters a), b) and c) correspond to those of Figs.5.28 and 5.30.

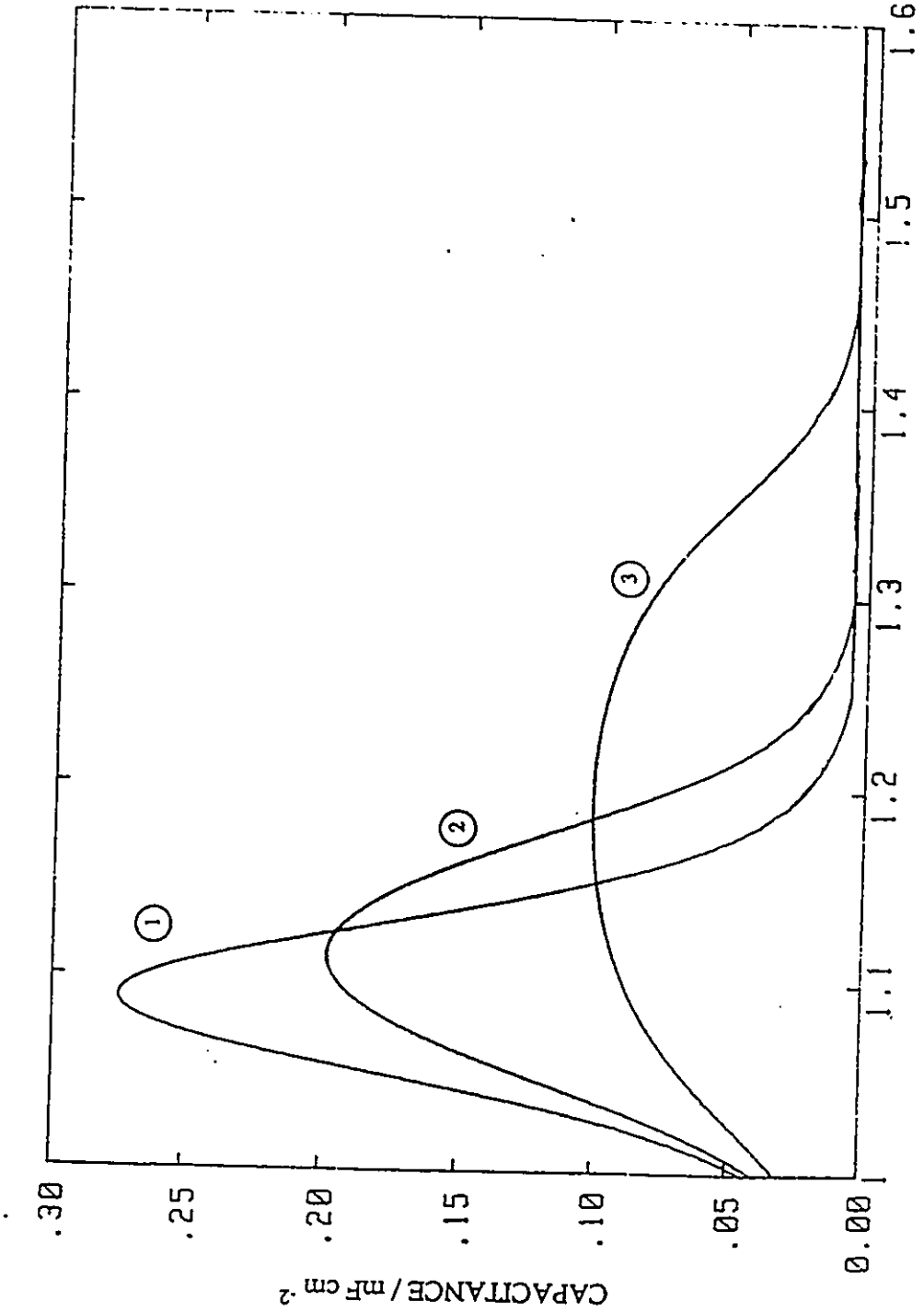

Fig.5.34 Calculated plots of C_d vs V according to eqn.[2.39] taking K_1 = 0.8, k_r = 0, k_3 = 4.87×10^{-9} and q = 30 μC cm^{-2}. (1), (2) and (3) represent the behaviour for three values of g = 0, 2, and 10, respectively.

interaction becomes materially changed.

The small value of q, 30 $\mu C\ cm^{-2}$, is quite close to the experimental value of ca. 27 - 30 $\mu C\ cm^{-2}$. This amount of charge is only about 13% of the 210 $\mu C\ cm^{-2}$ for the normal monolayer, which indicates that only about 13% of the surface area makes a contribution to the Cl_2 evolution reaction.

5.2.4. A.c. Impedance Spectra for Pt in the Non-aqueous TFA Solution System

As was seen for the reduced .Pt electrode in an aqueous medium, the a.c. impedance spectra for the Cl_2 evolution reaction at Pt in the non-aqueous TFA solution show clearly two semi-circles in the complex-plane plots, Figs.5.35a-d show the results for various potentials: (a) 1.1 V, (b) 1.2 V, (c) 1.3 V and (d) 1.4 V vs Ag/AgCl. The first semi-circle in the high-frequency region corresponds to the double-layer capacitance and the second, at lower frequencies, to the capacitance due to the adsorbed $Cl^{\cdot}$ intermediate. The double-layer capacitance does not change much with potential but the pseudocapacitance does significantly. As the anode potential increases, the second semi-circle rapidly becomes smaller. The clear observation of two semi-circles in the a.c. impedance behaviour (Fig.5.35) indicates the existence of the effect expected when a significant adsorption of $Cl^{\cdot}$ arises as is also indicated by the potential-relaxation transient measurements.

Figs.5.35a-d also show the equivalent circuit fitting results for the a.c. impedance spectra plotted in the complex-plane. As before, the solid line represents the theoretical which has excellent fit to the experimental points represented by the small crosses. The fitting parameters; R_{∞}, R_p, and C_p (Table 5.7) show only a small tendency to decrease with increasing potential but the decrease of R_p is substantially greater. The value of the double-layer capacitance is quite small here; however, it may qualitatively represent the true situation since it is detected over a relatively high frequency region (the top point frequency is ca. 5 kHz).

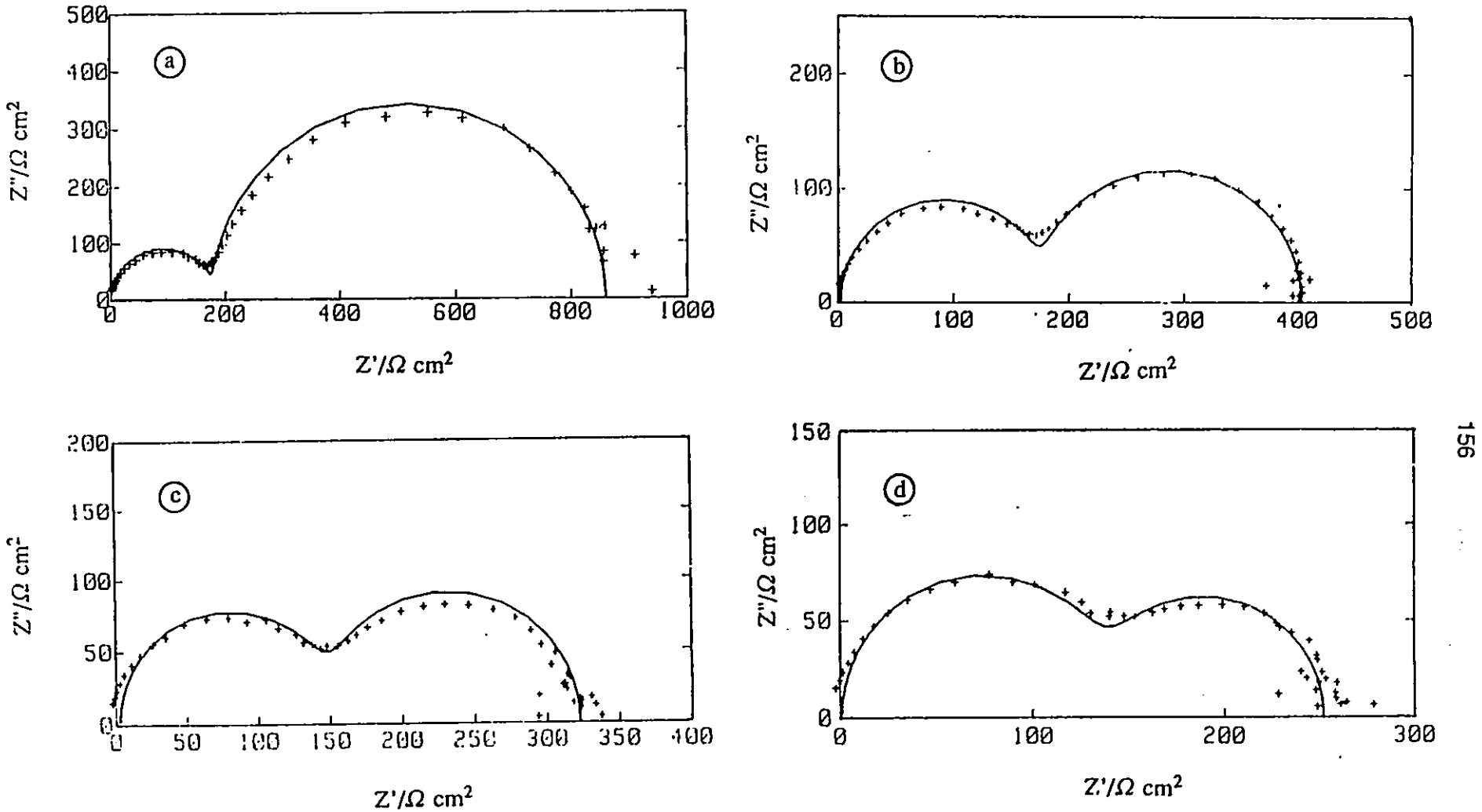

Fig.5.35 The a.c. impedance plots in the complex-plane for Cl_2 evolution at Pt electrodes in non-aqueous TFA solution at various potentials (vs Ag/AgCl) : a) 1.1 V; b) 1.2 V; c) 1.3 V and d) 1.4 V as indicated in the diagrams. "+" represents the experimental points and the lines represent the theoretical simulations.

Table 5.7 List of A.C. Fitting Parameters for the Behaviour of Pt in the Non-aqueous Solution

Parameters / Potential vs Ag/AgCl	R_∞ ($\Omega\,cm^2$)	R_P ($\Omega\,cm^2$)	C_P ($F\,cm^{-2}$)	C_{dl} ($F\,cm^{-2}$)
1.1 V	187	691	6.8×10^{-5}	1.2×10^{-6}
1.2 V	182	203	6.0×10^{-5}	1.2×10^{-6}
1.3 V	157	148	6.1×10^{-5}	1.2×10^{-6}
1.4 V	140	124	2.9×10^{-5}	1.2×10^{-6}

The simulation of the a.c. impedance behaviour in terms of the rate constants approach is shown in Figs.5.36 and 5.37 for the log| Z | vs log(ω) and phase angle vs log(ω) plots, respectively. Once again, excellent fits are obtained between the simulations and the experimental data. The numbers 1, 2, 3 and 4 correspond to the letters a, b, c and d in Fig.5.35, respectively.

From the values of the rate constants (Table 5.10), required for good fitting, it is found that $k_3 >> k_2$, which indicates, for a non-aqueous solution, that the recombination path is again the preferred desorption process. The mechanism, for the TFA experimental conditions, can be indicated as

$$Pt + Cl^- \quad ==== \quad Pt\text{-}Cl + e$$

and

$$2Pt\text{-}Cl \quad \longrightarrow \quad 2Pt + Cl_2 \uparrow$$

with the step

$$Pt\text{-}Cl + Cl^{\cdot} \longrightarrow Pt + Cl_2 \uparrow$$

contributing only about 0.1 % to the whole current. The above represents the kinetic behaviour of the Cl_2 evolution reaction at Pt in a non-aqueous TFA solution and explains the limiting current obtained in the Tafel plot as reported by Conway and Novak (refs.85,86).

Compared with their behaviour in an aqueous solution, both rate constants k_1 and k_3 are much smaller in a non-aqueous TFA solution. This may be due to the possibility of stronger bonding between the Pt atom and adsorbed $Cl^{\cdot}$ which makes recombinative $Cl^{\cdot}$ desorption relatively less facile than the competitive adsorption of TFA molecules or their anions as referred earlier.

Table 5.8 List of kinetic rate constants simulation of the a.c. impedance data for Pt electrode in non-aqueous TFA solution.

Rate constant / Potential vs Ag/AgCl	k_1 ($cm\,s^{-1}$)	k_{-1} ($cm\,s^{-1}$)	k_2 ($cm\,s^{-1}$)	k_3 ($mol\,cm^{-2}\,s^{-1}$)	q_o ($C\,cm^{-2}$)	C_{dl} ($F\,cm^{-2}$)
1.1 V	7×10^{-9}	1×10^{-11}	3.8×10^{-14}	1.8×10^{-9}	3×10^{-5}	1.2×10^{-6}
1.2 V	4.2×10^{-10}	1×10^{-11}	3.8×10^{-14}	2.7×10^{-9}	1.8×10^{-5}	1.2×10^{-6}
1.3 V	1×10^{-10}	1×10^{-11}	3.8×10^{-14}	1.8×10^{-9}	1.8×10^{-5}	1.2×10^{-6}
1.4 V	1×10^{-10}	1×10^{-11}	3.8×10^{-14}	1×10^{-9}	2×10^{-5}	1.2×10^{-6}

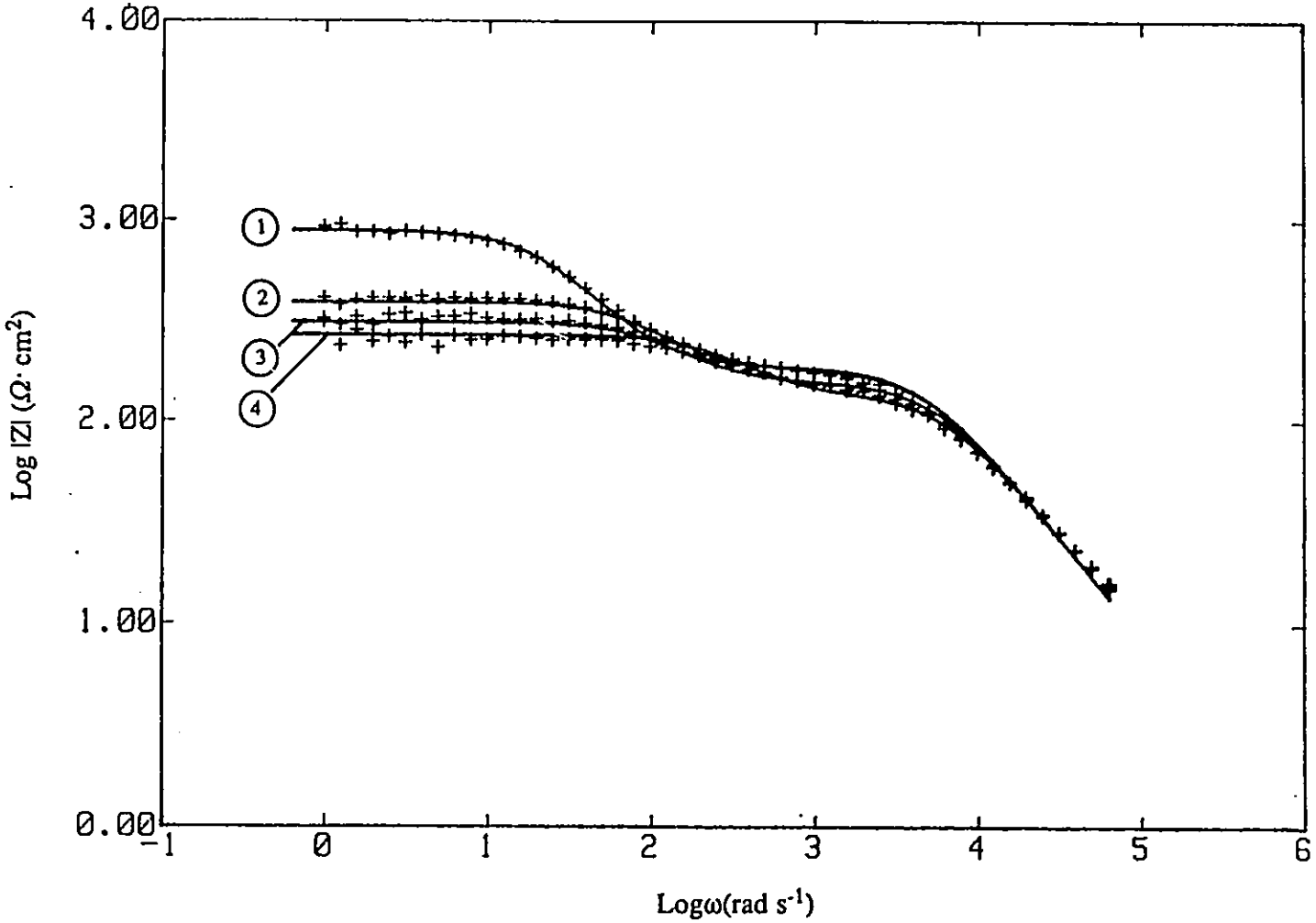

Fig.5.36 Experimental (crosses) and simulated (solid lines) Bode plots for Cl_2 evolution at Pt electrodes in non-aqueous TFA solution. The experimental conditions and values of simulation parameters for curves 1), 2), 3) and 4) are the same as those for Figs.5.35 a), b) c) and d), respectively.

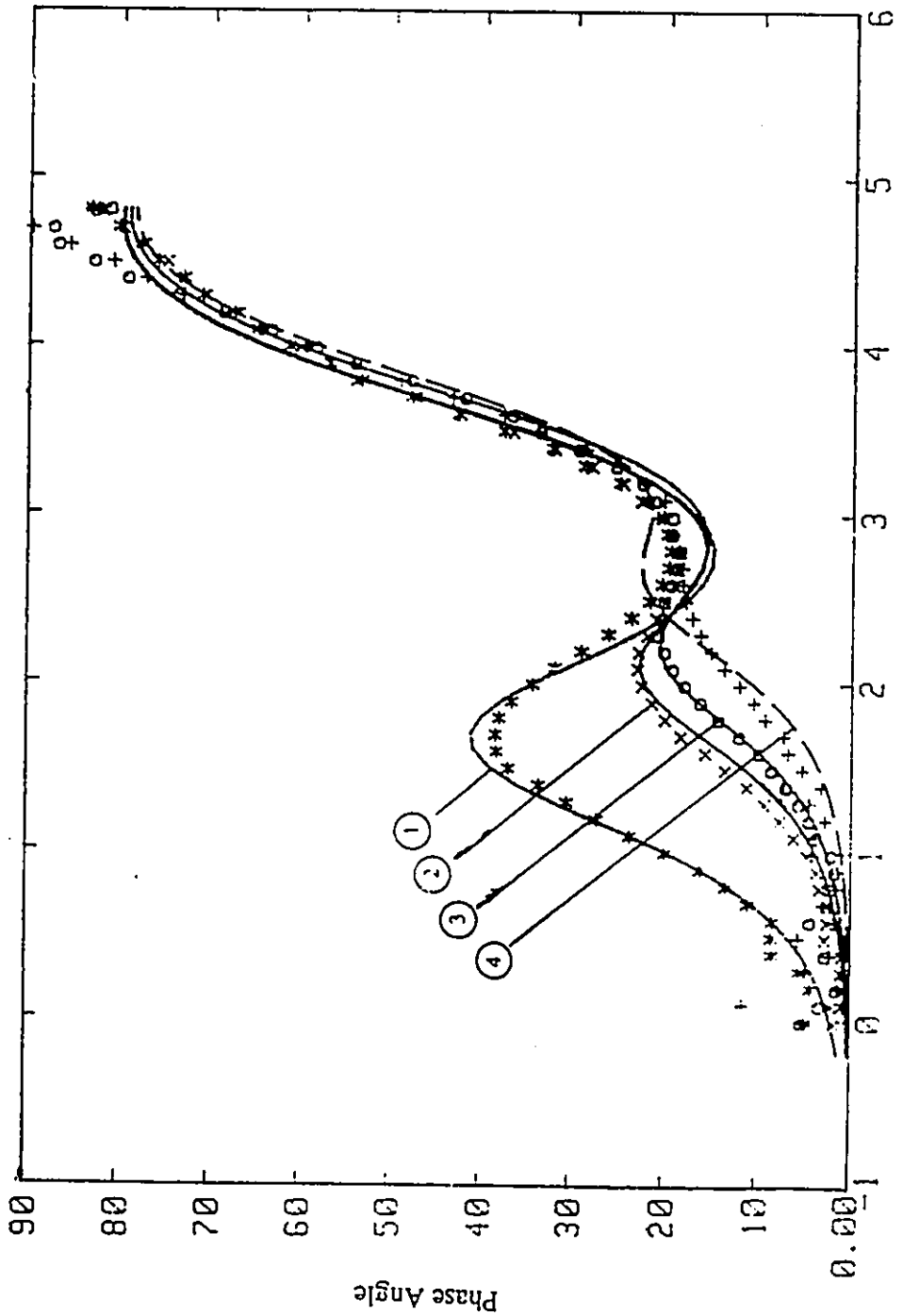

Fig.5.37 The same experimental and simulation behaviour as in Fig.5.36 but plotted as phase angle vs log(ω). Lines and points represent the theoretical simulation and experimental data, respectively. "*", "x", "o" and "+" correspond to a), b), c) and d) in Fig.5.37.

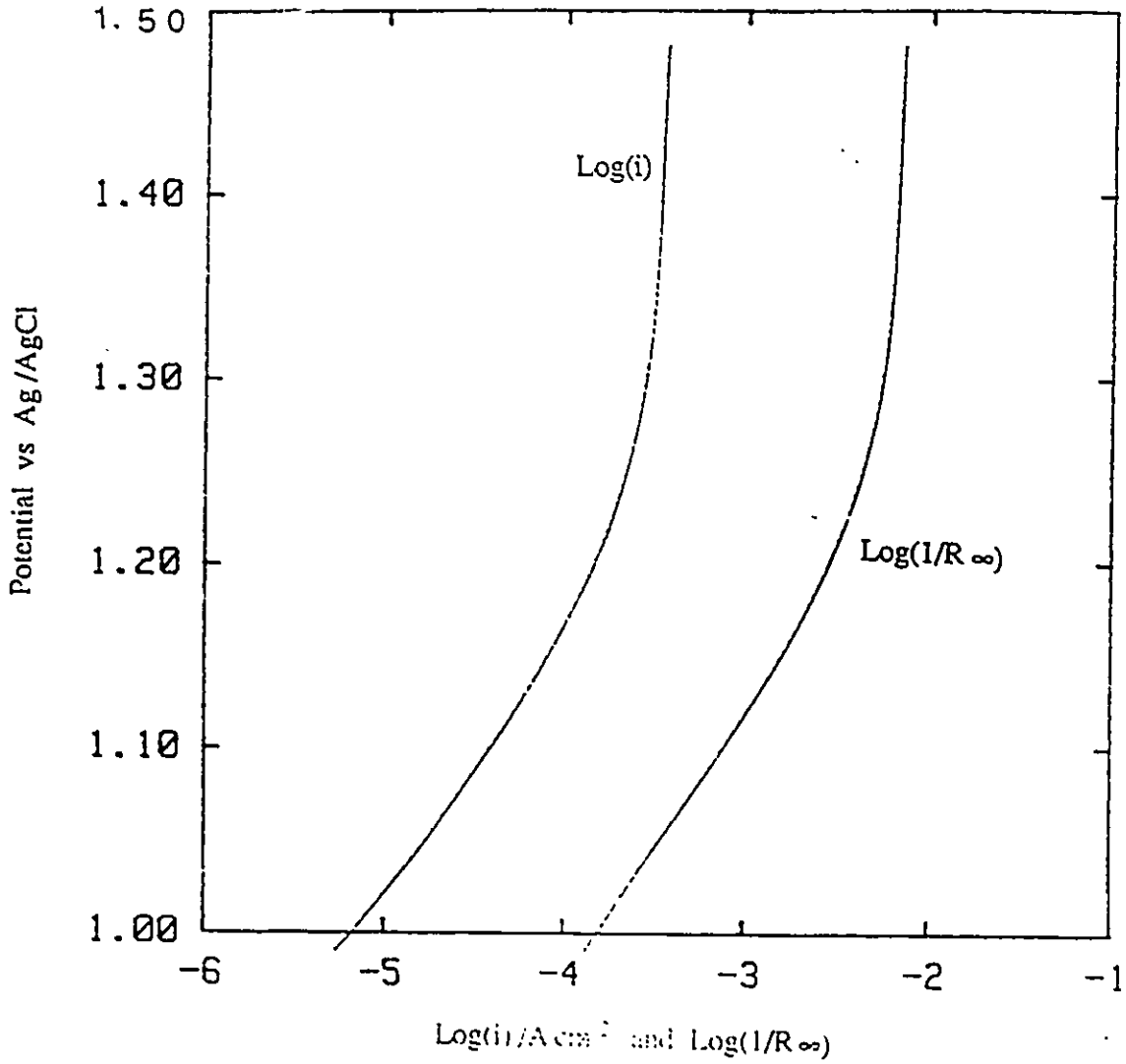

Fig.5.38 Simulated log(i) vs V and log(1/R_) vs V behaviour for anodic Cl_2 evolution in non-aqueous TFA solution at a Pt electrode according to eqns.[4.81], [4.82a] and [4.82c] using the rate constant values k_1 = 2.0x10^{-6}; k_{-1} = 1.0x10^{-11}; k_2 = 3.8x10^{-14}; k_3 = 1.8x10^{-9} mol cm^{-2} s^{-1}.

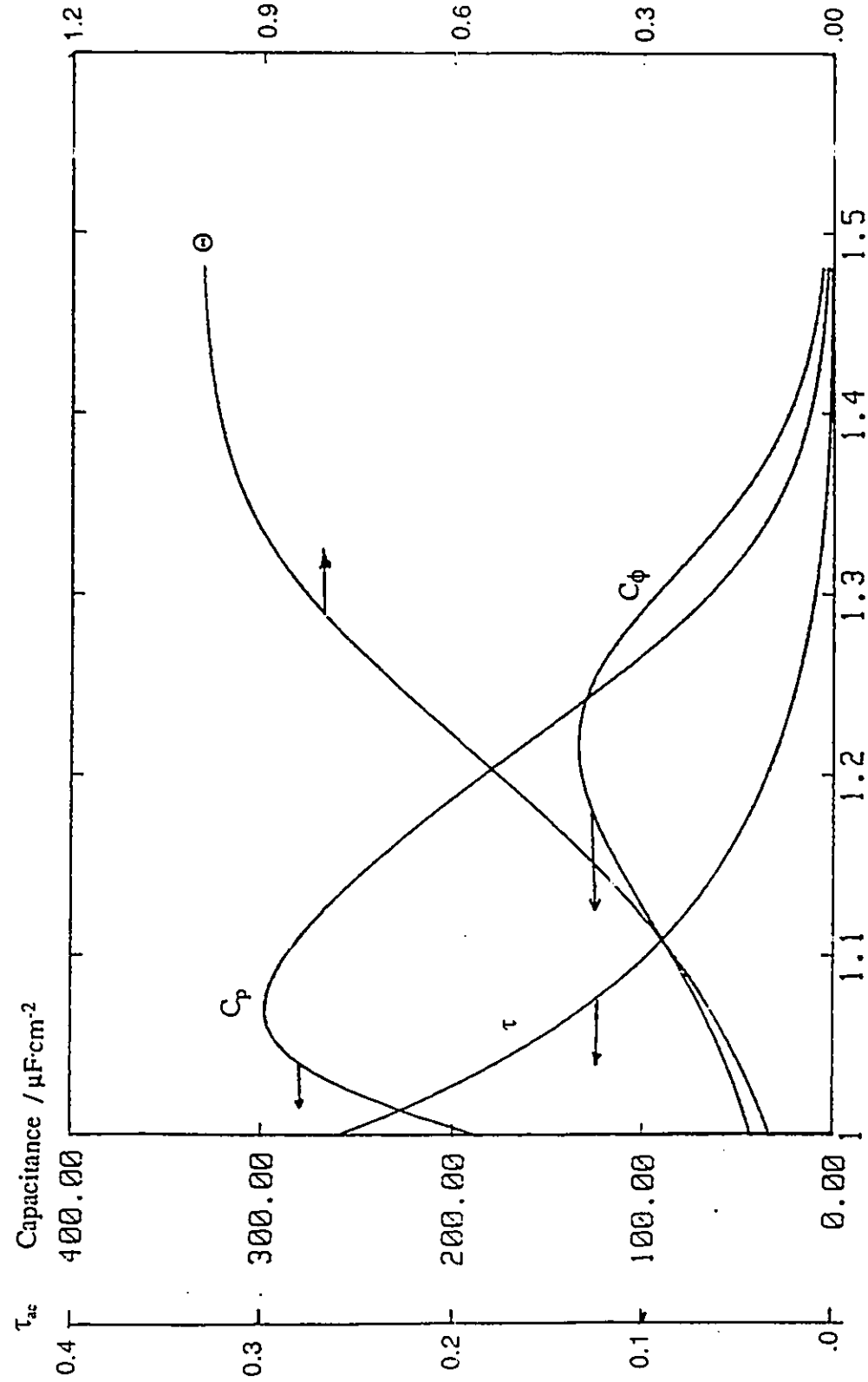

Fig.5.39 Simulated C_p vs V, C_ϕ vs V, θ vs V and τ vs V behaviour for the Cl_2 evolution reaction in non-aqueous TFA solution at a Pt electrode according to eqns.[4.82e], [4.80], [4.79] and [4.82d] using rate constants $k_1 = 2.0\times10^{-10}$; $k_{-1} = 1.0\times10^{-11}$; $k_2 = 3.8\times10^{-14}$; $k_3 = 1.8\times10^{-9}$ mol cm^{-2} s^{-1}.

The q value required for the fitting is ca. 18-30 $\mu C\ cm^{-2}$ which is close to that for the potential relaxation measurements. This is consistent with view that an inhibition effect plays an important role in Cl_2 evolution in a TFA solution. The simulated $\log(1/R_{ac})$ and log(i) behaviours for the non-aqueous TFA solution are shown in Fig.5.38 and as well the behaviours of C_p, C_ϕ, θ and τ_{ac} are shown in Fig.5.39.

5.2.5. Brief Conclusions on the Cl_2 Evolution Mechanism at Pt

It is useful now to summarize the behaviour of the Cl_2 evolution reaction at Pt in both an aqueous and a non-aqueous TFA solution.

(i) Limiting current-densities arise in the Tafel plot at both the reduced and pre-oxidized Pt electrodes; they are independent of the rotation rate and can only be explained kinetically in terms of the recombination mechanism.

(ii) The a.c. impedance fitting results show that the recombination rate constants, k_3, are much larger than those, k_2, of the electrochemical desorption step, thus further indicating that the recombination mechanism for Cl· desorption is preferred.

(iii) The rates of Cl_2 evolution at Pt in a non-aqueous TFA solution are also controlled by the recombination pathway, since limiting currents are observed in the Tafel plots and the a.c. impedance fitting results show that $k_3 >> k_2$.

(iv) The surface oxide species play a very important role in the anodic Cl_2 evolution reaction at Pt in an aqueous solution. The co-deposited O or OH species block the active-sites, making it more difficult for Cl⁻ adsorption and Cl· desorption to occur. This is also indicated by the a.c. impedance fitting results since the rate constant k_3 for reduced Pt is larger than that for the pre-oxidized Pt surface. The C(V) vs V profiles derived from the potential relaxation measurements support this conclusion.

(v) Oxide films generated for study in a non-aqueous solution seem to reduce the strong bonding between the Pt atom and the Cl· species but do not change the Cl_2 evolution mechanism.

(vi) Significant adsorption of the Cl· intermediate can be detected and quantita-

tively characterized in the anodic Cl_2 evolution reaction both in aqueous and non-aqueous solutions by means of potential-relaxation and a.c. impedance measurements.

CHAPTER VI

Cl_2 Evolution at other Noble Metal Electrodes (Pd, Ru, Ir and Rh)In Non-aqueous TFA Solution

In this section, some exploratory complementary work on the Cl_2 evolution reaction at other noble metals (Pd, Ru, Ir and Rh) in a non-aqueous 0.5 M RbCl + TFA solution, studied also by means of potential relaxation and a.c. impedance methods, will be presented. The results show again that the TFA has a strong inhibition effect on the kinetics of Cl_2 evolution at these electrodes and, when the potential is sufficiently high, a Kolbe type reaction may become involved.

6.1 Primary Steady-state Polarization Study

As discussed in Chapter V, the rate of the Cl_2 evolution reaction at a Pt electrode in an aqueous solution is much larger (45 times, refs.85,86) than that in a non-aqueous TFA solution. The smaller reaction rate in the non-aqueous solution arises first on account of strong chemisorption of Cl^- at the oxide-free metal and second, because of the inhibition effect of the adsorbed organic solvent, TFA, or its anion. Therefore, it is understandable that a smaller rate of Cl_2 evolution arises also at metals other than Pt in this non-aqueous solution.

The steady-state Tafel behaviour of the Cl_2 evolution reaction at Pd, Ru, Ir and Rh electrodes in the non-aqueous TFA solution are shown in Fig.6.1. The current densities are small compared with those in an aqueous medium, being only about 10^{-6} to 10^{-4} Amp cm^{-2}. The current densities are all smaller than those at the Pt electrode, Pd being the best of these metals (Ru, Ir and Rh).

The Tafel plot for the Cl_2 evolution reaction at the Pd electrode starts with a

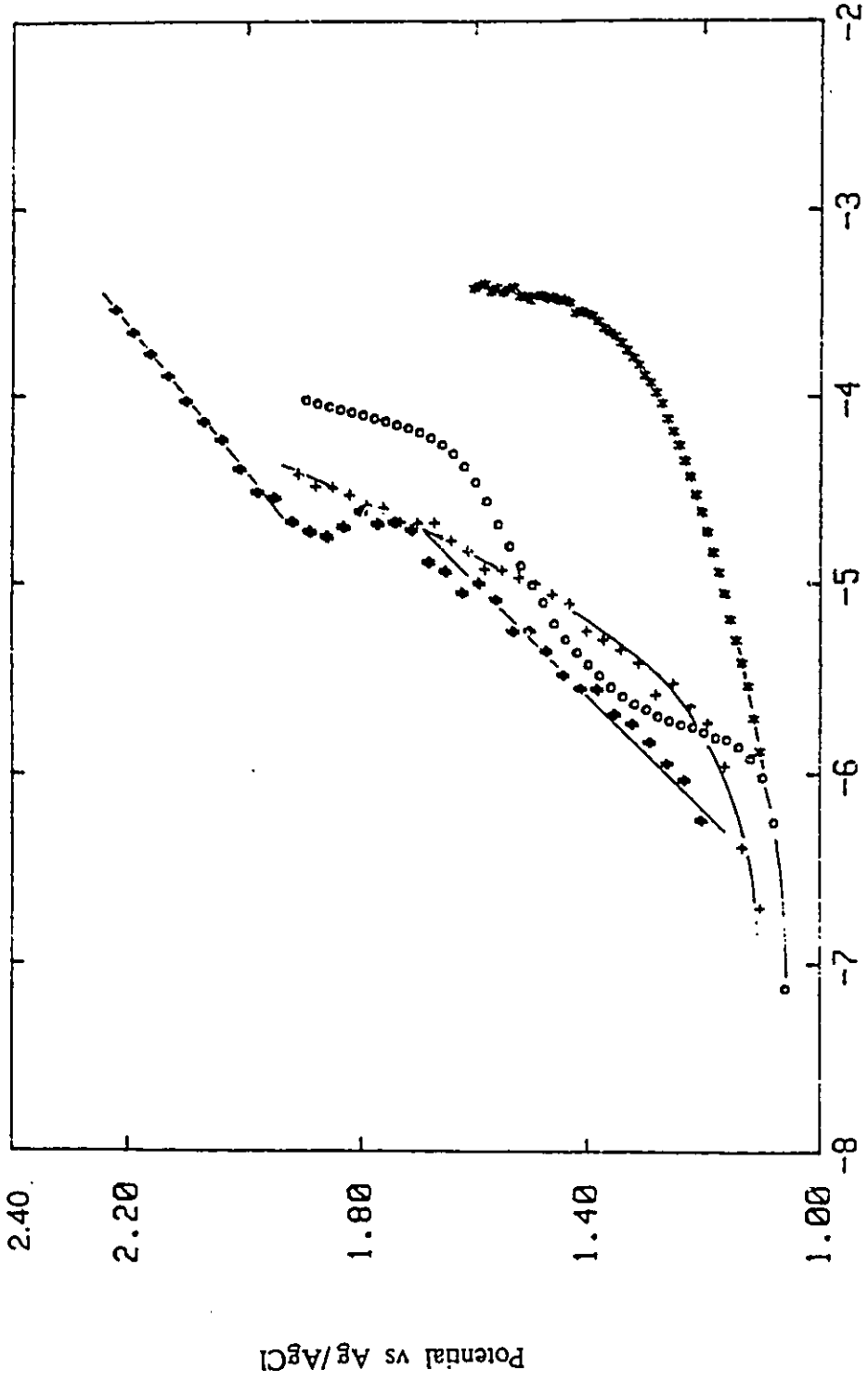

Fig.6.1 Log[current-density] vs overpotential relations for the Cl_2 evolution reaction (298 K) in 0.5 mol dm^{-3} RbCl + TFA non-aqueous solution at various noble metal electrodes. "+" for Rh; "*" for Pd; "o" for Ru and "#" for Ir electrodes.

densities are smaller, the Rh electrode also exhibits two distinguishable regions in its Tafel plot, with a slope of 48 mV per decade in the low potential range from 1.1 to 1.25 V vs Ag/AgCl and a limiting current at high potentials up to 1.9 V vs Ag/AgCl.

It is interesting that at the Ru electrode four regions arise in the Tafel plot, the first having a slope of 34 mV per decade, which probably indicates that the combination step controls the kinetics of the Cl_2 evolution reaction at low Cl· coverage. The second region shows a limiting current, corresponding also to the recombination mechanism proceeding at full Cl· coverage. Regions (1) and (2), from 1.1 to 1.5 V, are presumably associated with the Cl_2 evolution reaction but, in region (3), from 1.5 to 1.7 V , the slope changes to 180 mV per decade, which may be due to the onset of the Kolbe reaction, i.e. the TFA discharge step since, at a sufficiently high potential range, the following reactions can arise:

$$Ru + CF_3COOH \longrightarrow Ru\text{-}CF_3COO\cdot + H^+ + e \qquad [6.1]$$

$$Ru\text{-}CF_3COO\cdot \longrightarrow Ru\text{-}CF_3\cdot + CO_2 \text{ (barrierless)} \qquad [6.2]$$

as reported by Conway and Vijh[163,164]. In region (4), beyond 1.7 V, a limiting current arises again which may be due to the following recombination reaction involving CF_3· rather than Cl·:

$$2Ru\text{-}CF_3 \longrightarrow C_2F_6\uparrow + 2Ru \qquad [6.3]$$

or

$$Ru\text{-}CF_3 + Ru\text{-}Cl \longrightarrow 2Ru + CF_3Cl \qquad [6.4]$$

In contrast, the Ir electrode exhibits no limiting current over the entire studied potential range. The Tafel line below 1.9 V has a transition region (which may involve some Cl_2 but a very insignificant amount). Beyond 1.9 V, the current increases with a slope of 295 mV per decade, which is a typical value for the Kolbe reaction as discussed by Conway and Vijh[163,164] for the Kolbe reaction at Pt.

6.2. Potential Relaxation and Pseudocapacitance Behaviour

Investigations of the potential-relaxation behaviour of the Cl_2 evolution reaction at Pd, Ru, Ir and Rh electrodes in a non-aqueous TFA solution were also made and

results are shown as V vs log(t) plots in Figs.6.2a-d and with the corresponding log(-dV/dt) plots in Figs.6.3a-d, respectively. As can be seen, there are differences in the Tafel plots, the V vs log(t) and the V vs log(-dV/dt) plots, as may be expected, the metals showing their own individual characteristics.

First, we examine Figs.6.2a and 6.3a: the potential decay plots for Pd electrodes, which behave quite similarly to Pt as described in section 5.2, show basically two regions, a flat one from the time t = 10^{-5} to 10^{-2} s, and a second starting from 10^{-2} to ca. 10 s, which declines to the reversible potential. In the latter region, discharge of both the double-layer capacitance and the pseudocapacitance due to the Cl· adsorbed intermediate takes place. The corresponding V vs log(-dV/dt) plots (Fig.6.3a) have similar shapes but in reverse, becoming almost coincident at potentials lower than 1.4 V (vs Ag/AgCl).

The potential relaxation behaviour of the Ru electrode is quite different. In Curve (1), in Fig.6.2b, can barely be seen four regions which may correspond to the four regions which are observed in the Tafel plot. However, as the decaying potential becomes small, only two regions can be seen (see curves 5 in Fig.6.2b); this may be because the Kolbe reaction is not involved over a low potential range. A similar situation is also illustrated in the V vs log(-dV/dt) plots, which may be a hint that two kinds of adsorbed intermediates are involved in the electrochemical process.

For the Ir electrode (Fig.6.2c), two regions of the potential decay curve are barely differentiated but they are probably related in the usual way to the double-layer capacitance and the pseudocapacitance discharge processes. The C_ϕ, associated with the Cl· adsorbed intermediate of the Cl_2 evolution reaction, may not be significant and that for CF_3· and/or CF_3COO· for the Kolbe reaction may arise since the potential range covered (above 1.9 V) corresponds to that for onset of the Kolbe reaction. The log(-dV/dt) vs V plots are similar but opposite to the corresponding V vs log(t) plots.

The Rh electrode behaves in a different manner than the others. Its V vs log(t) plots (Fig.6.2d), taken from various initial potentials, are not superimposable over the

Fig.6.2 Digitally recorded potential-relaxation transients, V(t) vs log(t), from a series of 5 initial anodic overpotentials for the Cl_2 evolution at various electrodes in non-aqueous TFA solution. a) for Pd; b) for Ru; c) for Ir and d) for Rh electrodes. Numbers on the graphis indicate the initial potentials. For the Pd electrode: 1) 1.60 V; 2) 1.55 V; 3) 1.50 V; 4) 1.45 V; 5) 1.40 V. For the Ru electrode: 1) 1.90 V; 2) 1.80 V; 3) 1.70 V; 4) 1.60 V; 5) 1.50 V. For the Ir electrode: 1) 2.50 V; 2) 2.40 V; 3) 2.30 V; 4) 2.20 V; 5) 2.10 V. For the Rh electrode: 1) 1.90 V; 2) 1.80 V; 3) 1.70 V; 4) 1.60 V; 5) 1.50 V. All are vs Ag/AgCl.

Fig.6.3 Computer-plotted values of log[-dV/dt] vs V derived from the data of Fig.6.2 for different electrodes, represented by letters, at various initial anodic polarization overpotentials. Curves numbered, respectively, as in Fig.6.2.

Fig.6.4 Capacitance derived from the potential-relaxation transients and Tafel plots for the Cl_2 evolution reaction at the various electrodes in non-aqueous TFA solution. Letters and numbers correspond to those in Figs.6.2 and 6.3.

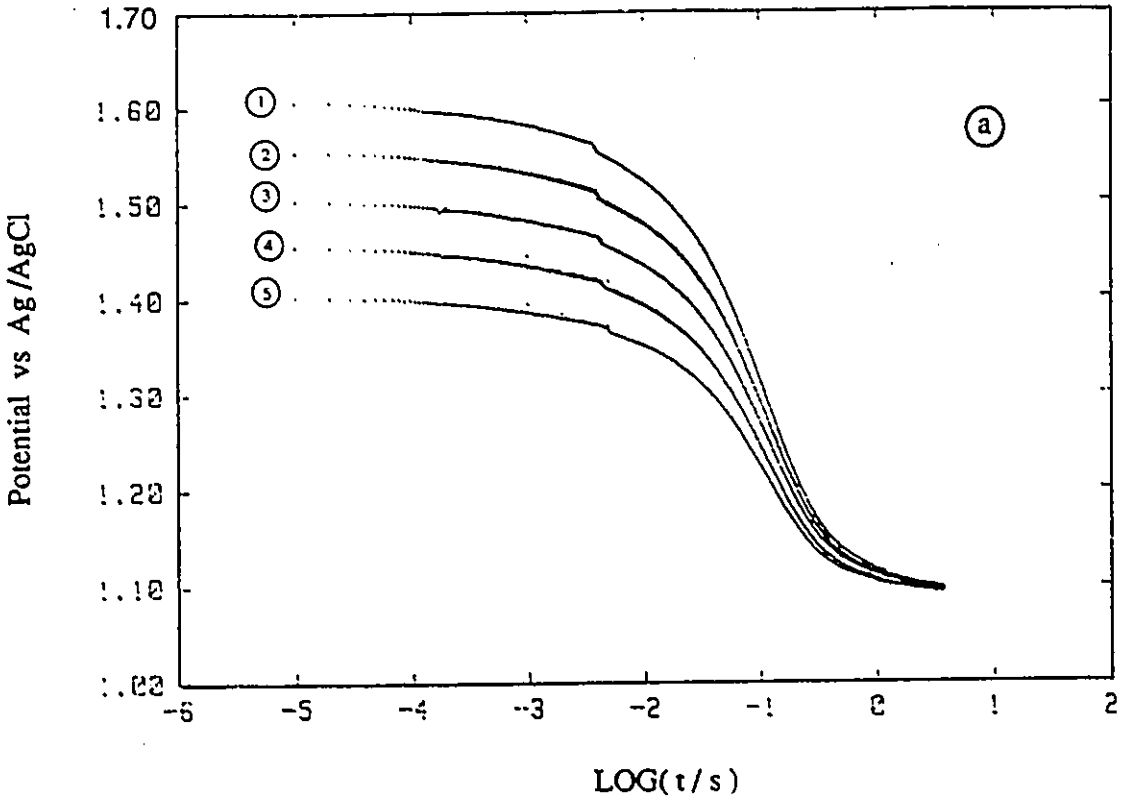
1.70
1.60
1.50
1.40
1.30
1.20
1.10
1.00
-6
-5
-4
-3
-2
-1
0
1
2
Potential vs Ag/AgCl
LOG(t/s)
a
1
2
3
4
5

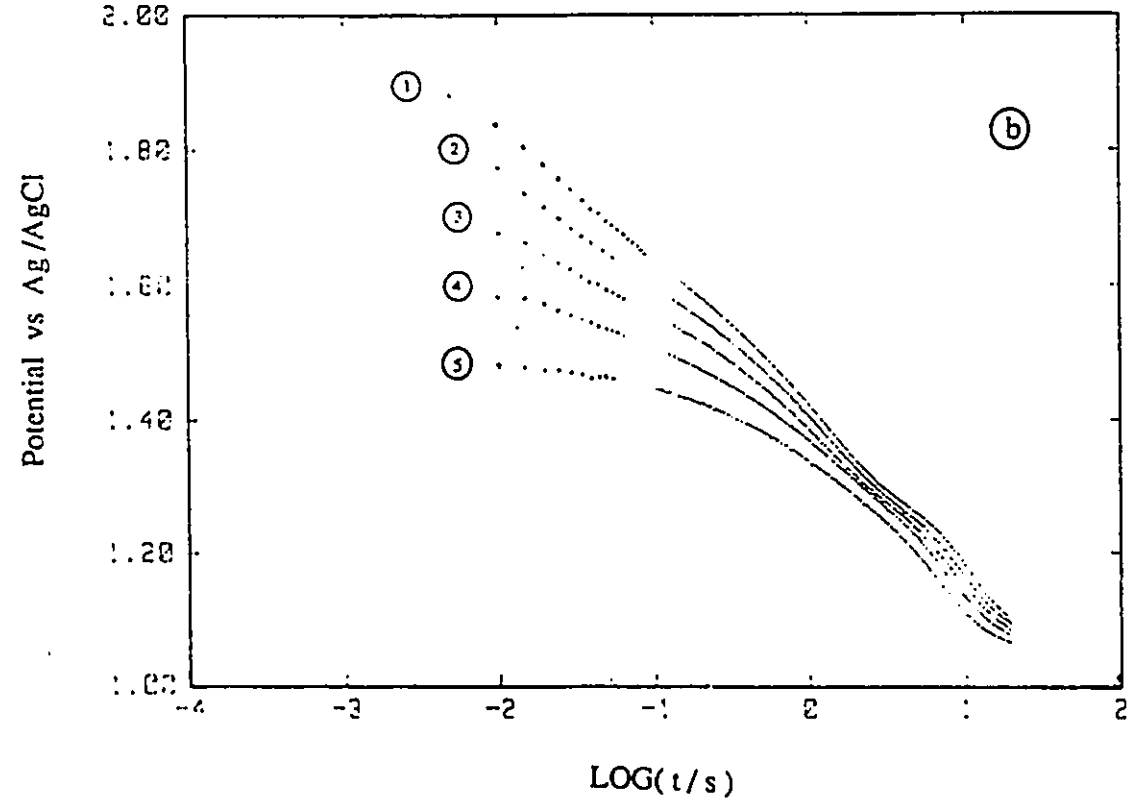
2.00
1.80
1.60
1.40
1.20
1.00
-4
-3
-2
-1
0
1
2
Potential vs Ag/AgCl
LOG(t/s)
b
1
2
3
4
5

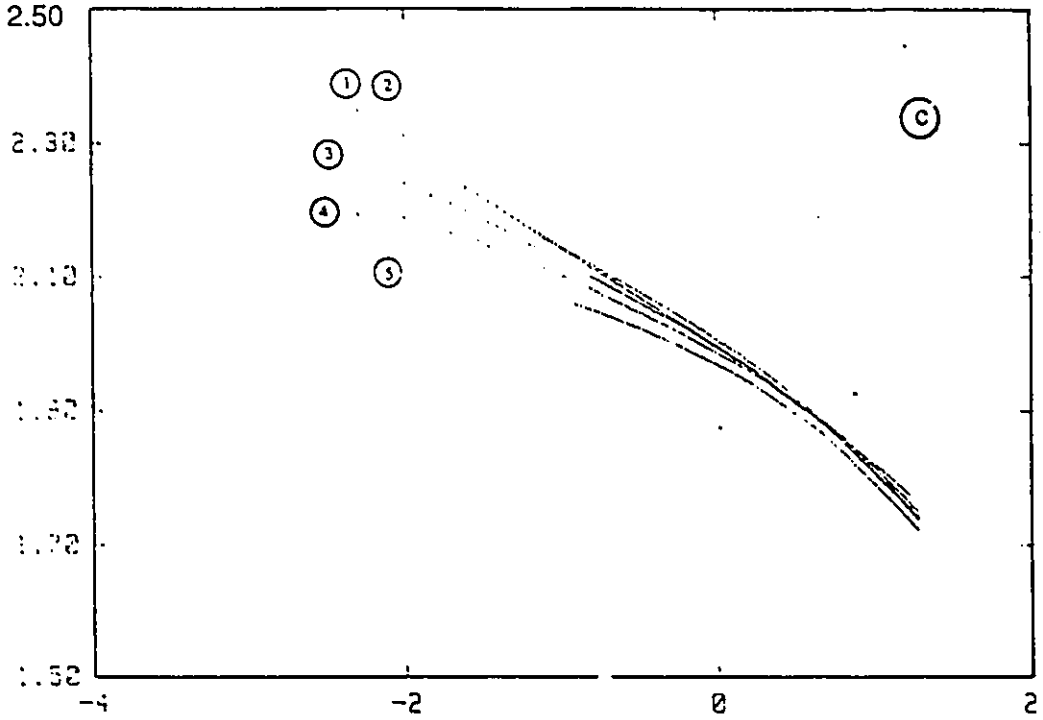
2.50
2.30
2.10
1.90
1.70
1.50
-4
-2
0
2
LOG(t/s)
c
1
2
3
4
5

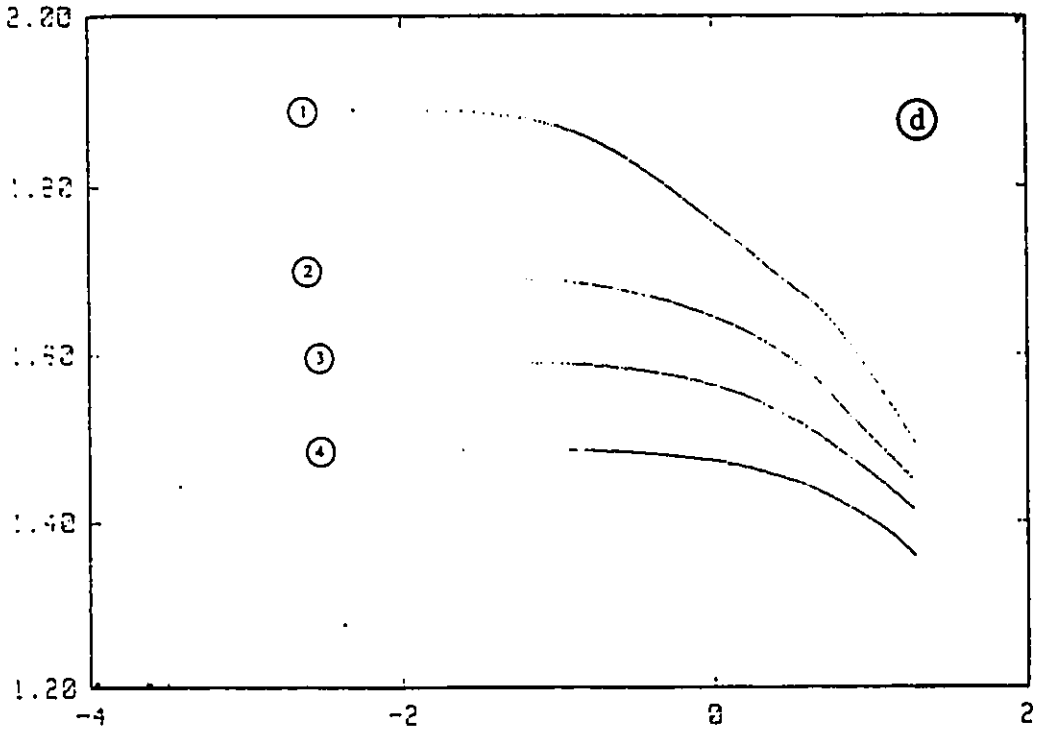
2.20
2.00
1.80
1.60
1.40
1.20
-4
-2
0
2
LOG(t/s)
d
1
2
3
4

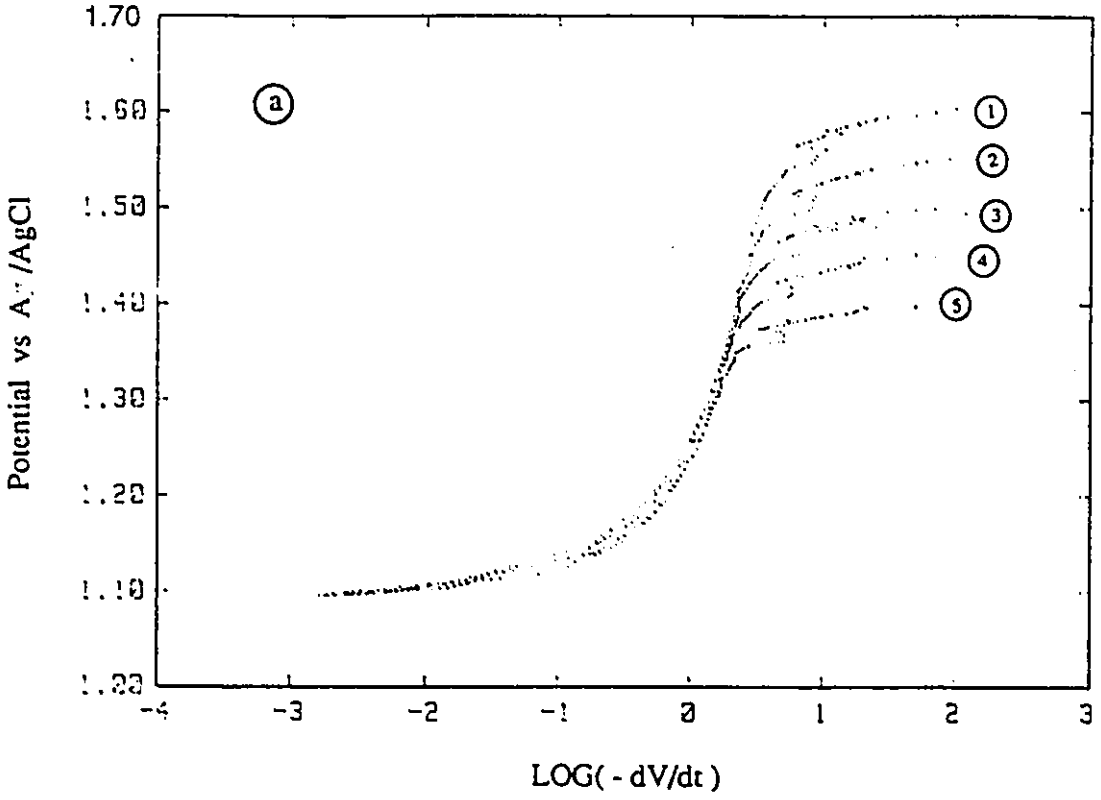
a
1
2
3
4
5
1.70
1.60
1.50
1.40
1.30
1.20
1.10
1.00
-4
-3
-2
-1
0
1
2
3
Potential vs Ag/AgCl
LOG(- dV/dt)

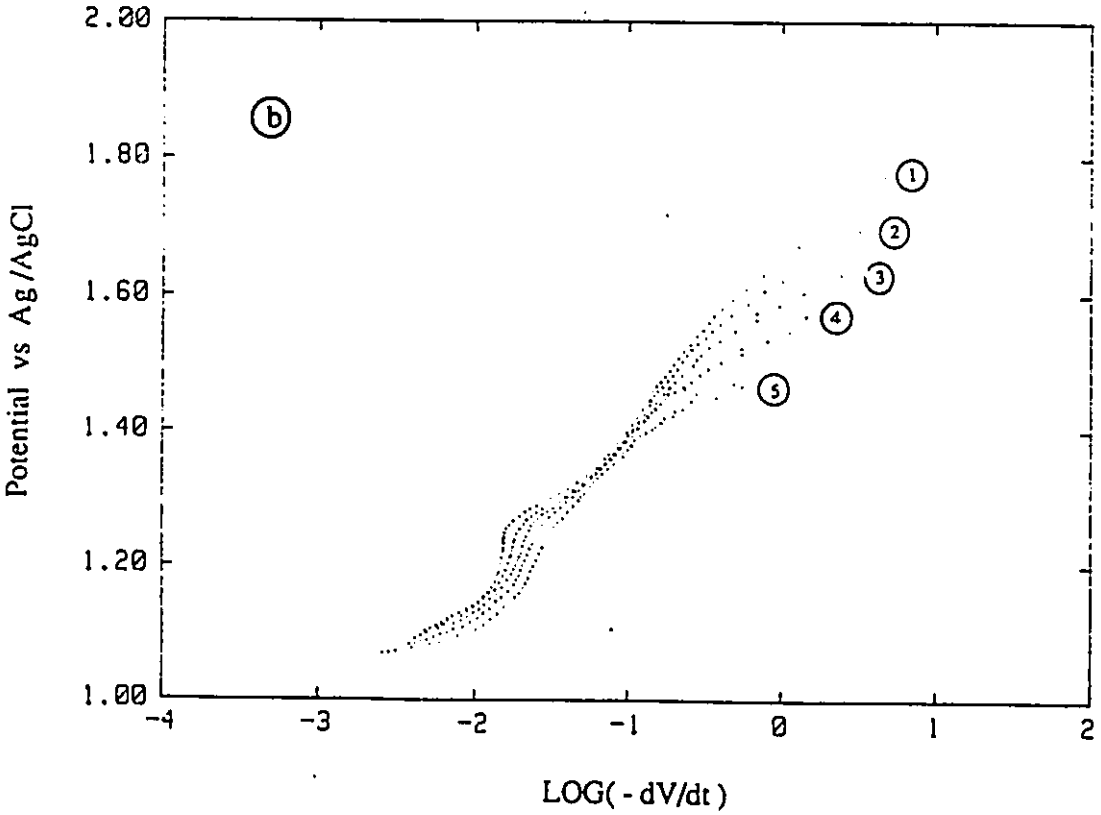
b
1
2
3
4
5
2.00
1.80
1.60
1.40
1.20
1.00
-4
-3
-2
-1
0
1
2
Potential vs Ag/AgCl
LOG(- dV/dt)

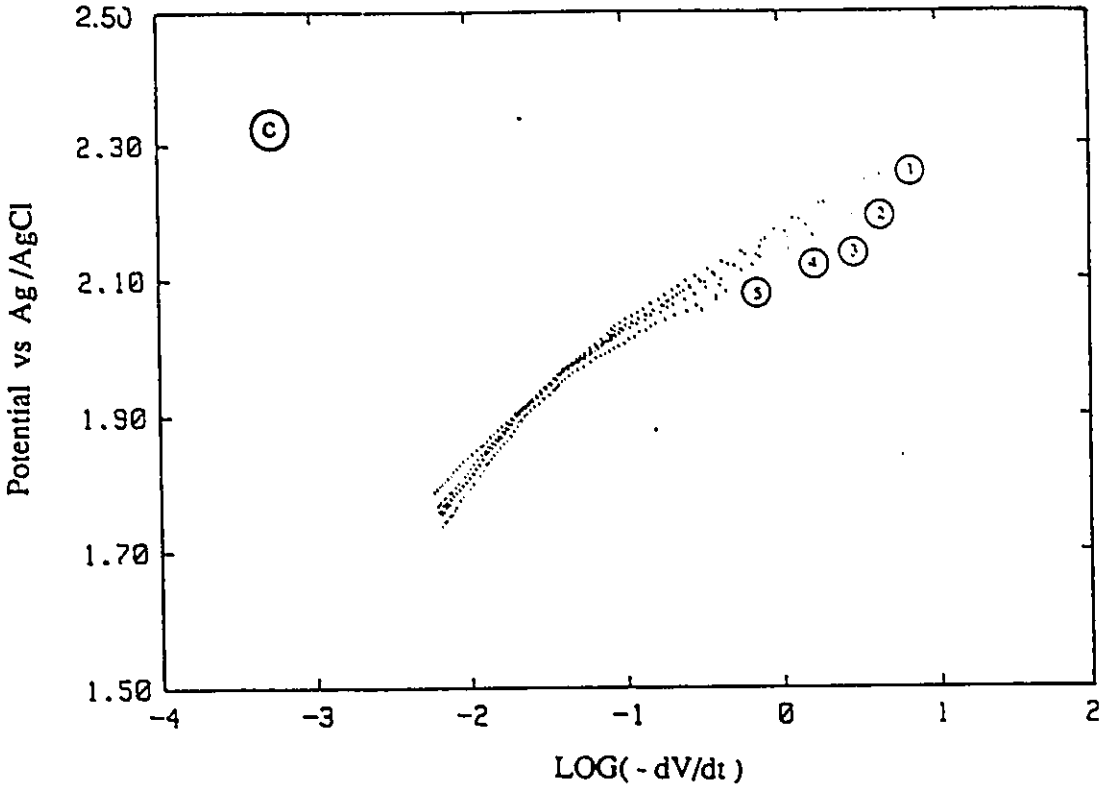
2.50
2.30
2.10
1.90
1.70
1.50
-4
-3
-2
-1
0
1
2
Potential vs Ag/AgCl
LOG(- dV/dt)
c
1
2
3
4
5

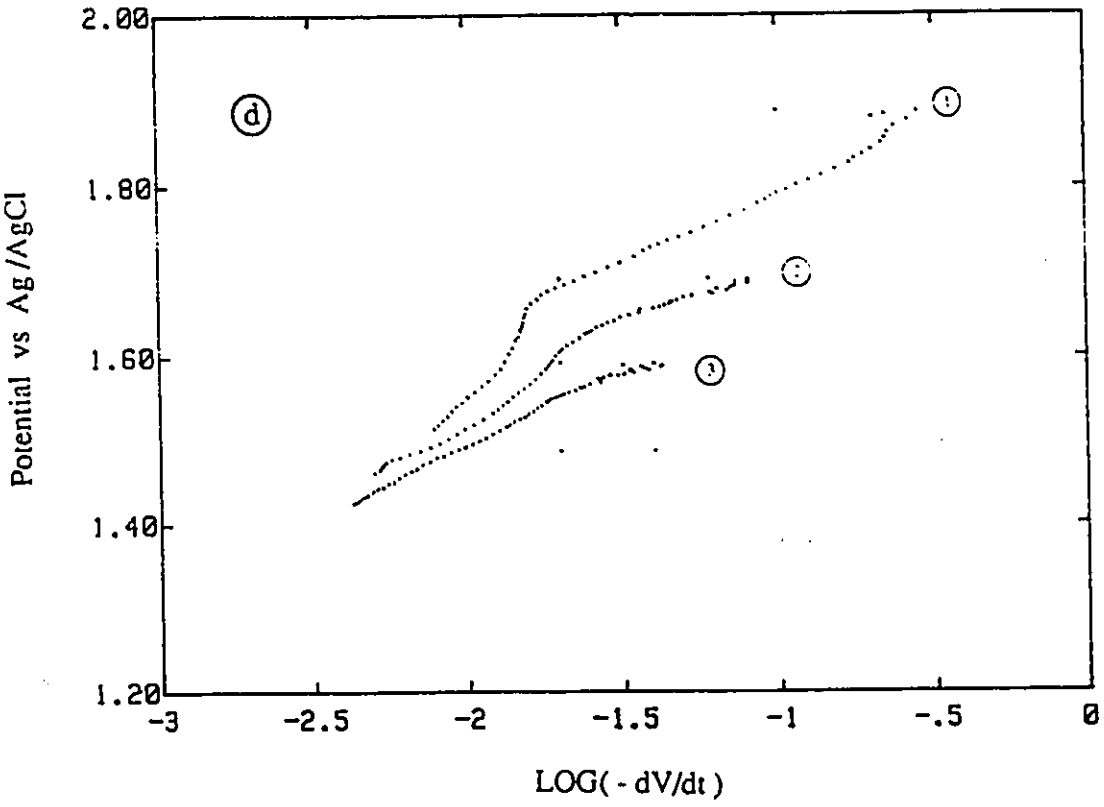
2.00
1.80
1.60
1.40
1.20
-3
-2.5
-2
-1.5
-1
-.5
0
Potential vs Ag/AgCl
LOG(- dV/dt)
d
1
2
3

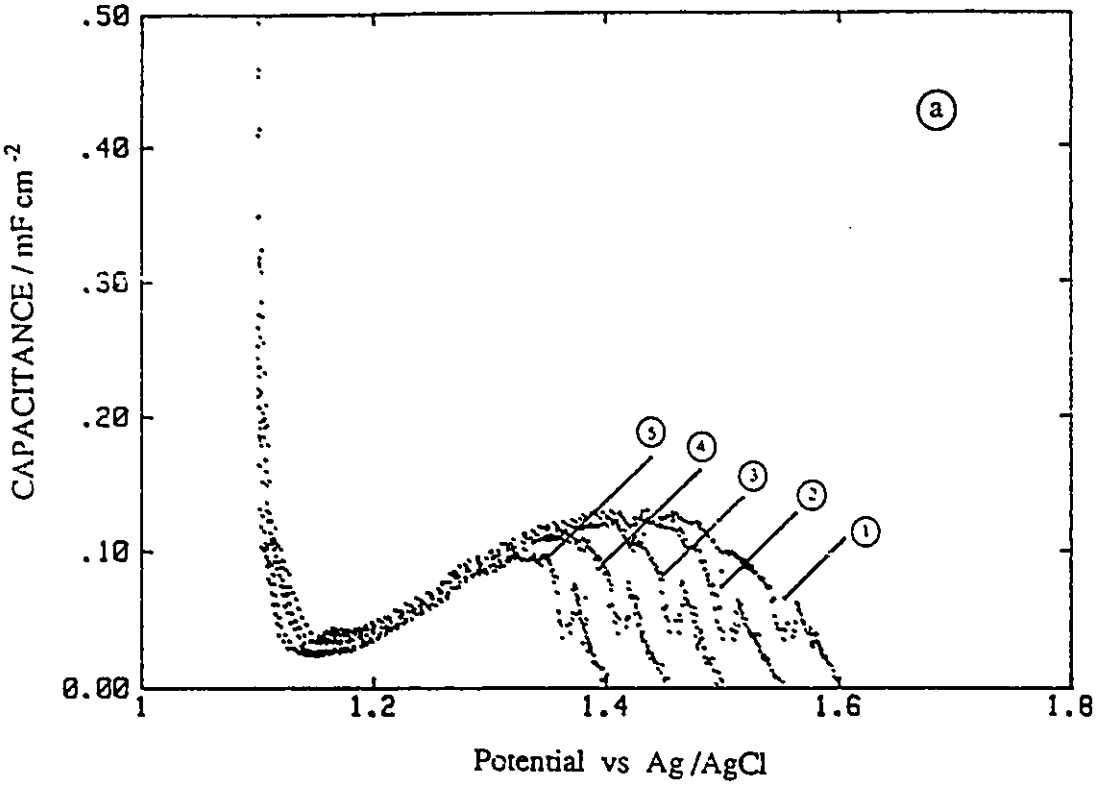
.50
.40
.30
.20
.10
0.00
CAPACITANCE / mF cm -2
a
5
4
3
2
1
1
1.2
1.4
1.6
1.8
Potential vs Ag/AgCl

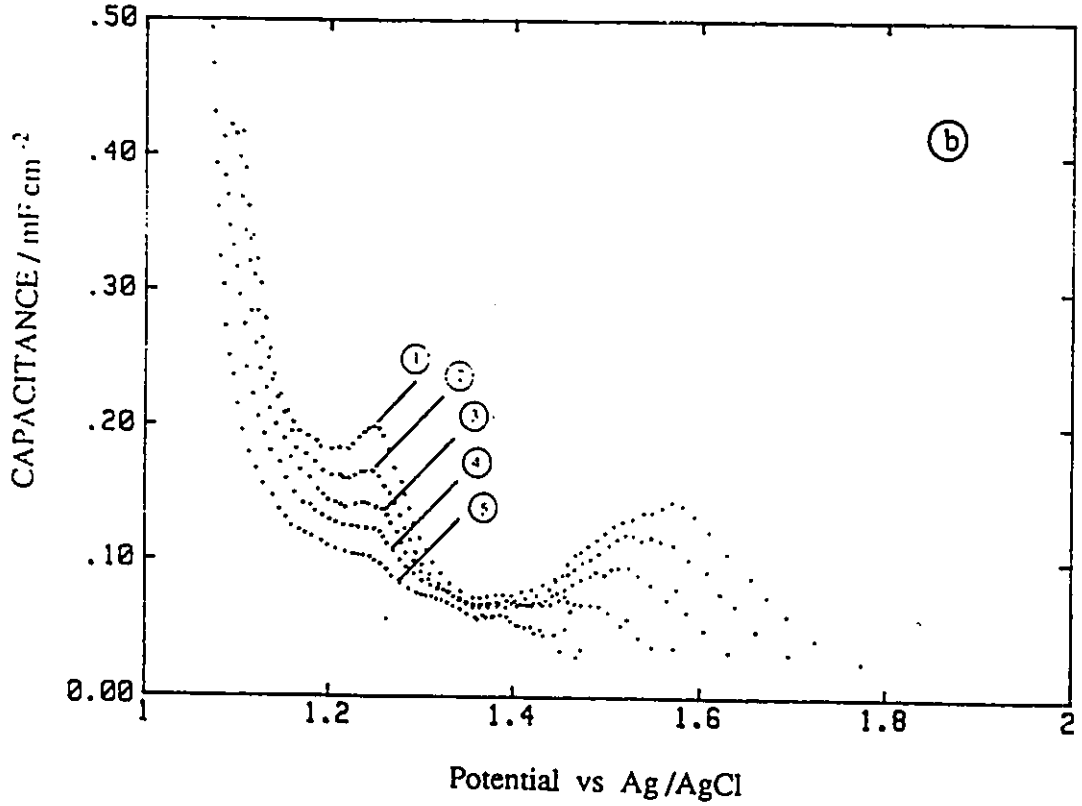
.50
.40
.30
.20
.10
0.00
CAPACITANCE / mF cm -2
b
1
2
3
4
5
1
1.2
1.4
1.6
1.8
2
Potential vs Ag/AgCl

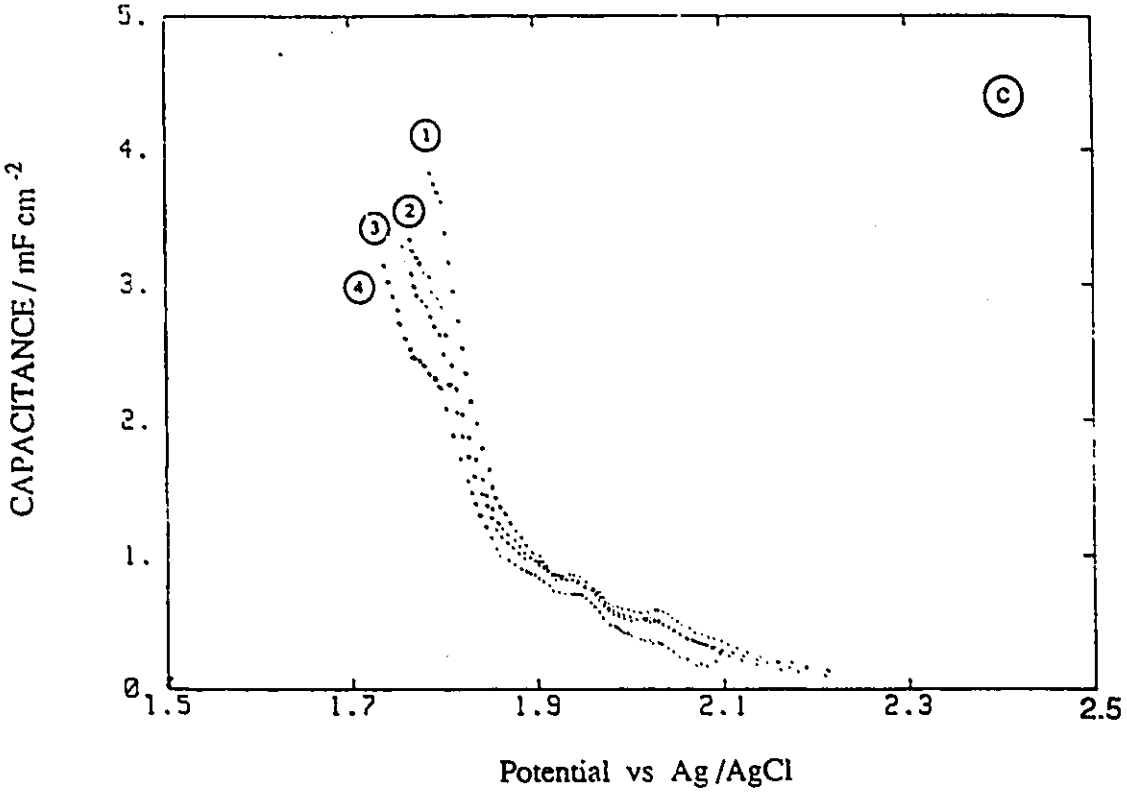
CAPACITANCE / mF cm -2
5.
4.
3.
2.
1.
0
1.5
1.7
1.9
2.1
2.3
2.5
Potential vs Ag /AgCl
c
1
2
3
4

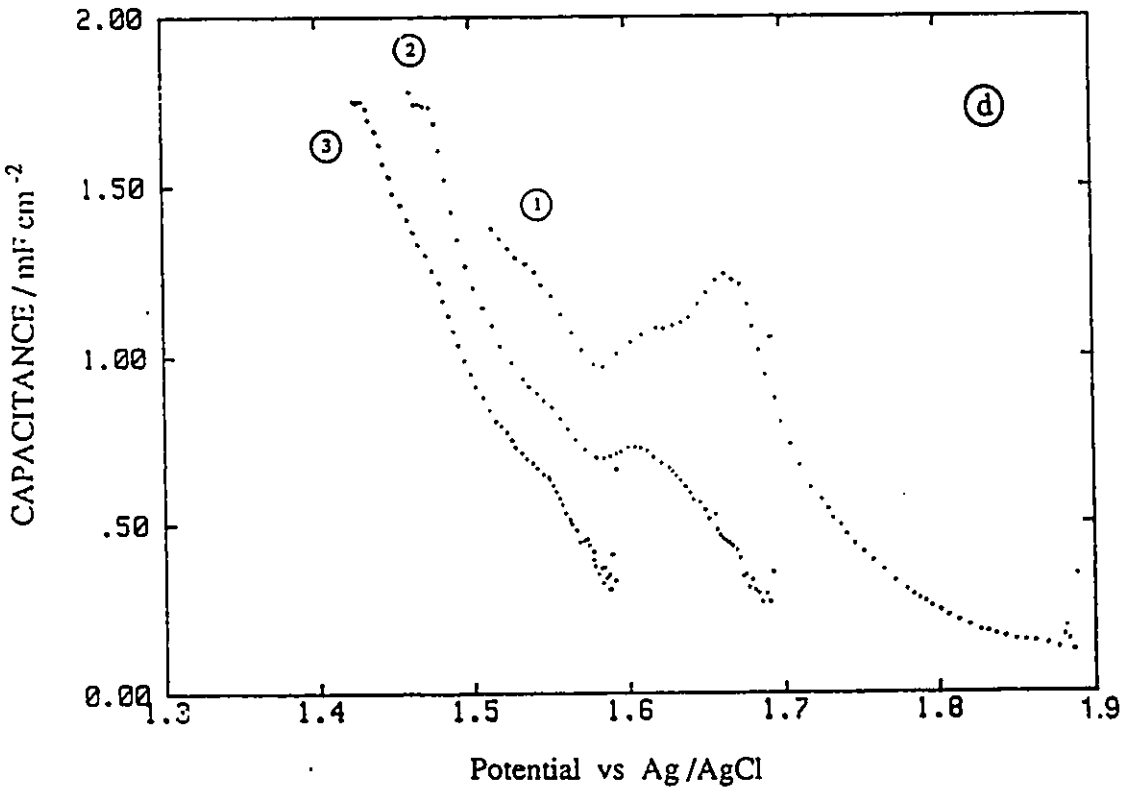
CAPACITANCE / mF cm -2
2.00
1.50
1.00
.50
0.00
1.3
1.4
1.5
1.6
1.7
1.8
1.9
Potential vs Ag /AgCl
d
1
2
3

whole potential decay range. This suggests that the surface condition is changing with polarization potential. Also, in these curves, two regions only can be seen at low initial potentials but three at high. Again, this implies that at least two capacitative components are involved in the process.

The capacitance behaviour of the adsorbed $Cl^{\cdot}$ intermediate in the Cl_2 evolution reaction (or $CF_3^{\cdot}$ and $CF_3COO^{\cdot}$, if the Kolbe reaction is also involved) has also been derived from the steady-state data together with the derivative of the decay transients, i.e. (-dV/dt), using eqn.[4.1] as reiterated below:

$$C(V) = -i(V)/(-dV/dt) \qquad [6.5]$$

The resulting C(V) vs V profiles for these four electrodes (Fig.6.4a-d) are very interesting: each of the electrodes shows its own characteristic behaviour. For the Pd electrode, a wide capacitance peak extends from 1.2 V to 1.6 V with a maximum of ca. 150 $\mu F\ cm^{-2}$ at 1.45 V. This capacitance peak must correspond to the adsorption of the $Cl^{\cdot}$ species in the Cl_2 evolution reaction since, in the potential range covered (1.2 - 1.6 V vs Ag/AgCl), no Kolbe reaction nor any Pd dissolution process can be involved; the Cl_2 evolution reaction is the one that is predominant. (Only at high potentials, up to +2.0 V vs Ag/AgCl, does dissolution of the Pd electrode arise leading to an orange coloured precipitate).

Another interesting result is the C(V) vs V profile for the Ru electrode, which shows two capacitance maxima at 1.2 and 1.55 V, having values of 200 and 150 $\mu F\ cm^{-2}$, respectively. As the initial potential for decay decreases, the peak at high potentials disappears. These peaks, perhaps, correspond to the adsorption of the intermediate $Cl^{\cdot}$ of the Cl_2 evolution reaction over the low potential range and $CF_3^{\cdot}$ or/and $CF_3COO^{\cdot}$ for the Kolbe reaction at the higher potential range. It is reasonable to assign the C(V) peak at low potentials to $Cl^{\cdot}$ adsorption in the Cl_2 evolution reaction and the peak at higher potentials to intermediates of the Kolbe reaction since these two peaks correspond to the observed two limiting currents in the steady-state plot (see Fig.6.1). This experiment also suggests that the potential-relaxation method could

be useful for detecting more than one adsorbed species in a complex electrode process.

Since the decay rates at electrodes of Ir and Rh are relatively slow over the studied time scale, as shown in Figs.6.4c-d, only a peak of C(V) is observed. However, the capacitances are potential dependent, being again associated presumably with the adsorbed species $Cl^{\cdot}$ or CF_3 and/or $CF_3COO^{\cdot}$ For the Ir electrode, the C(V) vs V profile (Fig.6.4c) corresponds to only one side of a peak owing to the inaccessibility of a wider range of data, but rises to ca. 4 mF cm^{-2}, which is a value greater than that for Pd, Ru and even Pt. This large capacitance is probably due to the adsorbed $CF_3COO^{\cdot}$ or $CF_3^{\cdot}$ intermediates of the Kolbe reaction since the studied potential region extends to that where the Kolbe reaction commences as indicated by its Tafel plot for which a slope of ca. 295 mV per decade of current-density is observed. For the Rh electrode, on the other hand, the capacitance behaviour shows a peak in the high potential range and maybe another peak at lower potentials which is not fully resolved in Fig.6.4d due to insufficiency of data. However, a significant rise of C(V) at 1.4 V vs Ag/AgCl is seen. As the initial decay potential decreases, the peak in the higher potential region disappears as was found at Ru. Again, this could indicate that both $Cl^{\cdot}$ for the Cl_2 evolution reaction and $CF_3COO^{\cdot}$ or $CF_3^{\cdot}$ for the Kolbe reaction are involved.

6.3. Brief A.C Impedance Study

As the adsorbed species ($Cl^{\cdot}$ or $CF_3^{\cdot}$ and $CF_3COO^{\cdot}$) are detectable by the potential-relaxation method, it is expected that two semi-circles would also be observed in the a.c. impedance complex-plane plots, which is a complementary indication that adsorbed intermediate(s) may be involved at appreciable coverage in an electrode process. Therefore, a.c. impedance experiments were made at each of the electrodes Pd, Ru, Ir and Rh under the conditions of the Cl_2 evolution reaction in a non-aqueous TFA solution in order to study the behaviour of the adsorbed species

and the interfacial capacitances.

Figs.6.5.a-d show the complex-plane plots for Pd at 1.3 V, Ru at 2.4 V, Ir at 2.2 V and Rh at 1.6 V, respectively. All the diagrams show clearly two semicircles (except for the Rh electrode at which the current is too small to complete the second semi-circle since a very low frequency has to be attained). The first semi-circle, as was the case for the Pt electrode, must originate from a relaxation involving the double-layer capacitance. The second one, in the case of Pd electrode, may be mainly due to adsorbed $Cl^{\cdot}$ species but adsorbed $CF_3^{\cdot}$ and $CF_3COO^{\cdot}$ may also be involved in the other cases since the potentials are sufficiently high for the Kolbe reaction to commence.

This brief a.c. exploration of the impedance behaviour serves only to provide a complementary proof of the involvement of the adsorbed species; more detailed studies will be carried out by another researcher in order to provide a better understanding of the electrode kinetics and mechanism under these conditions. However, the a.c. results do reveal some important information about the behaviour of the adsorbed species even though only in a qualitative way at the moment.

6.4. Brief Summary

It has to be stressed that it is difficult to give a so-called "summary" based on such limited experimental data. However, the author tries here only to describe what may be provisionally concluded in order to provide useful information for further work in this direction.

(a) Phenomenologically, the smallness of the current densities that are observed for the Cl_2 evolution reaction in a non-aqueous TFA solution may be on account of the inflection in the current vs potential plot due to the inhibition by the strong bonding between the free surface metal atoms and the adsorbed $Cl^{\cdot}$ species.

(b) The mechanism of the Cl_2 evolution reaction at Pd and Ru in a non-aqueous TFA solution is probably again, as with Pt, the $Cl^{\cdot}$ recombination process:

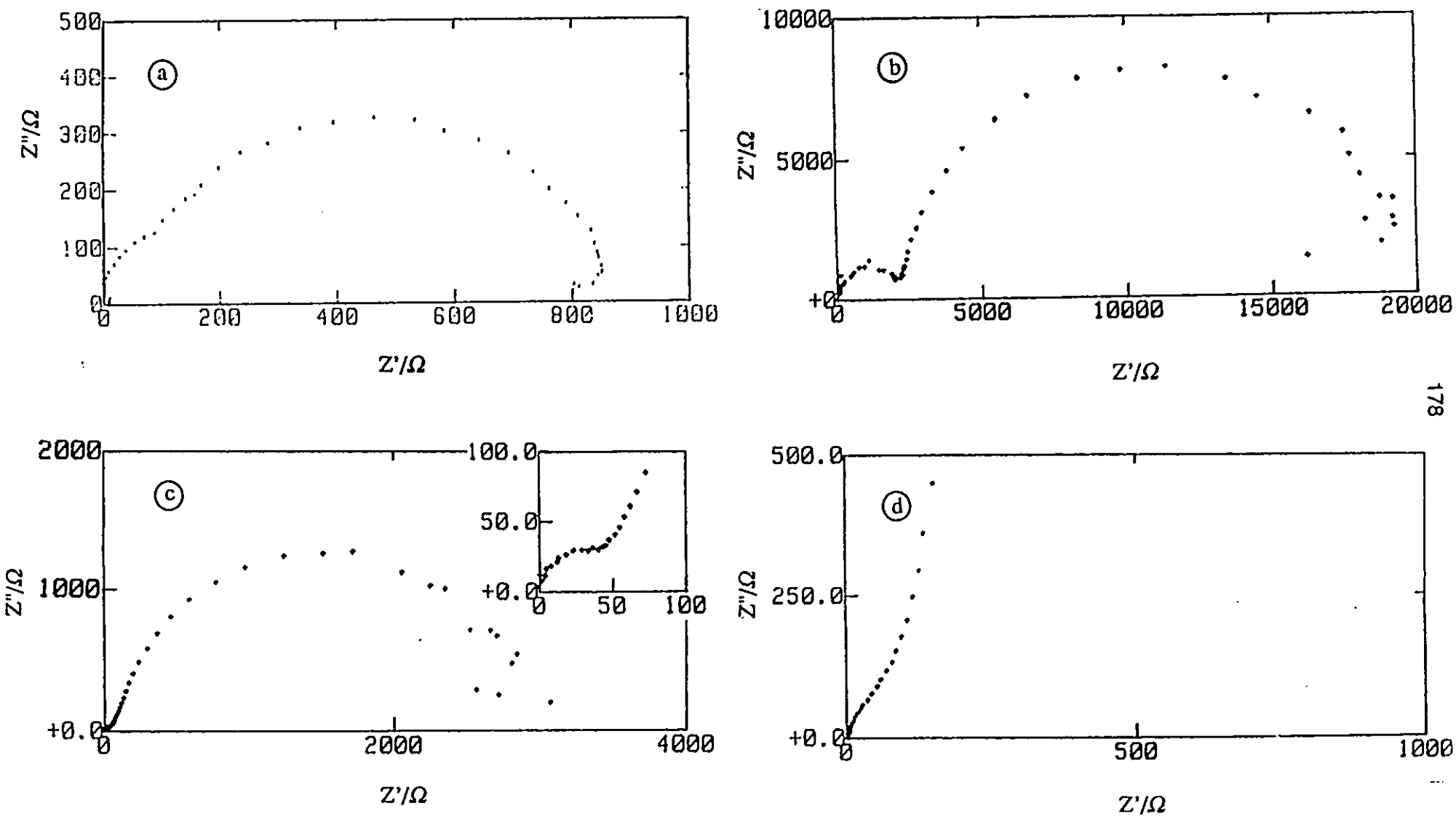

Fig.6.5a-d The a.c. impedance plot in the complex-plane for Cl_2 evolution at different electrodes in non-aqueous solution at various potentials (vs Ag/AgCl): a) for Pd at 1.3 V; b) for Ru at 2.4 V; c) for Ir at 2.2 V and d) for Rh at 1.6 V.

$$(Pd \text{ or } Ru) + Cl^- \equiv\equiv\equiv (Pd \text{ or } Ru)\text{-}Cl + e \qquad [6.6]$$

$$2(Pd \text{ or } Ru)\text{-}Cl \longrightarrow Cl_2 \uparrow + (Pd \text{ or } Ru) \qquad [6.7]$$

in the low potential region but, in the higher potential range, the Kolbe reaction may be involved. At Ir and Rh electrodes, the inhibition effect is much stronger so that the behaviour of Cl^- adsorption cannot be well characterized.

(c) The adsorption behaviour of the intermediates has been evaluated by means of potential relaxation and a.c. impedance methods. The adsorbed intermediates involved are not only Cl^- but also probably CF_3^- and/or CF_3COO^-, depending on the polarization potentials attained.

CHAPTER VII

Cl_2 Evolution Reaction at RuO_2-TiO_2 Ti Substrate Electrodes

After the first paper on the fundamental properties of RuO_2, the essential active component of the so-called DSA electrode used in the chlor-alkali industry, appeared in 1971 (refs.11,12,100), basic research on this material has expanded exponentially, both quantitatively and qualitatively. However, there are still many unclear matters relating to why such oxide materials lead to extremely satisfactory performance. In particular, the mechanisms of the electrocatalysis of Cl_2 evolution on this type of oxide electrode are still not well understood because there is insufficient knowledge of the diversity between the catalytic properties of a metal and its oxide surface. In this chapter will be reported the results of studies on Cl_2 evolution kinetics at RuO_2-TiO_2 electrodes having various compositions and morphology, arising from the application of relatively new electrochemical techniques.

The electrochemical kinetic behaviour of the Cl_2 evolution reaction at RuO_2-TiO_2 film electrodes, prepared by the thermal decomposition of $RuCl_3$-$Ti(OC_4H_9)_4$ solutions on metallic Ti supports has been investigated in 1 mole dm^{-3} solutions of Cl^- ion. Cyclic-voltammetry, steady-state polarization, potential-relaxation and a.c. impedance methods have been applied in the work to be described here. On thin-film RuO_2-TiO_2 materials, kinetic control of the Cl_2 evolution reaction seems to occur via Cl^- discharge to the adsorbed $Cl^\cdot$, followed by its recombination, as indicated by the observed unique linearity of Conway-Novak test plots (refs.85,86) for the recombination mechanism. As for the other cases, analysis of the potential relaxation transients enables the pseudocapacitance, C_ϕ, for the adsorbed $Cl^\cdot$ intermediate to be determined. C_ϕ shows ascent to large values below 50 to 100 mV overpotential, depending on the temperature. Roughness factor problems arise, however, in considering the adsorption

behaviour in relation to expectations associated with recombination control.

7.1 Composition and Surface Morphology of the RuO_2-TiO_2 Electrodes

Since many factors can affect the mechanism and electrocatalytic properties of RuO_2-TiO_2 electrodes, such as porosity, morphology and composition of the active layer together with the behaviour of the adsorbed intermediates, the procedure for preparation of the electrode is quite important. In the experiments described in this section, five RuO_2-TiO_2 electrode preparations either having various percentages of Ru (as RuO_2) or different morphologies of their surfaces, were examined.

Electrodes numbered #1 to #4 were prepared by coating with very dilute Ru-Ti solutions having various compositions while #5 was coated with a more concentrated one. All the electrodes were then baked at a temperature of ca. 450°C for 2 hours in air to form the active layer of mixed RuO_2-TiO_2. The oxidative dissociation of the anhydrous ruthenium chloride, represented by the reaction

$$RuCl_3 + O_2 \dashrightarrow RuO_2 + 3/2\ Cl_2 \qquad [7.1]$$

is usually carried out at temperatures below 500°C since a significant weight loss of the Ru can otherwise take place by the formation of volatile species such as RuO_3 and RuO_4 via the following reactions (ref.105):

$$RuO_2 + 1/2O_2 \dashrightarrow RuO_3 \qquad [7.2]$$

$$RuO_2 + O_2 \dashrightarrow RuO_4 \qquad [7.3]$$

The scanning electron micrographs (SEM) of the electrodes #1 to #5 are shown in Figs.7.1a-e, respectively. As expected, these five electrodes have very different surface structures (as well as compositions). From the microphotographs, it can be seen that electrodes #1 to #4 have a very thin oxide film with a relatively smooth surface (but some tiny pores can still be seen in the micrographs). In contrast, electrode #5 (Fig.7.1e) has a thicker film, ca. 2 μm, with a mud-crack morphology of the kind usually seen at DSA electrodes.

Table 7.1 The Compositions of the RuO_2 Films

Composition / Electrode	Ru (Weight %)	Ti (Weight %)
# 1	9	91
# 2	29	71
# 3	38	62
# 4	50	50
#5	22	78

The chemical compositions of the films were determined by means of an x-ray energy dispersive microanalyzer on the SEM. The components of the oxide films forming the surfaces of the five electrodes are presented in terms of the percentage of Ru and Ti as listed in Table 7.1. The proportional compositions of the films are found to be quite different from those of the respective coating solutions, especially for the thin films (#1 to #4). For example, the percentages of Ru in the coating solutions are, respectively, 30, 60, 80 and 100% for electrodes #1 to #4. However, the x-ray analysis results show only 9, 29, 38, 50 % Ru, respectively. This could be explained by some penetration of the Ru atoms into the Ti oxide substrate, or probably by some migration of bulk Ti atoms into the oxide film. For a thick film, this difference is not significant, e.g. at electrode #5.

(a)

(b)

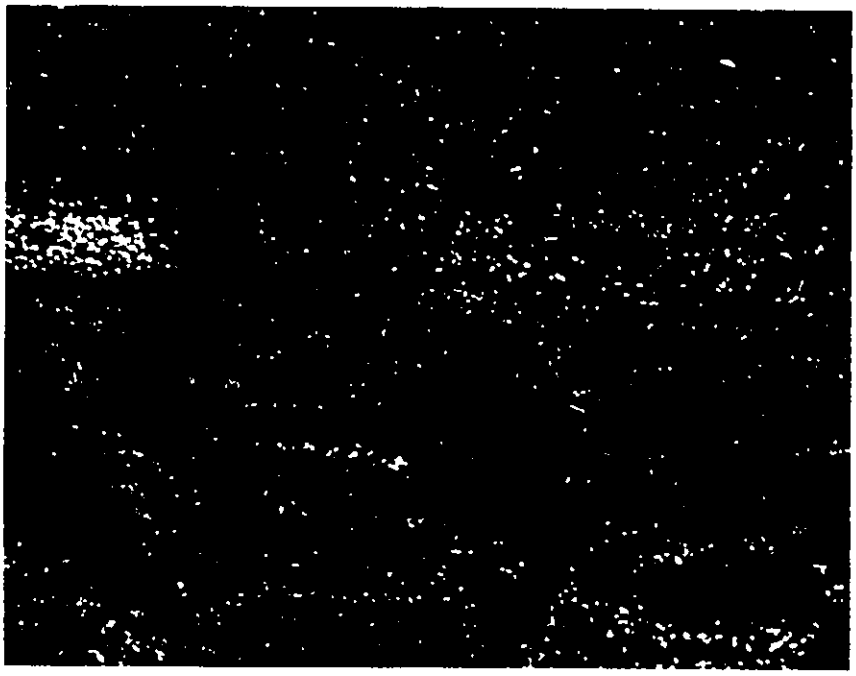

(c)

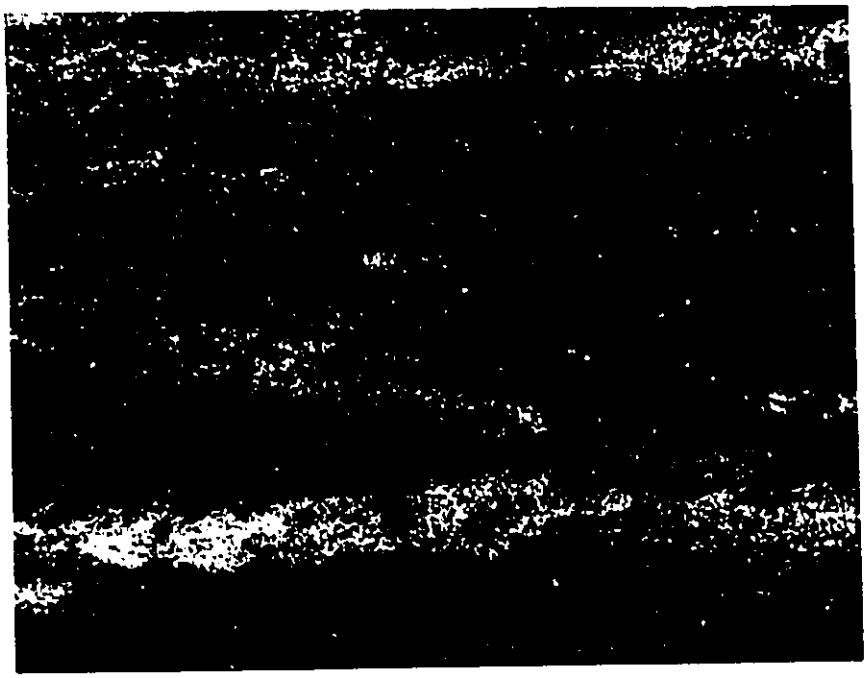

(d)

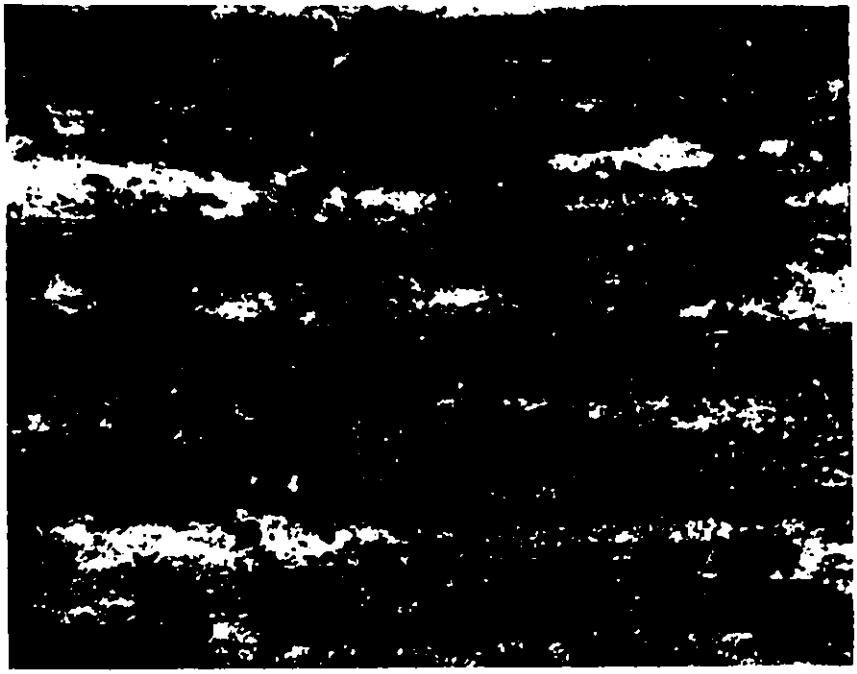

(f)

Fig.7.1 SEM photos for RuO_2-TiO_2 electrodes. (a) for electrode #1; (b) for #2; (c) for #3; (d) for #4 and (e) for #5.

7.2. Cyclic-Voltammetry Study

Typical i/V curves for RuO_2 electrodes examined by means of cyclic-voltammetry at a scanning speed of 100 mV s^{-1} are shown in Figs.7.2a-e for electrodes #1 to #5, respectively. The oxygen evolution process (peak 5) starts at about 1.4 V and two pairs of peaks are also seen at about 1.1 V (peaks 2 and 3) and at 0.7 V (peaks 1 and 4) for electrode #4 (Fig.7.2.d). However, peaks 2 and 3 do not arise in Figs.7.2a and e and are hardly detected in Figs.7.2b and c. Peaks 2 and 3 can be attributed to the Ru_2O_3/RuO_2 couple and peaks 1 and 4 to the RuO_2/RuO couple. Peak 6 is thought to be due to the solid-state reduction of RuO_2, i.e. to penetration of atomic hydrogen into the lattice. The disappearance of peaks 2 and 3 may be related to the distribution of Ru atoms in the surface of the oxide films. The trend of the behaviour is that the higher the Ru concentration the greater the tendency for peaks 2 and 3 to be resolved.

The qualitative and quantitative reproducibility of the cyclic-voltammograms taken at RuO_2-TiO_2 electrodes is excellent. Repeated potential cycling between the potentials for O_2 and H_2 evolution does not affect the shape of the curves.

The anodic charge injected, q_a, into the electrodes can be evaluated by integration of the i/V curves above the zero current line, i = 0. Fig.7.3 shows that these charges are almost a linear function of the potential, as in the case of a capacitor. The slopes of the lines then give values of the apparent capacity about 0.32-4.57 mF cm^{-2} which may correspond to a double-layer capacitance, allowing for the large real/apparent area ratio. The total anodic injected charge probably relates to the composition and the morphology of the oxide film, i.e. its porosity and the thickness. The electrode having the higher concentration of Ru takes a larger injected charge; for example, charges for #3 and #4 are larger than those for #1 and #2. The surface roughness and thickness of the oxide film could also give rise to a large effect, since if the layer of RuO_2 is porous, the depth of the pores could increase with thickness, thus

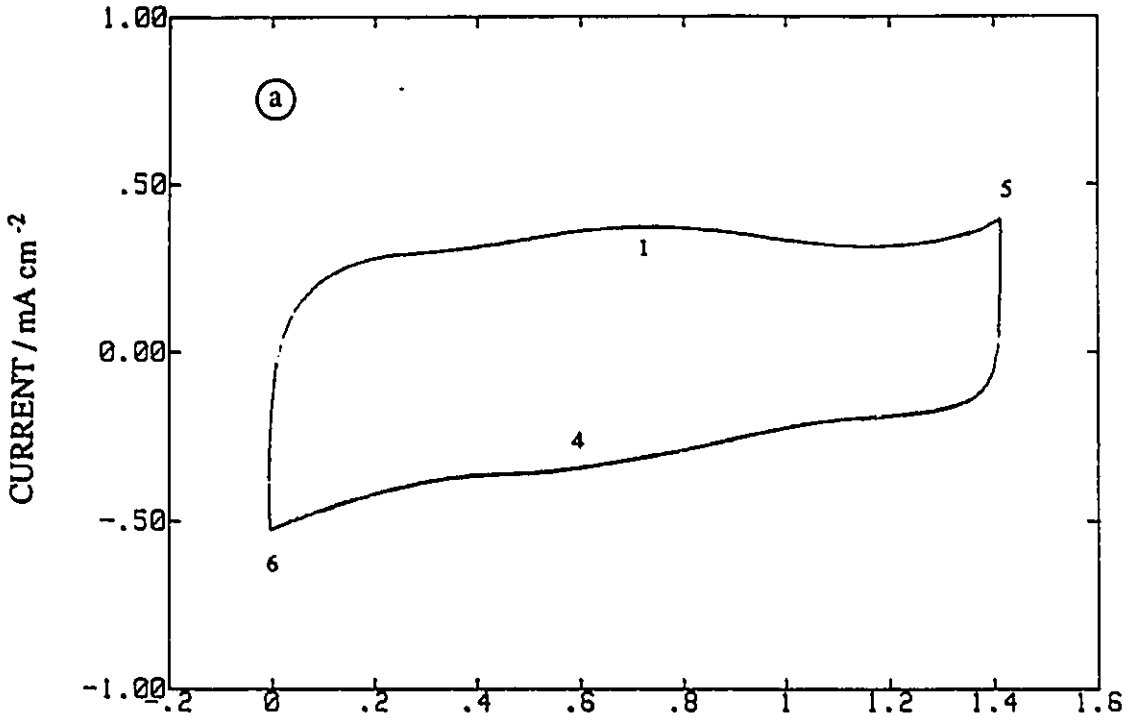
a
1.00
.50
0.00
-.50
-1.00
-.2
0
.2
.4
.6
.8
1
1.2
1.4
1.6
1
4
5
6
CURRENT / mA cm -2
POTENTIAL / V vs RHE

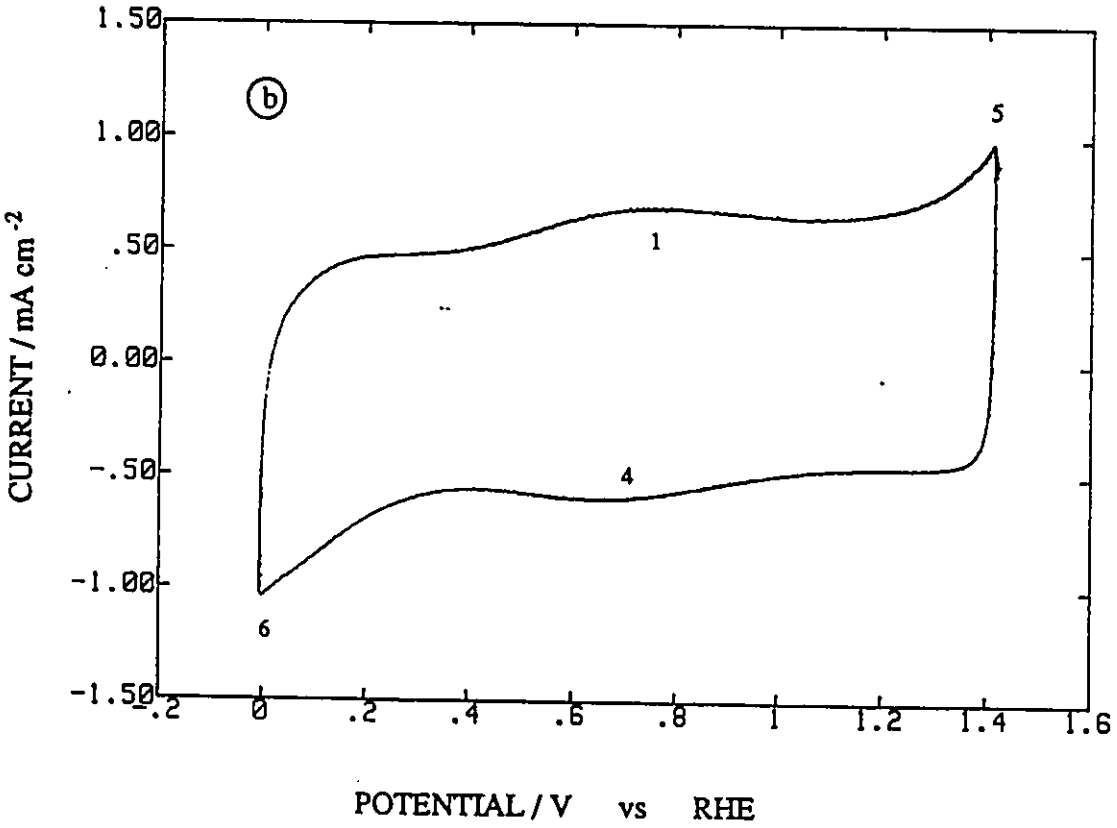
b
1.50
1.00
.50
0.00
-.50
-1.00
-1.50
-.2
0
.2
.4
.6
.8
1
1.2
1.4
1.6
1
4
5
6
CURRENT / mA cm -2
POTENTIAL / V vs RHE

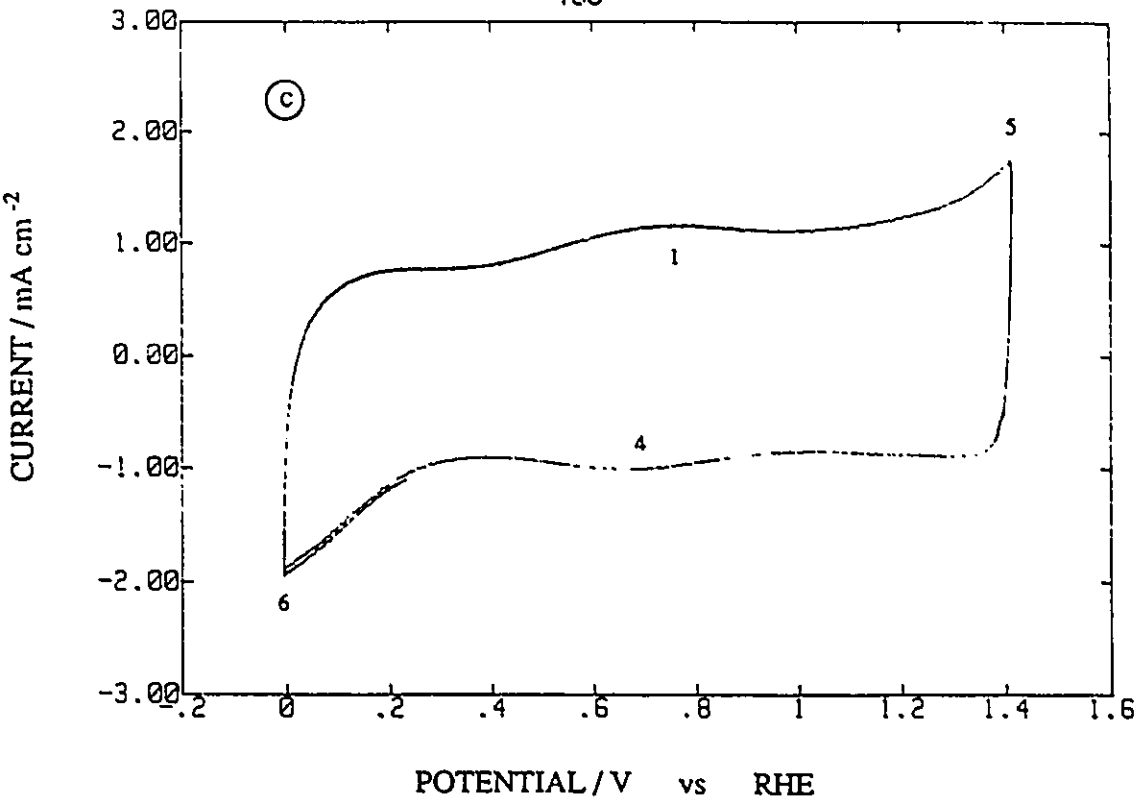
3.00
2.00
1.00
0.00
-1.00
-2.00
-3.00
CURRENT / mA cm -2
c
1
4
5
6
.2
0
.2
.4
.6
.8
1
1.2
1.4
1.6
POTENTIAL / V vs RHE

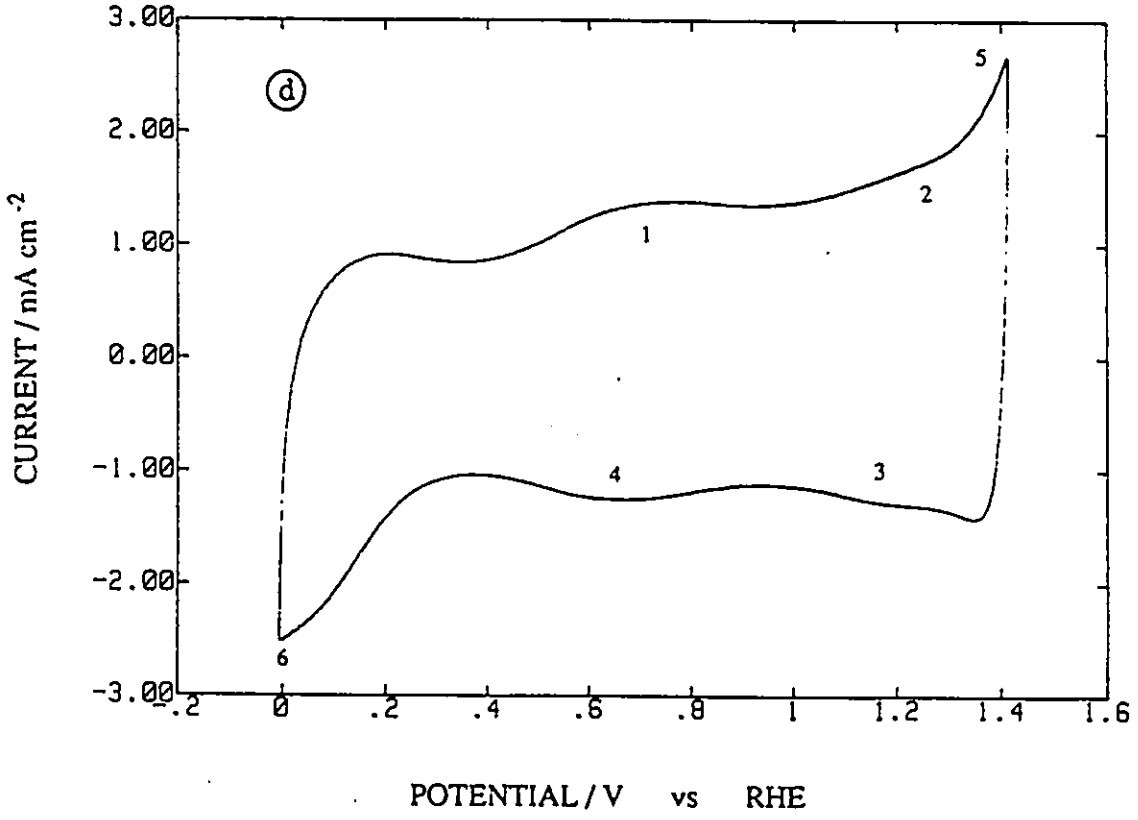
3.00
2.00
1.00
0.00
-1.00
-2.00
-3.00
CURRENT / mA cm -2
d
1
2
3
4
5
6
.2
0
.2
.4
.6
.8
1
1.2
1.4
1.6
POTENTIAL / V vs RHE

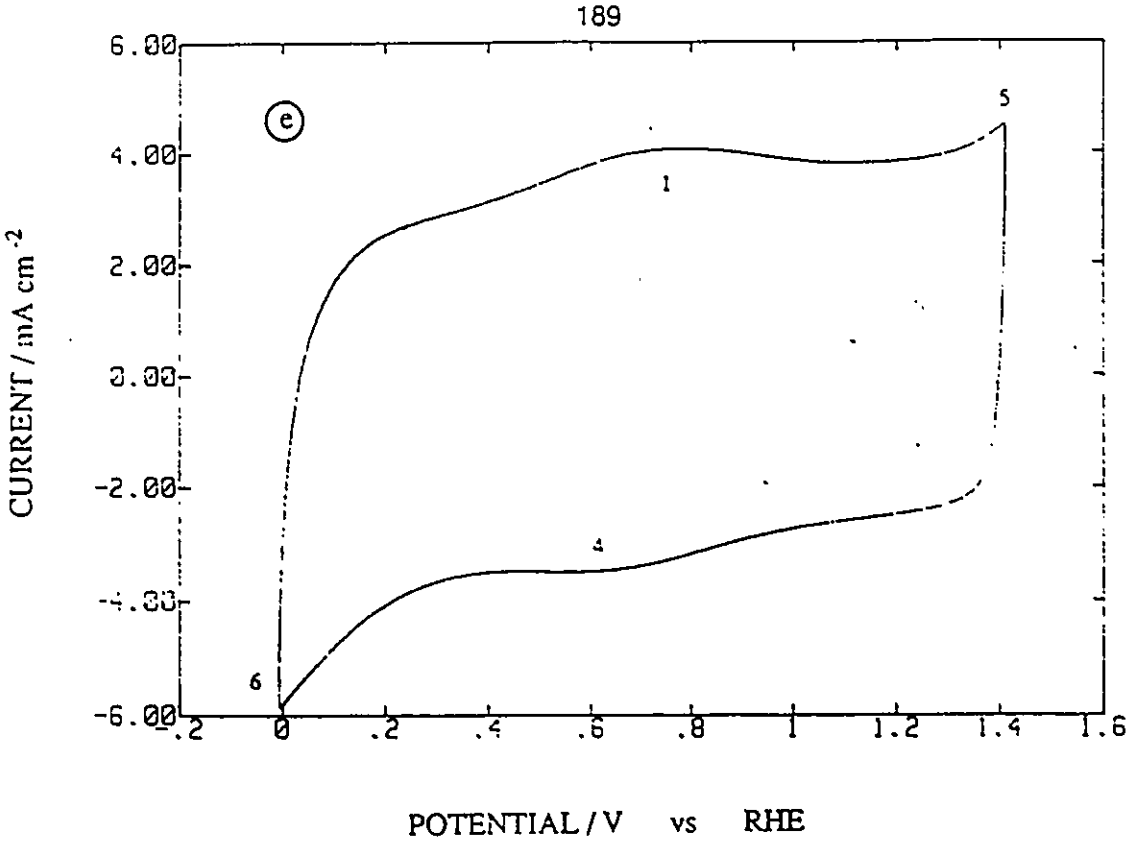

Fig.7.2 Cyclic-voltammograms of the five RuO_2-TiO_2 electrodes in 0.1 M H_2SO_4 solution: (a) for #1; (b) for #2; (c) for #3; (d) for #4 and (e) for #5.

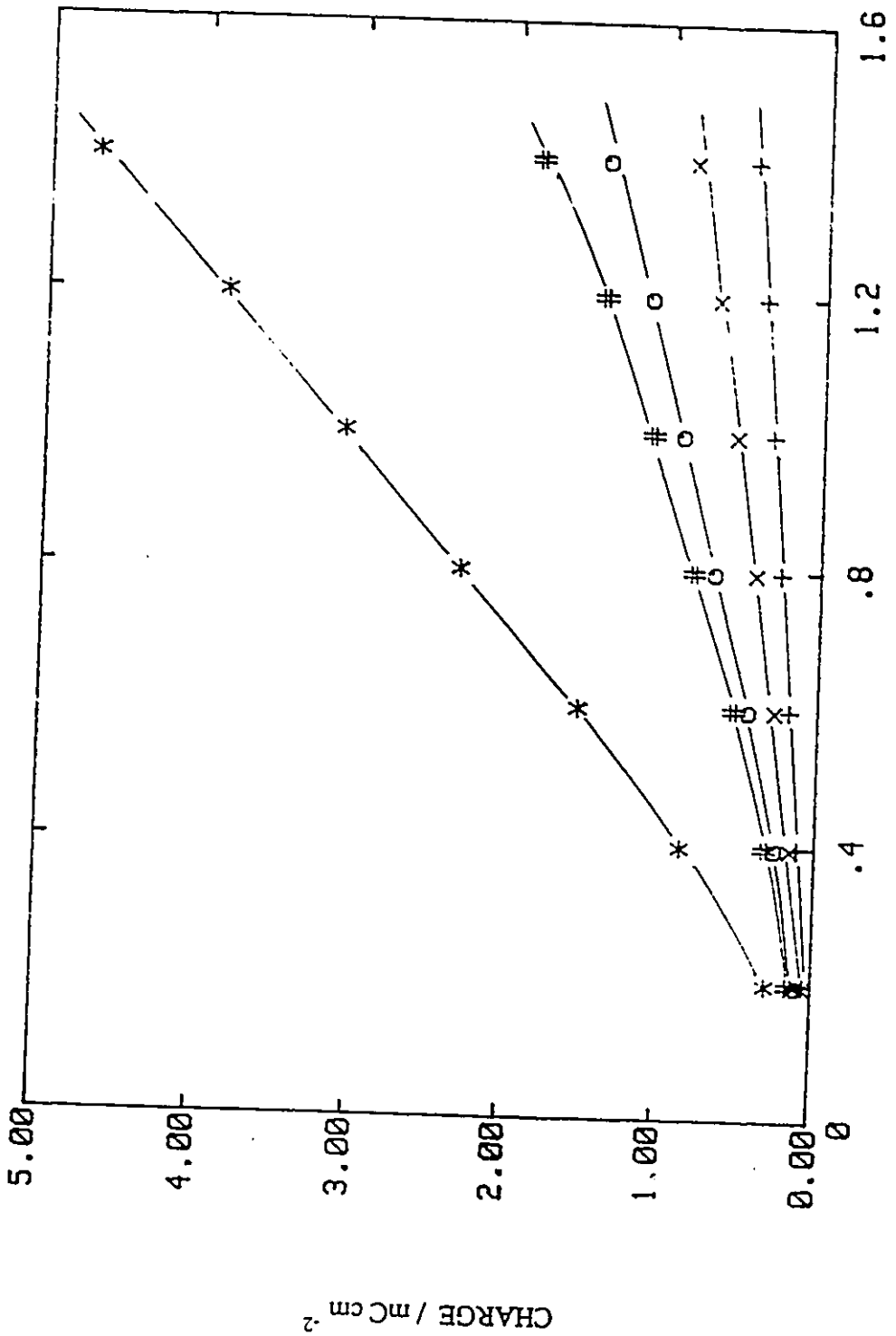

Fig.7.3 Integrated values of the anodically injected charge from Fig.7.2 for the five RuO_2-TiO_2 electrodes. The "+" for #1; "x" for #2; "o" for #3; "#" for #4 and "*" for #5.

increasing the real surface area. In this case, the amount of charge for double-layer charging could also increase. This is why the electrode #5 takes a much larger anodically injected charge than the others since it is very "rough". Table 7.2 gives the anodically injected charges and corresponding apparent capacitances per apparent cm^2 for comparison.

Table 7.2 The Anodically Injected Charge

Electrode	Anodically injected charge / mC cm^{-2}
# 1	0.44
# 2	0.87
# 3	1.42
# 4	1.84
# 5	4.68

7.3. Primary Kinetic Study

7.3.1. Anodic Polarization Characteristics

The steady-state polarization curves for the Cl^- evolution reaction at RuO_2-TiO_2 and RuO_2 electrodes measured potentiostatically at a temperature of 298 K, are shown in Fig.7.4 and for various concentrations of Cl^- up to 4.1 mole dm^{-3} in Fig.7.5. The Tafel plots all seem to be non-linear, with apparent approaches to limiting currents in the -1 to 0 decade of i. It is important to note that the data plotted are already the IR-corrected overpotentials so that the behaviour observed here cannot be due to the influence of uncompensated resistance effects in the measurement system.

Therefore, an experiment in which a RuO_2-TiO_2 electrode (#5) was rotated up to 6400 rpm (Fig.7.6), was conducted in order to establish if the approach to the limiting currents was due to a concentration-overpotential effect (mass-transfer limited current or supersaturation of Cl_2). Since similar behaviour is found even in 4.1 M NaCl, a possible concentration overpotential effect could hardly arise on account of a mass-transfer limitation involving the Cl^- ion itself. However, (ref.159) a supersaturation effect arising on account of dissolved, anodically generated Cl_2, could give rise to such behaviour but such supersaturation should be spun away at a rotated electrode.

The results in Fig.7.4 show, however, only a rather small effect of electrode rotation (up to 6400 rpm) on the curved shapes of the V vs log(i) relations, thus the curvature must be attributed to an activation-controlled kinetic effect rather than to either (or both) IR-drop and mass-transfer effects. This is an important experimental conclusion for the subsequent discussion of the results and reaction mechanism.

In all the plots of Figs.7.4 and 7.5, and those also of 7.6, there appears to be no clear linear sections of the Tafel plots for anodic Cl_2 evolution at these electrodes of the kind found for other types of RuO_2 surfaces investigated e.g. by Krishtalik and Erenburg[87,88] who found a linear Tafel region having a slope of ca. 42 mV. We believe it should be stressed that it is unlikely that any definite or absolute value for the Tafel slope for the anodic Cl_2 evolution reaction at RuO_2 can be stated because it must depend very much on the surface state of the thermochemically or the anodically formed RuO_2 deposit, and its microscopic structure and atomic surface composition. For example, the real/apparent area ratio for various RuO_2 materials prepared by Trasatti [102,5] was shown to be dependent on the baking temperature, The surface charge density associated with ionization or ion adsorption also depends on the preparation history of the RuO_2 materials. Indeed, anodically and thermochemically prepared RuO_2 films can behave in substantially different ways, so that the electrocatalytic behaviour of the RuO_2 surfaces for anodic Cl_2 evolution reaction should be related to the state and preparation history of the surface at which the kinetics are

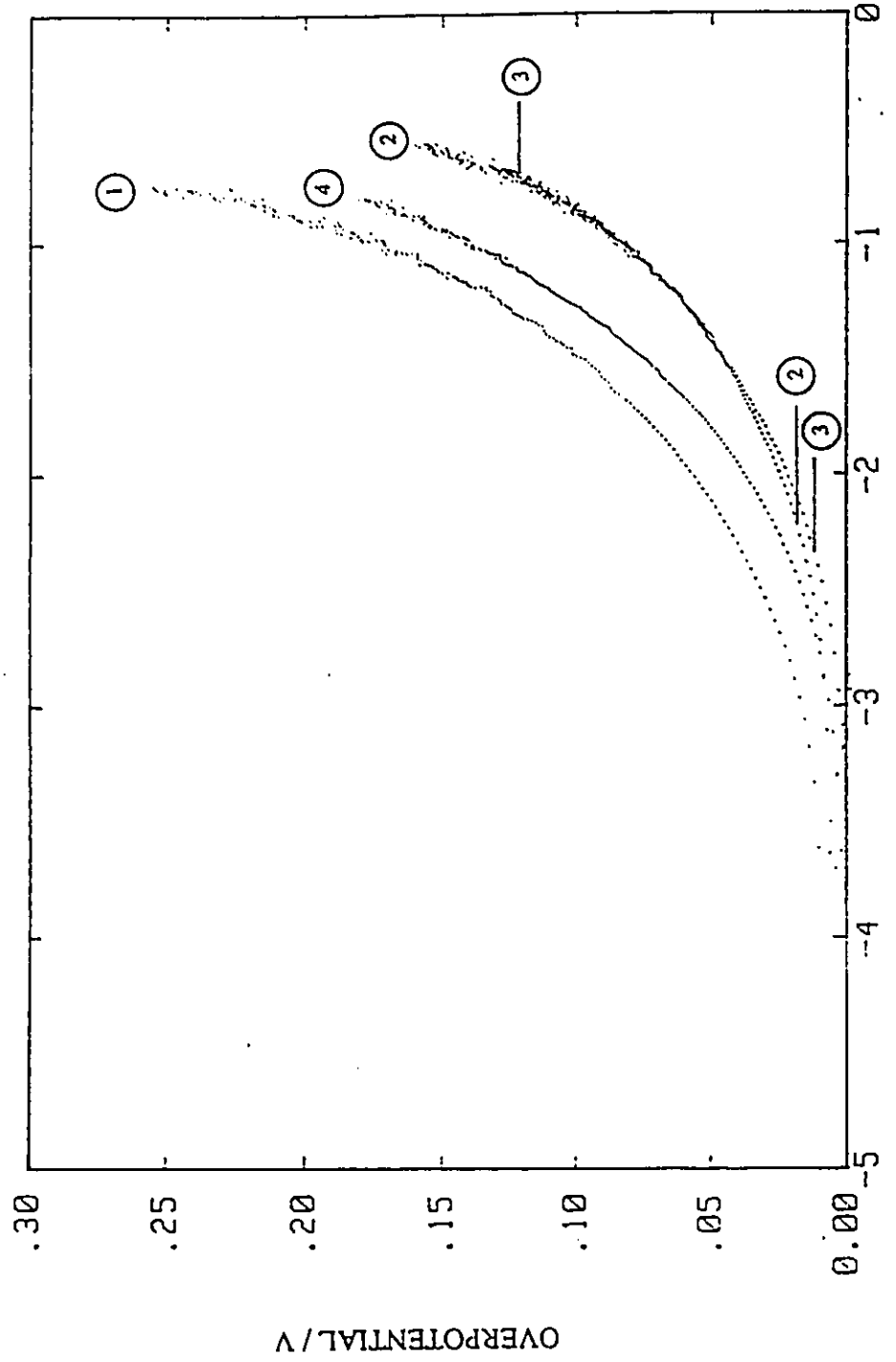

Fig.7.4 Tafel plots for the Cl_2 evolution reaction at the four RuO_2-TiO_2 electrodes (#1 to #4) in 0.1 M HCl + 0.9 M NaCl solution. Numbers 1, 2, 3 and 4 represent the behaviour of electrodes #1 to #4, respectively.

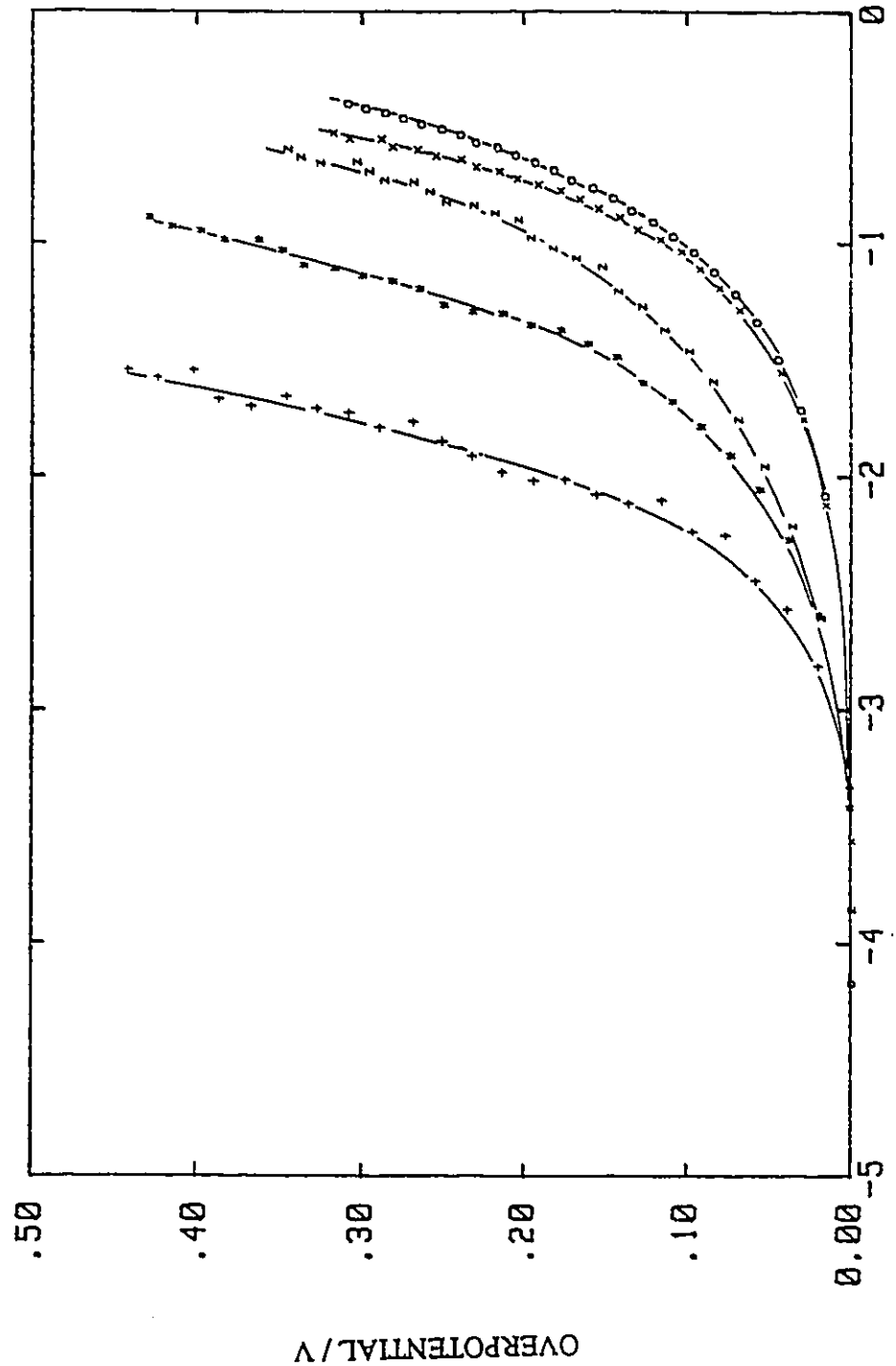

Fig.7.5 Tafel plots for the Cl_2 evolution reaction at electrode #4 at various concentrations of Cl^- (at constant ionic strength). The "+" represents the concentration of Cl^- $5x10^{-4}$ M; "*" represents 0.1 M of Cl^- "z" 0.5 M ; "x" 1.0 M and "o" 4.1 M.

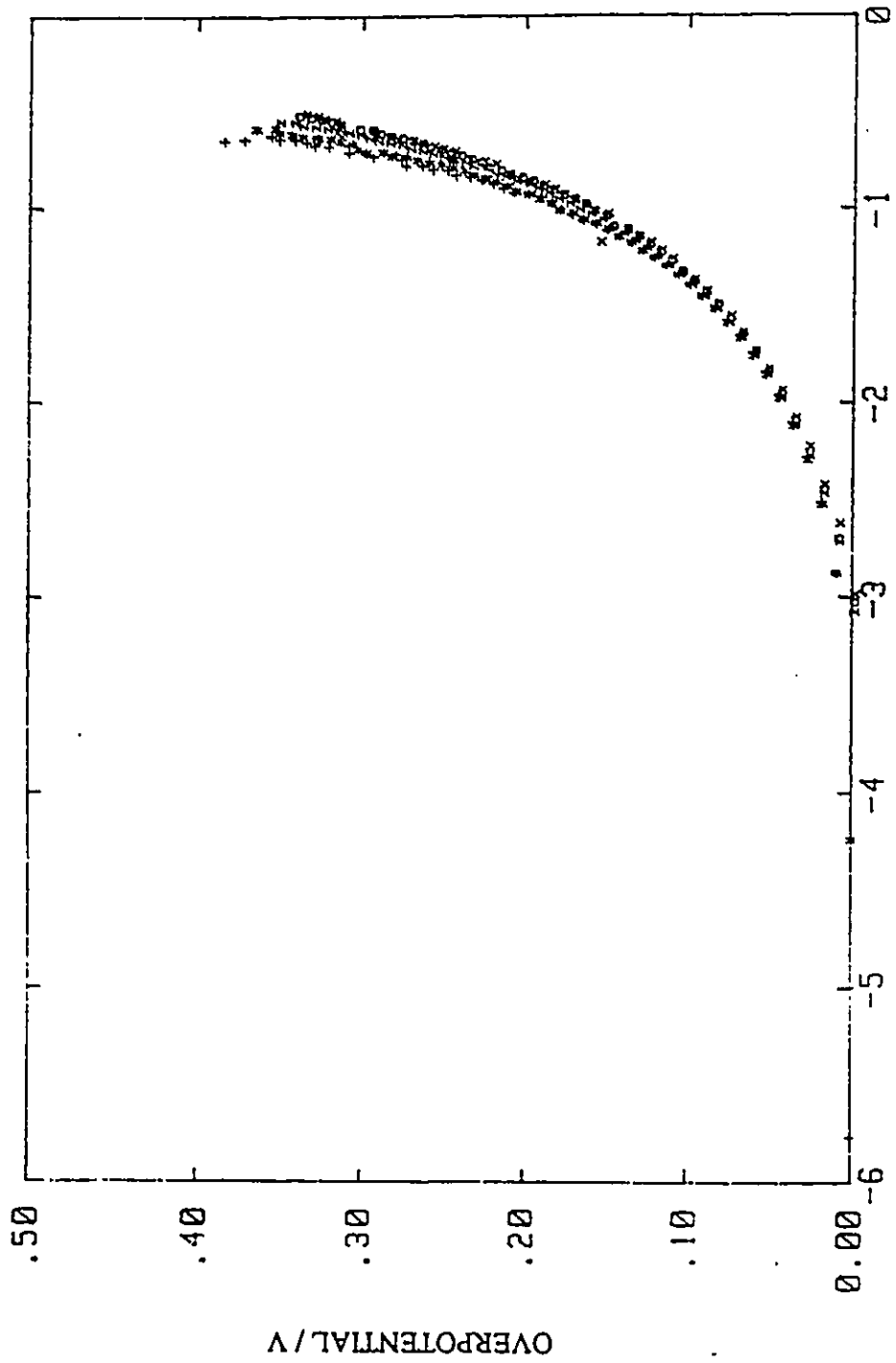

Fig.7.6 Tafel plots for the Cl_2 evolution reaction at a rotated RuO_2 electrode for various rotation rates in 0.1 M HCl + 0.9 M NaCl solution: "+" 400 rpm; "*" 900 rpm; "z" 2500 rpm; "o" 3600 rpm and "x" 6400 rpm.

characterized. Furthermore, the adsorption of the reactant Cl^- ion probably depends on the state of the RuO_2 anode surface but unfortunately this adsorption behaviour cannot be so conveniently and accurately determined as that at a Pt metal anode, evaluated in ref.80 by means of quantitative competitive surface oxidation experiments.

In general, the higher the concentration of Ru in the RuO_2-TiO_2 mixed films, the better the electrocatalytic behaviour but the structure of the oxide film surface sometimes also plays a significant role in the catalysis. It may give rise to the behaviour of electrode #4 which does not have as good kinetic behaviour as electrodes #2 and #3 (Fig.7.4). This may be due to the surface structure, as it can be seen in the SEM photo (Fig.7.1d), that there are some big black areas which are lower than the normal main surface area, which may be the result of some fault in the RuO_2-TiO_2 film structure.

7.3.2. Exp[VF/RT]/$i^{-1/2}$ vs Exp[VF/RT] Plots

Since there are evidently continuously curved relationships between V and log(i) (Figs.7.4 and 7.5), tests were made by means of Conway-Novak plots[85,86] to examine if the kinetic behaviour was associated with recombination control ($2Cl^- \longrightarrow Cl_2 \uparrow$, equation [III]) in the reaction mechanism. Such tests involve plotting exp[VF/RT]/$i^{-1/2}$ vs exp[VF/RT]; a resulting linear plot indicates recombination control and from the slopes and intercepts of such plots, the recombination rate constant, k_3, and the quasi-equilibrium constant, K_1, for $Cl^- \equiv Cl^\cdot + e$ (equation [I]) can be determined as was described in the section on kinetics at the Pt electrode in an aq. Cl^- solution. Such plots, shown in Fig7.7 for the four electrode (#1 to #4) surfaces at 298 K, evidently indicate the probability of recombination control under the present conditions, with electrode preparations 2 and 3 exhibiting similar k_3 values. This conclusion is not necessarily in conflict with that of Krishtalik and Erenburg[87,88] since their preparation of the RuO_2 film was different from that in our experiments, as mentioned earlier. Qualitatively, it is of interest that this implication of recombination control is also

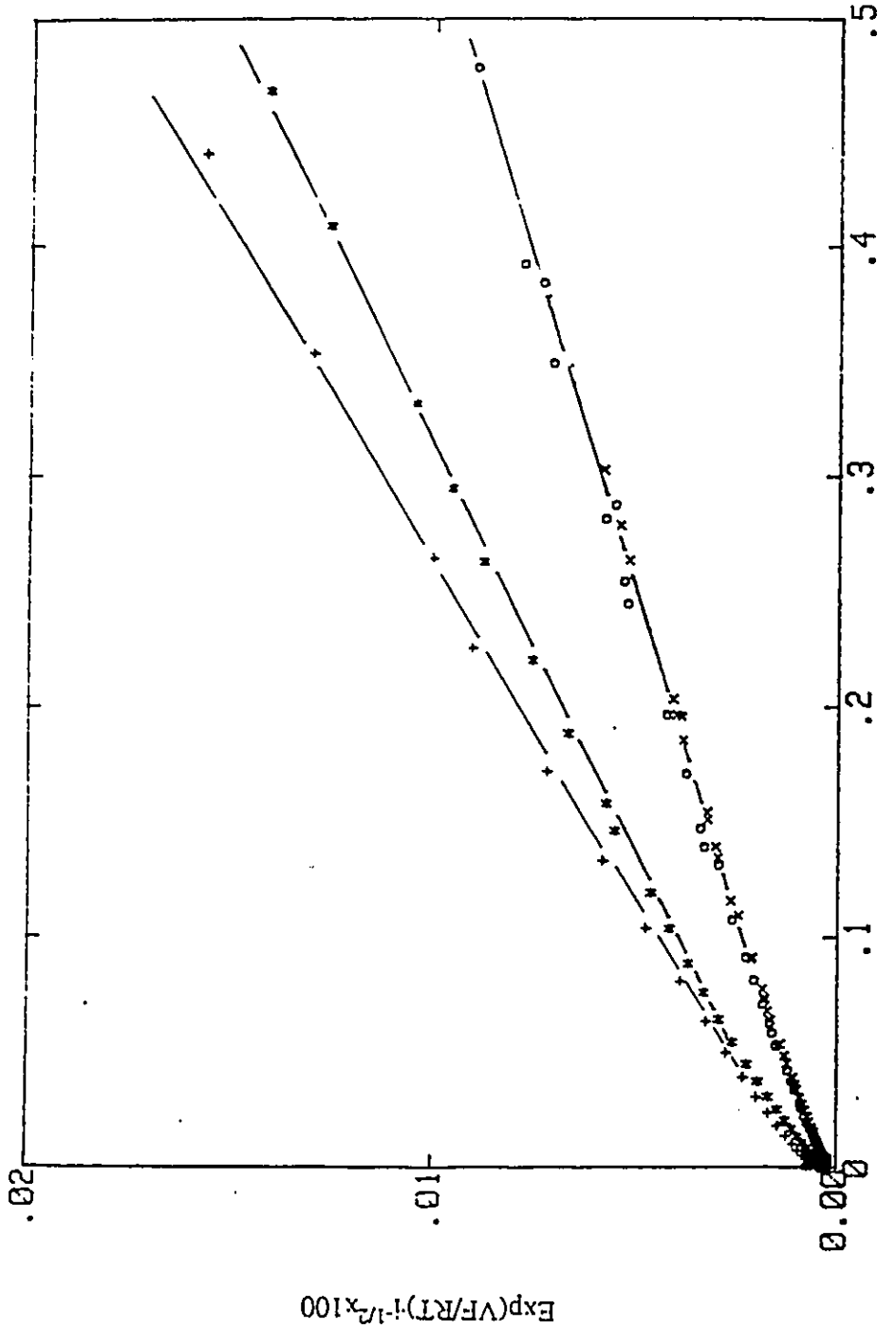

Fig.7.7 Conway-Novak test plots for the recombination-controlled mechanism of anodic Cl_2 evolution at electrodes #1 to #4. "+" #1; "o" #2; "x" #3 and "*" #4 from the same data as those of Fig.7.5.

found[85,86] for Pt electrodes and somewhat else reported by Fiata and Fiori[2].

Further information on electrocatalysis in anodic Cl_2 evolution at these RuO_2 surfaces is afforded by analysis of the results of the potential relaxation experiments (see section 7.4) and derived data, as well as a.c. impedance results (see section 7.5).

7.4. Potential relaxation behaviour

7.4.1. Log(t) and Log(-dV/dt) vs overpotential

Five sets of the digitally acquired, potential-relaxation data for the five electrodes (#1 to #5) in 0.1 M HCl + 0.9 M NaCl solution are shown in Figs.7.8a-e. These potential relaxation curves exhibit an interesting dependence on the initial polarization overpotentials which cover a wide range of 100-500 mV. The observation of non-straight lines implies that the decay behaviour does not obey eqn.[4.6] or in other words, eqn.[4.6] is too simple to express the complicated decay behaviour associated with the pseudocapacitance, C_ϕ arising in the generation of the Cl_{ad} intermediate.

In order to make it more convenient for discussion, the decay curves are divided into four regions as shown in Figs.7.8a-e.

Region I : for the electrodes #1 to #5, the first region starts from the beginning of the decay curve and ends at about $t = 10^{-4}$ sec. This part is believed to be related to the small dielectric capacitance due to the thermally formed oxide film itself. As reported in reference 119, the same phenomenon appears in potential relaxation curves for anodic O_2 evolution on a Co_3O_4 film thermally deposited on a Ti substrate electrode but not on a Ni substrate where a conducting NiO film is present. At Ti, the TiO_2 film is non-conducting. The oxide film may be represented by an $R_{ox}C_{ox}$ parallel circuit where R_{ox} is the resistance of the oxide film and C_{ox} its dielectric capacitance. When R_{ox} is small, the capacitance would discharge quickly, such as in the case of electrodes #2 and #3.

Region II : this starts from $t = 10^{-4}$ and ends at $t = 10^{-2} - 10^{-1}$ s. Normally, this

region is due to the discharge of the double-layer capacitance. The decay slopes in this part correspond quite closely to the respective Tafel slopes in the low overpotential region (see Table 7.3).

Region III: This can only be clearly distinguished in the cases of electrodes #2 and #3 which have the best electrocatalytic properties. It may be suggested that this region III of slow potential decay is an indirect result of the porosity of the oxide films in the sense that some Cl_2 is formed in the pores from desorptive recombination of previously adsorbed $Cl^{\cdot}$ atoms, giving rise to supersaturation and an enhanced local positive potential. This slow region III is then to be associated with relaxation of this supersaturation, with diffusion of Cl_2 out of microscopic pores in the oxide film. This may be the reason why a small but significant effect of electrode rotation arises in the potential relaxation transients (Figs.7.8e and f) and the Tafel plot (Fig.7.6).

Region IV: this corresponds to the final decay of overpotential to the reversible potential with a small decay slope, less than 13 mV per decade of time. After a long time decay, the surface coverage, θ, of adsorbed intermediates approaches the equilibrium value and this region is usually dominated by the $Cl^{\cdot}$ desorption process.

Rotation of the electrode (#5) to 3600 rpm produces a small but significant effect on the course (but not the shape) of the V(t) vs log(t) plots (Fig.7.8f). Correspondingly, there is a small rotation effect in plots of V(t) vs log[-dV/dt] as seen in Fig.7.9f. In Figs.7.9a-e are shown the V(t) vs log[-dV/dt] plots resulting from the application of eqn.[4.14] to the results. Mainly, two straight regions are observed (i.e. II and IV), which qualitatively correspond to the interfacial capacitances involved.

Table 7.3 lists all slopes d(log(t))/dV and d[log(-dV/dt)/dV] for the five electrodes:

Figs.7.8a-f The potential relaxation data plotted as V vs log(t) relations for the Cl_2 evolution reaction at RuO_2 films in 0.1 M HCl + 0.9 M NaCl solution at 298K. (a) #1; (b) #2; (c) #3; (d) #4; (e) #5 at zero rotation rate and (f) #5 with rotation at 3600 rpm. The numbers indicate the various initial polarization potentials: for electrodes #1 to #4, (1) 500 mV; (2) 450 mV; (3) 400 mV; (4) 350 mV; (5) 300 mV, and for electrode #5, (1) 550 mV; (2) 500 mV; (3) 450 mV; (4) 400 mV; (5) 350 mV (6) 300 mV.

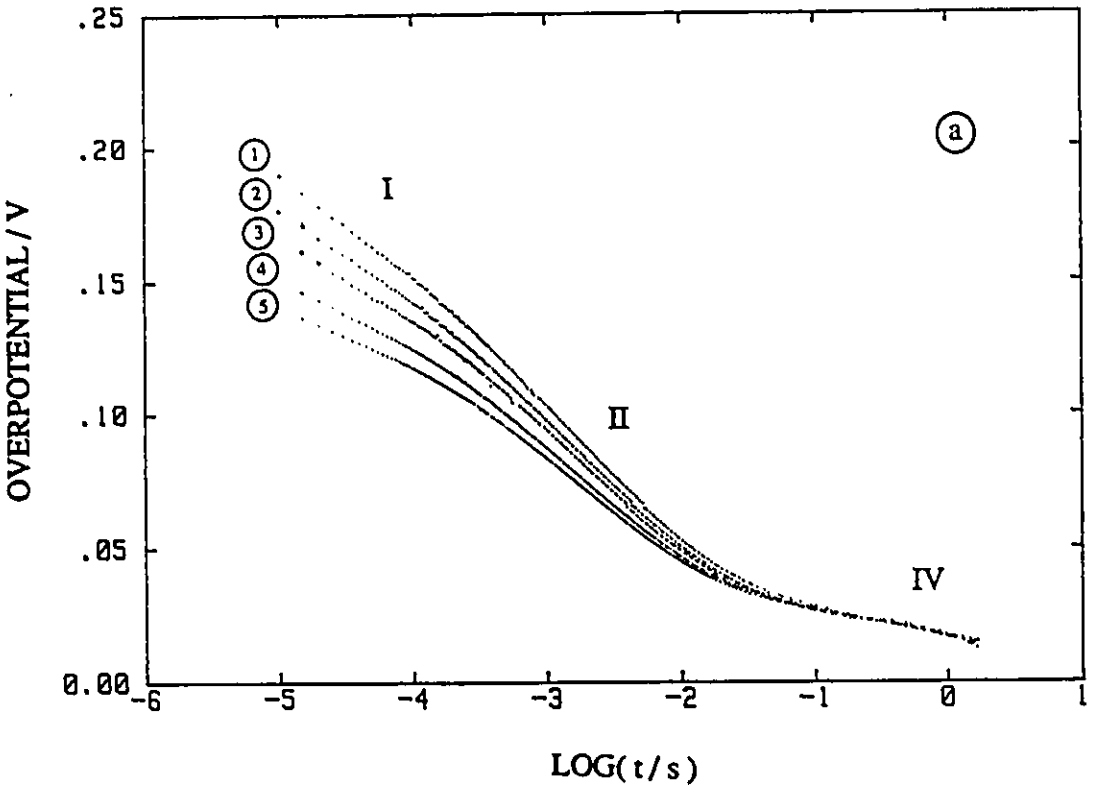
.25
.20
.15
.10
.05
0.00
OVERPOTENTIAL / V
a
1
2
3
4
5
I
II
IV
-6
-5
-4
-3
-2
-1
0
LOG(t / s)

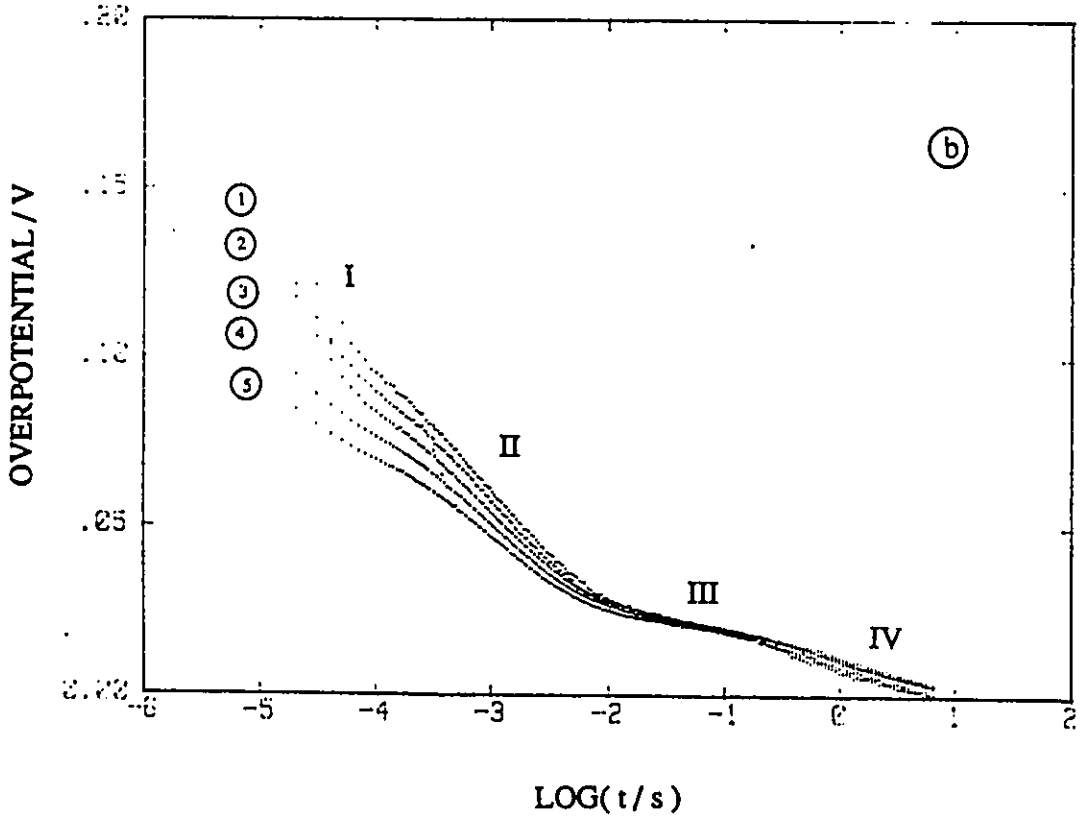
OVERPOTENTIAL / V
b
1
2
3
4
5
I
II
III
IV
-6
-5
-4
-3
-2
-1
0
1
2
LOG(t / s)

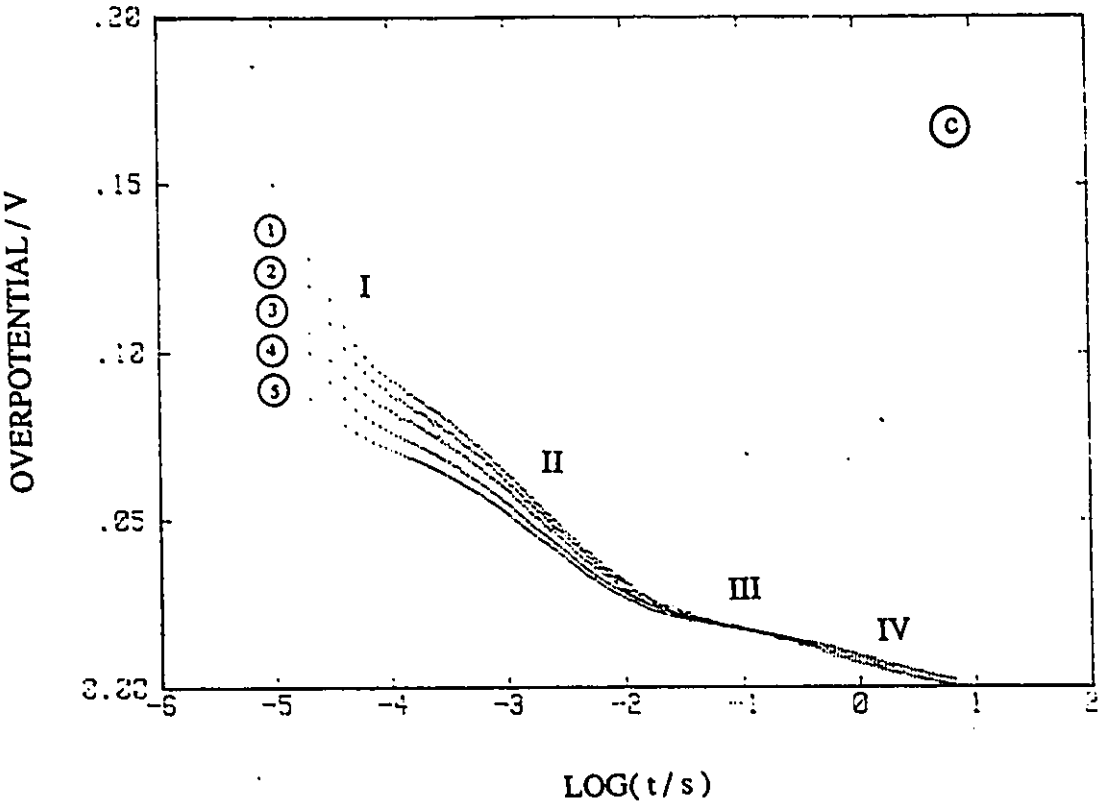
OVERPOTENTIAL / V
.20
.15
.10
.05
0.00
-6
-5
-4
-3
-2
-1
0
1
c
1
2
3
4
5
I
II
III
IV
LOG(t / s)

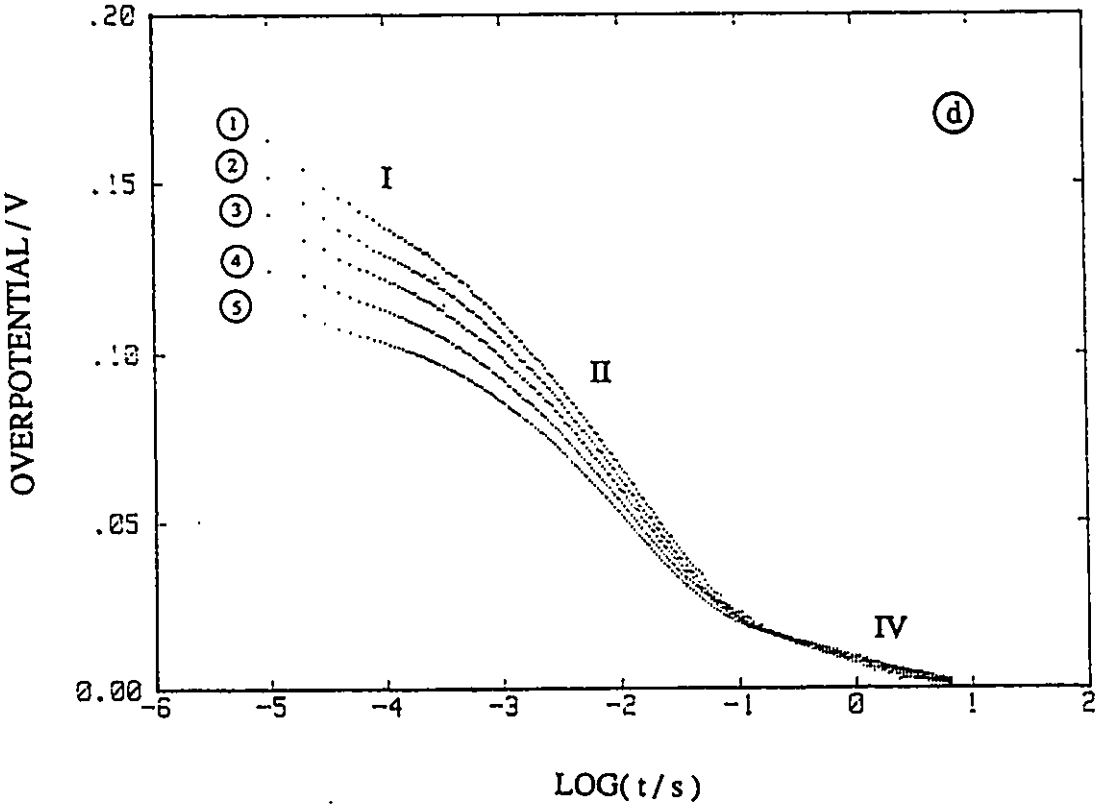
OVERPOTENTIAL / V
.20
.15
.10
.05
0.00
-6
-5
-4
-3
-2
-1
0
1
2
d
1
2
3
4
5
I
II
IV
LOG(t / s)

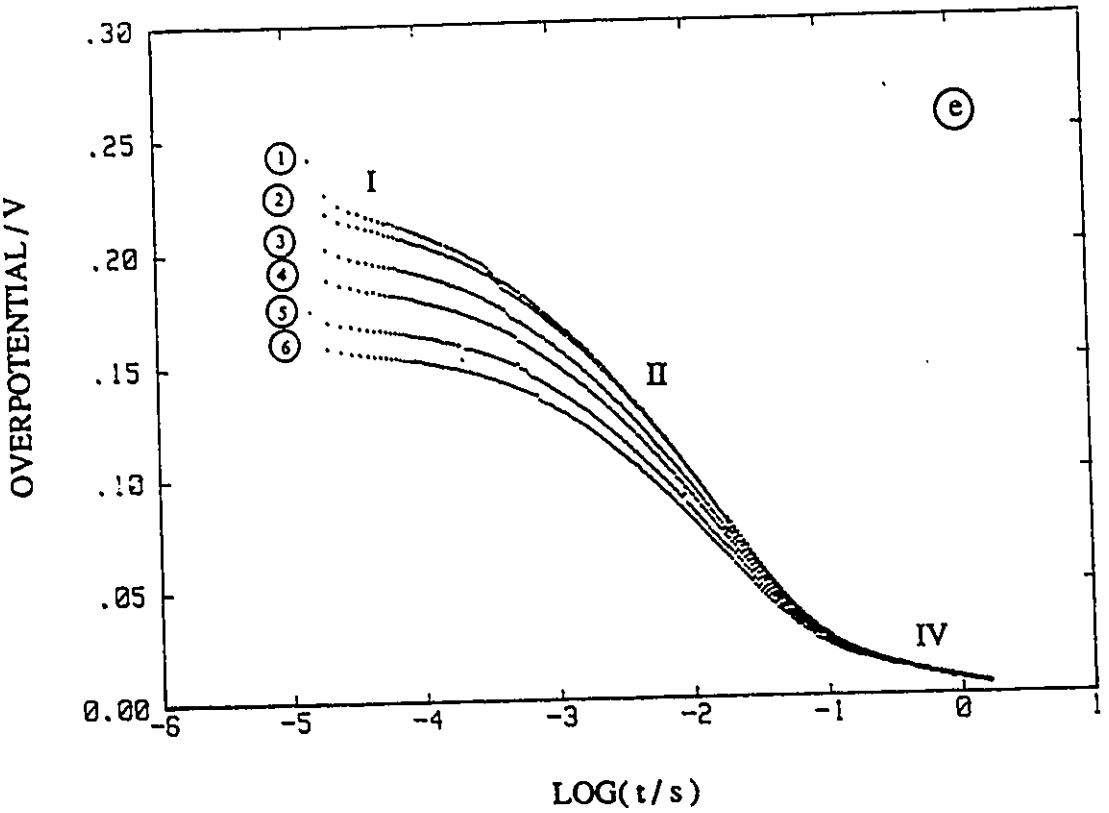
OVERPOTENTIAL / V
.30
.25
.20
.15
.10
.05
0.00
-6
-5
-4
-3
-2
-1
0
1
LOG(t/s)
e
I
II
IV
1
2
3
4
5
6

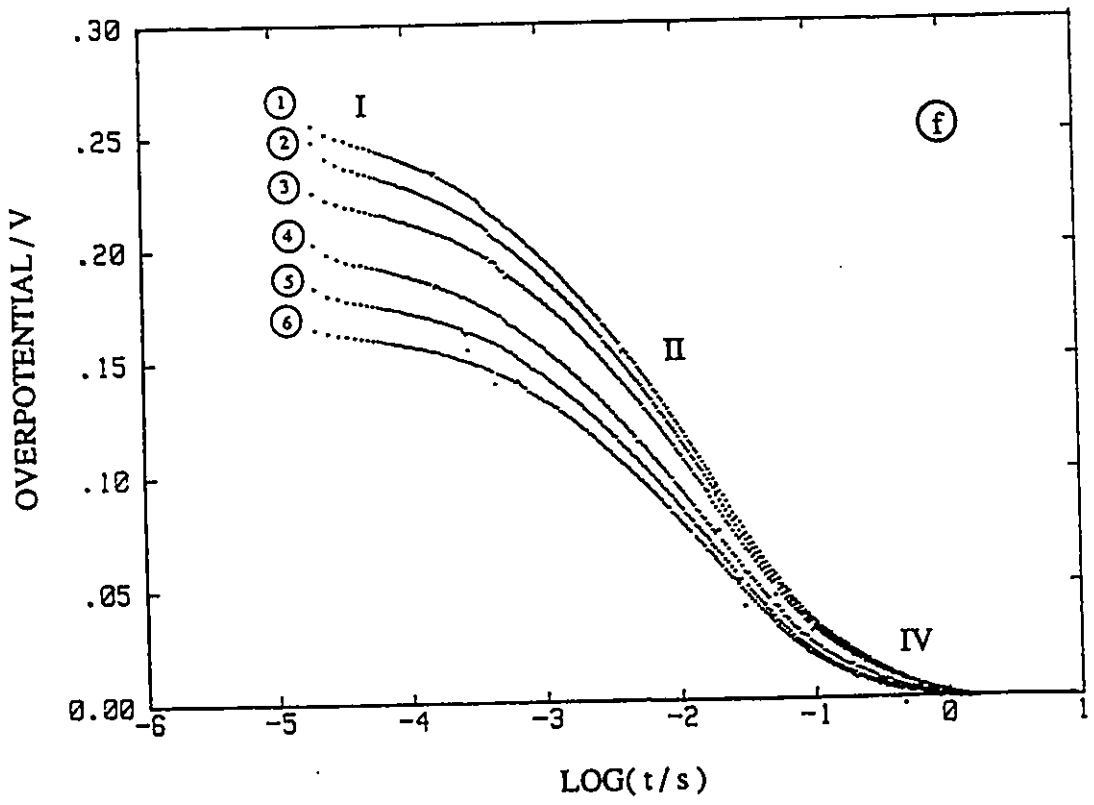
OVERPOTENTIAL / V
.30
.25
.20
.15
.10
.05
0.00
-6
-5
-4
-3
-2
-1
0
1
LOG(t/s)
f
I
II
IV
1
2
3
4
5
6

Figs.7.9a-f The V vs log(-dV/dt) relations derived from the same data as in Figs.7.8a-f.(a) #1; (b) #2; (c) #3; (d) #4; (e) #5 with zero rotation rate and (f) #5 with rotation at 3600 rpm. The numbers indicate the various initial polarization potentials as indicated in Figs.7.8.

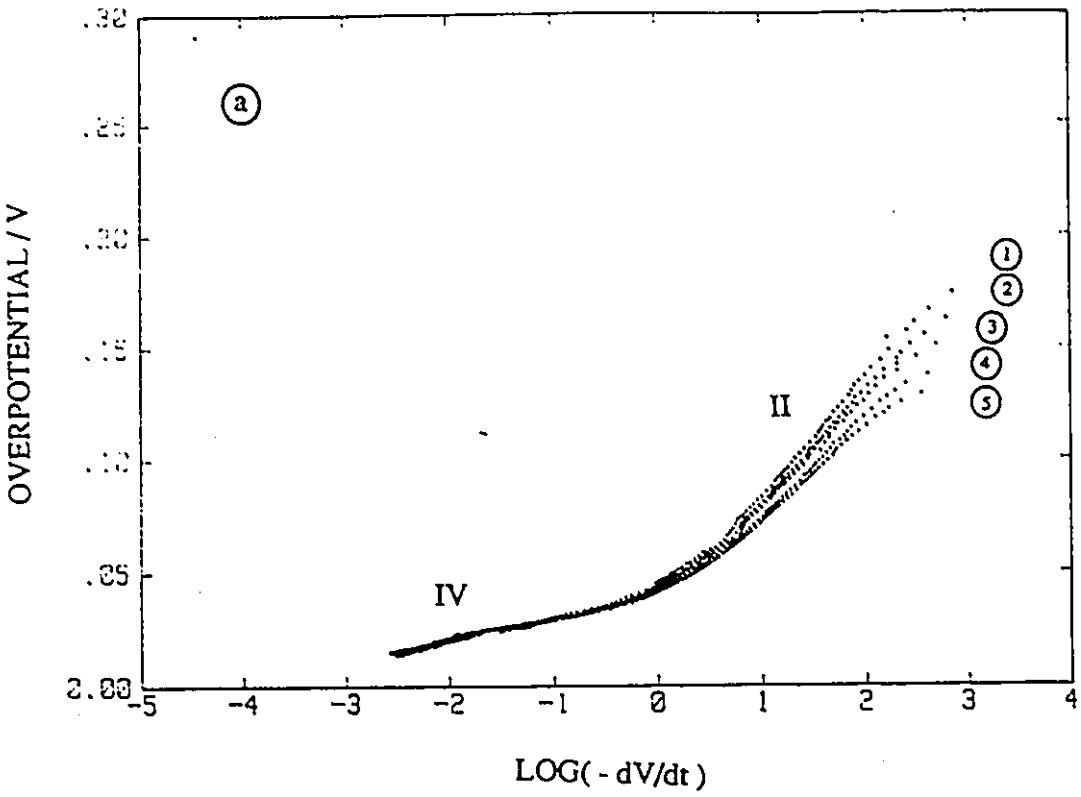
a
II
IV
1
2
3
4
5
OVERPOTENTIAL / V
LOG(- dV/dt)

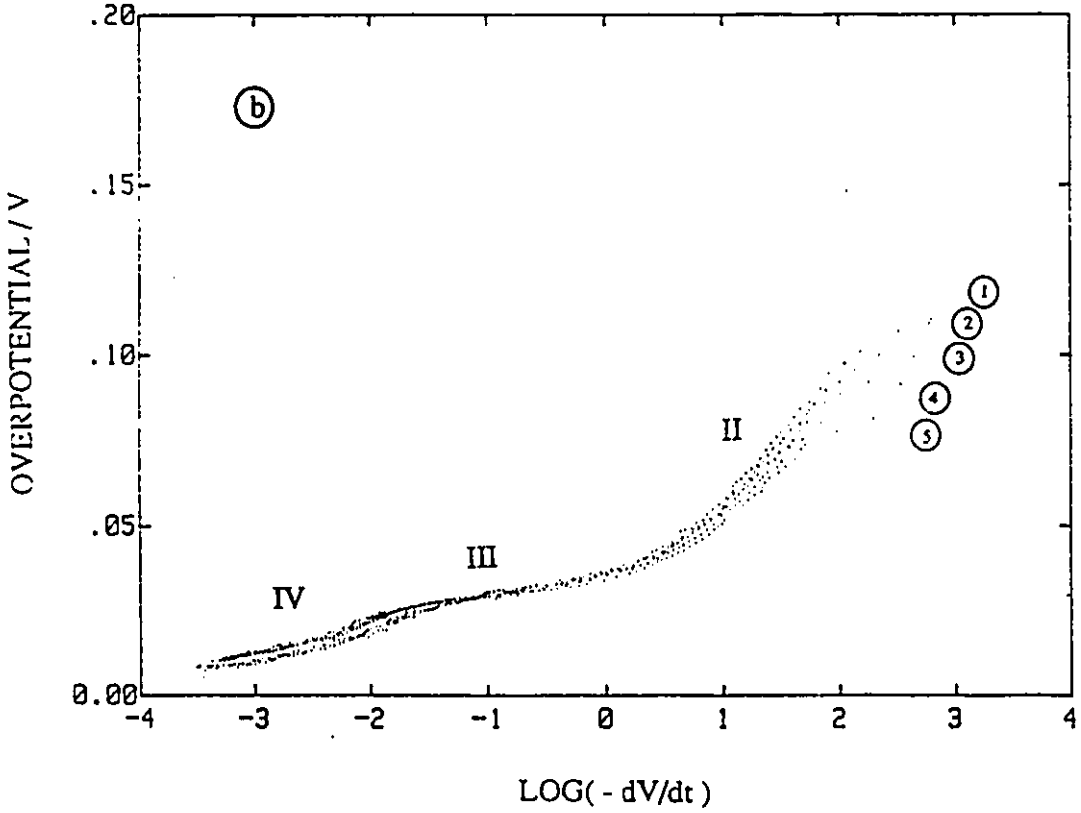
b
II
III
IV
1
2
3
4
5
.20
.15
.10
.05
0.00
-4
-3
-2
-1
0
1
2
3
4
OVERPOTENTIAL / V
LOG(- dV/dt)

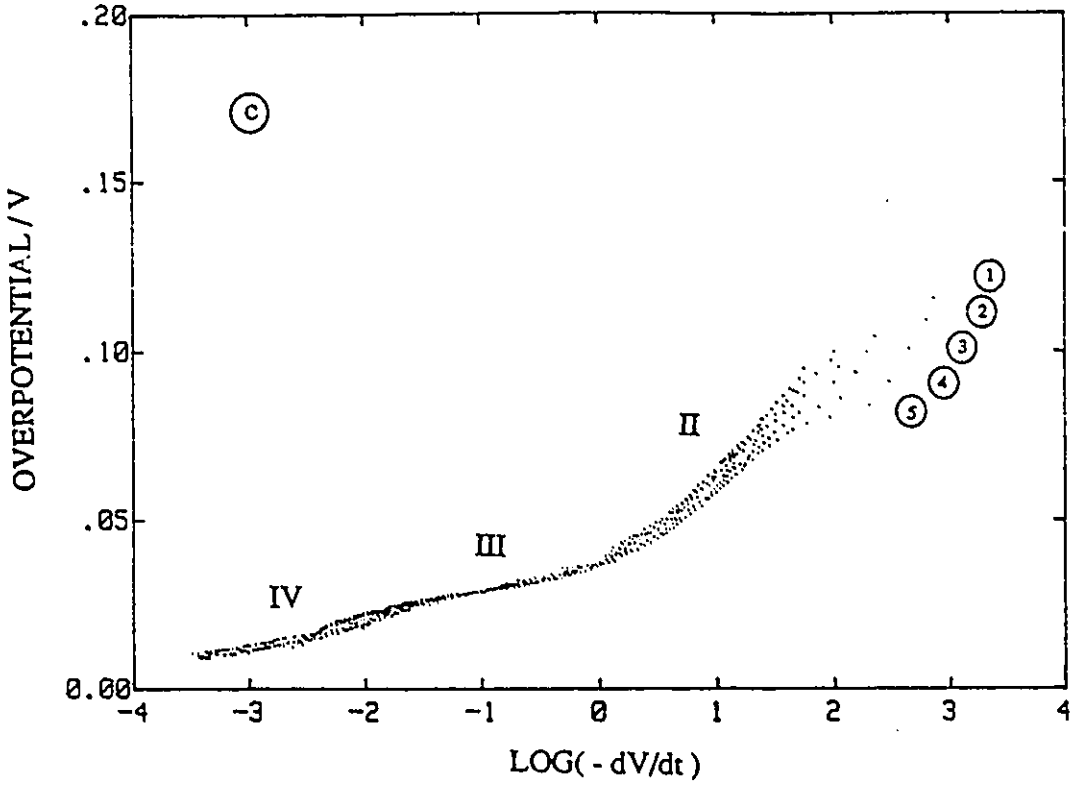
.20
.15
.10
.05
0.00
OVERPOTENTIAL / V
c
II
III
IV
1
2
3
4
5
-4
-3
-2
-1
0
1
2
3
4
LOG(- dV/dt)

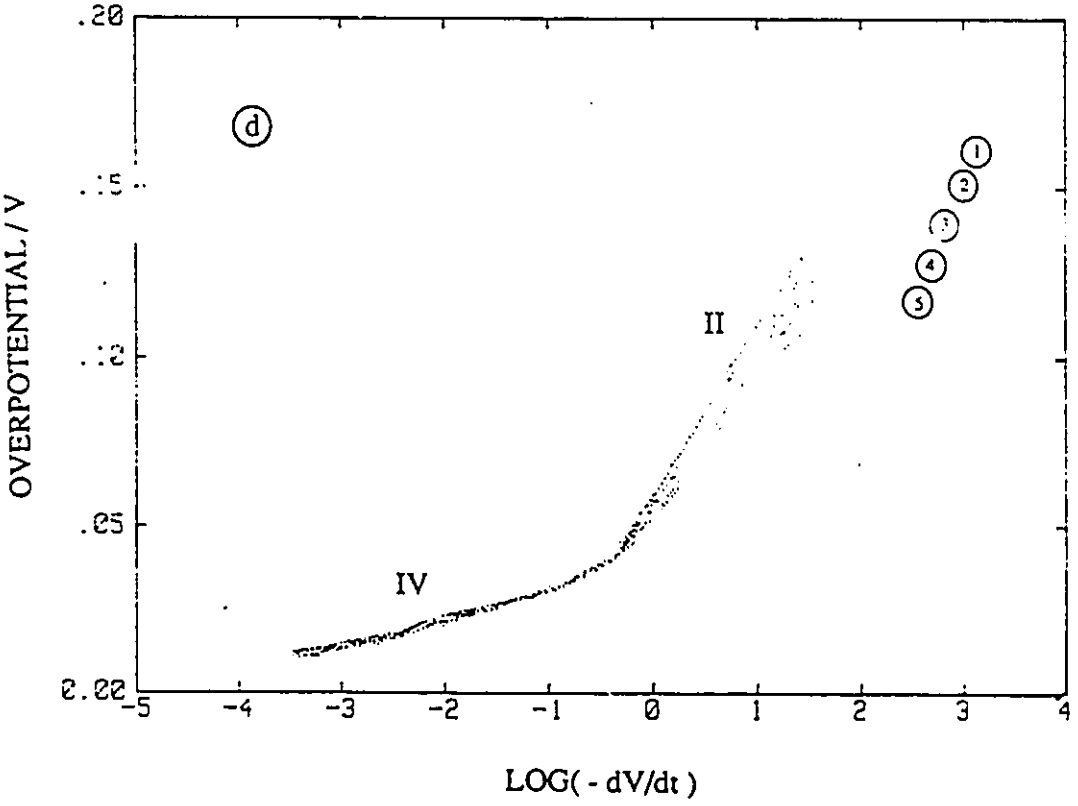
.20
.05
OVERPOTENTIAL / V
d
II
IV
1
2
3
4
5
-5
-4
-3
-2
-1
0
1
2
3
4
LOG(- dV/dt)

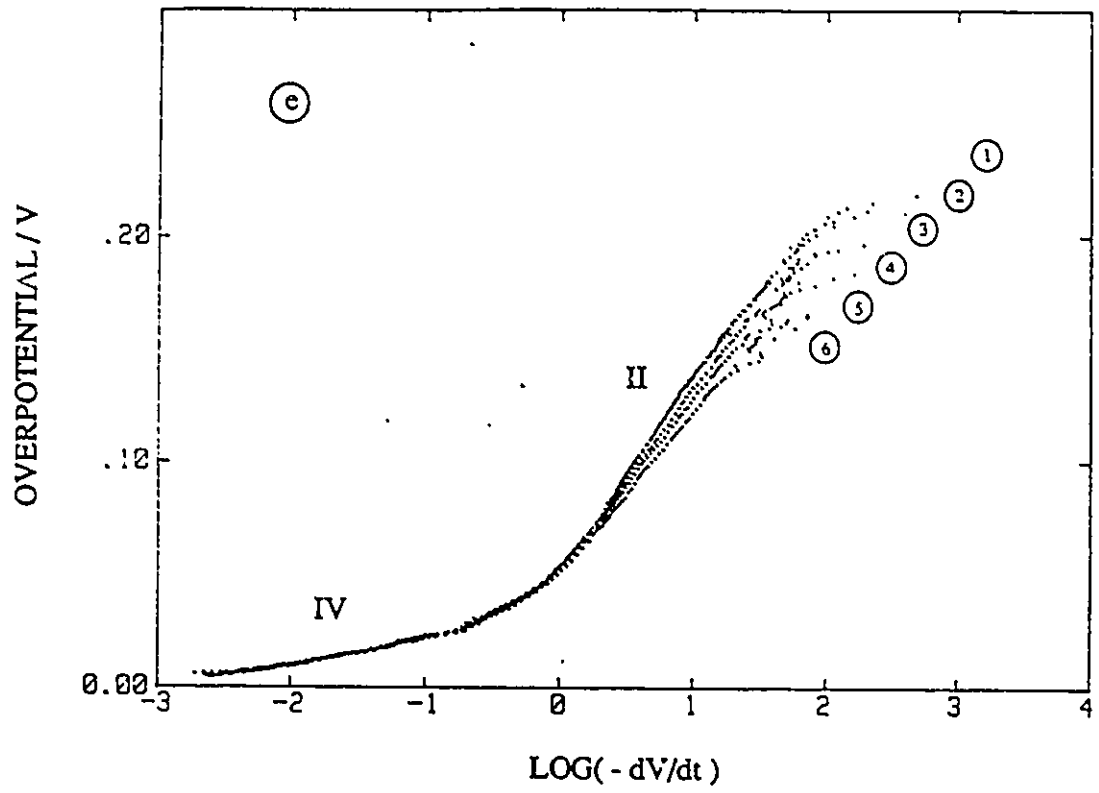
e
OVERPOTENTIAL / V
.20
.10
0.00
-3
-2
-1
0
1
2
3
4
II
IV
1
2
3
4
5
6
LOG(- dV/dt)

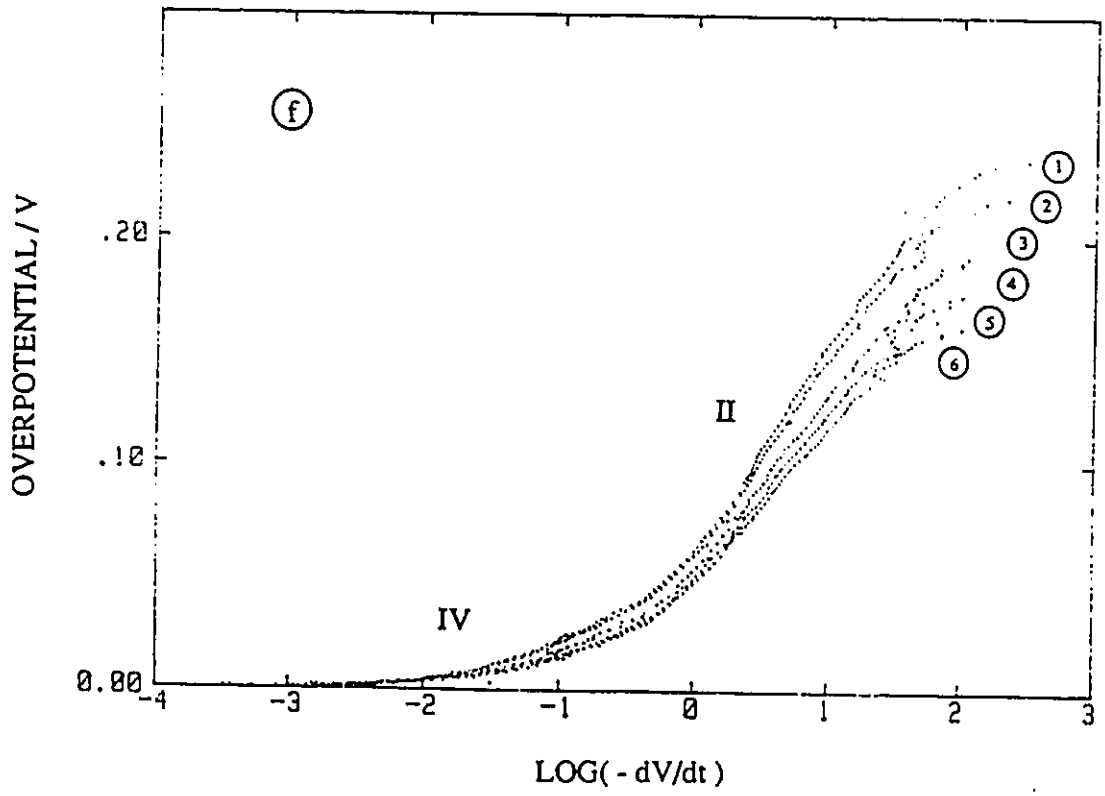
f
OVERPOTENTIAL / V
.20
.10
0.00
-4
-3
-2
-1
0
1
2
3
II
IV
1
2
3
4
5
6
LOG(- dV/dt)

Table 7.3 List of slopes of d(log(t))/dV and d[log(-dV/dt)/dV] for the five electrodes.

Slopes / Electrode	- dV/dlog(t) / mV			dV/d(log(-dV/dt)) /mV		
	II	III	IV	II	III	IV
# 1	52-41	----	10	51-44	----	9.8
# 2	38-27	7.2	12	41-29	6.0	9.6
# 3	34-26	6.4	9.6	35-29	7.2	8.0
# 4	47-38	----	9.6	48-43	----	8.0
# 5	83-63	----	16	85-71	----	12

7.4.2. Pseudocapacitance Information

The pseudocapacitance behaviour of the adsorbed Cl· species, evaluated from C = i(V)/(-dV/dt) (eqn.4.1) using the differentiated decay transients and current-potential relationships for Cl_2 evolution at the RuO_2-TiO_2 electrodes, are shown in Figs.7.10a-f. Unlike the single peaked C(V) curve for H species observed for the case of the H_2 evolution reaction at Ni (refs.136,143), or the curves for "reduced" Pt surface with Cl·, the C(V) profiles in Figs.7.10a-f have a hyperbolic shape over the potential range studied.

These plots all show a rapid rise of C with decreasing V, below V ≈ 50 mV, corresponding to the flattening out and/or arrest in the V(t) vs log(t) plots of Figs.7.8a-f. Results of similar experiments on the behaviour of the adsorbed intermediates in

the H_2 and O_2 evolution reactions at Pt show quite different behaviour within 50 ~ 100 mV of the reversible potential, where the expected[124] maximum in C is observed, which is comparable to the overpotential-deposited H in the H_2 evolution reaction (HER) at active Pt. It is possible that a maximum in C for Cl^- adsorption does exist at lower V values, towards the reversible potential, but is not observable over the range of potentials covered in the present experiments.

It may be thought that the rapid ascent of values of C which arise when V < 50 mV is an artefact due to the appearance of the back-reaction current. However : (a) it is the net anodic - minus-cathodic current that determines the potential relaxation behaviour according to eqn.[4.1], i.e. C(V) is determined by dV/dt and the net observed current, which includes any back-reaction component; and (b) a similar situation for the back-reaction current arises in the case of the HER at active Pt, for which a maximum in C is actually observed[123-125]. Therefore, it is to be concluded that the observed rapid rise of C with decreasing potential, V, for the five electrodes is a true characteristic feature of the Cl_2 evolution reaction at the RuO_2 surfaces. For surfaces #3 and #4 (see Figs.7.10c,d), the rise in C sets in at somewhat higher V values, 0.07 ~ 0.1 V, than for surfaces #1 and #2.

Around V = 0.04 V, the apparent values of C rise to ca. 40 mF (per apparent $cm^2)^{-1}$. While it was not possible to obtain an estimate of the real area per apparent cm^2, previous estimates of the real/apparent area ratio, R, for commercial-type, thermochemically formed RuO_2 films give a figure R = 300 ~ 400; then the above value of C would be ca. 115 $\mu F\ cm^{-2}$. Since the present electrodes (#1 to #4) are SEM-visibly smoother (Figs.7.1a-d) than commercial DSA-type surfaces, a smaller R value may reasonably apply, giving a C possibly of the order 500 ~ 1000 $\mu F\ cm^{-2}$ in the rising limit, i.e. in the range of pseudo-capacitance associated with appreciable coverage by Cl^-

Comparative experiments were also conducted at a lower temperature, 278 K. The results are qualitatively similar to those at 298 K but the following differences in

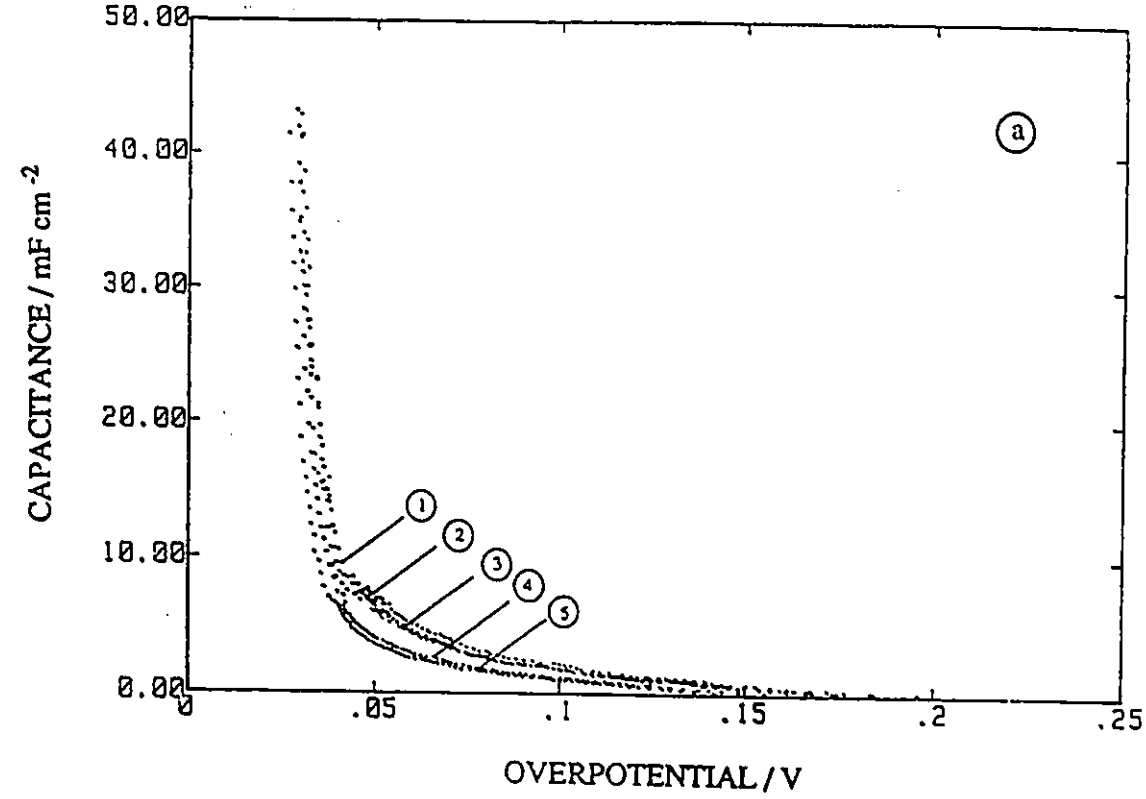
50.00
40.00
30.00
20.00
10.00
0.00
0
.05
.1
.15
.2
.25
CAPACITANCE / mF cm -2
OVERPOTENTIAL / V
a
1
2
3
4
5

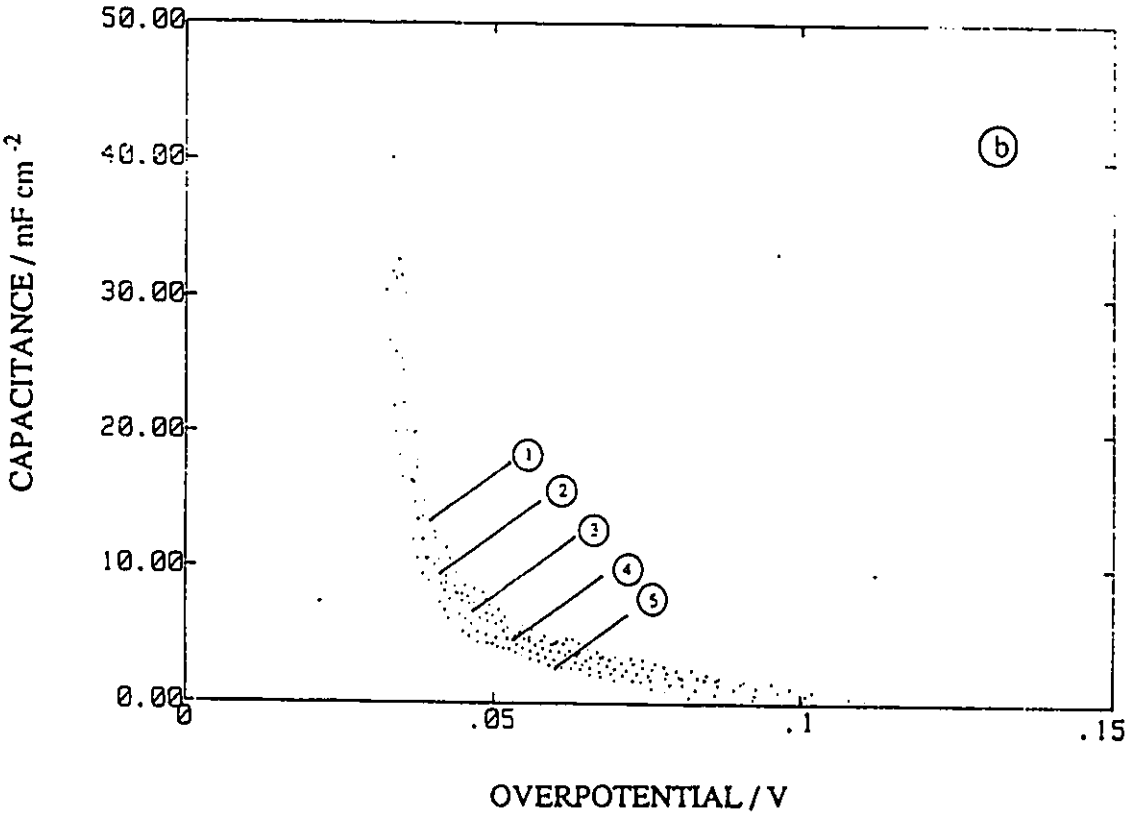
50.00
40.00
30.00
20.00
10.00
0.00
0
.05
.1
.15
CAPACITANCE / mF cm -2
OVERPOTENTIAL / V
b
1
2
3
4
5

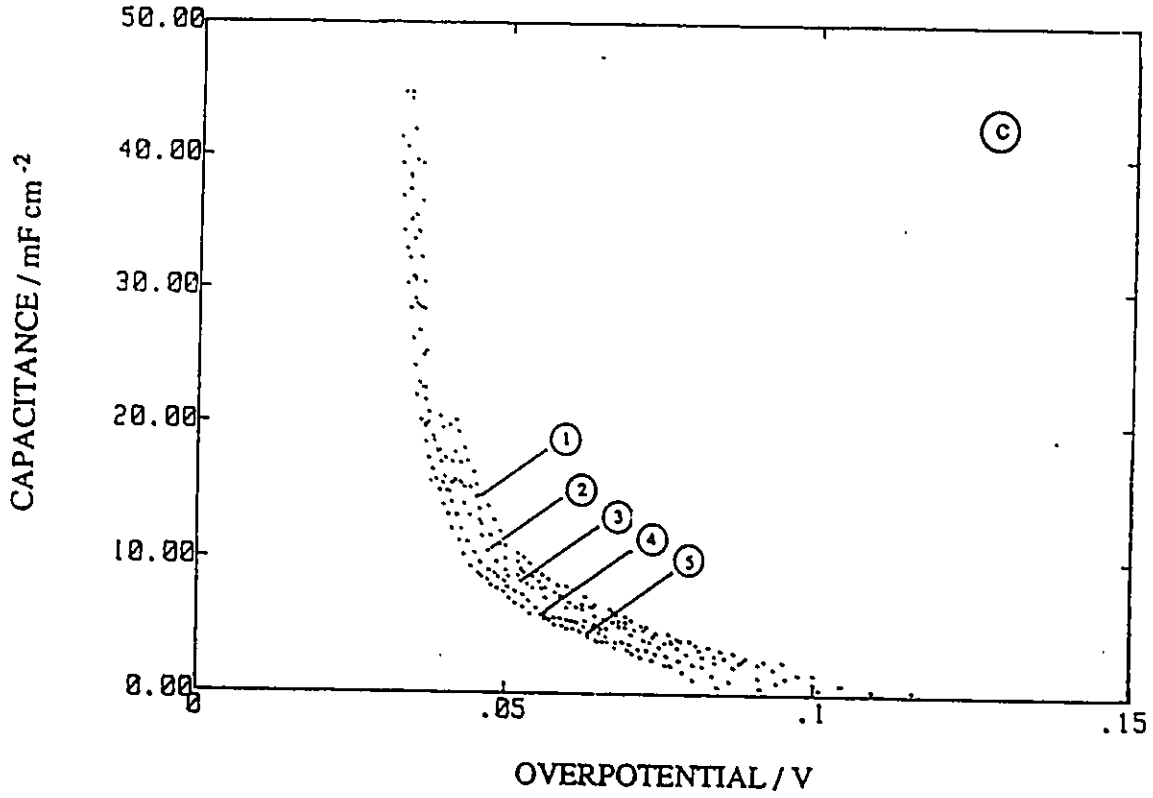
50.00
40.00
30.00
20.00
10.00
0.00
0
.05
.1
.15
CAPACITANCE / mF cm -2
OVERPOTENTIAL / V
c
1
2
3
4
5

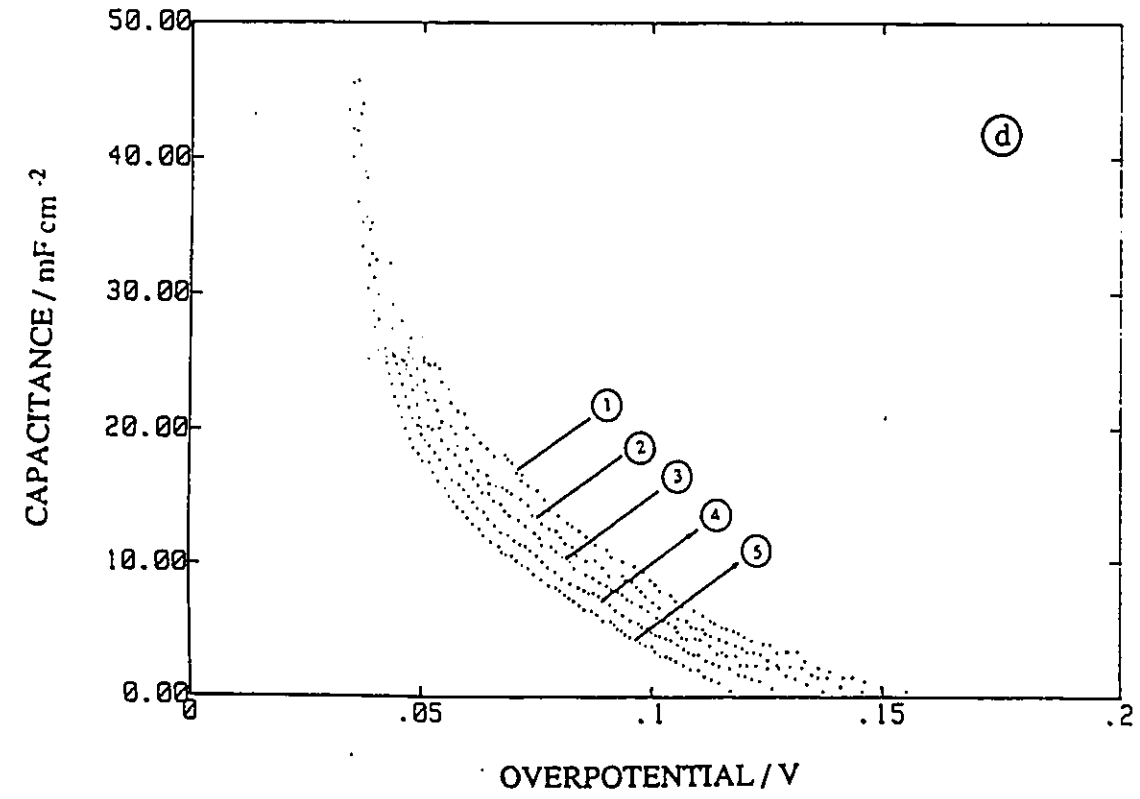
50.00
40.00
30.00
20.00
10.00
0.00
0
.05
.1
.15
.2
CAPACITANCE / mF cm -2
OVERPOTENTIAL / V
d
1
2
3
4
5

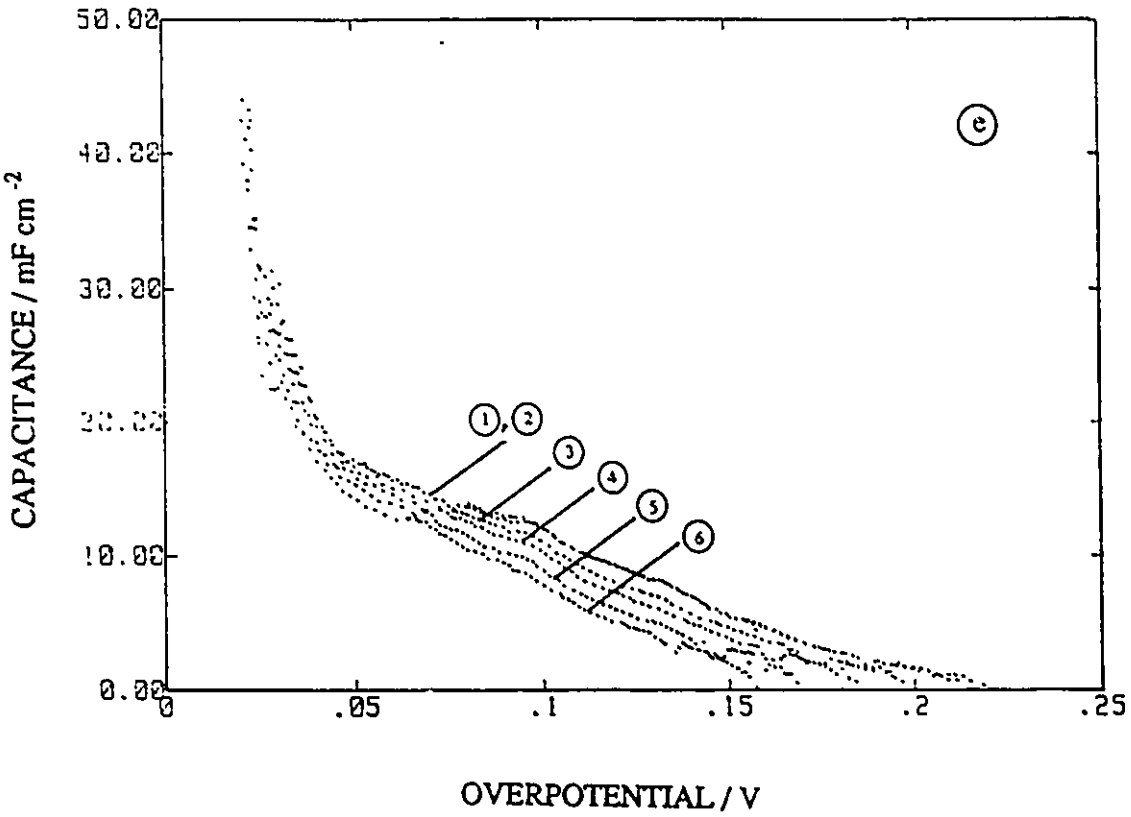

Figs.7.10a-e The C(V) vs V plots derived from the data in Figs.7.9a-e for electrodes #1 to #5. (a) #1; (b) #2; (c) #3; (d) #4; (e) #5. The numbers represent the various initial polarization potentials as indicated in Figs.7.9.

detail are significant : (i) the current densities at a given V are smaller, as expected (the activation energy effect); (ii) the potential relaxation transients, taken from different initial potentials (exemplified in Figs.7.11a,b) do not tend to become superimposable at longer times (say log(t) > -3) in the theoretically expected way, as actually observed for the HER at Ni[124]. This contrast is confirmed by the clearly non-coincident series of plots of V(t) vs log[-dV/dt] for 278 K shown in Figs.7.12a,b corresponding to the respective data in the plots of Figs.7.11 a,b. The corresponding derived C vs V plots (Figs.7.13a,b) for 278 K also depend much more on the initial potentials at which potential relaxation was initiated, than those for 298 K.

This type of behaviour suggests that the state of the RuO_2 surface determining the kinetics of the Cl_2 evolution reaction, and particularly the adsorption of Cl^-, depends appreciably on the anodic potential from which the relaxation transient is initiated. Such an effect could arise from a potential-dependent change of state of surface oxidation of the RuO_2; for example, states of surface oxidation up to Ru(VI) are possible[102], as indicated by ESCA experiments. We have mentioned that, for the HER, no such effect arises at Ni or Pt; however, at Pd, a somewhat similar effect is found and this must arise, we believe, because the state of the surface of Pd (for H chemisorption and electrocatalysis in the HER) can depend on the history of the electrode, in potential and time, depending on the extent of 3-dimensional sorption of H in the Pd[160,161].

Comparing the various C(V) plots, they have some common features: (i) different initial decay potentials gives significantly different C(V) profiles. This may be because the adsorption situation of Cl^- is not exactly the same for various polarization potentials; e.g. the surface concentration of Cl^- adsorbed ions and the extent of surface oxidation of the oxide film (for example, the extent of RuOOH formation, etc.). This phenomenon can also be seen in the V vs log(t) plots where curves from various initial potentials never become coincident, especially at the lower temperature 278K; (ii) for potentials higher than 50 mV, the capacitances have relatively small values that

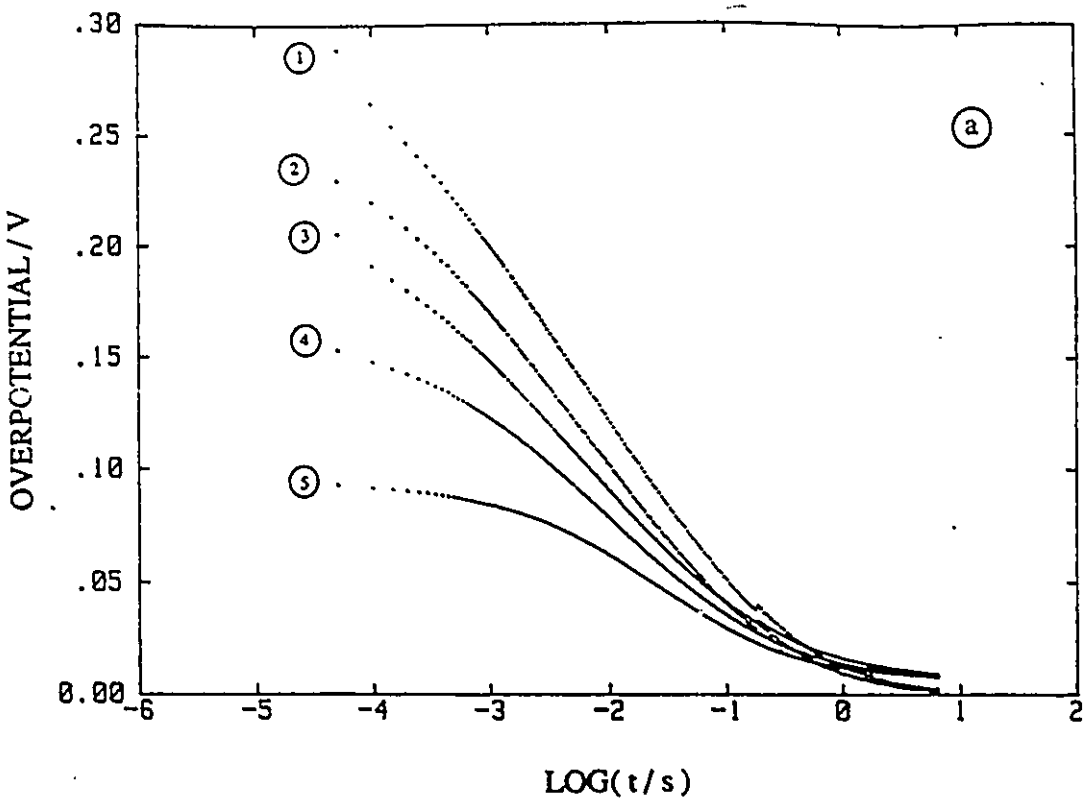

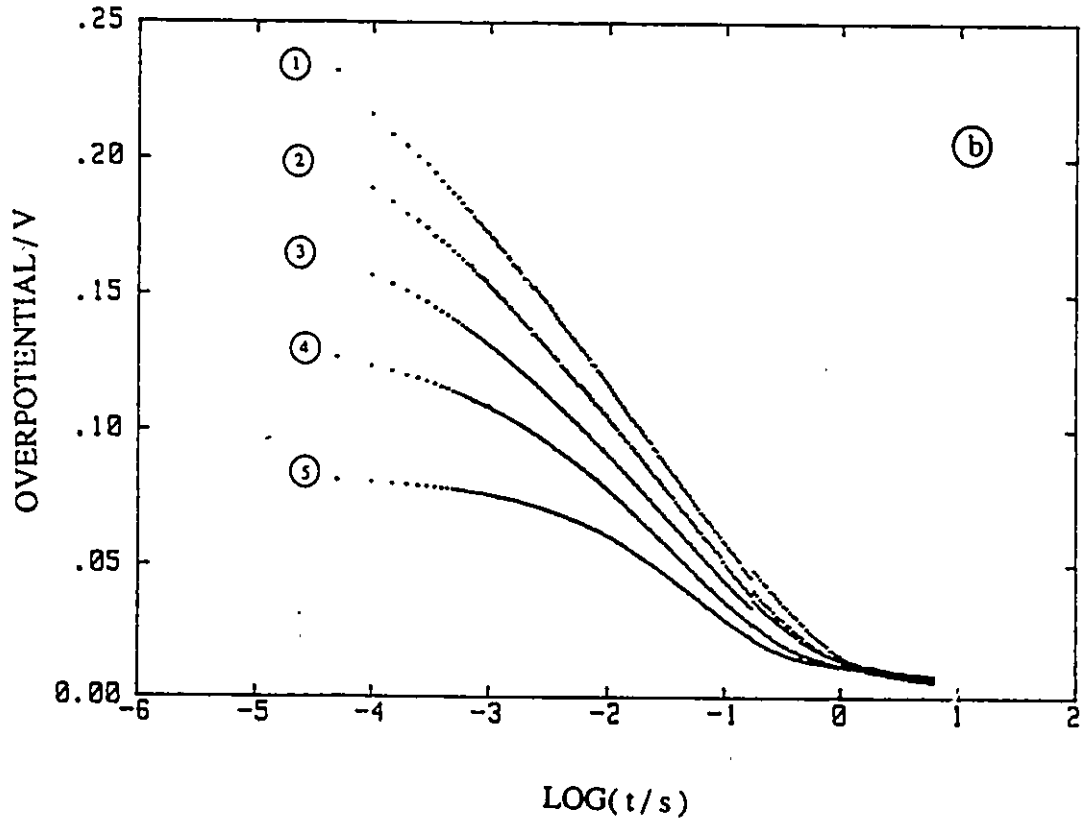

Figs.7.11a,b Two examples of potential decay V vs log(t) plots for the Cl_2 evolution reaction at 278K in 0.1 M HCl + 0.9 M NaCl solution: (a) for #1 and (b) for #4. The numbers indicate the various initial polarization potentials; (1) 500 mV; (2) 450 mV; (3) 400 mV; (4) 350 mV; (5) 300 mV.

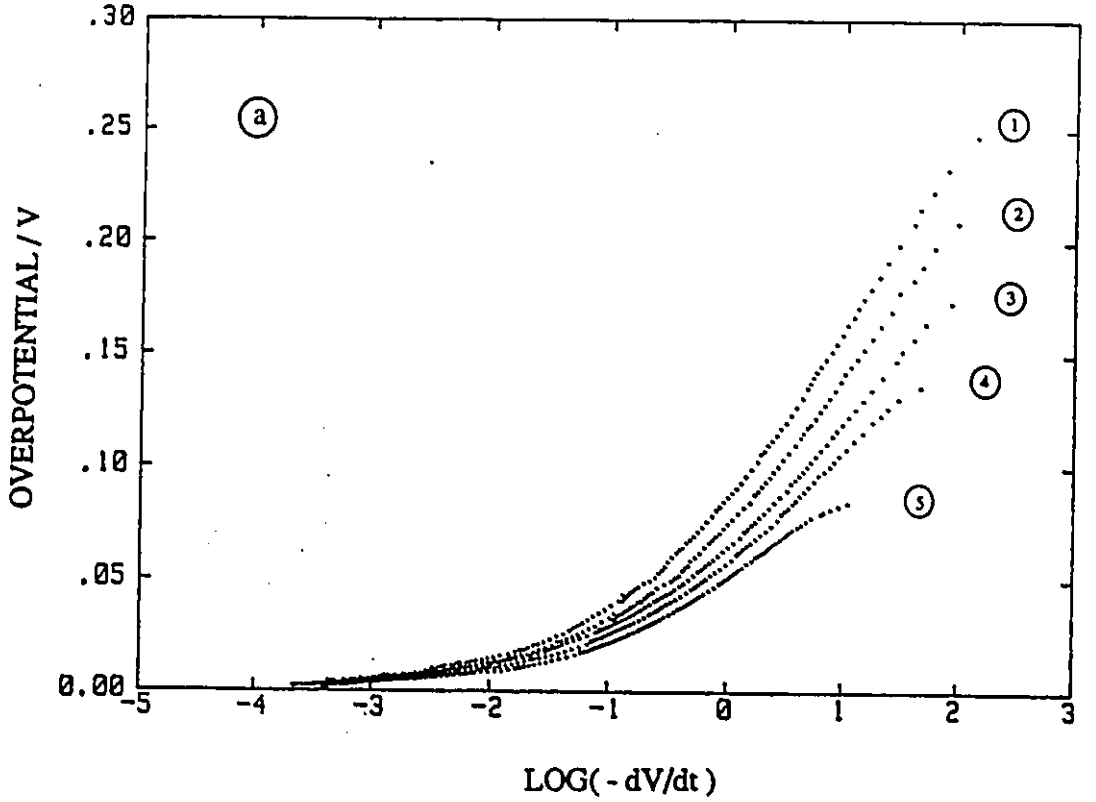

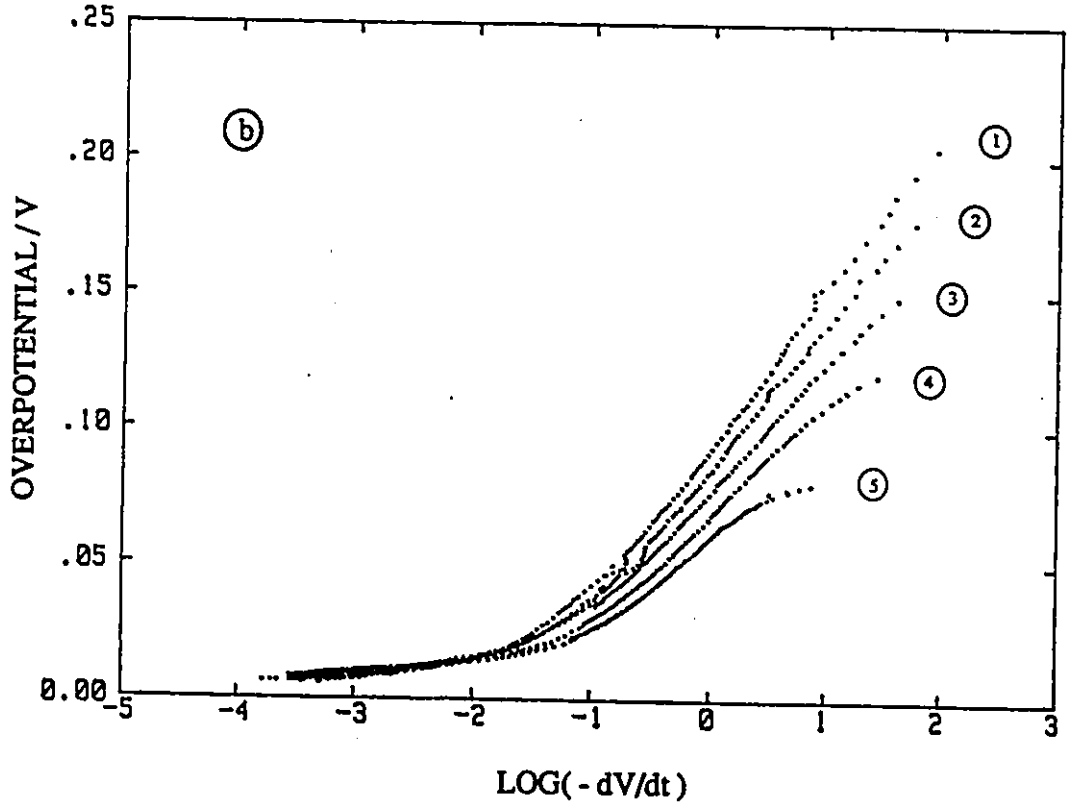

Figs.7.12 The V vs log(-dV/dt) plots based on the same data as in Figs.7.10a,b : (a) for #1 and (b) for #4. The numbers indicate the various initial polarization potentials as indicated in Fig.7.11.

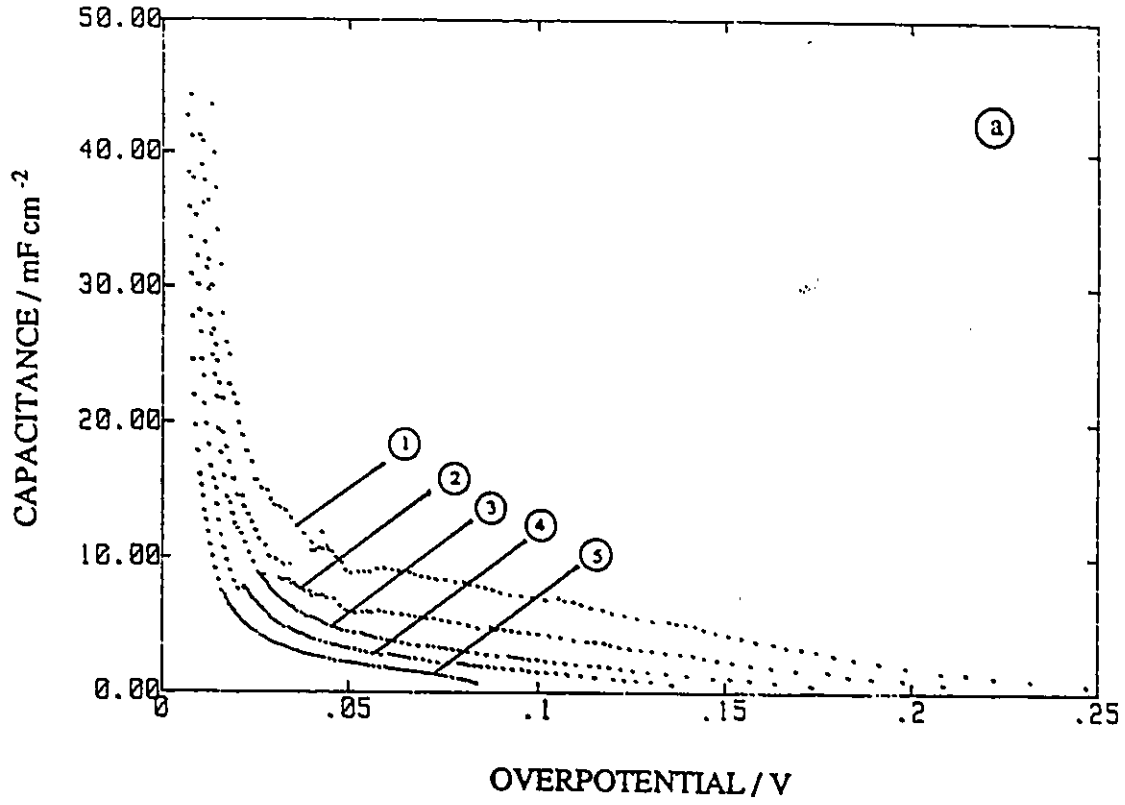

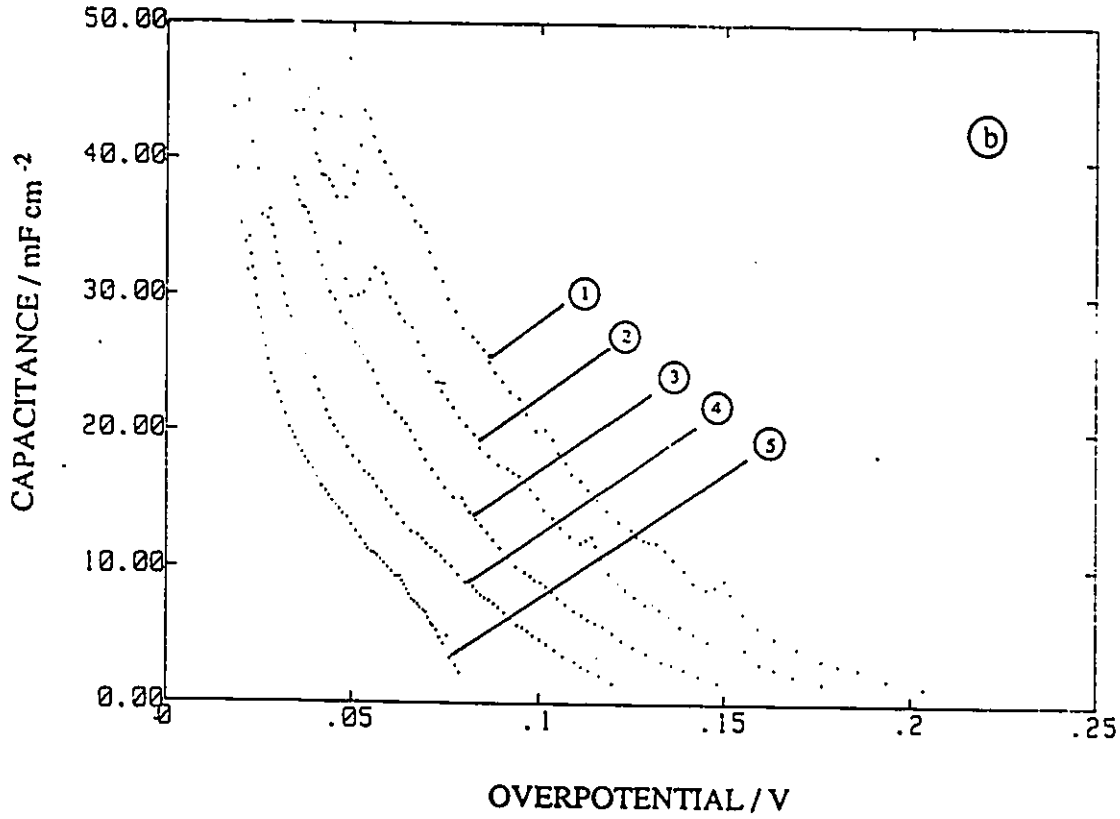

Figs.7.13a,b The C(V) vs V plots corresponding to the data of Figs.7.12a,b : (a) for #1 and (b) for #4. The numbers indicate the various initial polarization potentials as indicated in Figs.7.11a,b.

may be mainly attributed to the double-layer capacitance of the oxide interface since this part corresponds to decay region II, and the C value is about 10 to 50 mF cm^{-2} which is reasonable value for the porous electrodes that have relatively large surface area; and (iii) in all the C(V) profiles, a very rapid rise of capacitance begins at 50 mV or lower. This part corresponds to region IV of the V vs log(t) where the process involves desorption of the adsorbed Cl^- species. Another basis for the explanation of this behaviour is that, since the electrodes are porous, the desorption of Cl^- species may arise both from the top region of the film and also from deeper inside the pores. In the other words, the adsorbed Cl^- (surface) might diffuse out of these "pores" giving a rapid change of charge with potential, leading to the rising region of the capacitance. However, over the potential range covered, no actual peak in the capacitance is observed. The roughness can also affect the a.c. impedance spectra and in the later discussion, this question will be addressed further.

7.4.3. Relation of Cl^- Adsorption to the Indicated Recombination-Controlled Kinetics

It is always a matter of contemporary interest to understand the mechanism of the Cl_2 evolution reaction at RuO_2-TiO_2 electrodes since they are of great importance to the whole Cl_2 industry. Unfortunately, this is not easy because a number of factors simultaneously influence, in various ways, the Cl_2 evolution mechanism at RuO_2-TiO_2 electrodes. Such factors include : porosity, removal of the product Cl_2, bubble formation, morphology, composition of the active layer, the specific adsorption of the Cl^- ion, and even the hydration of the oxide film and competition with the O_2 evolution reaction.

However, a simplified mechanism model is used here in order to provide a basis for discussion of the chemical and catalytic aspects of the mechanism of the Cl_2 evolution reaction at these oxide electrodes. Normally, the two accepted paths for the Cl_2 evolution reaction in aqueous solution are the electrochemical desorption step (II) and the "chemical" recombination desorption step (III).

Taking the competitive O_2 evolution reaction and hydration of the oxide film (M_{ox}) into account, in the general case the proposed mechanism would be represented by :

$$M_{ox} + xH_2O \dashrightarrow M_{ox}(H_2O)_x \quad [VI]$$

$$M_{ox}(H_2O) \quad ==== \quad M_{ox}\text{-}OH + H^+ + e \quad [VII]$$

$$M_{ox}\text{-}OH \quad ==== \quad M_{ox}\text{-}O + H^+ + e \quad [VIII]$$

$$M_{ox}\text{-}OH + Cl^- \quad ==== \quad M_{ox}\text{-}HOCl + e \quad [IX]$$

$$M_{ox}\text{-}HOCl + Cl^- \dashrightarrow M_{ox}\text{-}OH + Cl_2\uparrow + e \quad [X]$$

$$2M_{ox}\text{-}HOCl \dashrightarrow 2M_{ox}\text{-}OH + Cl_2\uparrow \quad [XI]$$

where M_{ox} represents the RuO_2-TiO_2 film and $M_{ox}OHCl$ represents a co-deposited state of discharged OH^* and Cl^* at the electrode surface rather then an hypochlorite species. Step [VI] represents "hydration" of a pre-formed oxide film and happens as soon as the electrode is immersed in the electrolyte. Steps [VII] and [VIII] are the pathways for the O_2 evolution reaction but normally, in the presence of Cl^-, this process is not kinetically favoured, i.e. step [VIII] is relatively slow. Steps [IX], [X] and [XI] are the pathways for the Cl_2 evolution reaction. It is to be noted that the introduction of the state M_{ox}-HOCl is not to be confused with the HOCl mentioned by Krishtalik[87,88] but merely

represents a possible state of co-deposition of the OH and Cl^* species. Since the O_2 evolution reaction is normally insignificant, the kinetically observed behaviour can actually be represented by the mechanism proposed in section (2.3). In the present treatment, the back reactions for steps [X] and [XI] are also taken into account. The relevant rate equations for Cl_2 evolution are then:

$$v_9 = k_9(1-\theta)\exp(\beta V f) \quad [7.2]$$

---

*At the Pt metal anode, the initial process, prior to Cl_2 evolution, is chemisorption of Cl^* ions in competition with initial stages of formation of an OH + O film. Cl_2 evolution then proceeds on this anodically formed film as discussed earlier. In the RuO_2 case, Cl^* discharge takes place, of course, on the surface and in the pores of the already thermochemically formed oxide film.

$$v_{-9} = k_{9}\theta C_{Cl^-}\exp(-(1-\beta)Vf) \quad [7.3]$$

$$v_{10} = k_{10}\theta\exp(\gamma Vf) \quad [7.4]$$

$$v_{-10} = k_{10}(1-\theta)C_{Cl^-}\exp(-(1-\gamma)Vf) \quad [7.5]$$

$$v_{11} = k_{11}\theta^2 \quad [7.6]$$

$$v_{-11} = k_{11}(1-\theta)^2 \quad [7.7]$$

where f = F/RT, ß, γ are symmetry factors for charge transfer. Taking ß = γ = 0.5, the total net current density can be expressed in the form

$$i = 2F(v_{10} - v_{-10}) + (v_{11} - v_{-11}) \quad [7.8]$$

and represents the situation of the recombination and the electrochemical desorption steps being involved as parallel pathways. The contribution to the overall reaction rate of each of the parallel pathways depends, of course, on the respective rate constants. Fig.7.14 represents a simulated Tafel plot calculated for the parallel mechanism using eqn.[7.8] combined with eqns [7.2] to [7.7]. The circle points are the experimental data while the solid lines result from the simulation. Curve (a) is for the rate constants taken as: K_1 = 0.8; $k_2 = 1\times10^{-12}$; $k_3 = 4.87\times10^{-8}$, and curve (b) for k_2 = 0 and (c) with k_3 = 0. From the figure, one can see how the recombination pathway can be dominant for the values of k's chosen which provide a best fit to the experimental behaviour.

The trend to possible recombination-controlled limiting currents in Figs.7.4 and 7.5 suggests that levels of full coverage by Cl^- are approached. According to the derivation on the basis of the Conway-Novak plots of Fig.7.7, the approach to full coverage should follow a Langmuir (g = 0) or Frumkin type (g = 0) isotherm :

$$\theta/(1-\theta) = K_1C_{Cl^-}\exp[VF/RT]\exp[-g\theta] \quad [7.9]$$

The corresponding pseudocapacitance relations for non-equilibrium conditions were worked out by Gileadi and Conway[110] for various values of g. The sharpness of the ascent of the C value when V ≤ 50 mV (at 298 K), albeit in the absence of an observable maximum, suggests that g actually has negative values, so that θ can change from a small value to near 1 over a relatively small potential range (for Langmuir conditions [g = 0], this range for 0.05 < θ < 0.95 is ca. 200 mV). Fig.7.15

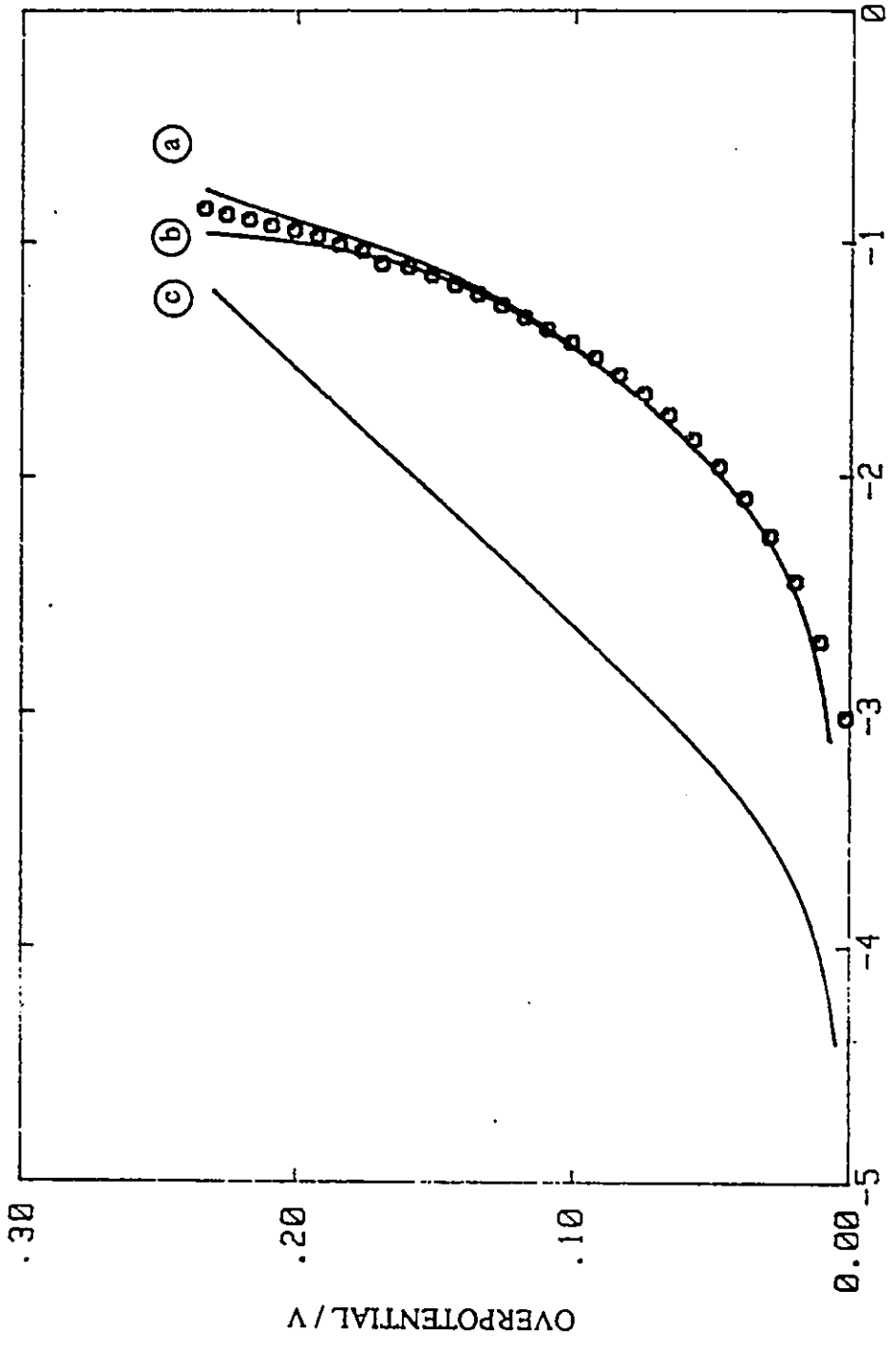

Fig.7.14 Numerical simulation of the Tafel plot for Cl_2 evolution on RuO_2-TiO_2 electrodes. The circles represent the experimental points; curve (a) is derived with K_1 = 0.8; k_2 = 10^{12}; k_3 = 4.87×10^{4}; curve (b) with k_2 = 0; and curve (c) with k_3 = 0 mole s^{-1}.

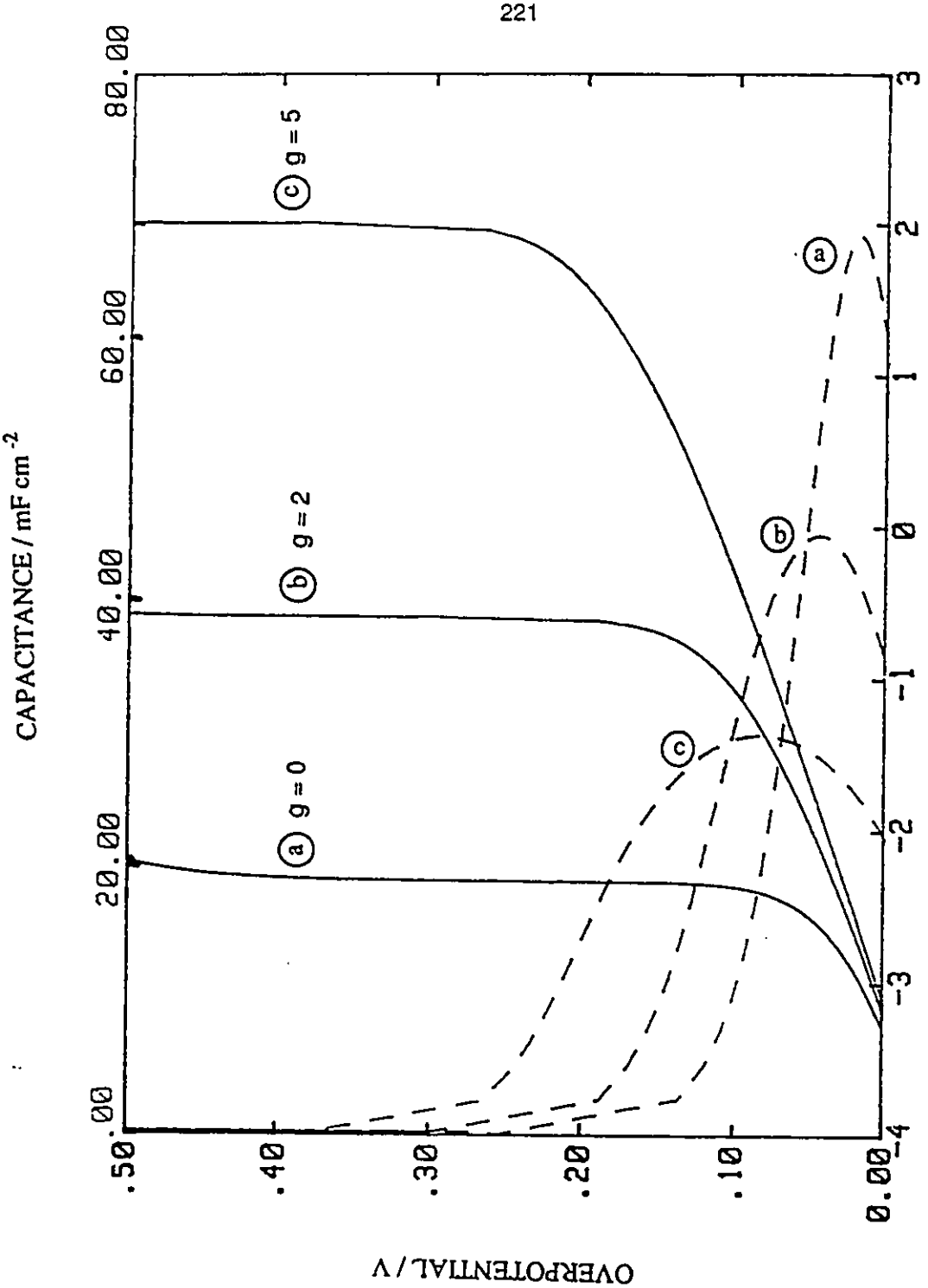

Fig.7.15 Theoretical simulation of the V vs log(i) (solid lines) and C(V) vs V dashed lines) behaviour taking the rate constants K_1 = 0.5; k_2 = 10^{-12}; k_3 = 4.87×10^{-8}; and q = 7 mC cm^{-2}. Curves (a), (b) and (c) are derived for three values of g taken as 0, 2, and 5, respectively.

shows the theoretical simulation of the C(V) vs V profile taking K_1 = 0.5; k_2 =10^{-12}; k_3 = 4.87x10^{-8} mole s^{-1} and q = 7 mC cm^{-2}. Curves (a), (b) and (c) represent the effect of different values of a g = 0, 2 and 5, respectively, on the C(V) maximum. The case for g = 0 in Fig.7.15 gives the sharp C(V) peak; however, the potential corresponding to the maximum of the capacitance peak, in fact, depends on the values of K_1, the equilibrium constant of step I. The potential of the maximum in C shifts to more negative values as K_1 is increased. It should also be noted that the approach to the limiting current condition depends very much on g and the actual limiting currents attained increase rapidly with g (Fig.7.15).

7.5. A.C. Modulation Study of the Cl_2 Evolution Reaction at RuO_2-TiO_2 Electrodes

One of the most useful techniques for the study of electrochemical interfacial processes is impedance analysis. If the system is perturbed by a small amplitude alternating signal, the resulting linear response may be analyzed to yield data on rate and diffusion coefficients, and capacitances etc, as has been shown in earlier chapter. However, a common complication that restricts the usefulness of impedance analysis is the non-trivial apparent frequency-dependence of the elements of the equivalent circuit which causes dispersive behaviour in complex-plane impedance plots, manifested as a depression of the diameter-chord of the semi-circle plots below the Z' axis.

7.5.1. A.C. Impedance Spectra

The a.c. impedance spectra for the Cl_2 evolution reaction at RuO_2-TiO_2 electrodes used in the present work (#1 to #5) are given in Figs.7.16 a-e for three d.c. level potentials in each case. All diagrams show only one distorted semi-circle observed in the frequency range studied. The capacitance values were estimated, in the usual way, from the top-point frequencies of the respective complex-plane impedance plot. These values, listed in Table 7.4, show qualitatively that the electrode prepared with

the highest concentration of Ru has the largest value of capacitance compared with the others. The same tendency is revealed in the results from the potential-relaxation method but not quantitatively, i.e. there are differences in the measured capacitances by these two techniques. This is because, at a porous electrode, the surface conditions corresponding to open-circuit and closed-circuit experiments are different.

Considering a porous electrode, the adsorbed species (Cl_{ad}) would be formed within the micro-structure of the oxide film, or in other words, the Cl_{ad} species would be adsorbed inside the tiny "holes" of the oxide film. In the open-circuit potential relaxation measurements, the diffusion of Cl_2 species under supersaturation out of the "holes" in the oxide film will affect the form of the capacitance curve depending on the diffusion time in relation to the duration of the potential decay, so that the potential-decay technique may then include the influence of diffusion effects. However, in the a.c. impedance measurement, no open-circuit situation is involved, so that those Cl_{ad} which have been generated within the oxide film micro-structure will tend to remain there. When a small amplitude sinusoidal signal is applied, the signal cannot totally penetrate (even at low frequency) the micro structure of the oxide film, i.e. less response will arise from capacitance associated with adsorbed Cl_{ad} inside those "holes". Therefore, a.c. impedance only senses (in a frequency-dependent manner) those adsorbed Cl_{ad} species on the outer surface region of the electrode, which can follow the sinusoidal signal. However, the degree of "penetration" of the a.c. signal will depend on frequency.

Table 7.4 The Estimated Values of Capacitance

Overpotential / Electrode	Capacitance (mF/cm^2)		
	10 mV	30 mV	50 mV
# 1	3.45	3.36	3.00
# 2	5.44	4.62	4.56
# 3	9.20	8.25	8.20
# 4	23.1	20.3	20.2
# 5	8.11	6.78	5.82

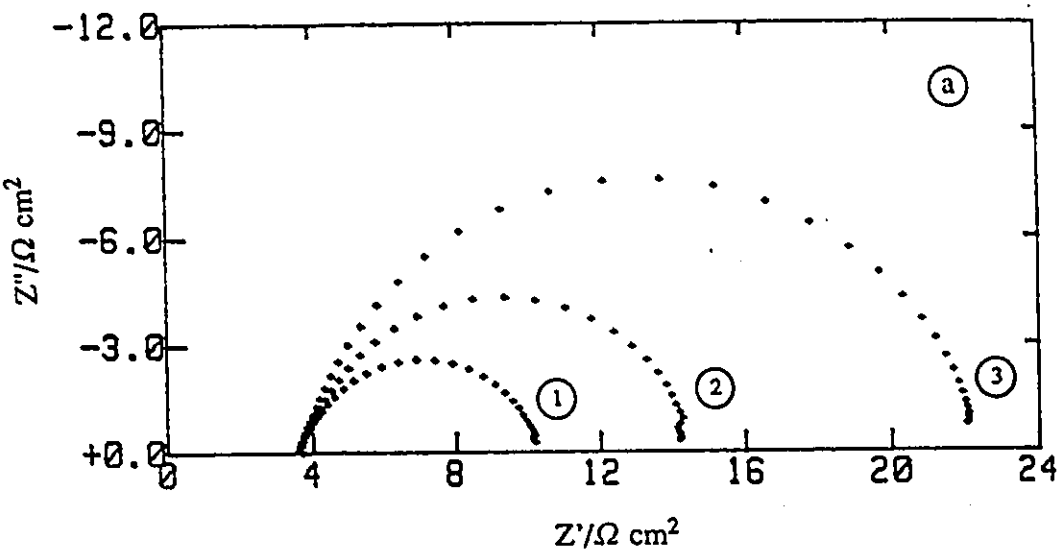
-12.0
-9.0
-6.0
-3.0
+0.0
0
4
8
12
16
20
24
Z''/Ω cm²
Z'/Ω cm²
a
1
2
3

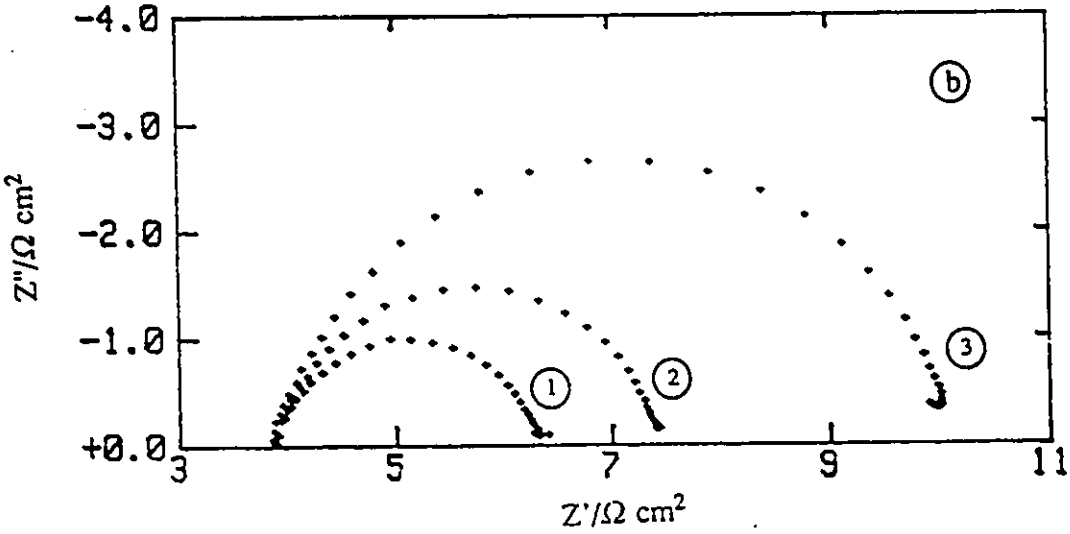
-4.0
-3.0
-2.0
-1.0
+0.0
3
5
7
9
11
Z''/Ω cm²
Z'/Ω cm²
b
1
2
3

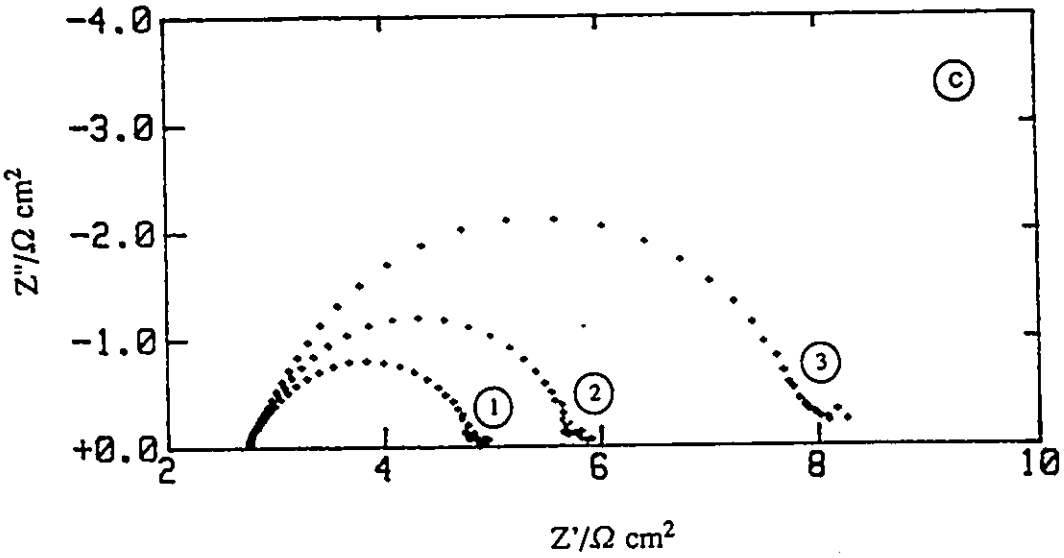
-4.0
-3.0
-2.0
-1.0
+0.0
2
4
6
8
10
Z''/Ω cm²
Z'/Ω cm²
c
1
2
3

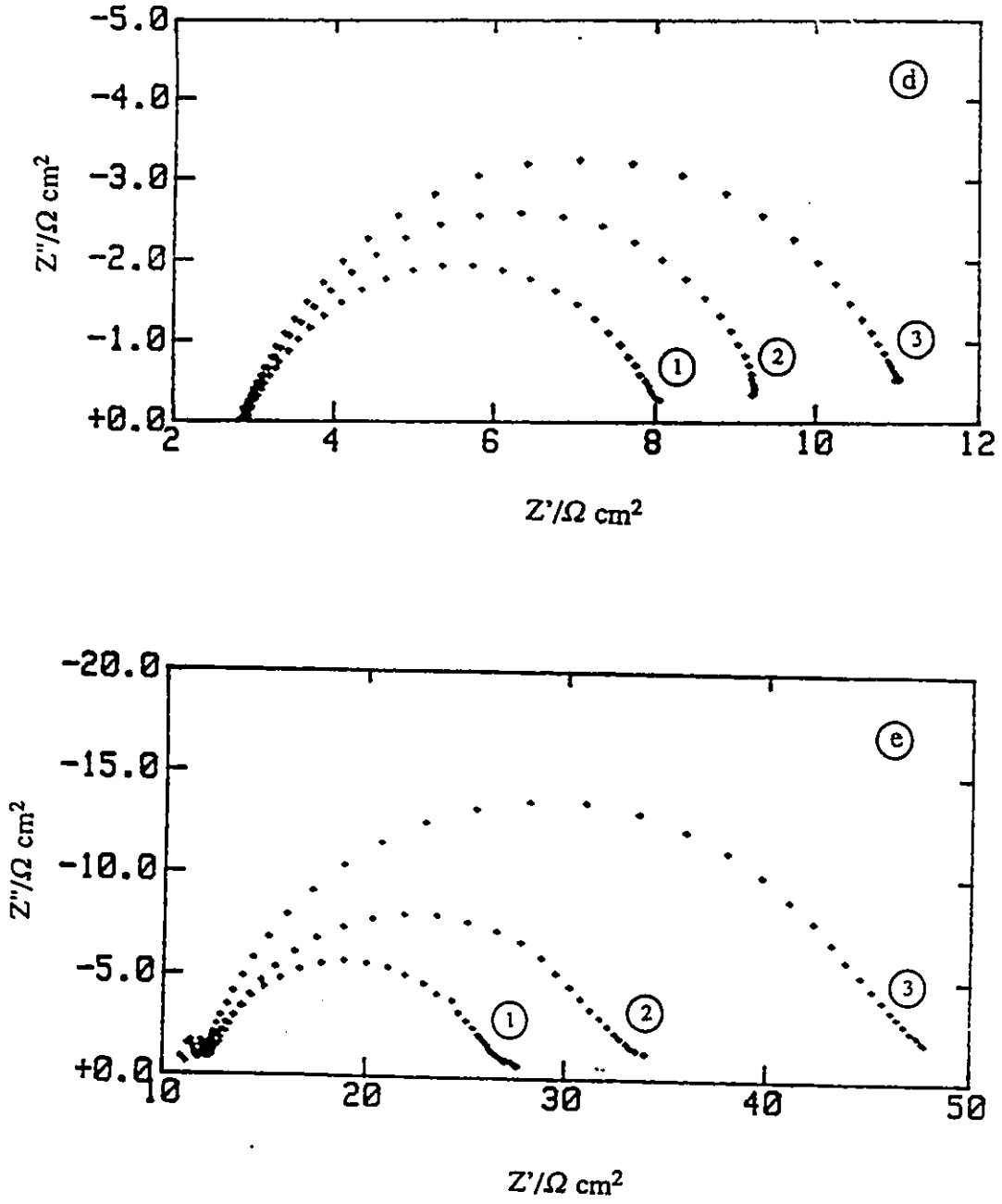

Fig.7.16 The a.c. impedance spectra as complex-plane plots for the Cl_2 evolution reaction in 0.1 M HCl + 0.9 M NaCl solution at RuO_2-TiO_2 electrodes for various polarization potentials. (1), (2) and (3) represent the behaviour at overpotentials of 10, 30 and 50 mV, respectively. (a) #1; (b) #2; (c) #3; (d) #4; (e) #5 electrodes.

Another factor can introduce some error into the evaluation of the capacitance. Since the evaluation depends on the identification of the co-called top-frequency and the diameter in Z' of the semi-circle, it is important that the semi-circle be well developed; this means that no depression of the semi-circle on the Z' axis should arise. Unfortunately, all the semi-circles observed in these experiments are depressed, so this can bring some uncertainty in the evaluation of C but this is not significant in comparison with the possible influence of diffusion from the pores. The distorted semi-circles may arise on account of the porous structure of the electrodes but the significance of depression angles is still not clear in a quantitative way. It should be mentioned that depression of complex-plane Z' vs Z" plots also arises for a number of other processes, e.g. cathodic H_2 evolution at smooth solid metal electrodes and in a related way in the dispersive of dielectric relaxation times of dielectrics.

Table 7.5 List of the Depression Angles

Electrodes	Depression Angle (degrees)
# 1	11.5
# 2	10
# 3	13
# 4	14.5
# 5	12.5

7.5.2. Surface Roughness and Frequency Dispersion

The first attempt to calculate the effect of surface roughness on impedance was by de Levie[165,166] who derived the impedance associated with V-shaped grooves in a flat electrode surface, under the assumption that the grooves are straight and infinite in length. Recently an attempt to calculate the impedance of a porous electrode using a random network model, numerically solved the resulting set of Kirchoff's equations, proposed by Nyikos and Pajkossy proposed, or so-called N-P model[167-172], It is a general treatment of the effect of surface roughness on the behaviour of ideally polarized electrodes in terms of factual geometry, surface irregularity which is characterized by the effective factual dimension, D. However, the N-P model has been questioned by Wang[173,174] because it lacks experimental proof.

It is useful, at this point, to draw attention to the frequency-dependent impedance following the general form :

$$Z_p(\omega) = A_1\omega^{-\alpha} - iA_2\omega^{-\alpha} \qquad [7.9]$$

where α is related to the factual dimension, D, according to $\alpha = 1/(D-1)$ in N-P's model and its value is usually between 0.5 to 1. A_1 and A_2 are constants which represent the contributions to the real and the imaginary parts of Z, respectively.
In the special case of $A_1 = A_2$, then

$$Z_p = A_1(\omega^{-\alpha} - i\omega^{-\alpha}) \qquad [7.10]$$

and when $A_1 = 0$;

$$Z_p = - iA_2\omega^{-\alpha} \qquad [7.11]$$

which is the empirical relationship widely used in treatments of porous electrode impedance behaviour.

In order to simulate the a.c. impedance spectra, an equivalent circuit can be proposed, taking the frequency-dependent element associated with roughness into account, as shown in Fig.7.17. Perhaps surprisingly, the fitting results (exemplified in Fig.7.18), for the Cl_2 reaction at RuO_2-TiO_2 electrodes at overpotentials of 30 and 50 mV, have an excellent overlay with the experimental data represented by small

crosses. The solid line represents the numerical simulation taking the frequency-dependent element into account, i.e. the total impedance in Fig.7.17, and the dashed line illustrates the case (Fig.4.5c) without the frequency-dependent element being included. The required simulation parameters are listed in Table 7.6.

The interesting and important fact is that, by using the same set of parameters, the dashed line (without Z_p) actually shows two semi-circles but the solid line (with Z_p) corresponds to only one. This implies that, when a frequency-dependent element is involved, the actual apparent a.c. impedance spectrum would, in some cases, not be seen as expected, i.e. two semi-circles may not be actually observed. What is actually seen is the apparent spectrum : a distorted semi-circle in the complex-plane plot.

However, identification of the causes of the frequency-dependent element is a complicated problem. Mainly, two factors are to be considered : (i) the surface is uneven or rough; this is believed to be the main cause of the depression of the complex-plane impedance plots by various authors [176-179] and as also considered by present author as well; but (ii) the adsorbed intermediates could also give rise to the depression effect since the depression of an a.c. impedance complex-plane plot must relate to the structure of the interfacial region which determines the interfacial capacitances. Therefore, any factor that affects the surface structure would tend to have effects on the surface capacitance, as revealed in the a.c. impedance spectrum; thus, the adsorption of intermediates can itself introduce a micro-heterogeneity that could possibly lead to some influence on the depression of the impedance plots. Additionally, as found in other work in this laboratory, ion size and specific adsorption can also give rise to the depression effect even at an apparently smooth electrode but not at Hg.

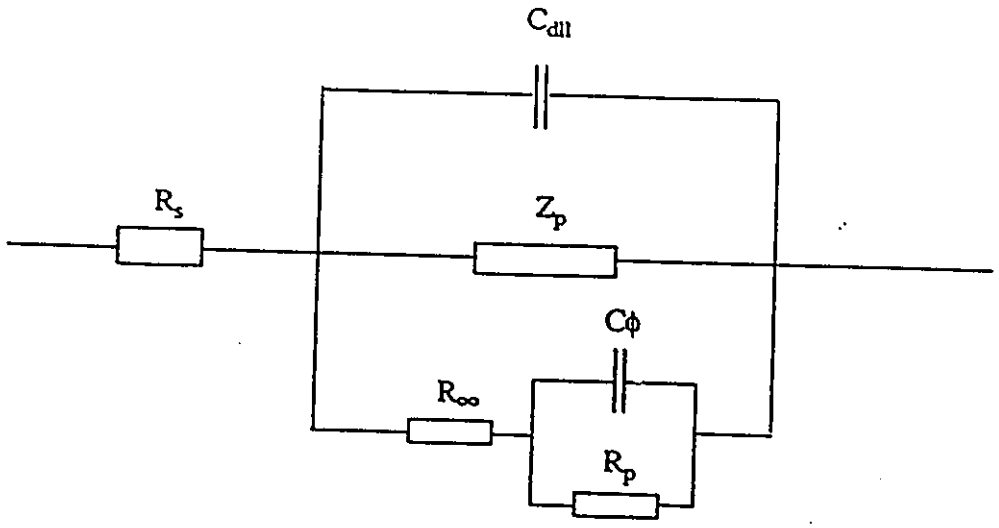

Fig.7.17 The equivalent circuit taking the frequency-dependent element, Z_p into account.

Table 7.6 The parameters required for simulation of the behaviour in Fig.7.18.

Case	R_∞ Ωcm^2	R_p Ωcm^2	A_1	A_2	α	C_{dl} F/cm^2	C_p F/cm^2	V mV
a	0.53	0.70	40	150	0.95	$3x10^{-4}$	$4x10^{-2}$	30
b	0.64	0.34	40	150	0.95	$3x10^{-4}$	$5x10^{-3}$	50

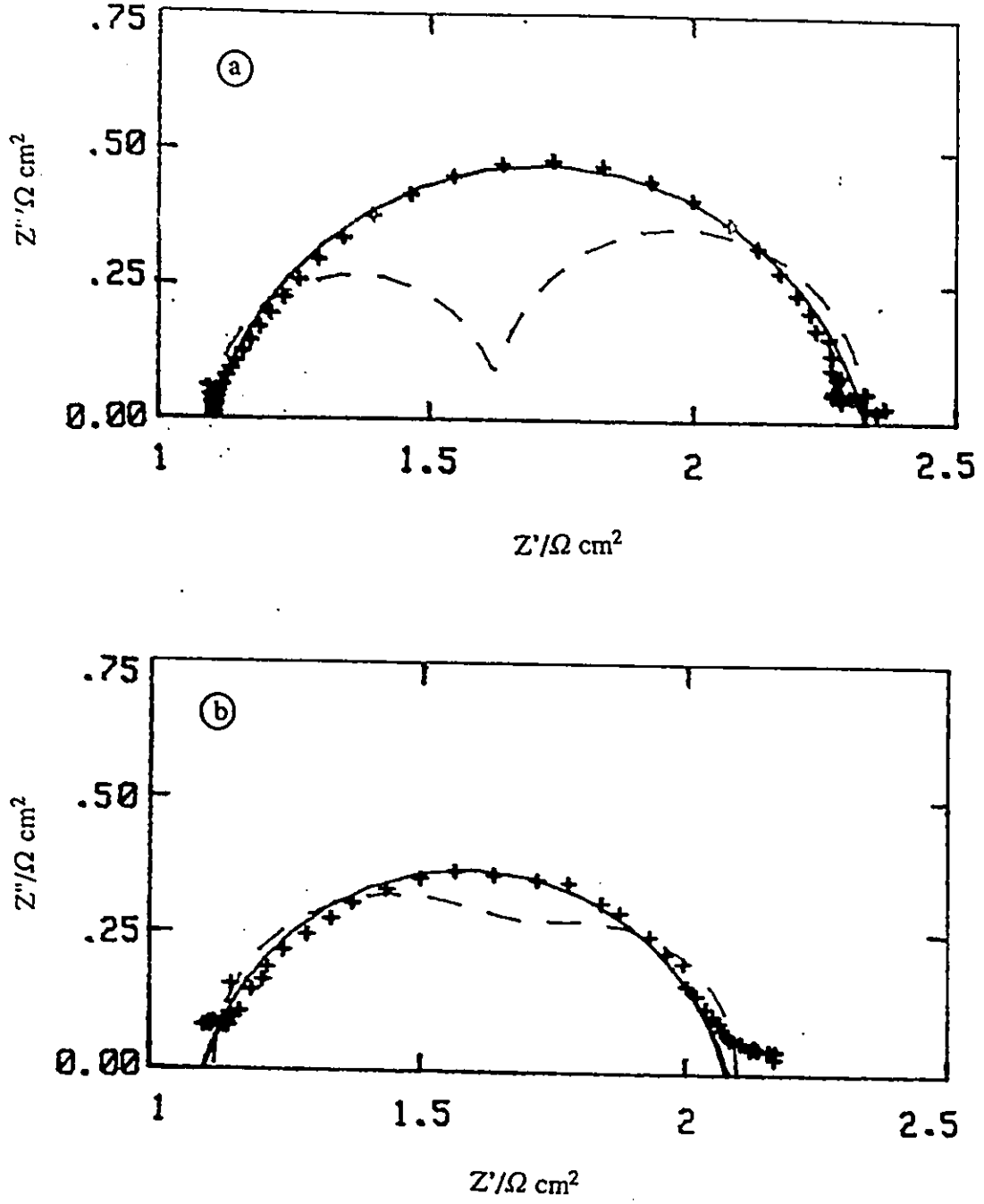

Fig.7.18 Examples of plots of simulated a.c. impedance behaviour using the equivalent circuit shown in Fig.7.17. The solid line illustrates the case with the Z_p and the dashed line that without Z_p.

7.6. Conclusions

(a) The determination of kinetic parameters for the Cl_2 evolution reaction at oxide electrodes can be vitiated by the complicating effects of a number of variables which, in previous work, have not always been taken adequately into consideration. In many cases, the determination of Tafel slopes alone is insufficient to deduce the mechanism.

(b) The mechanism of Cl_2 evolution on oxide electrodes is complicated by the specific features of the surface of the materials such as morphology and the procedure of preparation of the active oxide film.

(c) The formation of an higher local state of surface oxidation at some site, prior to Cl^- discharge, appears, as has been discussed in some papers, to be an important feature of the mechanism of the Cl_2 evolution reaction.

(d) The mechanism of the Cl_2 evolution reaction at the presently investigated thin-film RuO_2 electrodes is dominated by Cl^- recombination-control, and does not appear to change as the reaction rate is increased.

(e) The Cl^- adsorption behaviour has been determined by means of potential-relaxation transients. The resulting potential-dependent pseudocapacitance has been clearly observed at overpotentials of less than 50 mV.

(f) The a.c. impedance observations lead to only single semi-circles in the complex-plane plots which, through numerical simulation, give information about Cl^- adsorption in the anodic Cl_2 evolution reaction.

(g) The behaviour associated with the depression of Z' vs Z" semi-circle in complex-plane plots can be related to the porosity of the RuO_2 oxide films. Introduction of a frequency-dependent impedance element, Z_p, can lead to significant change of the Z' vs Z" plots, relative to the behaviour in the absence of distributed impedance effects represented by Z_p.

Contribution to Original Research

1) By means of potential-relaxation method, the role of $Cl^{\cdot}$ adsorption in the mechanism and kinetics of the Cl_2 evolution reaction, both in aqueous and non-aqueous solutions, have been further studied. The results reveal new information about the $Cl^{\cdot}$ adsorption and the predominant role of the $Cl^{\cdot}$ recombination pathway in the mechanism of anodic Cl_2 evolution at Pt and RuO_2 electrodes.

2) A new procedure of data acquisition and processing by using a digital oscilloscope and main-frame computer was developed. This method is able to fit entire open-circuit potential-relaxation transients, and it has been used to evaluate the capacitative components of an electrode reaction.

3) The behaviour of pseudocapacitance of the Cl_2 evolution reaction at the reduced, pre-oxidized and oxide-free Pt electrodes, has been carefully investigated. It is experimentally observed that the co-deposited OH or O species prevents further $Cl^{\cdot}$ or $Cl^{\cdot}$ adsorption or/and desorption but does not change the chlorine evolution mechanism.

4) The information concerning the adsorbed $Cl^{\cdot}$ intermediate, at both reduce and pre-oxidized and oxide-free Pt electrodes, was able to be observed by a.c. impedance techniques. The theoretical analysis of the obtained data by applying a newly developed kinetic constants and an equivalent circuit model showed a agreement with the information from potential-relaxation.

5) Some exploratory experiments have been made in a non-aqueous TFA solution for the Cl_2 evolution reaction at noble metals, i.g., Pd, Ir, Ru and Rh. From their corresponding capacitance curves, a second C maximum was observed, which may be attributed by a Koble reaction.

6) Detailed kinetic studies of the Cl_2 evolution reaction at DSA electrodes, RuO_2-TiO_2, has also been made by using potential-relaxation and a. c. impedance techniques.

The results coupled with the polarization behaviour support the recombination mechanism.

10) A interesting comparison of the simulation with and without taking the roughness element into account shows that, in some cases, two semi-circles in complex-plane may not be necessarily seen if the frequency dependent elements involves.

REFERNCES

1. G. Bianchi, J. Appl. Electrochem. , 1 (1971) 231.
2. G. Faita, G. Fiori and N. Nidola, J. Electrochem. Soc. , 117 (1970) 1333.
3. L. J. J. Janssen and J. G. Hoogland, Electrochim Acta, 15 (1970) 1667.
4. S. Trasatti and G. Buzzanca, J. Electroanal. Chem., 29 (1971) app. 1.
5. D. Galizzioli, F. Tantardini and S. Trasatti, J. Appl. Electrochem., 4 (1974) 57., and also, ibid. 5 (1975) 203.
6. C. Iwakura, H. Tada and H. Tamura, Electrochim. Acta, 22 (1977) 217.
7. J. S. Mayell and S. H. Langer, Electrochim. Acta., 9 (1964) 1411.
8. A. T. Kuhn and P. M. Wright, J. Electroanal. Chem., 38 (1972) 291.
9. T. Dickinson, R. Greef and Lord Wynne-jones, Electrochim. Acta, 14 (1969) 467.
10. F. T. Chang and H. Wick, Z. Phys. Chem., 33 (1935) 129.
11. K. J. O'Leary, U.S. Patent 3,776,834 (1973).
12. H. B. Beer, Neth. Pat. Appl. 216,199 (1957); U.S. Pat. 3,236,756 (1966).
13. D. J. Ives and G. I. jantz, Eds., Reference Electrodes, Academic Press, New York (1961) Chap. II, 111.
14. A. J. Bard, Ed. Encyclopaedia of Electrochemistry of the Elements, Vol.1 Marcel Dekker Inc. New York (1973), p.1.
15. L. Young, Anodic Oxide Films, Academic Press, London, New York, (1961).
16. A. K. Vijh, Electrochemistry of Metals and Semiconductors, Marcel Dekker Inc. New York, (1973) P. 129.
17. J. W. Diggle, T. C. Downie and C. W. Goulding, Chem. Rev., 69 (1969) 365.
18. J. P. Hoare, The Electrochemistry of Oxygen, Interscience, New York, (1968).
19. S. Schuldiner and R. M. Roe, J. Electrochem. Soc., 110 (1963) 332.
20. M. W. Breiter, C. A. Knorr and W. Volkl, Z. Elektrochem., 59 (1955) 881.
21. M. W. Breiter, K. Francke and C. A. Knorr, Z. Elektrochem., 63 (1959) 226.

22. F. G. Will and C. A. Knorr, Z. Elektrochem., 64 (1960) 258. And also, ibid., 64 (1960) 270.

23. K. J. Vetter, J. W. Schultze, J. Electroanal. Chem., 34 (1972) 131.

24. K. J. Vetter, J. W. Schultze, J. Electroanal. Chem., 34 (1972) 141.

25. J. W. Schultze, Z. Phys. Chem. NF, 73 (1970) 29.

26. H. Angerstein-Kozlowska, B. E. Conway, and W. B. A. Sharp, J. Electroanal. Chem., 43 (1973) 9.

27. B. V. Tilak, B. E. Conway, and H. Angerstein-Kozlowska, J. Electroanal. Chem., 48 (1973) 1.

28. J. P. Hoare, R. Thacker, and C. R. Wiese, J. Electroanal. Chem., 30 (1971) 15.

29. M. W. Breiter, Electrochim. Acta, 8 (1963) 447.

30. M. W. Breiter, Electrochim. Acta, 8 (1963) 457.

31. S. Schuldiner and T. B. Warner, J. Electrochem. Soc., 112 (1965) 212.

32. N. Sato and N. Cohen, J. Electrochem. Soc., 111 (1964) 572.

33. S. Barnartt, J. Electrochem. Soc. 106 (1959) 106.

34. B. E. Conway, W. B. A. Sharp, H. Angerstein-Kozlowska, and E. E. Criddle, Anal. Chem. 45 (1973) 1331.

35. B. M. W. Trapnell and D. O. Hayward, Chemisorption, W. E. Garner Ed., Butterworths, London, Washington, D. C. (1964) P.210.

36. A. K. N. Reddy, M. A. Genshaw and J. O'M Bockris, J. Electroanal. Chem., 8 (1964) 406.

37. A. K. N. Reddy, M. A. Genshaw and J. O'M Bockris, J. Chem. Phys. 48 (1968) 671.

38. R. Greef, J. Chem. Phys., 51 (1969) 3148.

39. B. E. Conway and S. Gottesfeld, J. Chem. Soc. Faraday Trans.1 69 (1973) 1090.

40. B. E. Conway, Symp., Faraday Soc., 41 (1970) 94.

41. J. L. Ord and F. C. Ho, J. Electrochem. Soc., 118 (1971) 46.

42. D. Gilroy and . E. Conway, Can. J. Chem. 46 (1968) 875.

43. D. Gilroy, J. Electroanal. Chem., 71 (1976) 257.

44. D. Gilroy, J. Electroanal. Chem., 83 (1977) 329.

45. A. Damjanovic and A. T. Ward, MTP, International Review of Science, Physical Chemistry, Series II, Butterworths, London (1973) P.103.

46. A. Damjanovic and B. Jovanovic, J. Electrochem. Soc., 123 (1976) 374.

47. A. T. Ward, A. Damjanovic, E. Gray, and M. O'Jea, J. Electrochem. Soc., 123 (1976) 1599.

48. Mott and Cabrera, Rep. Proc. Phys. 12 (1949) 163.

49. P. Stonehart, H. A. Kozlowska, and B. E. Conway, Proc. R. Soc. London Ser. A 310 (1969) 541.

50. W. Böld and M. W. Breiter, Z. Elektrochem., 64 (1960) 897.

51. S. W. Feldberg, C. C. Enke, and C. E. Bricker, J. Electrochem. Soc., 110 (1963) 826.

52. S. Gilman, Electrochim Acta, 9 (1964) 1025.

53. T. Biegler and R. Woods, J. Electroanal. Chem., 35 (1969) 73.

54. D. Gilroy and B. E. Coway, J. Phys Chem., 69 (1965) 1259.

55. M. Fleischmann, i. R. Mansfield, and W. F. K. Wynne-Jones, J. Electroanal. Chem., 10 (1965) 511.

56. A. K. Vijh and B. E. Conway, Z. Anal. Chem., 224 (1967) 160.

57. S. Shibata, Bull. Chem. Soc. Japan, 36 (1963) 525.

58. S. Shibata, Electrochim. Acta, 22 (1977) 175.

59. J. Llopis, I. M. Tordesillas, and J. M. Alfayate. Electrochim. Acta, 11 (1966) 623.

60. J. Llopis, J. M. Gamboa, and J. M. Alfayate, Electrochim. Acta, 12 (1967) 57.

61. V. V. Gorodetskii, M. M. Pecherskii, Ya. B. Skuratnik, M. A. Dembrovskii, and V. V. Losev, Electrokhim., 9 (1973) 894.

62. S. Hadzi-Jordanov, H. Angerstein-kozlowska, and B. E. Conway, J. Electroanal. chem., 60 (1975) 359.

63. S. Hadzi-Jordanov, M. Vukovic, H. Angerstein-kozlowska, and B. E. Conway, J. Electrochem. Soc., 125 (1978) 1471.

64. W. böld and M. W. Breiter, Electrochim. Acta, 5 (1961) 169.

65. A. Capon and R. parsons, J. Electroanal. Chem., 39 (1972) 275.

66. M. W. Breiter, z. Phys. Chem. NF, 52 (1967) 73.

67. B. D. Kurnikov, A. I. Zhurin, V. V. Chernyi, Yu. B. Vasil'ev, and V. S. Bagotskii, Elektrokhim., 9 (1973) 833.

68. D. A. J. Rand and R. Woods, J. Electroanal. Chem., 55 (1974) 375.

69. J. M. Otten and W. Visscher, J. Electroanal. Chem., 55 (1974) 1.

70. B. E. Conway and S. Gottesfeld, J. Chem. Soc., Faraday Trans. 1, 69 (1973) 1090.

71. J. M. Otten and W. Visscher, Electrochim. Acta, 55 (1974) 13.

72. J. Mozota and B. E. Conway, Electrochim. Acta, 28 (1983) 1.

73. J. Mozota and B. E. Conway, Electrochim. Acta, 28 (1983) 9.

74. J. P. Hoare, in Advances in Electrochemisrty and Electrochemical Engineering, P. Delahay, ed., Vol. 6, Interscience, N.Y. (1967).

75. S. E. S. El Wakkad and A. M. S. El Din, J. Chem. Soc.,(1954) 3094.

76. A. Hickling and G. Vrjosek, Trans. Faraday Soc., 57 (1961) 123.

77. S. Shibata, Bull. Chem. Soc. Japan, 38 (1965) 1330.

78. E. I. Khrushcheva, N. A. Shumilova and M. R. Tarasevich, Elektrokhim., 2 (1966) 277.

79. M. W. Breiter, Electrochim. Acta, 8 (1963) 925.

80. B. E. Conway and D. M. Novak, Croat. Chem. Acta, 53 (1980) 183.

81 B. E. Conway and D. M. Novak, J. Chem. Faraday Trans,1. 75 (1979) 2454.

82 V. S. Bagotskii, Y.B. Vasil'ev, J. Weber, and J.N. Pirtskhalava, J. Electroanal. Chem. 27 (1970) 31.

83. B. E. Conway and J. Mozota, J. Chem. Soc., Faraday Trans.1. 78 (1982) 1717.

84. S. G. Roscoe and B. E. Conway, J. Electroanal. Chem., 224 (1987) 163.

85. B. E. Conway and D. M. Novak, J. Chem. Soc. Faraday Trans. 1, 75 (1979) 244.

86 B. E. Conway and D. M. Novak, J. Electroanal. Chem., 99 (1977) 133.

87. R. G. Erenburg, L. I. Krishtalik, and V. I. Bystrov, Elektrokhim. 8 (1972) 1240.

88. H. G. Erenburg, L. I. Krishtalik, and I. P. Yaroshevskaya, Elektrokhim., 11 (1975) 1068.

89. J. M. Honig, "Defects and Transport in Oxides", M. S. Seltzer and R. J. Jaffee, Eds., Plenum Press, New York (1974) P.315.

90. J. O'M. Bockris and H. Wroblowa, J. Electroanal. Chem. 7 (1964) 428.

91. A. Damjanovic and A. T. Ward, Electrochemistry, the past thirty years and the next thirty years, H. Bloom and F. G. Gutmann, Eds., Plenum Press, N.Y. (1977) Chap.6, P.107.

92. J. O'M. Bockris and A.K.M.S. Huq, Proc. Roy. Soc. London Ser. A237 (1956) 271.

93. A. Damjanovic and V. Brusic, Electrochem. Acta., 12 (1967) 1171.

94. A. K. Vijh, Electrochemistry of metals and Semiconductors, Marcel Dekker Inc., New York (1973).

95. J. W. Schultze and K. J. Vetter, Electrochem. Acta., 18 (1973) 889.

96. A. K. Vijh, Electrochim. Acta., 14 (1969) 921.

97. T. Arikado, C. Iwakura and H. Tamura, Electrochim. Acta., 22 (1977) 229.

98. T. Arikado, C. Iwakura and H. Tamura, Electrochim. Acta., 23 (1978) 9.

99. L. F. Mattheiss, Phys. Rev. 13 (1967) 2433.

100. J. B. Cotton, E. C. Willians and A. H. Barber, U.K. Pat. 877901 (1961).

101. D. M. Novak, B. V. Tilak and B. E. Conway, in Modern Aspects of Electrochemistry, Vol. 14 Eds. by J. O,M Bockris, B. E. Conway and R. E. White. p.195.

102. "Electrodes of Conductive Metallic Oxide", S. Trasatti and G. Lod, Ed. by S. Trasatti, Part B.

103. S. Glasstone, K. J. Laidler and H. Eyring, Theory of Rate Processes, McGraw-Hill

Book Co., Inc. New York, (1940).

104. B. E. Conway, Theory and Principles of Electrode Processes, The Ronald Press (1965).

105. T. Yokoyama and M. Enyo, J. Electroanal. Chem., 136 (1982) 185.

106. B. E. Conway and D. M. Novak, J. Electroanal. Chem. 136 (1982) 191.

107. T. Yokoyama and M. Enyo, Electrochim. Acta, 15 (1970) 1921; 13 (1968) 1631.

108. I. Langmuir, J. Amer. Chem. Soc., 38 (1916) 2221.

109. M. I. Temkin, Zh. Fiz. Khim., 15 (1941) 246; also see A. N. Frumkin, Z. Physik. Chem. 116 (1925) 466: Z. Physik., 35 (1926) 792.

110. B. E. Conway and E. Gileadi, Trans. Faraday Soc., 58 (1962) 2493.

111. B. E. Conway and P. L. Bourgault, Trans. Faraday Soc. 58 (1962) 593.

112. S. Srinivasan and E. Gileadi, Electrochim. Acta, 11 (1966) 321.

113. M. W. Breiter, C. A. Knorr and W. Volki, Z. Elektrochem. 59 (1955) 681.

114. M. W. Breiter, H. Kammermaier and C. A. Knorr, Z. Elektrochem. 60 (1956) 37.

115. M. W. Breiter, Symposium on Electrode Processes, the Electrochem. Soc. Ed. E. Yeager, J. Wiley and Sons, N. Y. (1961) 307.

116. A. N. Frumkim, J. Res. Inst. Catalysis 15 (1967) 61.

117. A. N. Frumkin, Advances in Electrochemisrty and Electrochemical Engineering, P. Delahay, ed., Vol. 3, Interscience, N.Y. (1963) p278.

118. T. Biegler, D.A.J.Rand, and R. Words, J. Electroanal. Chem. 29 (1971) 269.

119. B. E. Conway and T. C. Liu, Ber. Bunsenges hys. Chem. 91 (1987) 461.

120. H. A. Kozlowska, in Comprehensive Treatise of Electrochemistry, Vol.9 Eds. E. Yeager, J. O'M. Bockris, B. E. Conway and S. Sarangapani, Plenum Publ. Corp. 1984.

121. B. E. Conway and D. M. Novak, J. Phys. Chem., 81 (1977) 1459.

122. P. Britz, J. Electroanal. Chem. 88 (1978) 309.

123. B. E. Conway, L. Bai and D. F. Tessier, J. Electroanal. Chem., 161 (1984) 39.

124. B. E. Conway and L. Bai, J. Chem. Soc. Faraday Trans. I, 81 (1985) 1841.

125. B. E. Conway and L. Bai, J. Electroanal.Chem., 198 (1986).

126. P. C. Milner, J. Electrochem. Soc. Vol. 107, No. 4 (1960) 343.

127. K. Aoki, Y. Nishki, K. Tokuda and H. Matsuda, Denki Kagaku 55 No.1 (1987) 74.

128. D. A. Harrington and B. E. Conway, J. Electroanal. Chem., 221 (1987) 1.

129. B. V. Tilak and B. E. Conway, Electrochem. Acta., 21 (1976) 745.

130. B. V. Tilak and B. E. Conway, Electrochim. Acta., 22 (1977) 1167.

131. J. E. B. Randlos, Disc. Faraday Soc., 1 (1947) 11.

132. H. Gerischer, Z. Phys. Chem., 198 (1951) 286.

133. H. Gerischer, Z. Phys. Chem., 201 (1952) 55.

134. W. Lorenz, Naturforsch., 9a (1954) 716.

135. W. Lorenz, Z. Phys. Chem. N. F. 19 (1959) 377.

136. M. Fleischmann, S. K. Rangarajan and H. R. Thirsk, Trans. Faraday Soc., 63 (1967) 1240.

137. H. Gerischer and W. Mehl, Z. Elektrochem., 59 (1955) 1049.

138. I. Epelboin and M. Keddam, J. Electrochem. Soc. 117 (1970) 1052.

139. R. D. Armstrong, R. E. Firman and H. R. Thirsk, Fraraday Disc. Soc., 56 (1973) 244.

140. R. D. Armstrong, J. Electroanal. Chem. 34 (1972) 387.

141. R. D. Armstrong, H. R. Thirsk, Electrochim. Acta., 17 (1972) 171.

142. R. D. Armstrong, T. D. Dickinson, P. M. Willis, J. Electroanal. Chem., 48 (1973) 47.

143. R. D. Armstrong, K. Edmondson, Electrochim. Acta, 18 (1973) 937.

144. R. D. Armstrong, M. F. Bell, R. E. Firman, J. Electroanal. Chem. 48 (1973) 150.

145. R. D. Armstrong, K. Edmindson, ibid., 53 (1974) 371.

146. J-P. Diard, B. Le Gorrec and C. Montella, J. Eelectroanal. Chem. 205 (1986) 77.

147. J-P. Diard, P. Landaud, B. Le Gorrec and C. Montella, J. Electroanal. Chem., 255 (1988) 1.

148. W. I. Archer and R. D. Amstrong, in A. J. Bard (Ed), Electroanalytical Chemistry,

Vol.7, Narcel Dekker N. Y. p157.

149. S. Iseki, K. Ohashi and S. Nagaura, Electrochimica Acta, 17 (1972) 2239.

150. R. D. Amstrong, M. F. Bell and A. H. Metcalfe in A. J. Bard (Ed), Electroanalytical Chemistry, Vol.6, Narcel Dekker N. Y. p99.

151. M. Sluyters-Rehbach and J. H. Sluyters, in A. J. Bard (Ed), Electroanalytical Chemistry, Vol.4, Narcel Dekker N. Y. p1.

152. K. S. Cole and A. H. Cole, J. Chem. Phys., 9 (1941) 61.

153. M. Rehbach and J. H. Sluyters, Recl. Trav. Chim. Phys. Bas., 80 (1961) 469; 81 (1962) 301; 82 (1963) 525.

154. I. Epelboin and M. Keddam, Electrochim. Acta, 17 (1972) 177.

155. B. V. Erschler, Disc. Faraday Soc. 1 (1947) 269.

156. B. D. Cohan and C. T. Chen. J. Electrochem. Soc. 129 (1982) 700.

157. D. A. Harrington and B. E. Conway, Electrochim. Acta, 32 (1987) 1703.

158. L. Bai, D. A. Harrington and B. E. Conway, Electrochim. Acta, 32 (1987) 1713.

159. I. V. Kadija, J. Electrochem. Soc., 131 (1964) 601.

160. M. Elam and B. E. Conway, J. Electrochem. Doc., 135 (1987) 1678.

161. M. Elam and B. E. Conway, J. App. Electrochem. 17 (1987) 1002

162. L. D. Burke and M. E. G. Lyons, in Modern Aspects of Electrochemistry, Vol. 18 Eds. by J. O'M Bockris, B. E. Conway and E. White. p169.

163. B. E. Conway and A. K. Vijh, J. Physical Chemistry, 71 (1967) 3637.

164. B. E. Conway and A. K. Vijh, J. Physical Chemistry, 71 (1967) 3655.

165. R. de Levie, J. Electroanal. Chem. 9 (1965) 117.

166. R. de Levie, Electrochim. Acta, 10 (1965) 113.

167. L. Nyikos and T. Pajkossy, Electrochim. Acta 30 (1985) 1533.

168. L. Nyikos and T. Pajkossy, J. Electrochem. Soc., 133 (1986) 2061.

169. L. Nyikos and T. Pajkossy, Electrochim. Acta, 31 (1986) 1347.

170. L. Nyikos and T. Pajkossy, Electrochim. Acta, 34 (1989) 171.

171. L. Nyikos and T. Pajkossy, Electrochim. Acta, 34 (1989) 181.

172. L. Nyikos and T. Pajkossy, Electrochim. Acta, 33 (1988) 713.

173. J. C. Wang, Electrochim. Acta, 33 (1988) 707.

174. J. C. Wang, Electrochim. Acta, 34 (1989) 987.

175. M. Keddam and H. Takenouti, Electrochim. Acta, 33 (1988) 445.

176. J.C. Wang and J. B. Bates, Solid State Ionics 18&19 (1986) 224.

177. S. H. Liu, Physical Review Letters, 55 (1985) 529.

178. A. Le Mehaute, Electrochim. Acta., 34 (1989) 591.